Asymptotic expansions and causal representations through the loop-tree duality

Thesis submitted for the Degree of Doctor of Philosophy

Author:

Judith Plenter

Director:

Germán V. Rodrigo García

Universitat de València

3126 Programa Oficial de Doctorat en Física

Instituto de Física Corpuscular, Departament de Física Teórica
Universitat de València – Consejo Superior de Investigaciones Científicas

February 2022

Declaration of authorship

I, Judith Plenter, hereby certify that this thesis, titled *Asymptotic expansions and causal representations through the loop-tree duality*, has been composed by myself. All the work contained herein is my own except where explicitly stated otherwise, and all main sources of help have been properly referenced and acknowledged.

The work presented in this thesis is based on original results previously published by myself, in collaboration with Germán Rodrigo, J. J. Aguilera-Verdugo, F. Driencourt-Mangin, R. J. Hernández-Pinto, S. Ramírez-Uribe, A. E. Rentería Olivo, G. Rodrigo, G. F. R. Sborlini, W. J. Torres Bobadilla, S. Tracz, R. M. Prisco and F. Tramontano. Chapters 2 and 4, in particular, are based on the following publications:

Articles

[1] J. J. Aguilera-Verdugo *et al.*, "A Stroll through the Loop-Tree Duality," *Symmetry* **13** no. 6, (2021) 1029, arXiv:2104.14621 [hep-ph]

[2] J. Plenter and G. Rodrigo, "Asymptotic expansions through the loop-tree duality," *Eur. Phys. J. C* **81** no. 4, (2021) 320, arXiv:2005.02119 [hep-ph]

[3] J. J. Aguilera-Verdugo, F. Driencourt-Mangin, R. J. Hernández-Pinto, J. Plenter, S. Ramirez-Uribe, A. E. Renteria Olivo, G. Rodrigo, G. F. R. Sborlini, W. J. Torres Bobadilla, and S. Tracz, "Open Loop Amplitudes and Causality to All Orders and Powers from the Loop-Tree Duality," *Phys. Rev. Lett.* **124** no. 21, (2020) 211602, arXiv:2001.03564 [hep-ph]

[4] J. J. Aguilera-Verdugo, F. Driencourt-Mangin, J. Plenter, S. Ramírez-Uribe, G. Rodrigo, G. F. R. Sborlini, W. J. Torres Bobadilla, and S. Tracz, "Causality, unitarity thresholds, anomalous thresholds and IR singularities from the loop-tree duality at higher orders," *JHEP* **12** (2019) 163, arXiv:1904.08389 [hep-ph]

An additional article arose from a collaboration during my PhD studies and is not covered in this thesis:

[5] S. Holz, J. Plenter, C. W. Xiao, T. Dato, C. Hanhart, B. Kubis, U. G. Meißner, and A. Wirzba, "Towards an improved understanding of $\eta \to \gamma^*\gamma^*$," *Eur. Phys. J. C* **81** no. 11, (2021) 1002, arXiv:1509.02194 [hep-ph]

Proceedings

[6] J. J. Aguilera-Verdugo, F. Driencourt-Mangin, J. Plenter, S. Ramírez-Uribe, G. Rodrigo, G. F. R. Sborlini, W. J. Torres Bobadilla, and S. Tracz, "Unsubtractions at NNLO," *CERN Yellow Reports: Monographs* **3** (2020) 169–176

[7] J. Plenter, "Asymptotic Expansions Through the Loop-Tree Duality," *Acta Phys. Polon. B* **50** (2019) 1983–1992

Presentations about the topic were given at the following conferences:

- 1st Workshop on High Energy Theory and Gender, CERN, Geneva (Switzerland), September 2018
- Amplitudes 2019, Dublin (Ireland), July 2019
- Matter to the Deepest, Chorzów/Katowice (Poland), September 2019
- GenT workshop on Precision probes of New Physics, Paterna (Spain), December 2019

Abstract

Large-scale particle physics experiments have provided a vast amount of high-quality data during the last decades. A leading role has been played by the Large Hadron Collider where the evaluation and analysis of its second run is currently still in progress while the third run is about to start, promising ever higher precision data of particle collisions and subsequent decays. The agreement between experimental observations and theoretical predictions using the Standard Model of Particle Physics is excellent. Indeed, this is a problem since there are currently few clues for how genuine shortcomings of the model can be overcome. New physics phenomena can appear either at higher energies, which would require the construction of an even larger particle collider, or as small deviations accessible only through precision calculations. These involve higher-order quantum corrections which pose technical challenges. An alternative to the traditional method has been proposed in the form of the loop-tree duality theorem. In this work a newly found purely causal representation of the dual integrands and the definitions of several classes of multiloop topologies as well as their loop-tree duality representations are presented. The main part of this work is focused on the development of a framework for using asymptotic expansions in the context of the loop-tree duality. Previously found expansions in the leading order Higgs boson decay are analyzed and a general method is derived for defining asymptotic expansion of scattering amplitudes within the loop-tree duality formalism. This method is applied and analyzed for the scalar two- and three-point functions at one-loop order and applied to highly boosted Higgs boson production.

Acknowledgements

First of all, I am very grateful for the four years of support by my thesis director, Germán Rodrigo. He always made time for answering my questions and helped me to find positive perspectives. Without his unwavering belief in me and the project I certainly would not have been able to finish this thesis.

For explaining big parts of the LTD framework, and all of the details hidden in the calculations, I want to thank Félix. Your help and patience with my unwillingness to accept some of the steps and results was immense. Even now, years after you have left IFIC, I have been using your thesis template and following much of your advice.

No voy a olvidar, por supuesto, la ayuda que me prestaron los demás miembros del grupo LTD. Will, tu apoyo tanto con los cálculos como con el manejo de Mathematica era imenso. Germán (Sborlini), te agradezco mucho la energía y motivación por la física que me mostraste, especialmente cuándo a mí me faltaban. Me ha gustado ver creciendo el grupo LTD: Andrés, Selomit, Jesús – gracias por todas las discusiones y colaboraciones.

A todos los del *Escuadrón IFIC* os agradezco cada una de las comidas, meriendas y cenas que hemos pasado juntos. Estos últimos años, con pandemia y la mayoría de vosotros ya doctores, os he echado mucho de menos. De este doctorado me llevaré, a parte de representaciones duales, también muchos recuerdos de rutas en bici, sábados de asados, cumpleaños celebrados juntos, días de playa, montaña y sol. Una mención especial es necesaria para Víctor y Ana: vuestra ayuda para manejar la burocracia del depósito ha sido imprescindible.

Joan, tú has sufrido conmigo en los momentos más difíciles de este trabajo. Gracias por apoyarme y asegurarme una y otra vez de que llegaría a entregar la tésis en algún momento. En los meses de pandemia asumiste el rol de compañero de despacho y ni quiero imaginarme la alternativa de haber pasado la cuarentena sólo acompañada por el documento vacío de la tesis.

Natürlich kann in dieser Liste meine Familie nicht fehlen. Es war sicher oft nicht einfach mit mir, aber trotzdem seid ihr nie von meiner Seite gewichen – es mögen uns die letzten Jahre 2000km getrennt haben, alleine habe ich mich aber dank eurer beständigen Unterstützung nie gefühlt.

This PhD thesis has been possible thanks to funding from the European Union Horizon 2020 research and innovation program under the Marie Skłodowska-Curie grant agreement No. 713673 and "La Caixa" Foundation (ID 100010434). The fellowship code is LCF/BQ/IN17/11620037. This work has also been supported by the Spanish Government (Agencia Estatal de Investigación) and ERDF funds from European Commission (Grant No. FPA2017-84445-P), Generalitat Valenciana (Grant No. PROMETEO/2017/053), Consejo Superior de Investigaciones Científicas (Grant No. PIE-201750E021) and the COST Action CA16201 PARTICLEFACE.

Gran parte de la inspiración para este trabajo la he conseguido gracias a las montañas de Valencia y sus senderos. A ellas dedico la portada de esta tesis.

Preface

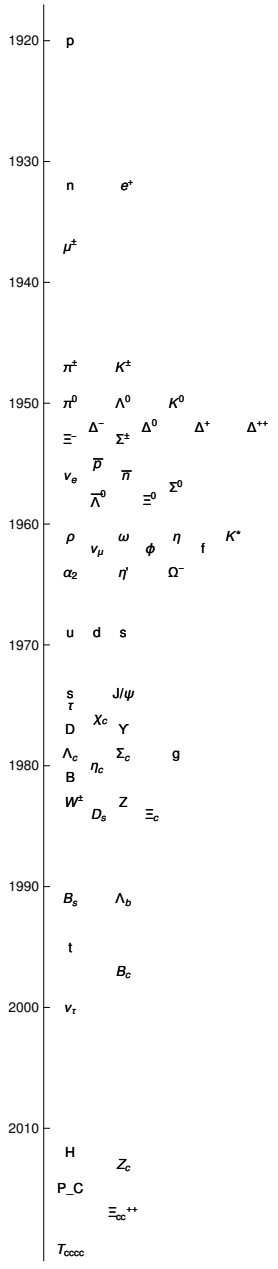

Figure 1: A selection of the experimental particle discoveries in the last centuries.

The field of elementary particle physics has emerged from the human desire to understand what the world around us is composed of. The idea that everything in nature is made up of different combinations of simpler underlying substances has appeared in various ancient cultures. With the introduction of the periodic table of elements in 1869 D. Mendeleev took an important step towards the systematization of the structure of matter. Only a few decades later two important observations in conflict with classical physics, the black-body radiation problem and the photoelectric effect, were explained by Max Planck and Albert Einstein through the introduction of the concepts of quantized energy and the correspondence between energy and frequency. These discoveries opened the door to quantum physics and lead to the major developments of quantum mechanics by W. Pauli, E. Schrödinger, W. Heisenberg and M. Born in the mid-1920s. Finally, in 1928 P. Dirac managed to combine quantum mechanics and special relativity to obtain a consistent description of the electron.

At this point, with quantum mechanics and special relativity well established as a framework to describe electromagnetic radiation, only few particles were known: the proton, electron and photon, with the positron and neutron having been proposed. Both were promptly discovered in 1932. The observation of continuous energy spectra in β decay led Pauli to propose an additional neutral particle, the neutrino, in 1930 and Fermi proposed a theory to describe the weak interaction underlying this decay in terms of a contact force between four fermions. Shortly after, in 1935, H. Yukawa explained the range of the strong nuclear force by introducing a mediator particle he called *pion*. When a heavy particle was detected in cosmic rays only two years later, it was commonly thought to be this mediator. Upon realizing that the newly discovered particle was in fact a heavier version of the electron, nowadays known as the muon, the apparently short list of elementary particles started becoming longer. This,

together with the development of sophisticated experiments and particle accelerators, started an era of rapid particle discoveries, visualized in Fig. 1, and the presumed order of the microscopic world collapsed.

Since the discovery of the neutron, a particle without electromagnetic charge, as part of the atomic nuclei, it had become apparent that the electromagnetic theory was insufficient for describing all particle interactions. Many of the newly discovered particles indeed appeared to be sensitive to the strong nuclear force. These so-called hadrons were grouped into multiplets with the same spin and same transformation properties under parity. Those multiplets were then identified with the irreducible representations of the symmetry group SU(3). In this system, proposed by M. Gell-Mann as the Eightfold Way and independently by G. Zweig, hadrons are built from the more fundamental quarks. In fact, the quarks were originally introduced as fictitious constituents in order to facilitate the group-theoretical classification of the hadron spectrum. Only after the substructure of the hadrons was experimentally probed were their components identified with quarks and gluons as mediators of the strong interaction in 1968.

The understanding of the dynamics between those particles that do not undergo the strong interaction, called leptons, improved significantly when it was proposed by S. Glashow that both electromagnetism and the weak nuclear force can be joined in a common framework. The description of the unified electroweak force by A. Salam and S. Weinberg in the 1960s led to the prediction of a neutral mediator particle, the Z boson. The non-zero mass of the mediator particles was explained shortly after by P. Higgs, R. Brout and F. Englert through the concept of symmetry breaking predicting another neutral particle, the Higgs boson.

The joint description of electroweak and strong interactions in terms of a Quantum Field Theory (QFT) is called the Standard Model of particle physics (SM). It has been exceedingly successful in describing and explaining a vast range of observations both in particle physics and in astrophysics to high precision. Thus, it is agreed upon, at least as an effective theory in a limited energy range, among virtually all physicists. Indeed, it is commonly claimed that the SM works *too well* since it is tremendously difficult to find discrepancies between the SM predictions and observations. Nonetheless, there are fundamental inconsistencies that it cannot solve like the matter-antimatter asymmetry observed in the current universe. In attempts to pinpoint what sector of the SM needs to be modified experiments like those at CERN's Large Hadron Collider (LHC) have been increasing both their precision and energy range significantly. In fact, current theoretical calculation techniques have difficulty matching the experimental precision. Facilitating the inclusion of additional higher order quantum contribu-

tions to the QFT predictions is thus at the forefront of current research. A short overview of QFT and some details on the SM are collected in Chapter 1.

Among others, the framework of the loop-tree duality (LTD) has been proposed to provide an alternative to the traditional method in perturbative QFT. It has the advantage of allowing calculations to be performed without changing the number of spacetime dimensions. Both its foundation and new developments for determing an entirely causal representation at leading order and beyond are found in Chapter 2.

The various theories for physics beyond the SM (BSM) typically become distinguishable from the SM prediction in a specific energy range or kinematic limit of particular observables. It is thus most important to calculate a precise prediction in those relevant limits. The LTD provides an ideal starting point for the development of asymptotic expansions at integrand-level since the LTD integrand is a function of Euclidean three-momenta. Cancellations between different components of Minkowski momenta that hinder the clear determination of the scaling within integrand expressions are thus avoided. The first asymptotic expansions in the context of the LTD were found in the leading order amplitude for the decay of the Higgs boson into two photons. The calculation of this process is provided in Chapter 3 and the nature and convergence behavior of the expansions is discussed therein.

The main part of this thesis in Chapter 4 is the development of a systematic approach for determining asymptotic expansions for the dual propagator and thus LTD amplitudes. The found expansions are tested at one-loop level. Asymptotic expansions for an important multiloop configuration are also provided. In Chapter 5 an application to the physically relevant process of highly boosted Higgs production is explored.

Contents

Abbreviations

BSM	beyond the Standard Model
CP	charge parity (symmetry)
CKM	Cabibbo-Kobayashi-Maskawa (matrix)
DREG	dimensional regularization
FDU	four-dimensional unsubtraction
IBP	integration by parts
IR	infrared
KLN	Kinoshita-Lee-Nauenberg (theorem)
LHC	Large Hadron Collider
LO	leading order
LTD	loop-tree duality
MI	master integral
MLT	maximal loop topology
MS	minimal subtraction
NLO	next-to-leading order
NMLT	next-to-maximal loop topology
NNLO	next-to-next-to-leading order
QCD	Quantum Chromodynamics
QED	Quantum Electrodynamics
QFT	Quantum Field Theory
SM	Standard Model (of particle physics)
SMEFT	Standard Model Effective Field Theory
SSB	spontaneous symmetry breaking
UV	ultraviolet

Chapter 1

Quantum Field Theory and the Standard Model of particle physics

The understanding of what the fundamental building blocks of matter and the universe are has changed over time. Until the middle of the 20th century the electron, proton and neutron were considered to be the indivisible constituents of the atoms. Together with the positron, an electron with inverted charge, and the muon, a heavier version of the electron, they were considered to be the fundamental particles at the time. The detection of the pion in 1947 began an era of rapid discovery revealing a multitude of new particles, made possible by the advancements in accelerator technology. The sheer amount, their diversity but also similarities between different particles created the expectation of a systematic explanation.

During the 1920s a novel theory was developed to describe the interactions between light and electrons called Quantum Electrodynamics. This was the first of many Quantum Field Theories to come. With the later implementation of the renormalization formalism to treat the singular quantum corrections and the development of gauge theories, the Standard Model of particle physics was formulated in the 1970s and has since been used successfully in describing and predicting a wide range of observations in particle colliders and other types of experiments.

1.1 Quantum Field Theory

The theoretical framework needed to describe the interactions of subatomic particles must be able to fulfill a set of requirements. Due to the small distance scales involved, inversely related to the energy of the processes through the uncertainty relation, a quantum theory is needed. This theory must be able to relate infinitely many degrees of freedom in order to describe concepts like the electromagnetic field, or seen from a different angle, the production of particle-antiparticle pairs from the vacuum at any point in spacetime. With velocities close to the speed of light it is also necessary to incorporate special relativity into the formalism. One of the theoretical constructs that fulfill these conditions is a *Quantum Field Theory*, and in fact, it is expected that whatever framework may be necessary to unite particle physics with gravity at the Planck scale, the corresponding effective theory describing nature at energy scales accessible in current particle physics experiments should be a QFT.

The general objective in particle physics is to predict the likelihood of scattering and decay events. These occur naturally or are provoked by accelerating particles to extremely high energies and facilitating their collision in large-scale

experiments like the LHC. The probability that an initial asymptotic state[1] of particles with momenta $\{p_1, \ldots, p_n\}$ evolves into a final asymptotic state with momenta $\{p'_1, \ldots, p'_n\}$ is given by the square of the so-called S-matrix element $< p'_1, \ldots, p'_n|S|p_1, \ldots, p_n >$. These matrix elements, needed for the calculation of scattering or decay processes, are generally written in terms of a Lorentz-invariant amplitude $\imath\mathcal{M}$. For the scattering of two initial particles into two final particles the S-matrix element is given by[2]

$$\langle p'_1 p'_2|S|p_1 p_2\rangle = \tag{1.1}$$
$$I + \imath(2\pi)^4\delta^4(p_1 + p_2 - p'_1 - p'_2)\frac{\mathcal{M}(p_1, p_2; p'_1, p'_2)}{(2E_1)^{1/2}(2E_2)^{1/2}(2E'_1)^{1/2}(2E'_2)^{1/2}},$$

where the identity matrix describes the scenario leaving the particles unaffected while their non-trivial interaction is described through the amplitude $\mathcal{M}$, which is directly related to the physical observables[3]. In a scattering experiment the likelihood of a particular final state is generally given in terms of the cross section σ since it is indicative of the physical process itself and allows comparison between different experiments. The differential cross section or $2 \to n$ scattering is thus given in terms of the amplitude as

$$d\sigma = \frac{(2\pi)^4|\mathcal{M}|^2}{4\sqrt{(p_1 \cdot p_2)^2 - m_1^2 m_2^2}}\, d\Phi_n(p_1 + p_2; p_3, \ldots, p_{n+2}), \tag{1.2}$$

where p_1 and p_2 are the momenta of the initial particles with masses m_1 and m_2, $\{p_3, \ldots, p_{n+2}\}$ are the momenta of the final particles and the element of n-body phase space is

$$d\Phi_n(P; p_1, \ldots, p_n) = \delta^4\left(P - \sum_{i=1}^{n} p_i\right)\prod_{i=1}^{n}\frac{d^3 p_i}{(2\pi)^3 2E_i}. \tag{1.3}$$

The amplitude can be calculated from the Lagrangian $\mathcal{L}$ of a QFT. For a non-interacting field theory a Lagrangian is made up of terms that contain the squares

[1] An initial (final) asymptotic state is defined as a (multi-particle) state in the limit $t \to \mp\infty$. In reality, it refers to the comparatively stable states before or after the interaction has occurred.

[2] Notation is chosen in agreement with [8], except for the sign of the amplitude. Some additional definitions relating Minkowski momenta p_i with Euclidean three-momenta $\boldsymbol{p}_i$ and on-shell energies E_i are given in Appendix A.

[3] Considering the interaction as no more than a perturbation is appropriate since the momentum eigenstates can contain no information about the position of the particle. This means that the likelihood of evaluating more than one field in close proximity is minimal and neither particle having an effect on the other is the (uninteresting) norm.

of one type of field. For a real scalar this is obtained directly from quantizing the classical Klein-Gordon field theory by imposing commutation relations between the creation and annihilation operators. This gives the free Lagrangian

$$\mathcal{L}_{KG} = \frac{1}{2}(\partial_\mu \phi)^2 - \frac{m^2}{2}\phi^2 \,, \tag{1.4}$$

where the quantum field $\phi(x)$ corresponds to a scalar particle with mass m. In an interacting field theory additional terms appear which couple three or more fields of the same or different types, called interaction terms $\mathcal{L}_I$. For the scalar field above a term describing a four-point interaction could be of the form

$$\mathcal{L}_{\phi^4} = -\frac{\lambda}{4!}\phi^4 \,, \tag{1.5}$$

with the coupling λ determining the strength of the interaction. From the interaction terms one calculates the scattering transition into asymptotic states as the exponential of their spacetime integral

$$S = T \exp\left\{ \imath \int d^4x \, \mathcal{L}_I \right\} \,, \tag{1.6}$$

where T is the time-ordering operator. Thus, to any given scattering process an infinite amount of terms with various powers of the interaction Lagrangian contribute. In those QFTs where the coupling appearing in the interaction term is small, these terms may be ordered in powers of the coupling. Then the expansion in the coupling can be used to calculate a process up to a specified order and thus to limited, but defined, precision. This procedure is referred to as *perturbation theory* and allows to write the amplitude in a perturbative expansion. For a theory with coupling λ this amounts to

$$\mathcal{M} = \lambda \mathcal{M}^{(1)} + \lambda^2 \mathcal{M}^{(2)} + \lambda^3 \mathcal{M}^{(3)} + \mathcal{O}\left(\lambda^4\right) \,, \tag{1.7}$$

with the leading order (LO) contribution denoted by $\mathcal{M}^{(1)}$, the next-to-leading order (NLO) contribution by $\mathcal{M}^{(2)}$ and the next-to-next-to-leading order (NNLO) contribution by $\mathcal{M}^{(3)}$. There are various techniques to obtain the terms contributing to the perturbative expansion at any given order. On a practical level the diagrammatic approach is most convenient, where particles are represented by lines whose crossing vertices signal interactions.

For the scalar field theory with the ϕ^4 interaction term of Eq. (1.5) the perturbative expansion can then be displayed as

$\mathcal{M} =$ 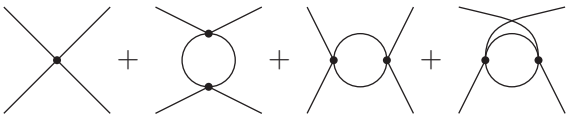 $+ \mathcal{O}\left(\lambda^3\right) \,.$ (1.8)

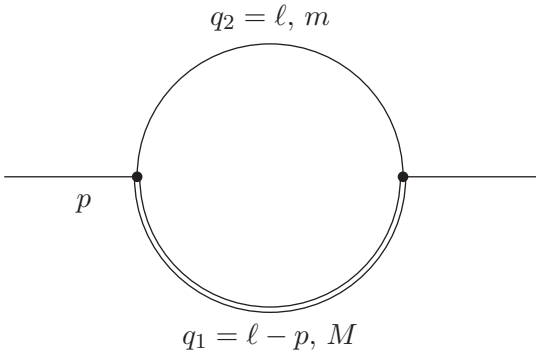

Figure 1.1: Diagram corresponding to the scalar two-point function of Eq. (1.10) with internal masses M and m.

In these so-called *Feynman diagrams* the lines and vertices have clear mathematical definitions derived from the given Lagrangian that are called *Feynman rules*. Specifically, the vertices always include a factor of the relevant coupling. Feynman diagrams like the first one in Eq. (1.8), without closed circuits, are called tree-level diagrams. Their value can be read off directly using the Feynman rules. Diagrams with closed circuits are called loop diagrams - their calculation involves solving an integral over the four-dimensional momentum running through the loop which in many cases leads to singularities and other technical difficulties. The internal lines correspond to Feynman propagators which are potentially divergent functions

$$G_F(q) = \frac{1}{q^2 - m^2 + \imath 0}\,, \tag{1.9}$$

where q is the four-momentum running along that line and m the mass of the particle it stands for. It is well-defined only with the infinitesimal imaginary regulator $\imath 0$ that circumvents the explicit singularity when the particle goes on shell.

1.2 Singularities, regularization and renormalization

A simple loop diagram, which will play an important role in the main part of this thesis, is the scalar two-point function as shown in Fig. 1.1. The goal of this section is to remind the reader of the multitude of steps that go into the calculation of even a simple Feynman diagram using the textbook method. With only scalar particles involved the numerator of this amplitude is trivial and the

loop integral over the four-momentum ℓ is given by

$$\mathcal{A}^{(1)}(p) = -\imath \int \frac{\mathrm{d}^4\ell}{(2\pi)^4}\, G_F(q_1;M)\, G_F(q_2;m)\ , \tag{1.10}$$

with $q_1 = \ell - p$ and $q_2 = \ell$. The textbook procedure for evaluating a Feynman integral starts with rewriting the product in the denominator of the integrand as a single expression raised to the power of the number of contributing Feynman propagators. This step is performed by employing so-called *Feynman parameters* and leads to

$$\begin{aligned} &G_F(q_1;M)\, G_F(q_2;m) \\ &\quad = \int_0^1 \mathrm{d}x\ \frac{1}{\left[x\left(\ell^2 - 2\ell\cdot p + p^2 - M^2 + \imath 0\right) + (1-x)\left(\ell^2 - m^2 + \imath 0\right)\right]^2} \\ &\quad = \int_0^1 \mathrm{d}x\ \frac{1}{\left[(\ell')^2 - \Delta^2\right]^2}\ , \end{aligned} \tag{1.11}$$

where the integration momentum is shifted by $\ell' = \ell - xp$ and the part of the expression independent of the integration variable is summarized as $\Delta^2 = -x(1-x)p^2 + (1-x)m^2 + xM^2 - \imath 0$. As long as the external momentum fulfills $p^2 < (m+M)^2$ it holds that $\Delta^2 > 0$ and the parameter Δ may thus be treated as an effective mass, the generalization to arbitrary external momenta can be obtained later on through analytic continuation. Understanding the behaviour of the integrand, and evaluating the integral, is obscured by the presence of Minkowski momenta. To circumvent this problem one performs a *Wick rotation*[1] consisting in the change to Euclidean integration variables by defining $\ell_0 = \imath \ell_{E,0}$, $\boldsymbol{\ell} = \boldsymbol{\ell}_E$, leading to a simplified integrand that can now be evaluated in four-dimensional spherical coordinates

$$\mathcal{A}^{(1)}(p) = \int \frac{\mathrm{d}^4\ell_E}{(2\pi)^4} \int_0^1 \mathrm{d}x\ \frac{1}{\left[\ell_E^2 + \Delta^2\right]^2} = \int \frac{\mathrm{d}\Omega_4}{(2\pi)^4} \int_0^1 \mathrm{d}x \int_0^\infty \frac{\mathrm{d}|\ell_E|\ \ell_E^3}{\left[\ell_E^2 + \Delta^2\right]^2}\ , \tag{1.12}$$

[1] The concept of the Wick rotation is based on solving the energy part of the integral through a contour integral, closing the integration path along the real axis with a semi-circle in the imaginary plane. Indeed, this is the concept on which the loop-tree duality is based as well, for the chosen integration path in the context of LTD see Fig. 2.1(a shift in the loop momentum would have to be performed there to allow a Wick rotation). Since the value of a contour integral is unaffected by smoothly changing the integration path, as long as no divergence is crossed, the contour may be rotated by 90°. The actual integration in the Minkowski energy ℓ_0 thus goes from $-\imath\infty$ to $+\imath\infty$, which is equivalent to the substitution mentioned in the main text.

where $\mathrm{d}\Omega_4$ is the solid angle element in four dimensions. It can be seen easily that the integral over the Euclidean momentum diverges logarithmically

$$\lim_{\Lambda\to\infty}\int_0^\Lambda \mathrm{d}|\ell_E|\ \frac{\ell_E^3}{\left[\ell_E^2+\Delta^2\right]^2} = -\frac{1}{2} + \lim_{\Lambda\to\infty}\log\frac{\Lambda}{\sqrt{\Delta^2}}\ . \tag{1.13}$$

The occurrence of a divergence like the one above, or an even more severe one, is not the exception but the rule for a loop integral. Indeed, higher-order calculations in perturbative QFTs most often involve having to deal with expressions that cannot be evaluated straight-forwardly in isolation and in four spacetime dimensions. Physical observables must necessarily be finite and QFT only became an accepted and widely used tool in particle physics when methods had been found to rewrite diverging expressions in a well-defined and consistent way. This process of removing overt singularities, often by making them explicit in terms of an infinitesimal parameter, is called *regularization*.

Actually, the most wide-spread regularization has already been introduced previously in the definition of the Feynman propagator Eq. (1.9). Here the mass of the internal particle has been given an infinitesimal negative imaginary part,

$$m^2 \to m^2 - \imath 0\ , \tag{1.14}$$

which assures that the propagator is never evaluated exactly on its pole and avoids thus the one point where the propagator is not well-defined. The pole of the Feynman propagators is only one of the types of singularities that can appear at integrand-level with many of them being integrable and leading to finite results.

While there are integrand-level singularities related purely to the calculation technique or chosen conventions (spurious singularities), which will cancel among themselves during the calculation, other divergences are of great physical importance. Most notably this is true for the singularities appearing in relation to the physical *unitarity threshold*. This is the kinematic configuration where the energy provided for the interaction is just sufficient to create a set of on-shell internal or final-state particles. This type of integrand-level singularity is integrable. In the example of the scalar two-point function used above threshold it appears when the external momentum squared is equal to or larger than the square of the summed up masses of the internal particles,

$$p^2 \geq (m+M)^2\ . \tag{1.15}$$

The origin, or rather explanation, of these physically relevant singularities goes much deeper than the calculation of a Feynman integral. To emphasize that they are not an artefact of the chosen calculation method but a physical necessity it is useful to consider them from the perspective of the S-matrix instead.

One of the postulates of S-matrix theory is the principle of maximal analyticity. This states that scattering amplitudes, considered as functions of Lorentz invariant energy variables, are analytic in the whole complex plane except for where there is a physical argument to the contrary. The common exceptions are pole singularities caused by resonances and branch cuts generated by multiparticle intermediate states. These examples of non-analytic behavior can be deduced from the fundamental principle of probability conservation by generalizing the notation of the S-matrix element defined in Eq. (1.1) for a generic initial particle state $|i\rangle$. Making sure that this state is normalised it may be written in terms of an orthonormal and complete set of states $|n\rangle$ as

$$|i\rangle = \sum_n a_n |n\rangle \,, \tag{1.16}$$

where the coefficients have to fulfill $\sum_n |a_n|^2 = 1$. The probability for the initial state to evolve into a final state $\langle f|$ is given by the square of the absolute value of the S-matrix element and since the total probability for the initial state to evolve into *any* final state has to be equal to one it is found that

$$\begin{aligned} 1 &= \sum_f |\langle f|S|i\rangle|^2 = \sum_f \langle i|S^\dagger|f\rangle\langle f|S|i\rangle = \langle i|S^\dagger S|i\rangle \\ &= \sum_{n,n'} a_n a^*_{n'} \langle n'|S^\dagger S|n\rangle \,. \end{aligned} \tag{1.17}$$

Since the choice of the coefficients cannot be restricted this leads to the unitarity condition for the S-matrix. Considering instead the total probability for an arbitrary, but specific, final state to evolve from any initial state leads to a comparable result and thus it is guaranteed that

$$S^\dagger S = S S^\dagger = 1 \,. \tag{1.18}$$

This important quality is transferred to the amplitude $\mathcal{M}$ connecting the initial state i with total momentum p_i to the final state f as

$$\mathcal{M}(i \to f) - \mathcal{M}^*(f \to i) = \imath \sum_n (2\pi)^4 \delta^{(4)}\left(k_n - p_i\right) \mathcal{M}(n \to f) \mathcal{M}^*(i \to n) \,, \tag{1.19}$$

where the sum extends over all permitted intermediate states n whose momenta sum up to k_n. For the elastic scattering of two spinless particles and total energies below the inelastic threshold this takes the concrete form

$$2\mathrm{Im}\mathcal{M}(p_1,p_2;p_1',p_2') = \int \frac{\mathrm{d}^3k_1}{(2\pi)^3 2E_1}\frac{\mathrm{d}^3k_2}{(2\pi)^3 2E_2}(2\pi)^4\delta^{(4)}\left(k_1+k_2-p_1-p_2\right) \times \mathcal{M}(k_1,k_2;p_1',p_2')\mathcal{M}^*(p_1,p_2;k_1,k_2)\,. \tag{1.20}$$

The important observation here is that the allowed intermediate states determine the imaginary part of the amplitude. The significance of the imaginary part becomes clear when considering the amplitude as a function of the center-of-mass energy $s = (p_1+p_2)^2$ and extending its domain of definition into the complex plane through analytic continuation. The physical amplitude is then defined as the value of the amplitude when evaluated with an infinitesimally positive imaginary part as

$$\mathcal{M}_{\text{physical}}(s) = \lim_{\varepsilon\to 0^+}\mathcal{M}(s+\imath\varepsilon)\,. \tag{1.21}$$

Being analytic in the upper half-plane the Schwarz reflection principle gives the imaginary part in the lower half-plane as

$$\mathrm{Im}\mathcal{M}(s) = -\mathrm{Im}\mathcal{M}(s^*)\,. \tag{1.22}$$

This shows that whenever the imaginary part is non-zero, the scattering amplitude has a branch cut along the real axis, starting at the two-particle production threshold that gives the lowest contributions to the unitarity condition above.

When increasing the total energy of the process in Eq. (1.20) sufficiently to permit inelastic scattering there are additional intermediate states that can be produced on their mass shell. These must be added with additional terms on the right-hand side of the unitarity condition, leading to an immediate and abrupt change in the imaginary part of the amplitude. The reason for this is that the elastic scattering matrix element has a branch point whenever the threshold for the production of an additional final state is reached.

These general observations must be fulfilled independently of the chosen method of calculating the amplitude, which in the case of Feynman diagrams involves integrating over a function that is in principle real (neglecting the regulator $\imath 0$). While the Riemann integral of a real function will produce a real result (if it exists), an integrand with singularities that can be integrated using complex analysis can produce an imaginary part in the result. The integrand-level

singularities related to the unitariy threshold are thus a necessity to produce the correct analytic structure of the scattering amplitude.

Depending on the topology and the kinematics of the amplitude it is possible for more internal particles to go on shell simultaneously than those that would be needed for producing an on-shell intermediate state (i.e. unitary cut). This scenario gives rise to an *anomalous threshold*. The most common example of this is the leading singularity of the triangle graph, where all three internal lines are set on shell, with all three particles necessarily moving forward (or backward) in time.

While both unitary and anomalous thresholds are an integral part of a scattering amplitude and spurious singularities cancel during the calculation, divergences related to the high-energy region of the integral, as the one found in Eq. (1.13) for the scalar two-point function, and divergences originating in the low-energy region of the momentum integral have to be regularized and treated carefully in order to obtain unambiguous results for the physical observables.

There is a variety of regularization schemes available that deal with the appearing divergences in different forms. The traditional schemes are based on changing the number of spacetime dimensions in intermediate steps of the calculation. Parts of this procedure will be explained in the following since it is the most commonly used regularization technique. A comparative overview of alternative regularization schemes can be found in Ref. [9], covering issues arising from the treatment of algebraic objects like metric tensors and Dirac matrices. Some of these regularization schemes are the four-dimensional formulation of dimensional reduction (FDF) [10], tools for the automation of one-loop calculations using dimensional reduction (GoSAM) [11], the framework of implicit regularization (IREG) [12–14], that allows calculations to be performed in the physical dimension of the underlying QFT, and four-dimensional regularization (FDR) [15].

1.2.1 UV singularities, DREG and renormalization

As seen above in Eq. (1.13), during the evaluation of the scalar two-point function a momentum cutoff was set as a regulator to allow the evaluation of the momentum integral in four spacetime dimensions. While the integrand does not diverge for large momenta, it also does not go to zero sufficiently fast, leading to the logarithmic divergence seen. This type of divergence can already be inferred from basic power counting since the behavior at large values of the integration

momentum is given by

$$\mathcal{A}^{(1)}(p) \sim \int \frac{\mathrm{d}^4\ell}{\ell^4}\,. \tag{1.23}$$

Higher order divergences are also common, with the integrand approaching a constant value different from zero or even increasing for high energies. Since it is the high-energy part of the momentum integral that produces these effects they are called *ultra-violet (UV) singularities*.

There are different regularization schemes available to treat UV singularities. As an alternative to setting a momentum cutoff, additional terms connected to artificial particles can be introduced which cancel the UV part of the amplitude (Pauli-Villars regularization). Both of these approaches lead to technical difficulties since they violate both gauge and Lorentz invariance. This is especially inconvenient since the gauge symmetries of a QFT lead to the Ward identities which are important both for the simplification of correlation functions and for the systematic treatment of UV divergences.

In the most common regularization technique calculations are performed in $d = 4 - 2\varepsilon$ spacetime dimensions. This leaves the problematic expressions mathematically well-defined as long as ε is not set to zero. In the case of the scalar two-point function the problematic integral now behaves as

$$\mathcal{A}_d^{(1)}(p) \sim \int \frac{\mathrm{d}^d\ell}{\ell^4} \tag{1.24}$$

at high energies and thus converges whenever d is smaller than four. An explicit result can thus be found and its dependence on the parameter ε encodes the singularity in an unambiguous way. This idea was introduced by G. 't Hooft and M. Veltman [16], and independently by J. Giambiagi and C. Bollini [17], in the seventies and is known under the name *dimensional regularization* (DREG).

The complete calculation of the scalar two-point function in d dimensions leaves the integral with the form

$$\mathcal{A}^{(1)}(p) = \int_0^1 \mathrm{d}x \int \frac{\mathrm{d}^d\ell_E}{(2\pi)^d} \frac{1}{\left(\ell_E^2 + \Delta^2\right)^2} = \int_0^1 \mathrm{d}x \int \frac{\mathrm{d}\Omega_d}{(2\pi)^d} \int \mathrm{d}|\ell_E| \frac{|\ell_E|^{d-1}}{\left(\ell_E^2 + \Delta^2\right)^2}\,. \tag{1.25}$$

The evaluation of the integral over the d-dimensional unit sphere gives $\int \mathrm{d}\Omega_d = 2\pi^{d/2}/\Gamma(d/2)$. The momentum integral can be solved by substituting $\ell_E^2 = y\Delta^2$

and bringing it into the shape of the Beta function which is given by

$$\int_0^\infty \mathrm{d}y\, y^{\alpha-1}(1+y)^{-\alpha-\gamma} = \frac{\Gamma(\alpha)\Gamma(\gamma)}{\Gamma(\alpha+\gamma)}\,, \tag{1.26}$$

allowing thus to express the integral with the singularity encoded in the Γ function. Only the integral over the Feynman parameter is then left to be solved and one finds

$$\mathcal{A}^{(1)}(p) = \frac{1}{(4\pi)^{\frac{d}{2}}}\frac{\Gamma(2-\frac{d}{2})}{\Gamma(2)}\int_0^1 \mathrm{d}x\,(\Delta^2)^{\frac{d}{2}-2}\,. \tag{1.27}$$

Inserting $d = 4-2\varepsilon$ the integrand and expanding the Γ function

$$(\Delta^2)^{\frac{d}{2}-2} = 1 - \varepsilon\log\left(\Delta^2\right) + \mathcal{O}(\varepsilon^2)\,, \tag{1.28}$$

$$\Gamma\left(2-\frac{d}{2}\right) = \frac{1}{\varepsilon} - \gamma_E + \mathcal{O}(\varepsilon)\,, \tag{1.29}$$

the divergent part of the integral can be identified as

$$\mathcal{A}^{(1)}(p) = \frac{1}{16\pi^2}\frac{1}{\varepsilon} + \text{finite}\,. \tag{1.30}$$

To obtain the finite part of the amplitude the integral over the Feynman parameter still has to be solved. By subtracting a counterterm containing the same divergent structure the amplitude is then left finite and the dimensions can be set to the physical value

$$\mathcal{A}_R^{(1)} = \mathcal{A}^{(1)} - \mathcal{A}_{\mathrm{UV}}^{(1)}\Big|_{d=4}\,. \tag{1.31}$$

The most striking quality of this approach is that it conserves all of the fundamental symmetries of the used theory. This makes it possible to not just regularize a specific amplitude but to render the entire theory well-defined in the UV. This process is based on recognizing that those parameters that appear in the Lagrangian, such as masses and couplings, are not necessarily the physically measurable properties of the particles described by the theory. During this so-called *renormalization* the bare parameters of the Lagrangian are redefined to absorb the appearing UV divergences by combining the unrenormalized

amplitude with the UV counterterm. Using the renormalized theory and its Lagrangian, written in terms of the observed masses and couplings, all amplitudes are then immediately free of UV singularities.

The parameters of the renormalized theory depend explicitly on the non-physical dimension. Thus this systematic subtraction is only possible within DREG. Nonetheless, having identified the counterterms needed in DREG it is possible to use these same expressions also within other frameworks, even four-dimensional ones. The direct subtraction of the counterterm and calculation of the renormalized amplitude in four dimensions is sufficient for the calculation of a specific observable.

1.2.2 Soft singularities

The other group of non-integrable divergences is related to the low-energy region of loop integrals and appears when one or more internal lines represent massless particles and carry almost zero energy. They are referred to as *infrared (*IR*)* or *soft singularities*.

The origin of these divergences lies in the curious fact that while one might be tempted, from a theoretical perspective, to define a $2 \to 2$ process purely through the S-matrix element connecting two initial-state with two final-state particles, this does not in fact correspond to reality. The precision of any experiment is limited, even theoretically. This means that the elastic scattering of two electrons cannot be distinguished from events where an additional soft photon is emitted with an energy so low that it lies below the detection threshold of the experimental setup. Thus the full experimental cross-section for the production of an n-particle final state, consisting at least partially of massless particles, out of the collision of two particles is obtained by taking Eq. (1.2) with $2 \to n$ and adding the corresponding expression that include additional massless final states where the additional massless particle's energy is restricted to undetectable values. At LO this amounts to including Eq. (1.2) for the $2 \to n+1$ process. Accordingly, during the theoretical construction of a physical observable it must always be taken into account which type of processes actually contribute to a given measurement.

It turns out that both the phase-space integral of the amplitudes describing the emission of additional low-energy massless particles (real emission contributions) as well as the virtual loop contributions diverge. Just as in the UV case, both the divergences in the real and in the virtual contributions must be regularized and parameterized in a controlled way in order to see that, in fact, the divergences cancel exactly between the real and the virtual contributions leading to an unambiguous and finite result. Constructing observables in a way that

guarantees their equivalence to an actual measurement leads to IR-safe observables.

Comparable cancellations take place when both the radiating and the radiated particle are massless and the angle separating their trajectories is so small that they can only be registered as one signal during experimental reconstruction. The so-called *collinear singularity* created in this scenario is again canceled by a part of the corresponding loop integral.

It has been shown with the Kinoshita-Lee-Nauenberg (KLN) theorem that up to all orders in perturbation theory the IR singularities of a QFT with massless fields cancel when summing over all virtual and real contributions. [18, 19] Physical observables are necessarily IR safe.

Different regularization schemes exist that allow to achieve this cancellation for an observable, for instance giving the problematic particle a fictitious mass, which is taken to zero only after the calculation, or setting an infrared cutoff. The most commonly used approach is based on using the KLN theorem to justify defining local counterterms in the shape of the real radiation contributions to cancel the divergences appearing in the loop integral. Different variants of this subtraction formalism are available [20–34] and many, but not all, are performed in the context of DREG. An informative overview of recent developments with a special emphasis on local cancellations, including various regularization schemes that allow computations to be performed in four spacetime dimensions, can be found in Ref. [35].

1.3 Anatomy of a loop calculation

There exist many techniques to perform and regularize a loop calculation with the most widely used being based on DREG. In practice, the steps described in Section 1.2 are very similar for a variety of amplitudes. Still, comparability is not always straight-forward since different choices in defining the Feynman parameters lead to analytically different integrands, whose equivalence may have to be checked numerically. Furthermore, additional simplifications are necessary for amplitudes with non-trivial numerators. For example, these appear in processes with external vector particles where the scattering amplitude is given by the product between the external polarization vectors and a reduced amplitude with tensor structure. For an amplitude with n external vector particles and $m - n$ external scalars this amounts to an expression of the shape

$$\mathcal{A}(p_1, \ldots, p_n, p_{n+1}, \ldots, p_m) = \varepsilon_{\mu_1}(p_1) \cdot \cdots \cdot \varepsilon_{\mu_n}(p_n) \mathcal{A}^{\mu_1 \cdots \mu_n}(p_1, \ldots, p_m)\,, \quad (1.32)$$

where the reduced amplitude $\mathcal{A}^{\mu_1\cdots\mu_n}$ can be written in terms of all n-tensors that can be constructed from the external momenta. With theses tensors $\mathcal{T}_i$ forming the basis $\mathcal{B}$ one can then decompose the reduced amplitude as

$$\mathcal{A}^{\mu_1\cdots\mu_n}(p_1,\ldots,p_m) = \sum_{i\in\mathcal{B}} \mathcal{T}_i^{\mu_1\cdots\mu_n} F_i\,, \tag{1.33}$$

where the functions F_i are scalar form factors depending on the scalar products between the external momenta. The integrand $f^{\mu_1\cdots\mu_n}$ appearing in the original expression in general depends on tensor structures that form a larger basis since they may additionally depend on any of the loop momenta

$$\mathcal{A}^{\mu_1\cdots\mu_n}(p_1,\ldots,p_m) = \int_{\ell_1}\cdots\int_{\ell_L} f^{\mu_1\cdots\mu_n}(p_1,\ldots,p_m,\ell_1,\ldots,\ell_L) \tag{1.34}$$

with the d-dimensional integration measure summarized in the notation

$$\int_\ell = -\imath\,\mu^{4-d}\int \mathrm{d}^d\ell/(2\pi)^d\,. \tag{1.35}$$

By defining projection operators $\mathcal{P}$ that fulfill the condition

$$\mathcal{P}_{i,\mu_1\ldots\mu_n}\cdot\mathcal{T}_j^{\mu_1\cdots\mu_n} = \delta_{ij}\,, \tag{1.36}$$

one obtains scalar integrals for the form factors given by

$$F_i = \int_{\ell_1}\cdots\int_{\ell_L} \mathcal{P}_{i,\mu_1\ldots\mu_n}\cdot f^{\mu_1\cdots\mu_n}(p_1,\ldots,p_m,\ell_1,\ldots,\ell_L)\,. \tag{1.37}$$

While the integrands of the form factors are now scalar they may still have non-trivial numerators. As an example, an expression like

$$I = \int_\ell \frac{c_1\ell^2 + c_2\;\ell\cdot p + c_3 m^2}{(\ell^2-m^2)\left((\ell-p)^2-m^2\right)} \tag{1.38}$$

could appear. Here the ℓ-dependent terms appearing in the numerator can be expressed in terms of the inverse propagators, abbreviated by $D_1 = (\ell^2-m^2)$ and $D_2 = ((\ell-p)^2-m^2)$, as

$$\begin{aligned} \ell^2 &= D_1 + m^2 \\ 2\ell\cdot p &= D_1 - D_2 + p^2\,. \end{aligned} \tag{1.39}$$

Using these identities the integral can be rewritten in terms of scalar integrals with trivial numerators as

$$I = c_1 \int_\ell \frac{1}{D_1} + \left((c_1 + c_3)\, m^2 + \frac{c_2}{2}\, p^2 \right) \int_\ell \frac{1}{D_1 D_2}\,, \tag{1.40}$$

where a shift in the integration momentum has been used to show that $\int D_1^{-1} = \int D_2^{-1}$. This example is a particular case of what is known as *Passarino-Veltman reduction* [36] which can be used to decompose any one-loop integral with up to four internal propagators into a small set of scalar *master integrals* (MIs).

At present, automatizations of both the tensor reduction and the decomposition into master integrals are available, most notably within the MATHEMATICA [37] package FeynCalc [38, 39] which has been used in the context of this thesis. Therein also the solutions for the MIs are provided, where those that were used in this work are given for reference in Appendix A.

Higher order corrections containing more than one loop integral need additional techniques since irreducible scalar products appear, which cannot be written in terms of the propagators. A standard approach lies in applying *Integration-by-Parts Identities* (IBPs) which allow to construct a system of linear equations from a set of Feynman integrals that depend on the same propagators elevated to different powers [40, 41]. Solving this system many Feynman integrals can be written in terms of a smaller basis of independent integrals which in this context are the MIs.

Generally, the difficulty of a loop calculation increases with the number of loops, the number of external particles, and the amount of independent energy scales (internal and external masses and Mandelstam variables). While certain physical processes have been calculated to five-loop precision even for some two-loop amplitudes with four external legs some MIs are as of yet unsolved for certain configuration of internal and external scales, making the study of calculation and regularization techniques within QFT an important field of current research.

1.4 The Standard Model of particle physics

As S. Weinberg famously stated, to construct a QFT one needs to know only the relevant degrees of freedom, i.e. the particles interacting at the considered energy scale, and the symmetries of the considered system [42]. The Lagrangian consists then of all possible terms that contain the allowed fields and respect the symmetries, including continuous Lorentz transformations. Using this Lagrangian to calculate an observable through perturbation theory one obtains the

most general possible S-matrix element that agrees with the assumed symmetries, analyticity, perturbative unitarity and the cluster decomposition principle. For the known fundamental particles such a Lagrangian can thus be constructed using the symmetries observed through experimental observation. The union of all renormalizable operators appearing in this Lagrangian defines the Standard Model of particle physics.

The particles considered within the scope of particle physics are grouped together as fermions, with half-integer spin, and bosons, with integer spin. Those particles that mediate the fundamental interactions are all bosons. For electromagnetism these are the photons and their counterparts for the strong interaction are called gluons. Weak interactions are mediated through the massive $W^{\pm}$ and Z bosons and lastly there is the Higgs boson connected to the mechanism for mass-generation. Among the fermions, which constitute the matter content of the SM, are the up and down quark, which are the primary constituents of protons and neutrons. Two heavier copies of this set have been found: overall there are six quarks affected by the strong interaction collected into pairs of increasing mass

$$\begin{bmatrix} u \\ d \end{bmatrix}, \quad \begin{bmatrix} c \\ s \end{bmatrix}, \quad \begin{bmatrix} t \\ b \end{bmatrix}. \tag{1.41}$$

The remaining fundamental fermions not affected by the strong interaction are called leptons. This group is composed of heavier versions of the electron and the corresponding neutrinos:

$$\begin{bmatrix} \nu_e \\ e^- \end{bmatrix}, \quad \begin{bmatrix} \nu_\mu \\ \mu^- \end{bmatrix}, \quad \begin{bmatrix} \nu_\tau \\ \tau^- \end{bmatrix}. \tag{1.42}$$

The differences between the sets appear to lie solely in the mass and they are thus considered to be three families with differing *flavor*. The fermions, their corresponding antiparticles, the gauge boson and the Higgs boson are what we currently understand to be fundamental particles and as such are the fields whose interactions are described by the SM.

Besides the basic requirement that the laws of physics, even of particle physics, are not to depend on the position or speed of the observer, that is they are required to be invariant under proper orthochronous Lorentz transformations, the SM is built up on the basis of gauge symmetries. These are connected to the fact that the fields used to describe particle interactions are not themselves physical objects that can be directly measured. Different configurations without physical relevance chosen for the fields must lead to exactly the same measurable outcome.

Operations converting one of these allowed configurations into another one are called *gauge transformations*. The gauge symmetries related to the electroweak and strong interactions together form the symmetry group of the SM

$$SU(3)_C \otimes SU(2)_L \otimes U(1)_Y \,. \tag{1.43}$$

The first subgroup of these is related to the strong interaction. Observable particles that are affected by this strong interaction are the hadrons. These occur as fermionic baryons and bosonic mesons and both of these still have an inner structure. Simplistically, mesons are identified with the bound state of a quark and an antiquark while the (anti-)baryons correspond to a state of three (anti-)quarks. It has been experimentally established through the measurement of the proton form factors in deep inelastic scattering experiments that quarks behave as nearly free particles at very short distances, leading to an experimental requirement called *asymptotic freedom*.

Using quarks to build up the entire hadronic spectrum one needs to introduce a new quantum number, the color charge: without it Fermi-Dirac statistics would be violated in the baryonic sector. Color itself cannot be observed directly since all asymptotic states are color singlets leading to the second experimental requirement for a theory describing the strong interaction: due to their color charge, quarks cannot appear outside of color-neutral bound states. This concept is called *confinement*. From measuring the ratio between the hadronic and leptonic τ decay widths the number of colors is determined to be three.

With all asymptotic states being color singlets the defining symmetry of the strong interaction is the invariance under rotations in the three-dimensional color space. Particularly, this symmetry should also hold when being promoted to a local one. Collecting the quark fields of the three different colors and common flavor f as a vector in color space, q_f, the Lagrangian has to be invariant under transformations of q_f in the form

$$q_f \overset{SU(3)_C}{\longrightarrow} \exp\{-ig_s\, \theta^a(x) T^a\}\; q_f \,. \tag{1.44}$$

Here $\theta^a(x)$ is an arbitrary function depending on spacetime, the operators T^a are the generators of $SU(3)_C$ and g_s is the strong coupling. This symmetry transformation can be used to construct the gauge theory of Quantum Chromodynamics (QCD) which is described by the Lagrangian

$$\mathcal{L}_{\text{QCD}} = \bar{q}_f\, i \not{D}\, q_f - \frac{1}{4} G^{\mu\nu}_a G^a_{\mu\nu} \,, \tag{1.45}$$

where the field-strength tensor $G_a^{\mu\nu}$ contains the gluon fields and D_μ is the covariant derivative acting as

$$D_\mu q_f = (\partial_\mu - i g_s \, T^a G_a^\mu(x)) \, q_f \, . \tag{1.46}$$

Its effect is the coupling of gluons and quarks in the form of

$$\mathcal{L}_{\mathrm{QCD}} \supset -g_s G_a^\mu \bar{q}_f^\alpha \gamma^\mu T_{\alpha\beta}^a q_f^\beta \, . \tag{1.47}$$

The QCD Lagrangian as derived from the gauge principle necessarily describes massless quarks. The experimentally known masses are obtained at a later stage of the formalism through the Higgs mechanism, described towards the end of this section.

The symmetry group at hand, being a non-Abelian Lie group, leads to the generation of gluon self-interaction diagrams. This results in the strong scale dependence of the QCD running coupling which explains the observed asymptotic behavior of the strong interaction: with increasing energy the strength of the strong interaction decreases, resulting in the phenomenon of asymptotic freedom and making the application of perturbation theory possible. In this perturbative region the predictions of QCD are consistent with all experimental data available. In the low-energy regime, on the other hand, the coupling increases. Thus quarks and gluons are confined within the color-neutral hadrons. Since in this regime QCD is non-perturbative the direct connection between QCD and the relevant hadronic degrees of freedom (mesons and baryons) cannot be calculated analytically.

The electroweak interaction as described by the SM contains both electromagnetic interactions mediated between charged particles by photons through Quantum Electrodynamics (QED) and the weak interactions which couple all fundamental fermions through the massive gauge bosons Z and $W^\pm$. These have in common that their couplings are sufficiently small for a perturbative treatment: transition amplitudes can be expanded in terms of the electromagnetic and weak couplings and calculated up to the needed level of accuracy.

Studying both the energy and angular distributions of β decays it has been revealed that they depend on the spin direction of the involved particles. In fact, only left-handed fermions and right-handed antifermions appeared to partake in these kind of interactions involving the flavor change of a massive lepton. The additional observation from neutrino scattering experiments that the number of leptons of any flavor is separately conserved, thus distinguishing neutrinos from antineutrinos, as well as theoretical arguments demanding a correct behavior of the theory at high energies has been sufficient for the development of the

electroweak theory. In this process the vector bosons and their masses were actually predicted and their existence later confirmed in experiments.

Processes like the β decays are mediated by the charged vector bosons $W^{\pm}$. Taking into account that only left-handed (right-handed) fermions (antifermions) are affected by these so-called *charged currents* it is clear that two important discrete symmetries are maximally broken: parity, which flips the sign of the spatial coordinate and thus interchanges left-handed particles with their right-handed counterparts, and charge conjugation, which replaces particles with their antiparticles and vice versa. The left-handed fermions couple to the charged vector bosons in the form of doublets, formed for a family f by

$$Q_{1,f} = \begin{pmatrix} u_f \\ d_f \end{pmatrix}_L , \tag{1.48}$$

where $u_f = (u, c, t)$ is the up-type quark of flavor f and $d_f = (d, s, b)$ the bottom-type quark. The lepton doublet is written as

$$L_{1,f} = \begin{pmatrix} \nu_f \\ l_f^- \end{pmatrix}_L . \tag{1.49}$$

Other processes like electron-positron scattering are mediated by neutral vector bosons: the massless photon and the massive Z boson. Since neither of these have electromagnetic charge these interactions are known as *neutral currents*. Both of these vector bosons couple to a fermion and the corresponding antifermion, thus they transform as singlets under the gauge transformation and are always flavor-conserving. Both couple to the left-handed particles forming the $SU(2)_L$ doublets and also to the right-handed fermions, besides the neutrino, which are encoded as

$$Q_{2,f} = u_{f,R} , \quad Q_{3,f} = d_{f,R} \quad \text{and} \quad L_{3,f} = l_{f,R}^- . \tag{1.50}$$

A QFT describing both the weak interaction with its doublet representation and electromagnetism can be obtained through the symmetry group

$$SU(2)_L \otimes U(1)_Y \tag{1.51}$$

where the second subgroup cannot be directly identified with the symmetry group of QED. The Lagrangian describing the electroweak interactions is then given by

$$\mathcal{L}_{\text{ew}} = \sum_f \sum_{j=1}^{3} \left(\imath \bar{Q}_{j,f} \not{D} Q_{j,f} + \imath \bar{L}_{j,f} \not{D} L_{j,f} \right) - \frac{1}{4} B_{\mu\nu} B^{\mu\nu} - \frac{1}{4} W^i_{\mu\nu} W_i^{\mu\nu} , \tag{1.52}$$

where the covariant derivative D_μ couples the fermions to the gauge bosons W^1_μ, W^2_μ, W^3_μ and B_μ derived from the symmetry in Eq. (1.51). The kinetic terms and self-interactions between these gauge bosons are found in the latter two terms of the Lagrangian. The charged current interaction terms $\mathcal{L}_{\mathrm{CC}}$ are found through the identification $W^\pm_\mu = (W^1_\mu \pm W^2_\mu)/\sqrt{2}$. Since the photon's coupling does not distinguish between right- and left-handed fermions it cannot be identified directly with either of the two neutral fields W^3_μ and B_μ. Instead the fields Z_μ and A_μ of the physical vector bosons mediating the weak and electromagnetic interactions are superpositions of the fields of the neutral gauge bosons given by

$$\begin{pmatrix} W^3_\mu \\ B_\mu \end{pmatrix} = \begin{pmatrix} \cos\theta_W & \sin\theta_W \\ -\sin\theta_W & \cos\theta_W \end{pmatrix} \begin{pmatrix} Z_\mu \\ A_\mu \end{pmatrix}, \tag{1.53}$$

in terms of the electroweak mixing angle θ_W. This allows the identification of the neutral current interaction terms $\mathcal{L}_{\mathrm{NC}}$ which may be separated into the QED Lagrangian and those terms providing the coupling to the Z boson as

$$\mathcal{L}_{\mathrm{NC}} = -eA_\mu \sum_f \left(\frac{2}{3}\bar{u}_f \gamma^\mu u_f - \frac{1}{3}\bar{d}_f \gamma^\mu d_f - \bar{l}_f \gamma^\mu l_f \right) + \mathcal{L}^Z_{\mathrm{NC}}\,. \tag{1.54}$$

Summarizing the self-interaction between 3 (4) gauge bosons as $\mathcal{L}_3$ ($\mathcal{L}_4$) the overview of the electroweak Lagrangian then is given by

$$\mathcal{L}_{\mathrm{ew}} = \mathcal{L}_{\mathrm{kin}} + \mathcal{L}_3 + \mathcal{L}_4 + \mathcal{L}_{\mathrm{CC}} + \mathcal{L}_{\mathrm{NC}}\,, \tag{1.55}$$

where all kinetic terms are collected in $\mathcal{L}_{\mathrm{kin}}$. Note that these do not contain any mass terms for fermions since these would mix the left- and right-handed component of the fields. Similarly, the gauge symmetry would be broken through the explicit introduction of mass terms for the vector bosons even though they are experimentally known to be massive.

For masses to be included in the theory the electroweak gauge theory has to be broken. This can be achieved while leaving the Lagrangian fully symmetric, and thus renormalizable, through breaking the symmetry spontaneously. In the case of the SM the *spontaneous symmetry breaking* (SSB) is realized in the form of the Higgs mechanism. The general idea is based on the introduction of two additional complex scalar fields which transform under $SU(2)_L$ as a doublet

$$\phi(x) = \begin{pmatrix} \phi^{(+)}(x) \\ \phi^{(0)}(x) \end{pmatrix} \tag{1.56}$$

and adding the corresponding kinetic terms equipped with a covariant derivative defined such that the Lagrangian is invariant under the gauge symmetry. Additionally, a potential is introduced to give

$$\mathcal{L}_S = (D_\mu \phi)^\dagger D^\mu \phi - V(\phi)\,, \quad V(\phi) = \mu^2 \phi^\dagger \phi + h\left(\phi^\dagger \phi\right)^2\,, \tag{1.57}$$

where the parameters of the potential are set as $h > 0$ and $\mu^2 < 0$ to guarantee the presence of an infinite set of degenerate states where the potential is minimized. These minima in the potential are found for

$$\left|\left\langle 0 \left| \phi^{(0)} \right| 0 \right\rangle\right| = \sqrt{\frac{-\mu^2}{2h}} = \frac{v}{\sqrt{2}}\,, \tag{1.58}$$

where the neutral scalar field has acquired a vacuum expectation value. The equation above can be fulfilled by an infinite number of configurations of the doublet due to the invariance of the Lagrangian under $SU(2)_L$ transformations. Parameterizing the excitation above the ground state as $H(x)$ the scalar doublet may be written as

$$\phi(x) = \exp\left\{\imath \frac{\sigma^i}{2}\theta^i(x)\right\} \frac{1}{\sqrt{2}} \begin{pmatrix} 0 \\ v + H(x) \end{pmatrix}\,. \tag{1.59}$$

The degenerate states with minimum energy are then obtained by varying $\theta^i(x)$ while maintaining the excitation at $H(x) = 0$. While the doublet is now written in terms of four real fields, ϕ^i and H, the gauge invariance allows to choose the configuration where the exponential function is trivial by setting $\theta^i = 0$, the unitary gauge, leaving only the field H. Having arbitrarily chosen a specific ground state the electroweak symmetry group is spontaneously broken to the electromagnetic one

$$SU(2)_L \otimes U(1)_Y \quad \xrightarrow{\text{SSB}} \quad U(1)_{\text{QED}}\,. \tag{1.60}$$

With the ground state parameterized as such and identifying $M_H = \sqrt{-2\mu^2}$ the potential takes the form

$$-V(\phi) = \frac{M_H^2 v^2}{8} - \frac{M_H^2}{2} H^2 - \frac{M_H^2}{2v} H^3 - \frac{M_H^2}{8v^2} H^4\,. \tag{1.61}$$

The field $H(x)$, identified with the Higgs boson, has thus acquired a mass as well as self-interaction terms. In the unitary gauge the couplings to the vector bosons

in the covariant derivative take the shape

$$(D_\mu\phi)^\dagger D^\mu\phi \overset{u.g.}{=} (\partial_\mu H)^\dagger \partial^\mu H + (1+2/vH+H^2/v^2)\left(\frac{v^2g^2}{4}W_\mu^\dagger W^\mu + \frac{v^2g^2}{8\cos^2\theta_W}Z_\mu Z^\mu\right), \tag{1.62}$$

producing thus the desired mass terms for the vector bosons and allowing to identify their masses as $M_W = vg/2$ and $M_Z = M_W/(\cos^2\theta_W)$. The value of the vacuum expectation value can then be determined from the measurement of the Fermi coupling to be

$$v = \left(\sqrt{2}G_F\right)^{-1/2} = 246\,\mathrm{GeV}\,. \tag{1.63}$$

The introduction of fermion masses needs an additional, but straight-forward, step: taking into account the scalar $SU(2)$ doublet the symmetry requirements allow adding terms to the Lagrangian which couple left-handed fermion doublets to their right-handed partners. This leads to the so-called Yukawa-Lagrangian which in unitary gauge and after SSB is given by

$$\mathcal{L}_Y = -\left(1+\frac{H}{v}\right)\sum_f \left(m_{u_f}\bar{u}_f u_f + m_{d_f}\bar{d}_f d_f + m_{l_f}\bar{l}_f l_f\right) \tag{1.64}$$

and thus provides the SM with mass terms for all fermions besides the neutrino. Concurrently, interaction terms between the fermion-antifermion pairs and the Higgs boson are introduced with the interaction strength being necessarily proportional to the fermion masses. The terms above are obtained by diagonalizing a more general Lagrangian where the different flavors of fermions are coupled together. This diagonalization introduces couplings to the W boson between fermions and antifermions of different flavors. The terms describing flavor-changing charged currents are then included in the Lagrangian through the Cabibbo-Kobayashi-Maskawa matrix $\boldsymbol{V}$ as

$$\mathcal{L}_{\mathrm{CC}} = -\frac{g}{2\sqrt{2}}\left(W_\mu^\dagger\left[\sum_{i,j}\bar{u}_i\gamma^\mu(1-\gamma_5)\boldsymbol{V}_{ij}d_j + \sum_l \bar{\nu}_l\gamma^\mu(1-\gamma_5)\,l\right] + h.c.\right). \tag{1.65}$$

Joining the descriptions of the strong interaction through QCD and the electroweak interaction the complete SM Lagrangian after SSB is given by

$$\mathcal{L}_{\mathrm{SM}} = \mathcal{L}_{\mathrm{QCD}} + \mathcal{L}_{\mathrm{ew}} + \mathcal{L}_S + \mathcal{L}_Y\,. \tag{1.66}$$

It has been exceedingly successful in describing not just a large variety of experiments in particle colliders but also in cosmological attempts to decipher the origin and evolution of the universe. This is true up to increasing precision: certain observables have been calculated including up to five loops of QED corrections.

1.5 The search for physics beyond the Standard Model

In spite of various decades of successful application of the SM there are various lines of evidence demonstrating that it cannot be a complete description of particle physics. While no groundbreaking discoveries have been made at the LHC since the Higgs boson, experimental observations such as the anomalous magnetic moment of the muon [43] or the B anomalies [44] hint at discrepancies between SM predictions and measurements. At the same time, there are parts of the SM that are not entirely satisfying from a theoretical point of view: the model requires a large number of unexplained parameters. These puzzles include the pattern of masses and of the mixing between the quarks but also the question of why there are exactly three families of fermions.

One obvious issue can be found in considering the neutrinos of the traditional SM which are massless. This directly contradicts the experimental observation of neutrino oscillations: Electron neutrinos produced in the sun do not reach detectors on earth at the expected rate since they have been partially converted into neutrinos of other flavors. Comparable observations have been made with anti-neutrinos produced in nuclear reactors and with atmospheric neutrinos. Oscillations between the different flavor states allow to measure the mass differences between the mass eigenstates of the neutrinos. Various mechanisms have been proposed to explain neutrino masses, ranging from the addition of sterile right-handed neutrinos to a right-handed Majorana mass term.

Besides the electromagnetic, strong and weak interactions there is a fourth fundamental force: the quantization of gravity and its unification with the SM has as of yet not been successful. This is of little importance when studying particle collisions and collider experiments since the relevant distance scales of gravity are many orders of magnitude larger than those considered in particle physics. For understanding the origin of matter and the history of the universe this changes. In cosmological models the interactions of fundamental particles, their agglomeration and the effects of gravity in creating larger structures have to be combined. Various observations show that the amount of matter far exceeds the observable matter. The SM does not offer an explanation as to the origin of this *dark matter*. To be in agreement with the observed accelerated expansion

of the universe it is further necessary to include the concept of *dark energy*, about which absolutely nothing is known, into the model. Lastly, our current understanding of the very early universe relies on the creation of significantly more baryons than antibaryons – otherwise they would have annihilated when the universe cooled down. This unequal behavior can only occur if the joined symmetry of parity and charge conjugation, CP, is violated. While the SM does allow CP violation to some degree, through the complex phase of the CKM matrix and an additional term of the QCD Lagrangian, the θ-term, the amount is not enough by a large margin to explain baryogenesis.

Any model proposed for physics beyond the SM (BSM) must not only provide a solution to at least one of the problems but first of all agree with all the available experimental data. Since this requirement is true for the SM the actual task at hand is to show that a proposed model reproduces the SM at low energies, treating it thus as an effective field theory. The Standard Model Effective Field Theory (SMEFT) has been introduced to provide a consistent framework for parameterizing possible deviations from the SM in a model-independent way by adding higher-dimensional operators involving the SM fields. These encapsulate new physics effects making it convenient to determine the impact the model has on the SMEFT operators instead of calculating the predictions for a vast number of observables for each specific model of new physics. The BSM effects on energy regimes currently accessible through experiments are necessarily very small. With decreasing experimental uncertainties it is clear that theoretical predictions at increasing precision are at the forefront of current research in order to confirm or reject deviations from the SM [45].

A relevant part of BSM physics is focused on the Higgs sector. The potential used in the Higgs mechanism, Eq. (1.57), was accepted as part of the SM not because there was no logical alternative but because it was the simplest one that lead to the desired effect of generating fermion and vector boson mass terms. Indeed, it is perfectly reasonable to include additional Higgs-like scalar particles. Studying the couplings and interactions of the Higgs boson to high precision is thus considered to be important.

The dominant Higgs boson production mechanism at the LHC is gluon fusion $gg \to H$. The ggH interaction vertex in the SM is almost entirely generated by loops of top quarks whose Yukawa coupling to the Higgs boson is fixed by the mass of the top quark and the electroweak vacuum expectation value. In reality though, the Yukawa coupling is determined experimentally to around 50% from ttH production. Therefore an additional effective point-like component to the

Hgg coupling has not been excluded yet: [46]

$$\frac{m_t}{v}\bar{t}tH \;\rightarrow\; -\kappa_g \frac{\alpha_s}{12\pi v} G^a_{\mu\nu} G^{\mu\nu,a} H + \kappa_t \frac{m_t}{v}\bar{t}tH. \tag{1.67}$$

In the limit of a large top quark mass the Higgs boson production cross-section $\sigma_{gg\to H}$ is proportional to the sum of the two couplings κ_g and κ_t therefore they cannot be constrained separately using only this process.

Instead, one may look at the production of Higgs bosons with large transverse momentum $p_\perp$. Assuming that the scale of new physics Λ_g is much larger than twice the top quark mass one finds that the kinematic region $2m_t \ll p_\perp \ll \Lambda_g$ allows to disentangle the top quark and BSM components of the term in Eq. (1.67) since only the latter can still be treated as point-like leading to different scaling behavior of the cross-section in these limits as [46]

$$\frac{d\sigma_H}{dp_\perp^2} \sim \frac{\sigma_0}{p_\perp^2} \begin{cases} (\kappa_g + \kappa_t)^2 & , \; p_\perp^2 < 4m_t^2, \\ \left(\kappa_g + \kappa_t \frac{4m_t^2}{p_\perp^2}\right)^2 & , \; p_\perp^2 > 4m_t^2. \end{cases} \tag{1.68}$$

A precise SM prediction in this kinematic regime is clearly needed. Although the theoretical description for the purely point-like region has reached N^{3}LO QCD accuracy for the inclusive rate [47] and NNLO QCD for the $p_\perp$ - distribution [48–52], the situation is less satisfying for region with $p_\perp^2 > 4m_t^2$. In the latter kinematic regime the Higgs boson is produced together with a gluon or quark.

Processes with gluons in the initial state typically have large (radiative) QCD corrections. The LO QCD calculation for the production of highly boosted Higgs bosons [53,54] is thus likely to be insufficient. The NLO calculation in the full SM involves the computation of two-loop four-point amplitudes involving elliptical integrals. The planar contributions have been calculated [55] but other MIs are still unavailable. Advancements towards an NLO result have been made in recent years both through numerical integration [56] and expansions in the Integration by Parts identities [46]. A recent analysis [57] provides approximate QCD predictions at NNLO by combining results obtained in heavy top quark effective theory available at NNLO [49–52] with both the numerical and the approximated SM result at NLO [46,56]. Work towards an alternative calculation using asymptotic expansions in the context of the loop-tree duality is shown in Chapter 5.

There are many similar observables for which an increase in theoretical precision is not necessarily needed for the full amplitude because specific limits are the window to test potential discrepancies between experiments and SM predictions. The interest in asymptotic expansions within perturbative QFT arises from their

potential to facilitate analytic results in specific kinematic configurations, particularly when full analytic calculations in DREG are not possible. While work on the solution for further master integrals is ongoing, an expanded result can still be of great interest since it showcases the relevant behavior of the amplitude in the needed kinematic limit. Furthermore, in the context of the local cancellation of IR singularities expanded integrands could be very convenient to reduce computation time. While maintaining the correct analytic structure in the divergent limit and thus allowing for the combination with the real-emission contributions, the less complicated form of the expanded virtual contributions is expected to evaluate faster during the point-by-point process of numerical integration.

The interest in asymptotic expansions becomes also clear noting that there are already well-developed methods for simplifying the integrands of Feynman amplitudes. Widely known among them is Expansion by Regions [58–64]. While this technique has been shown to provide correct results a general proof is still pending [65]. Additionally, the degree of UV divergence rises with every term in the expansion which can result inconvenient. Within this work the application of asymptotic expansions is explored in the context of the loop-tree duality theorem.

Chapter 2

Loop-tree duality

The need for a technique like DREG is founded in the difficulty of quantifying non-integrable integrals. Using this well-defined formalism on loop integrals and scattering amplitudes allows to write the divergent part as a pole in $\varepsilon = (d-4)/2$, where d is the number of spacetime dimensions, and define a counterterm to subtract the problematic terms. If this subtraction were to be performed at integrand-level the calculation itself could be done in four dimensions.

Various techniques have been developed in recent years to tackle this problem, many of them summarized in Ref. [9], among them the loop-tree duality (LTD) [3,4,66–82] and four-dimensional unsubtraction method (FDU) [83–85]. The basis of LTD is using the Cauchy residue theorem to integrate over one component of the loop momentum. Loop amplitudes can thus be expressed as a sum of residues which can be reformulated as so-called dual amplitudes. These consist of sums of tree-level like objects appearing as integrands of what essentially is a phase-space integral.

2.1 Loop integrals and the residue theorem

A general one-loop scattering amplitude with N external legs in the Feynman representation is given by

$$\mathcal{A}_N^{(1)} = \int_\ell a_N^{(1)} = \int_\ell \mathcal{N}\left(\ell, \{p_k\}_N\right) \left(\prod_{i=1}^{N} G_F(q_i)\right) , \tag{2.1}$$

where the loop integral measure in $d = 4-2\varepsilon$ spacetime dimensions is provided in Eq. (A.13) and the expression $\mathcal{N}\left(\ell, \{p_k\}_N\right)$ is a function of the loop momentum ℓ and the N external momenta $\{p_k\}_N$. The Feynman propagators $G_F(q_i) = (q_i^2 - m_i^2 + \imath 0)^{-1}$ carry momenta $q_i = \ell + k_i$, where k_i are linear combinations of the external momenta.

Interpreting a Feynman propagator $G_F(q_i)$ as a function of the energy component $q_{i,0}$ of its internal momentum allows to identify the poles through

$$G_F(q_i) = \frac{1}{\left(q_{i,0} - q_{i,0}^{(p,+)}\right)\left(q_{i,0} + q_{i,0}^{(p,+)}\right)} , \tag{2.2}$$

where the complex on-pole energies are defined as $q_{i,0}^{(p,+)} = \sqrt{\boldsymbol{q}_i^2 + m_i^2 - \imath 0}$. Thus, the integrand a_N of the one-loop amplitude with the loop energy ℓ_0 extended into the complex plane has $2N$ poles for

$$\ell_0 \to \ell_0^{(\pm i)} = \pm q_{i,0}^{(p,+)} - k_{i,0} = \pm\sqrt{\boldsymbol{q}_i^2 + m_i^2} - k_{i,0} \mp \imath 0 , \tag{2.3}$$

half of them with positive and the other half with negative imaginary part.

According to the residue theorem, and since $a_N^{(1)}(\ell_0)$ is analytic in $\mathbb{C}\backslash\{\ell_0^{(\pm i)}\}$, the line integral of $a_N^{(1)}$ over a closed curve γ is proportional to the sum of the residues of $a_N^{(1)}$ at the singular points that lie within the area enclosed by the curve

$$\oint_\gamma d\ell_0\, a_N^{(1)} = \pm 2\pi\imath \sum \mathrm{Res}(a_N^{(1)}, \ell_0^{(\pm i)})\,, \tag{2.4}$$

with the sum going over those $\ell_0^{(\pm i)}$ that lie within γ and the positive (negative) sign reflecting a positively-oriented (negatively-oriented) curve.

For connecting the above to the calculation of the one-loop integral the curve can be chosen along the real axis and is closed through a semi-circle either in the lower or upper half plane, as demonstrated in Fig. 2.1. Letting the radius of the semi-circle go to infinity assures that the integrand vanishes along the semi-circle. As an illustration one sees for a single propagator

$$\lim_{|\ell_0|\to\pm\infty} G_F(q_i) = \lim_{|\ell_0|\to\pm\infty} \frac{1}{(\ell_0 + k_{i,0})^2 - (\boldsymbol{\ell} + \mathbf{k}_i)^2 - m_i^2 + \imath 0} = 0\,. \tag{2.5}$$

Note that the above is true independently of the value of the loop three-momentum since any cancellation would only affect the real part of ℓ_0 - its imaginary part going to infinity will always let the integrand vanish. While the numerator can have an impact on this behavior, problems can only arise in the case of UV divergent amplitudes. Those will need to be renormalized locally (see for example Chapter 3), creating thus an integrand where neglecting the integral over the semi-circle would again be justified.

The scattering amplitude can thus be expressed as

$$\mathcal{A}_N^{(1)} = \int_{\vec{\ell}} \int \frac{d\ell_0}{-2\pi\imath}\, a_N^{(1)} = \pm \int_{\vec{\ell}} \sum_{\mathrm{Im}(\ell_0^{(\pm i)})\lessgtr 0} \mathrm{Res}(a_N^{(1)}, \ell_0^{(\pm i)})\,, \tag{2.6}$$

where the reduced integration measure is

$$\int_{\vec{\ell}} = -\,\mu^{4-d} \int \mathrm{d}^{d-1}\ell/(2\pi)^{d-1}\,. \tag{2.7}$$

The residue, whenever the index i refers to a simple pole, is given by

$$\mathrm{Res}(a_N^{(1)}, \ell_0^{(\pm i)}) = \frac{1}{\pm 2 q_{i,0}^{(+)}} \left(\mathcal{N}\left(\ell, \{p_k\}_N\right) \prod_{j\neq i}^{N} G_F(q_j) \right)_{\ell_0 = \ell_0^{(\pm i)}}\,. \tag{2.8}$$

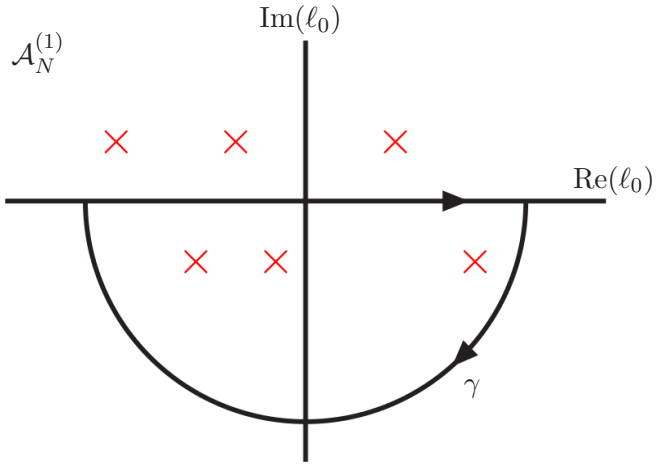

Figure 2.1: The position of the singularities of a one-loop amplitude in the complex plane of the loop energy ℓ_0. Half of the poles always lie in the area enclosed by the negatively-oriented integration path γ when the radius of the semi-circle is extended to infinity. Figure adapted from Ref. [66].

The generalization for one Feynman propagator appearing more than once and producing a pole of order n is obtained by the general formula for the residue

$$\mathrm{Res}(a_N^{(1)}, \ell_0^{(\pm i)}) = \frac{1}{(n-1)!} \lim_{\ell_0 \to \ell_0^{(\pm i)}} \frac{d^{n-1}}{d\ell_0^{n-1}} \left((\ell_0 - \ell_0^{\pm i})^n \, \mathcal{N}\left(\ell, \{p_k\}_N\right) \prod_{j=1}^{N} G_F(q_j) \right) , \tag{2.9}$$

taking care not to double-count residues in the sum. While a pole of higher order does not appear naturally in a one-loop amplitude, this type of integral can appear after applying IBP identities.

2.2 The loop-tree duality theorem

For a numerical application of the LTD writing the theorem in terms of the residues as in Eq. (2.6), or its generalization for more than one loop, is usually the most convenient. When aiming for an analytical result instead, it is useful to rewrite the residues as shown in the following, allowing thus simplifications,

the identification of cancellations and a more intuitive understanding of the amplitude. In any case, the different residues should not be treated independently. While different shifts in the loop momentum are in principle allowed, this has the potential to complicate the calculation. Maintaining the relation between the momenta q_i is important to conserve local cancellations.

As a first step it is convenient to notice that the remainder of the propagator producing the divergence in the residue of the simple pole, $1/(2q_{i,0}^{(p,+)})$, may be written in terms of the real on-shell energy

$$q_{i,0}^{(+)} = \sqrt{\boldsymbol{q}_i^2 + m_i^2} = |q_{i,0}^{(p,+)}| \,. \tag{2.10}$$

The imaginary part in $1/(2q_{i,0}^{(p,+)})$ can be dropped since the only singularity that could appear in this expression would be an endpoint singularity in the massless case, where the regulator $\imath 0$ would not be of use. The residue of a Feynman propagator evaluated at its pole in the negative half-plane can thus be written in terms of a modified delta functional $\tilde{\delta}\,(q_i) = 2\pi i\ \theta(q_{i,0})\delta(q_i^2 - m_i^2)$, in short, or $\tilde{\delta}\,(q_i; m_i) \equiv \tilde{\delta}\,(q_i)$ whenever it is necessary to make reference to the internal masses. This allows to recover the integral over the loop energy as

$$\begin{aligned}\int_{-\infty}^{\infty} d\ell_0\, \tilde{\delta}\,(q_i)\ f(\ell, \{p_k\}_N) &= 2\pi i \int_{-\infty}^{\infty} d\ell_0\, \frac{\delta(\ell_0 + k_{i,0} - q_{i,0}^{(+)})}{2q_{i,0}^{(+)}}\, f(\ell, \{p_k\}_N) \\ &= \frac{2\pi i}{2q_{i,0}^{(+)}}\, f(\ell, \{p_k\}_N)\bigg|_{\ell_0 = q_{i,0}^{(+)} - k_{i,0} = |\ell_0^{(+i)}|} \,. \end{aligned} \tag{2.11}$$

If one were to naively identify the generic function $f(\ell, \{p_k\}_N)$ with the product of numerator and Feynman propagators $\mathcal{N}\,(\ell, \{p_k\}_N) \sum_{i=1}^{N} \left(\prod_{j\neq i} G_F\,(q_j)\right)$ the expression would fail to reproduce the imaginary prescription of the propagators in the residue: evaluating a Feynman propagator at the complex pole energy we have

$$\begin{aligned} G_F(q_j)\Big|_{\ell_0 = \ell_0^{(+i)}} &= \frac{1}{\left(q_{i,0}^{(p,+)} - q_{j,0}^{(p,+)} + k_{ji,0}\right)\left(q_{i,0}^{(p,+)} + q_{j,0}^{(p,+)} + k_{ji,0}\right)} \\ &= \frac{1}{(k_{ji,0})^2 + 2q_{i,0}^{(p,+)} k_{ji,0} + (q_{i,0}^{(p,+)})^2 - (q_{j,0}^{(p,+)})^2} \,, \end{aligned} \tag{2.12}$$

where $j \neq i$ and $k_{ji} = q_j - q_i$. In this expression the imaginary parts of the on-

pole energies cancel.[1] With $k_{ji,0}$ being a sum of external energies and thus real, the imaginary prescription of the propagator in the so-called dual prescription is given by

$$\mathrm{Im}\left(2q_{i,0}^{(p,+)}k_{ji,0}\right) = -\imath 0\,\eta\cdot k_{ji}\,, \quad \eta = (1,\mathbf{0})\,. \tag{2.13}$$

Considering that the imaginary prescription is an integral part of the Feynman propagator and its evaluation, it makes sense to identify this modified expression by defining the *dual propagator* as

$$\begin{aligned} G_D(q_i;q_j) \equiv G_F(q_j)\Big|_{q_{i,0}=q_{i,0}^{(p,+)}} &= \frac{1}{q_j^2 - m_j^2 - \imath 0\,\eta\cdot k_{ji}}\Bigg|_{q_{i,0}=q_{i,0}^{(+)}} \\ &= \frac{1}{2q_i\cdot k_{ji} + m_i^2 + k_{ji}^2 - m_j^2 - \imath 0\eta\cdot k_{ji}}\Bigg|_{q_{i,0}=q_{i,0}^{(+)}}. \end{aligned} \tag{2.14}$$

Indeed, the only difference between G_D and G_F lies in the momentum-dependent prescription for the imaginary regulator and a lot of the qualities of LTD are directly related to cancellations made possible through this feature. For this reason a lot of emphasis is put in this chapter to differentiate between quantities with an infinitesimal imaginary part like $q_{i,0}^{(p,+)}$ and their absolute value or real part $q_{i,0}^{(+)}$. Only while maintaining this distinction are the following dual amplitudes and their limits unambiguous.

Using the shown properties we can see that identifying $f(\ell,\{p_k\}_N)$ with the product of the amplitude's numerator and the corresponding dual propagators does reproduce the residues

$$\begin{aligned} \int_{-\infty}^{\infty} d\ell_0\,\tilde{\delta}\,(q_i)\,\mathcal{N}\,(\ell,\{p_k\}_N)\prod_{j\neq i} G_D\,(q_i;q_j) \\ = \frac{2\pi i}{|2q_{i,0}^{(+)}|}\,\mathcal{N}\,(\ell,\{p_k\}_N)\prod_{j\neq i} G_F\,(q_j)\Bigg|_{\ell_0=\ell_0^{(+i)}}. \end{aligned} \tag{2.15}$$

Note that the imaginary parts are only relevant in so far as they regularize an otherwise undefined integral and therefore can be set to zero in the numerator.

[1] The cancellation between infinitesimal imaginary parts is admissible here only because no expansion implicitly modified their numerical value. On the contrary, the imaginary part of a comparable expression like $q_{i,0}^{(p,+)} - q_{j,0}^{(p,+)}$ is undefined. While due to the infinitesimal nature of the imaginary part of the on-pole energy one may generally write $q_{i,0}^{(p,+)} = q_{i,0}^{(+)} - \imath 0$, this involves the replacement $\imath 0/(2q_{i,0}^{(+)})| \to \imath 0$.

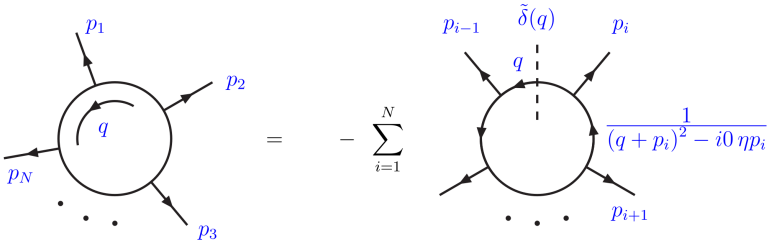

Figure 2.2: A one-loop amplitude with N external particles expressed on the left in the Feynman representation and on the right after the application of the LTD as given in Eq. (2.16). Figure taken from Ref. [66].

The original formulation of the loop-tree duality theorem as presented in Ref. [66] allows thus to rewrite the result of applying the residue theorem, with the curve closed in the lower half-plane, in a compact form

$$\mathcal{A}_N^{(1)} = -\int_\ell \mathcal{N}\left(\ell, \{p_k\}_N\right) \sum_{i=1}^{N} \tilde{\delta}\left(q_i\right) \left(\prod_{j\neq i} G_D\left(q_i; q_j\right)\right) \,. \tag{2.16}$$

The alternative option of closing the contour in the upper half-plane would correspond to multiplying the expression above by a factor of -1, due to the changed direction of the integration path, and redefining the delta functional to select the modes with negative energy. Since this process is equivalent to reversing the momentum flow of the loop $\ell \to -\ell$ it does not have to be considered separately. The choice $\eta = (1, \mathbf{0})$ corresponds to integrating out the energy component of the loop momentum, thus reducing the integration measure to the Euclidean space of the loop three-momentum as shown in the previous section. That calculation can be generalized to extend not the loop energy but a different component of the loop momentum into the complex plane. Therefore, in the general case η is an arbitrary future-like vector.

A different internal loop momentum is set on shell in each of the summands in Eq. (2.16), which are conventionally called dual contributions (also sometimes referred to as dual amplitudes or cuts). In each of these contributions the energy-component of the loop momentum is fixed through the delta functional leaving to be solved only the integral over the Euclidean three-momentum. This representation thus highlights how the original one-loop integral has been expressed in terms of a sum of tree-level like objects, in the sense that with one internal propagator on shell the dual contributions resemble the phase-space integral over

a tree-level amplitude as illustrated in Fig. 2.2.

The simplest amplitude to exemplify many of the properties of dual amplitudes is the scalar two-point function. As will be seen later on, many of the observations concerning this example can be extended to general one-loop amplitudes. Defining the loop momenta $q_1 = \ell + p_1$ and $q_2 = \ell$ one has

$$\mathcal{A}_2^{(1)} = \int_\ell G_F(q_1) G_F(q_2)\,, \tag{2.17}$$

which is written in the notation of the LTD as

$$\mathcal{A}_2^{(1)} = -\int_\ell \left(\tilde{\delta}\,(q_1)\, G_D(q_1; q_2) + \tilde{\delta}\,(q_2)\, G_D(q_2; q_1) \right) . \tag{2.18}$$

The direct relation to the amplitude in the Feynman representation is obtained with

$$\mathcal{A}_2^{(1)} = \int_{\vec{\ell}} \left(\frac{1}{2q_{1,0}^{(+)}} G_F(q_2)\Big|_{q_{1,0}=q_{1,0}^{(p,+)}} + \frac{1}{2q_{2,0}^{(+)}} G_F(q_1)\Big|_{q_{2,0}=q_{2,0}^{(p,+)}} \right) , \tag{2.19}$$

where in each dual contribution one of the internal lines is explicitly not just set on shell but evaluated at the pole energy. In most situations it will be more comfortable to handle mainly real quantities. The explicit dual prescription for the imaginary regulator allows just that. Factorizing the denominator in the integrand above permits the direct identification of the appearing singularities as

$$\begin{aligned} \mathcal{A}_2^{(1)} = \int_{\vec{\ell}} \Bigg(& \frac{1}{2q_{1,0}^{(+)}} \frac{1}{(q_{1,0}^{(+)} + q_{2,0}^{(+)} - p_{1,0})(q_{1,0}^{(+)} - q_{2,0}^{(+)} - p_{1,0}) + \imath 0 p_{1,0}} \\ & + \frac{1}{2q_{2,0}^{(+)}} \frac{1}{(q_{2,0}^{(+)} + q_{1,0}^{(+)} + p_{1,0})(q_{2,0}^{(+)} - q_{1,0}^{(+)} + p_{1,0}) - \imath 0 p_{1,0}} \Bigg) . \end{aligned} \tag{2.20}$$

This expression has been obtained by integrating the original four-dimensional integrand over the loop energy and fixing it at the energy value $q_{i,0}^{(+)}$ where either internal line is on shell and with positive energy. The on-shell energy still depends on the loop three-momentum and can still allow the remaining propagator to diverge.

2.3 Singularities in dual integrands

Singularities play an important role in the calculation of scattering amplitudes. As explained in Section 1.2 both IR and UV singularities persist in the integrated

amplitude and thus require a regularization procedure like DREG just to solve the integral (or even allow the integral to be well-defined). With LTD having provided an integrand as a function of Euclidean three-momenta, the objective in this case is to identify the regions of the integration domain that produce said singularities and define appropriate counterterms to regularize the integrand locally. In the case of UV singularities those local counterterms, when integrated, have to reproduce the counterterms known from DREG for comparability. Soft and collinear singularities cancel between virtual and real scattering amplitudes contributing to the same physical processes. If demonstrated that these are restricted to a compact region of the loop three-momentum, this cancellation may be achieved already at integrand-level by identifying and subtracting the corresponding terms.

Physically relevant are also threshold singularities at integrand-level: they appear whenever the kinematics of an amplitude permit the internal loop particles to go on shell. This type of singularity is the origin of the imaginary part of an integrated amplitude and has a fundamental impact on its analytic structure. Considering that the behavior of scattering amplitudes is influenced by their analytic properties more than anything else the importance of these integrand-level divergences becomes clear.

Lastly, the various propagators in an amplitude can produce additional singularities without physical impact. In the following it will be shown how within LTD these types of unphysical singularities necessarily cancel.

An intuitive analysis of the singularities present in the integrands of scattering amplitudes can be obtained by considering them as functions of primarily the energy component of the loop momentum. Divergences occur when the momentum running along one internal line respects the on-shell condition of a physical particle or antiparticle. This corresponds to the energy component of the loop energy taking the value

$$\ell_0 \to \pm\sqrt{\boldsymbol{q}_i^2 + m_i^2 - \imath 0} - k_{i,0} \tag{2.21}$$

as shown at the beginning of this chapter. These on-shell hyperboloids reduce to light-cones in the massless case. After applying the LTD theorem the loop momentum is fixed to the positive energy mode of a different on-shell hyperboloid for each dual contribution. The remaining integral over the loop three-momentum thus evaluates the integrand along the corresponding on-shell hyperboloid. Singularities in the dual integrand appear only in those places where one of the forward on-shell hyperboloids crosses any other hyperboloid. These hyperboloids are shown for the case of the scalar two-point function, as defined in Eq. (2.17),

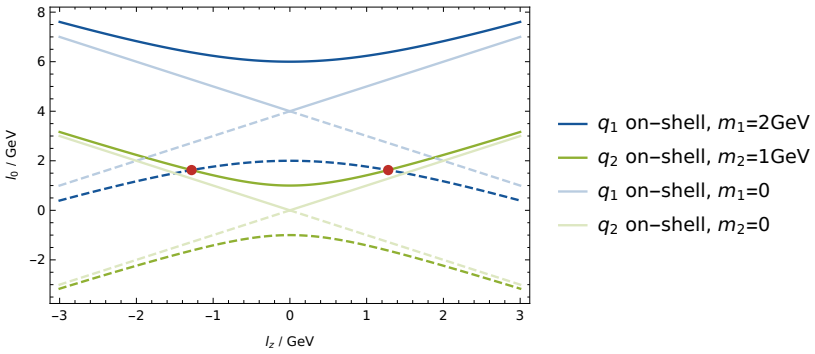

Figure 2.3: The on-shell hyperboloids for the scalar two-point function in Eq. (2.17) with $\boldsymbol{p} = 0$ and $p_{1,0} = -4\,\mathrm{GeV}$. Both massive and massless hyperboloids are shown, the latter ones in a lighter color. The red dots show the position of the physical thresholds. The integral over the loop three-momentum evaluates the dual integrand along the solid lines.

in Fig. 2.3 where they are described by

$$\ell_0^{\text{2-pt.-fct.}} \to \left\{ \pm\sqrt{(\boldsymbol{\ell}+\boldsymbol{p})^2 + m_1^2} - p_{1,0}, \pm\sqrt{\ell^2 + m_2^2} \right\} . \tag{2.22}$$

Physical thresholds appear whenever forward and backward on-shell hyperboloids intersect as happens for the kinematic conditions chosen in Fig. 2.3. The intersection between a positive energy mode $q_{i,0}^{(+)}$ with a negative energy mode $-q_{j,0}^{(+)}$ is realized when

$$\ell_0 = q_{i,0}^{(+)} - k_{i,0} = -q_{j,0}^{(+)} - k_{j,0} \, . \tag{2.23}$$

It is also possible that an intersection between either two forward or two backward on-shell hyperboloids appears. These do not have physical impact and always cancel between the dual contributions as will be shown in the following. Nonetheless, it can be inconvenient to deal with these types of unnecessary divergences. Often it can be worthwhile to redefine the amplitude in such a way that unphysical thresholds can be avoided altogether. As can be seen in Fig. 2.4 the two forward hyperboloids of the scalar two-point function intersect for a positive external energy, while this intersection is transferred to the backward hyperboloids when the external energy is negative. This second configuration is equivalent to changing the direction of the loop momentum $\ell \to -\ell$ when

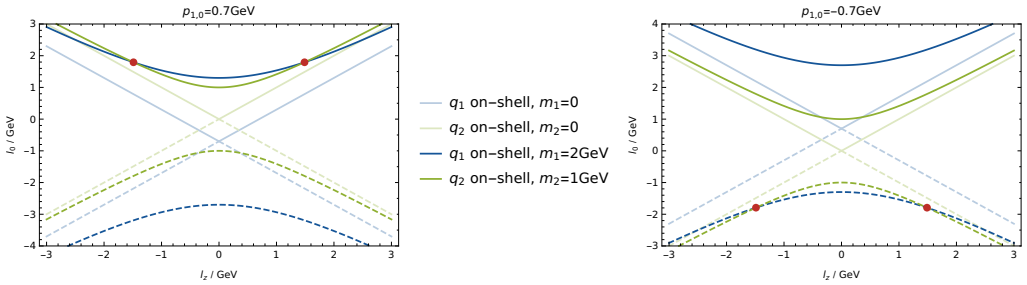

Figure 2.4: The on-shell hyperboloids for the scalar two-point function in Eq. (2.17) with $\boldsymbol{p} = 0$. The red dots show the position of the unphysical thresholds. On the left the kinematic configuration for a positive external energy can be seen, on the right the unphysical singularities are avoided with a negative external energy.

originally defining the amplitude and should generally be preferred since the integration goes along the forward hyperboloids and thus avoids the unphysical singularities.

Lastly, additional singularities appear when either only the internal or also the external particles are massless. Since the hyperboloids convert to light-cones for massless internal particles there is always an intersection at their origin, signaling a soft singularity. When on top of this two Feynman propagators are separated by a light-like distance $k_{ji,0}^2 = 0$, which in the case of the scalar two-point function can only be realized through a massless external particle, the forward light-cone of one propagator runs parallel to the backward light-cone of the other for a restricted range of the loop three-momentum, whenever $\boldsymbol{k}_{ji}$ is parallel or antiparallel to $\boldsymbol{\ell}$. This is referred to as a collinear singularity. Both types are shown in Fig. 2.5. While these singularities are not integrable, seeing as they are restricted to a compact region of the loop three-momentum their cancellation with the corresponding singularities appearing in real emission amplitudes can be performed locally.

The singular structure observed through the on-shell hyperboloids for the scalar two-point function can be easily extended to general one-loop amplitudes. Since the dual propagator $G_D(q_i; q_j)$ is $G_F(q_j)$ evaluated with $q_{i,0} = q_{i,0}^{(p,+)}$, and

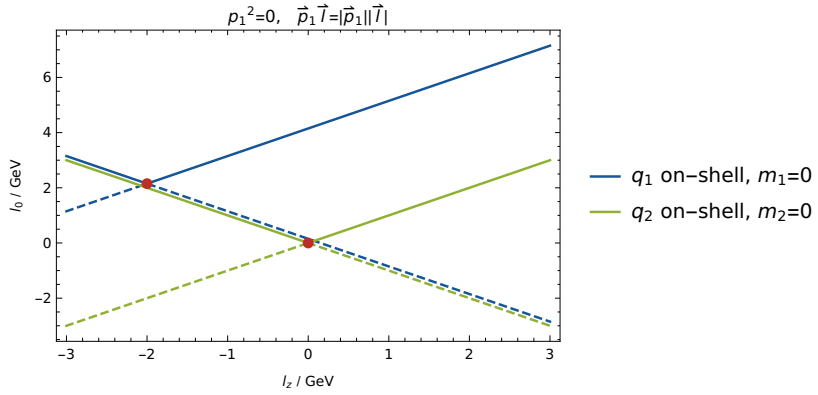

Figure 2.5: The on-shell light-cones for the scalar two-point function in Eq. (2.17). The red dots show the position of the soft singularities. Along the line between the dots is a collinear singularity.

vice versa, dual propagators always appear in pairs

$$\mathcal{A}_N^{(1)} = -\int_\ell \mathcal{N}\left(\ell, \{p_k\}_N\right) \left[\tilde{\delta}\left(q_i\right) G_D\left(q_i; q_j\right) \prod_{l\neq i,j} G_D\left(q_i; q_l\right) \right. \tag{2.24}$$
$$\left. + \tilde{\delta}\left(q_j\right) G_D\left(q_j; q_i\right) \prod_{l\neq j,i} G_D\left(q_j; q_l\right) + \sum_{k\neq i,j}^{N} \tilde{\delta}\left(q_k\right) \prod_{m\neq k} G_D\left(q_k; q_m\right) \right] .$$

A useful analysis to study the singularity structure of a dual amplitude is thus the generalization of the scalar two-point function

$$S_{ij}^{(1)} = (2\pi\imath)^{-1}\, \tilde{\delta}\left(q_i\right)\, G_D(q_i; q_j) + (i \leftrightarrow j) \tag{2.25}$$
$$= \frac{(2\pi\imath)^{-1}\, \tilde{\delta}\left(q_i\right)}{\lambda_{ij}^{++}\lambda_{ij}^{+-} - \imath 0 \eta\cdot k_{ji}} + \frac{(2\pi\imath)^{-1}\, \tilde{\delta}\left(q_j\right)}{\lambda_{ij}^{--}\lambda_{ij}^{+-} - \imath 0 \eta\cdot k_{ij}} ,$$

which diverges whenever either factor in the denominator vanishes. These are given by

$$\lambda_{ij}^{\pm\pm} = \pm q_{i,0}^{(+)} \pm q_{j,0}^{(+)} + k_{ji,0} \,. \tag{2.26}$$

Demanding that the limit $\lambda_{ij}^{++} \to 0$ be fulfilled leads to kinematic constraints. For a start it is obvious that with the on-shell energies by definition positive the term $k_{ji,0}$ must be negative. Further, one may use the definition of $\boldsymbol{k}_{ji} = \boldsymbol{q}_j - \boldsymbol{q}_i$,

the value of $k_{ji,0}$ in the limit above and the Cauchy–Schwarz inequality to see that

$$k_{ji}^2\Big|_{\lambda_{ij}^{++}=0} = \left(q_{i,0}^{(+)} + q_{j,0}^{(+)}\right)^2 - \left(\boldsymbol{q}_j - \boldsymbol{q}_i\right)^2 \geq (m_i + m_j)^2 \,, \tag{2.27}$$

showing that this limit in fact corresponds to the causal unitarity threshold. Further, a limiting requirement for the on-shell energies can be noted as well: λ_{ij}^{++} can only vanish when $q_{m,0}^{(+)} < -k_{ji,0}$, for $m \in \{i,j\}$, meaning that the acceptable on-shell energies are bounded. Assuming these kinematic conditions the limit of the sum of two single-cut dual contributions above may be taken by writing all denominators in terms of λ_{ij}^{++} leading to

$$\begin{aligned}\lim_{\lambda_{ij}^{++}\to 0} S_{ij}^{(1)} &= \Theta(-k_{ji,0})\Theta(k_{ji}^2 - (m_i+m_j)^2) \\ &\times \lim_{\lambda_{ij}^{++}\to 0} \frac{1}{\lambda_{ij}^{++} - 2q_{j,0}^{(+)}} \left[\frac{(2\pi\imath)^{-1}\,\tilde{\delta}\,(q_i)}{\lambda_{ij}^{++} - \imath 0 \frac{\eta\cdot k_{ji}}{-2q_{j,0}^{(+)}}} + \frac{(2\pi\imath)^{-1}\,\tilde{\delta}\,(q_j)}{\lambda_{ij}^{++} - 2q_{i,0}^{(+)} - 2q_{j,0}^{(+)} + \imath 0 \frac{\eta\cdot k_{ji}}{-2q_{j,0}^{(+)}}} \right],\end{aligned} \tag{2.28}$$

where λ_{ij}^{++} has been set to zero in the factor multiplying the infinitesimal imaginary part. The regulator may be dropped in the second term since it does not diverge in the considered scenario. Taking the limit thus gives

$$\begin{aligned}\lim_{\lambda_{ij}^{++}\to 0} S_{ij}^{(1)} &= \Theta(-k_{ji,0})\Theta(k_{ji}^2 - (m_i+m_j)^2) \\ &\times \lim_{\lambda_{ij}^{++}\to 0} \left[-\frac{1}{4q_{i,0}^{(+)} q_{j,0}^{(+)} (\lambda_{ij}^{++} + \imath 0 \eta\cdot k_{ji})} - \frac{1}{8q_{i,0}^{(+)} q_{j,0}^{(+)} (q_{i,0}^{(+)} + q_{j,0}^{(+)})} + \mathcal{O}\left(|\lambda_{ij}^{++}|\right) \right].\end{aligned} \tag{2.29}$$

Of course the result of the calculation is independent of the type of notation used and can thus also be performed with the imaginary prescription hidden in the definitions of $\lambda_{ij}^{\pm\pm}$ and the on-pole energies. In that case it is necessary to expand in $\mathrm{Re}(\lambda_{ij}^{++})$, ensuring that imaginary parts are considered correctly in every factor and only dropped when justified. The LTD representation with its explicit prescription for the imaginary part thus simplifies this type of calculations significantly.

The limit considered above, $\lambda_{ij}^{++} \to 0$, occurs when the forward on-shell hyperboloid of one propagator intersects with the backward on-shell hyperboloid of the complementary one (see Fig. 2.3). That is, when integrating the loop three-momentum along the positive energy mode of the first propagator, this integration

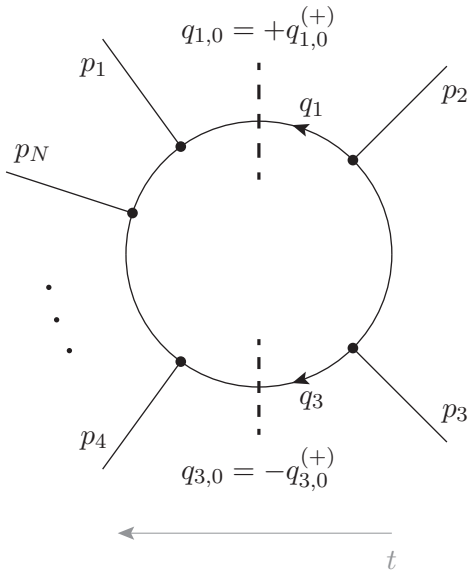

Figure 2.6: A general one-loop diagram with two propagators evaluated at their singularities, one on the positive energy mode, $q_{1,0} = +q_{1,0}^{(+)}$, and the other one on the negative energy mode, $q_{3,0} = -q_{3,0}^{(+)}$. This configuration is the causal threshold.

encounters a singular point when reaching the value for $\boldsymbol{\ell}$ that corresponds to the negative energy mode of the second propagator. Involving the combination of one backward and one forward on-shell hyperboloid, with the momentum defined continuously in the loop, the scenario described here corresponds to two physical particles propagating in the same direction in time as visualized in Fig. 2.6. For massless propagators, and light-like separation $k_{ji}^2 = 0$, the singular surface pinches to a collinear singularity along a finite segment. The complementary situation with the two singular propagators reversed is obtained in the limit $\lambda_{ij}^{--} \to 0$ where the condition on the external energy is $k_{ji,0} > 0$. Since the value of the external momenta is generally fixed, only one of these scenarios will be possible for any given process.

The only other possible singularity for $S_{ij}^{(1)}$ appears in the limit $\lambda_{ij}^{+-} \to 0$. For this limit to occur the external momenta are restricted by $k_{ji}^2 \leq (m_j - m_i)^2$. The effect of the dual prescription becomes apparent when the limit is taken

separately for the first of the two contributions

$$\begin{aligned}\lim_{\lambda_{ij}^{+-}\to 0} 2q_{j,0}^{(+)} G_D(q_i;q_j) &= \lim_{\lambda_{ij}^{+-}\to 0} \frac{2q_{j,0}^{(+)}}{\lambda_{ij}^{+-}(\lambda_{ij}^{+-}+2q_{j,0}^{(+)}) - \imath 0\eta\cdot k_{ji}} \\ &= \lim_{\lambda_{ij}^{+-}\to 0} \frac{1}{\lambda_{ij}^{+-} - \imath 0\eta\cdot k_{ji}} \left(1 - \frac{\lambda_{ij}^{+-}}{2q_{j,0}^{(+)}} + \frac{(\lambda_{ij}^{+-})^2}{(2q_{j,0}^{(+)})^2} + \mathcal{O}\left((\lambda_{ij}^{+-})^3\right)\right)\end{aligned} \tag{2.30}$$

and then for the other one, making sure to take into account the effect on the imaginary prescription caused by factoring out the singularity

$$\begin{aligned}\lim_{\lambda_{ij}^{+-}\to 0} 2q_{i,0}^{(+)} G_D(q_j;q_i) &= \lim_{\lambda_{ij}^{+-}\to 0} \frac{2q_{i,0}^{(+)}}{\lambda_{ij}^{+-}(\lambda_{ij}^{+-}-2q_{i,0}^{(+)}) + \imath 0\eta\cdot k_{ji}} \\ &= \lim_{\lambda_{ij}^{+-}\to 0} \frac{1}{\lambda_{ij}^{+-} - \imath 0\eta\cdot k_{ji}} \left(-1 - \frac{\lambda_{ij}^{+-}}{2q_{i,0}^{(+)}} - \frac{(\lambda_{ij}^{+-})^2}{(2q_{i,0}^{(+)})^2} + \mathcal{O}\left((\lambda_{ij}^{+-})^3\right)\right).\end{aligned} \tag{2.31}$$

Since the regulator of the singularity now has taken the same sign in both contributions they can be added up straightforwardly and demonstrate how their sum is in fact finite, giving

$$\begin{aligned}\lim_{\lambda_{ij}^{+-}\to 0} S_{ij}^{(1)} &= \frac{1}{4q_{i,0}^{(+)}q_{j,0}^{(+)}} \lim_{\lambda_{ij}^{+-}\to 0} 2q_{j,0}^{(+)} G_D(q_i;q_j) + (i\leftrightarrow j) \\ &= \frac{1}{4q_{i,0}^{(+)}q_{j,0}^{(+)}} \lim_{\lambda_{ij}^{+-}\to 0} \frac{1}{\lambda_{ij}^{+-} - \imath 0\eta\cdot k_{ji}} \left(-\lambda_{ij}^{+-}\frac{q_{i,0}^{(+)}+q_{j,0}^{(+)}}{2q_{i,0}^{(+)}q_{j,0}^{(+)}} + \mathcal{O}\left((\lambda_{ij}^{+-})^2\right)\right) \\ &= -\frac{q_{i,0}^{(+)}+q_{j,0}^{(+)}}{8(q_{i,0}^{(+)})^2(q_{j,0}^{(+)})^2}.\end{aligned} \tag{2.32}$$

This is unsurprising since the limit $\lambda_{ij}^{+-}\to 0$ does not correspond to a physical artifact and thus cannot have any noteworthy effect on the result. Its interpretation is the on-shell emission and on-shell reabsorption of one virtual particle. Limits of this type always appear entangled between two dual contributions as shown for the general one-loop amplitude in Eq. (2.24). The additional non-singular propagators do not affect the cancellation since

$$\lim_{\lambda_{ij}^{+-}\to 0} G_D(q_i;q_k) = G_D(q_j;q_k), \tag{2.33}$$

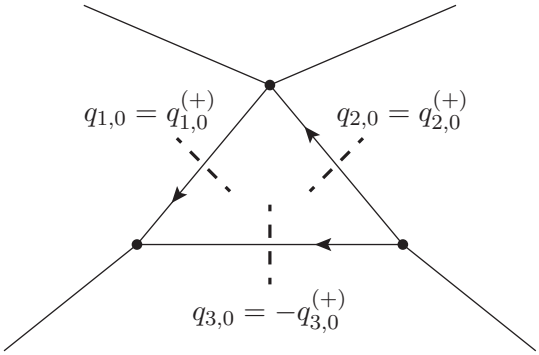

Figure 2.7: The leading singularity of the triangle graph is given by the anomalous threshold created when all three internal particles are on shell and travelling in a common direction in time. This is achieved when all three propagators are on shell simultaneously as shown here with two on the positive energy mode and one on the negative one.

based on the identity $q_{i,0}^{(+)} + k_{ki,0} = \lambda_{ij}^{+-} + q_{j,0}^{(+)} + k_{kj,0}$ relating the distinctive factors in their denominators.

At one-loop level there are other configurations with more than two internal particles on shell and moving in a common direction in time. These lead to physical singularities that are not covered by the description of the unitary threshold. Those type of singularities that do not correspond to inelastic thresholds are the anomalous thresholds, occurring for example in the leading singularity of the triangle graph where all three internal particles are on shell and moving forward (or backward) in time. A generalization of this scenario can be analyzed through the integrand function of three dual propagators

$$\mathcal{S}_{ijk}^{(1)} = (2\pi\imath)^{-1} G_D(q_i; q_k) G_D(q_i; q_j) \tilde{\delta}(q_i) + \text{perm.}\,. \tag{2.34}$$

The anomalous threshold arises in the intersection of two forward hyperboloids with one backward hyperboloid (or two backward hyperboloids with one forward hyperboloid). This describes the situation of all three particles travelling with positive on-shell energies in a common direction as shown in Fig. 2.7 and corresponds to the double limit $\{\lambda_{ij}^{++}, \lambda_{ik}^{++}\} \to 0$, achievable for kinematic conditions that give both $k_{ji,0}$ and $k_{ki,0}$ negative. The three-propagator integrand in this

limit is, similarly to the unitarity threshold above, given by

$$\lim_{\{\lambda_{ij}^{++},\lambda_{ik}^{++}\}\to 0} \mathcal{S}_{ijk}^{(1)} = \frac{1}{8q_{i,0}^{(+)}q_{j,0}^{(+)}q_{k,0}^{(+)}} \prod_{r=j,k} \theta(-k_{ri,0})\theta(k_{ri}^2-(m_i+m_r)^2) \tag{2.35}$$
$$\times \left(\frac{1}{-\lambda_{ir}^{++} - \imath 0 k_{ri,0}} - \frac{1}{2(q_{i,0}^{(+)}+q_{r,0}^{(+)})} + \mathcal{O}\left(|\lambda_{ir}^{++}|\right) \right).$$

Note that even though $\lambda_{jk}^{-+} = \lambda_{ik}^{++} - \lambda_{ij}^{++}$ vanishes in this limit, the expression is free of singularities in λ_{jk}^{-+}. This is to be expected due to the cancellations seen in the previous discussion on unphysical singularities. These were unaffected by the presence of additional propagators and are thus completely valid for this case as well.

2.4 Multiloop topologies and the causal representation

A general L-loop scattering amplitude with N external legs can be classified in terms of separate sets of internal momenta summarized as loop lines. These sets contain all internal momenta that share a common linear combination of the loop integration momenta ℓ_i with $i \in \{1,\dots,L\}$. Each set is identified by the index of the loop integration momentum, or linear combination thereof, defining it. To simplify the notation the letter ℓ will be used both to refer to the L integration momenta and to the remaining set-defining linear combinations as

$$\ell_i = \begin{cases} \text{loop integration momentum} & \text{for } i \leq L \\ \sum_{j=1}^{L} a_j \ell_j + p_i & \text{for } i > L \end{cases}. \tag{2.36}$$

Here p_i is a linear combination of external momenta attached to the amplitude through indices that join loop lines. While it is certainly possible to define an amplitude in such a way that the common momentum within a set is $\ell_i + p_i$ even for $i \leq L$, this would complicate the notation unnecessarily and it will be assumed that this choice is avoided.

The N_s+1 internal momenta within a given set s can then be written as $q_{s,i} = \ell_s + k_{s,i}$ with $k_{s,i} = \sum_{j=1}^{i} p_{s,j}$ in terms of the N_s external momenta exclusively attached to this loop line $\{p_{s,i}\}_{N_s}$ and with $k_{s,0} = 0$. The Feynman propagators of all internal lines within one set can then be summarized as

$$G_F(s) = \prod_{i=0}^{N_s} \left(G_F(q_{s,i})\right)^{a_{s,i}}, \tag{2.37}$$

where the exponent a_i is necessary to include more than one power of the same propagator which can occur naturally starting at two loops.

A generic L loop scattering amplitude may then be written as

$$\mathcal{A}_N^{(L)}(1,\ldots,n) = \int_{\ell_1,\ldots,\ell_L} \mathcal{N}\left(\{\ell_i\}_L, \{p_j\}_N\right) G_F(1,\ldots,n)\,, \tag{2.38}$$

where the argument of the amplitude $(1,\ldots,n)$ refers to the n sets of internal momenta and

$$G_F(1,\ldots,n) = \prod_{s=1}^{n} G_F(s)\,. \tag{2.39}$$

Using this definition to collect all the Feynman propagators of a set allows to simplify the arguments in many of the multiloop derivations and formulas. In practice, reversing to the full notation for including external particles does not impact the majority of the results.

The direct generalization of the LTD theorem to the multiloop case comes from iteratively applying the residue theorem to solve the integral over the energy component of each loop momentum. In the following this will be shown in detail for the two-loop sunrise scalar integral and generalized thereafter.

The generalized sunrise diagram in Fig. 2.8 is given by the amplitude

$$\mathcal{A}_{\ominus,N}^{(2)}(p) = \int_{1,2} G_F(1,2,12)\ , \tag{2.40}$$

with the third set defined through the linear combination $\ell_{12} = -\ell_1 - \ell_2 + p$. Considering the special case where the only external legs are the ones attached to the common vertices of the loop lines the three loop sets are reduced to only their defining loop momenta and the integral is explicitly written as

$$\mathcal{A}_{\ominus}^{(2)}(p) = \int_{1,2} G_F(\ell_1) G_F(\ell_2) G_F(\ell_{12})\ . \tag{2.41}$$

The short-hand notation $\ell_i \to i$ and $G_F(\ell_i) \to G_F(i)$ will be used hereafter. This integrand has singularities whose location depends on both loop momenta. When choosing to evaluate first the integral over ℓ_1, the propagator $G_F(\ell_2)$ is constant and the momentum ℓ_2 in the mixed propagator is to be regarded as fixed, though unspecified, and real. The location of singularities in the lower half of the complex plane of the integration variable $\ell_{1,0}$ is then given by

$$S_1 = \left\{ q_{1,0}^{(p,+)}, q_{12,0}^{(p,+)} - \ell_{2,0} + p_0 \right\}\ , \tag{2.42}$$

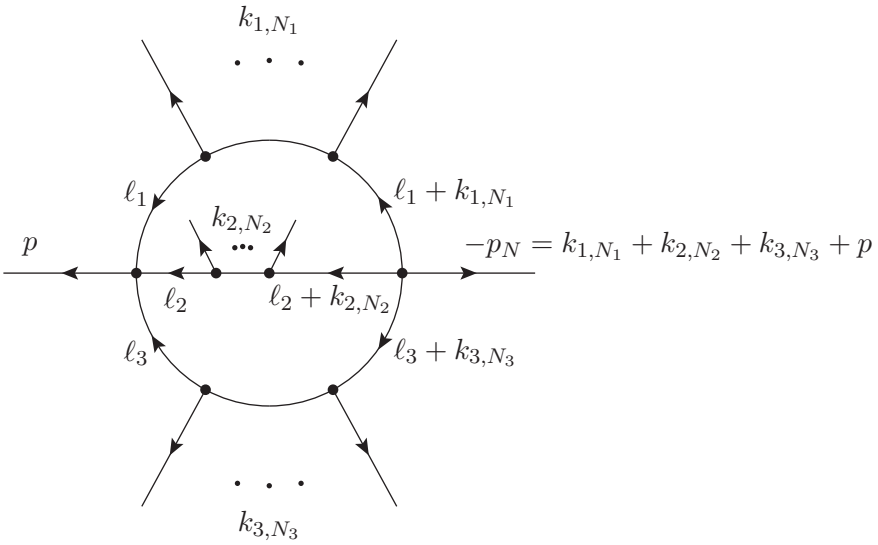

Figure 2.8: The two-loop sunrise diagram with external legs and the assigned loop momenta. The momenta of the external legs connected to the set defined through ℓ_i sum up to k_{i,N_i}. Arrows denote the direction in which the momenta are defined.

where $\ell_{2,0}$ is real[1]. Using the residue theorem to solve the integral over $\ell_{1,0}$ thus gives

$$\mathcal{A}^{(2)}_{\ominus}(p) = \int_{\vec{1},2} \sum_{\ell^{(p,+)}_{1,0} \in S_1} \text{Res}\left(G_F(1,2,12), \left\{\ell_{1,0} \to \ell^{(p,+)}_{1,0}\right\}\right) , \tag{2.43}$$

where the factor of $-2\pi\imath$ has been absorbed in the definition of the reduced-dimensional integration measure (see Eq. (A.14)). After evaluating this expression two propagators remain in each residue

$$\mathcal{A}^{(2)}_{\ominus}(p) = \int_{\vec{1},2} \left[\frac{1}{2q^{(+)}_{1,0}} \, G_F(2,12)\Big|_{\ell_{1,0}=q^{(p,+)}_{1,0}} + \frac{1}{2q^{(+)}_{12,0}} \, G_F(1,2)\Big|_{\ell_{1,0}=q^{(p,+)}_{12,0}-\ell_{2,0}+p_0} \right] . \tag{2.44}$$

[1]The LTD representation is obtained by solving the two integrals over the loop energies. These energies are, in principle, real and are only extended into the complex plain as a tool for solving the integral. It is therefore well justified to treat all loop energies as real, except the one that is currently being evaluated in terms of complex analysis.

Consecutively, the integral over the second loop energy may be evaluated, now extending also the energy component of the second loop momentum into the complex plane. The expression above still displays singularities for $\ell_{2,0}$ at the values

$$S_2 = \left\{ \pm q_{2,0}^{(p,+)}, \pm q_{12,0}^{(p,+)} - q_{1,0}^{(p,+)} + p_0, \mp q_{1,0}^{(p,+)} + q_{12,0}^{(p,+)} + p_0 \right\} , \tag{2.45}$$

where the first set of singularities appears in both residues caused by $G_F(2)$, the second set is caused by $G_F(12)$ and the third set is caused by $G_F(1)$ with $\ell_{1,0}$ set to $q_{12,0}^{(+)} - \ell_{2,0} + p_0$. For those singularity positions that involve the difference between two on-pole energies the sign of the imaginary part is unknown. A direct separation into those poles that appear in the upper or lower half of the complex plane is thus not possible. Nonetheless, the second energy integral may be calculated using the residue theorem, ensuring that only the poles in the lower half plane are counted through the inclusion of a Heavyside function as

$$\mathcal{A}_{\ominus}^{(2)}(p) = \int_{\vec{1},\vec{2}} \sum_{\ell_{2,0}^{(p,+)} \in S_2,\ \ell_{1,0}^{(p,+)} \in S_1} \Theta\left(-\mathrm{Im}(\ell_{2,0})\right) \times \tag{2.46}$$
$$\mathrm{Res}\left(\mathrm{Res}\left(G_F(1,2,12), \left\{\ell_{1,0} \to \ell_{1,0}^{(p,+)}\right\}\right), \left\{\ell_{2,0} \to \ell_{2,0}^{(p,+)}\right\}\right) .$$

We refer to this type of expression as a sum of *nested residues*.

Among the terms appearing in Eq. (2.46) there are those that upon evaluating the residue in $\ell_{1,0}$ do not diverge for $\ell_{2,0} \to \ell_{2,0}^{(p,+)}$ and thus evaluate to zero when calculating the outer residue. This is the case for terms like

$$\begin{aligned} &\mathrm{Res}\left(\mathrm{Res}\left(G_F(1,2,12), \left\{\ell_{1,0} \to q_{1,0}^{(p,+)}\right\}\right), \left\{\ell_{2,0} \to \mp q_{1,0}^{(p,+)} + q_{12,0}^{(p,+)} + p_0\right\}\right) \\ &\quad = \mathrm{Res}\left(\frac{1}{2q_{1,0}^{(+)}} G_F(2,12)\Big|_{\ell_{1,0}=q_{1,0}^{(p,+)}}, \left\{\ell_{2,0} \to \mp q_{1,0}^{(p,+)} + q_{12,0}^{(p,+)} + p_0\right\}\right) \\ &\quad = 0 \end{aligned} \tag{2.47}$$

which vanishes because the singularity in $\ell_{2,0}$ considered here originates in $G_F(1)$ which is already fixed.

The remaining nested residues involve setting two different internal lines on shell, although the momentum flow may be contrary to the original (and arbitrary) definition in the diagram. Anticipating the result diagrammatically in Fig. 2.9 we see that two further contributions cancel, leaving just three nested residues to be calculated. For a more intuitive and diagrammatic discussion it is

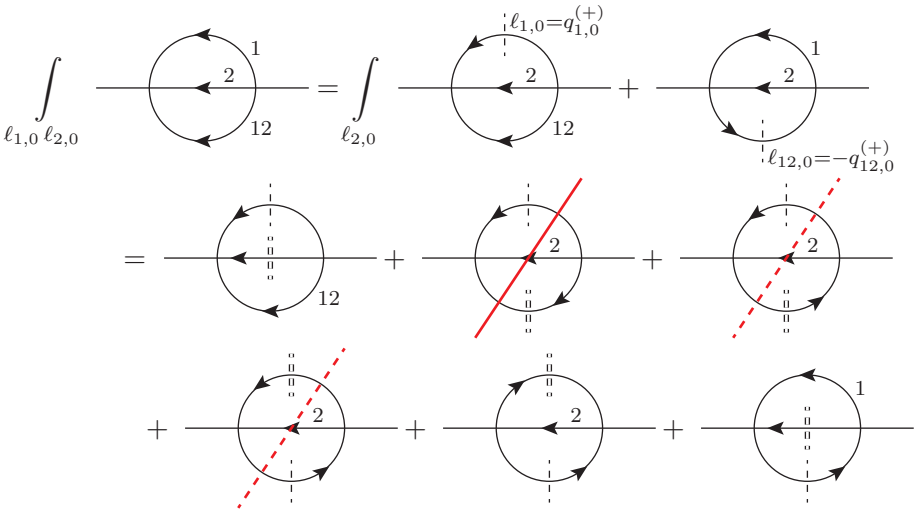

Figure 2.9: The various contributions to the sunrise diagram when solving the energy part of the loop integrals through the residue theorem, first in $\ell_{1,0}$, marked by a single dashed line, and then in $\ell_{2,0}$, marked by a double dashed line. The vanishing contribution of $\ell_{2,0} \to -q_{2,0}^{(p,+)}$ has been omitted. Similarly, the contribution representing the residue for $\ell_{2,0} \to -q_{12,0}^{(p,+)} - q_{1,0}^{(p,+)} + p_0$ vanishes due to the negative imaginary part of the pole and is therefore crossed out. Two further contributions that appear with ambigous imaginary part cancel each other and are thus crossed out with a dashed line. Three nested residues contribute thus to the result.

thus convenient to rewrite the residues in terms of the internal momenta corresponding to the cut internal lines instead of the poles appearing in the integration momenta. For this purpose it is convenient to point out two properties of residues. For a function f that is meromorphic on the complex plane with a simple pole at $x = x_0$ the residue can be rewritten as

$$\begin{aligned} \mathrm{Res}\left(f(x), \{x + a \to x_0 + a\}\right) &= \frac{1}{a}\mathrm{Res}\left(f(x), \{a \cdot x \to a \cdot x_0\}\right) \\ &= \mathrm{Res}\left(f(x), \{x \to x_0\}\right) . \end{aligned} \tag{2.48}$$

Applied to the residues appearing in the calculation of the sunrise diagram this property can be used to rewrite the residues in terms of the momentum that is

set on shell. With $\ell_{1,0} + \ell_{2,0} - p_0 = -\ell_{12,0}$ we thus have

$$\begin{aligned} \mathrm{Res}\left(G_F(1,2,12), \ell_{1,0} \to q_{12,0}^{(p,+)} - \ell_{2,0} + p_0\right) \\ = \mathrm{Res}\left(G_F(1,2,12), -\ell_{12,0} \to q_{12,0}^{(p,+)}\right) , \end{aligned} \tag{2.49}$$

motivating the introduction of a new notation for the dual propagator given by

$$G_D(i;j) = \mathrm{Res}\left(G_F(i,j), \left\{\ell_{i,0} \to q_{i,0}^{(p,+)}\right\}\right) . \tag{2.50}$$

The reversed momentum flow is indicated by $\bar{i}$ referring to $-\ell_i$. Here and in the following this new definition based on calculating the residue is distinguished from the previous definition in Eq. (2.14), employed primarily in one-loop calculations, through the use of arguments i, j instead of q_i, q_j. Both definitions are related through

$$G_D(i;j) = G_D(q_i;q_j)\Big|_{q_{i,0}=q_{i,0}^{(p,+)}} . \tag{2.51}$$

This definition can be straightforwardly extended to the nested residues by first including additional unrestrained propagators into the simple residue as

$$G_D(i;j,\ldots,n) = \mathrm{Res}\left(G_F(i,j,\ldots,n), \left\{\ell_{i,0} \to q_{i,0}^{(p,+)}\right\}\right) , \tag{2.52}$$

and setting further internal lines on shell by calculating the subsequent residues through

$$G_D(i,j;k,\ldots,n) = \mathrm{Res}\left(G_D(i;j,k,\ldots,n), \left\{\ell_{j,0} \to q_{j,0}^{(p,+)}\right\}\right) . \tag{2.53}$$

For the case of the sunrise amplitude all expressions are derived from a product of three Feynman propagators. These evaluate to

$$G_D(i,j;k) = \frac{1}{4q_{i,0}^{(+)}q_{j,0}^{(+)}} G_F(k)\Big|_{\ell_{i,0}=q_{i,0}^{(p,+)},\ell_{j,0}=q_{j,0}^{(p,+)}} , \tag{2.54}$$

where $\ell_{k,0}$ must be expressed through the internal momenta set on shell. Note that $G_D(i,j;k) = G_D(j,i;k)$ and the sign of this result is not influenced by considering expressions with reversed momentum flow since those give rise to two

minus signs during the calculation of the residue, leading to an overall positive result:

$$G_D(\bar{i};j) = \lim_{-\ell_{i,0}\to q_{i,0}^{(p,+)}} \frac{-\ell_{i,0} - q_{i,0}^{(p,+)}}{(\ell_{i,0} - q_{i,0}^{(p,+)})(\ell_{i,0} + q_{i,0}^{(p,+)})} G_F(j) \qquad (2.55)$$
$$= \frac{-1}{-2q_{i,0}^{(p,+)}} G_F(j)\Big|_{\ell_{i,0}=-q_{i,0}^{(p,+)}} .$$

Having introduced this notation it may be applied to simplify the contributions to the sunrise diagram in Eq. (2.46). The calculation of those terms where the on-shell momentum corresponds to an integration momentum is straightforward: the location of the singularity $\ell_{2,0}^{(p,+)}$ is inequivocally in either the lower or upper half plane and thus there is no doubt whether the residue contributes to the dual amplitude. As an example one may consider the contribution

$$\begin{aligned} &\mathrm{Res}\left(\mathrm{Res}\left(G_F(1,2,12),\left\{\ell_{1,0}\to q_{1,0}^{(p,+)}\right\}\right),\left\{\ell_{2,0}\to \pm q_{2,0}^{(p,+)}\right\}\right) \\ &\quad = \pm\mathrm{Res}\left(\mathrm{Res}\left(G_F(1,2,12),\left\{\ell_{1,0}\to q_{1,0}^{(p,+)}\right\}\right),\left\{\pm\ell_{2,0}\to q_{2,0}^{(p,+)}\right\}\right) \qquad (2.56) \\ &\quad = \begin{cases} G_D(1,2;12) \\ -G_D(1,\overline{2};12) \end{cases} , \end{aligned}$$

where the multiplication identity of the residue was used. Of course the contribution of $G_D(1,\overline{2};12)$ corresponding to $\ell_{2,0} = -q_{2,0}^{(p,+)}$ vanishes due to the presence of the Heavyside function.

There are certain terms where the imaginary part of the singularity position in the outer residue is unclear since it involves the difference between two on-pole masses. For the sunrise diagram two such contributions appear. The first one involves setting on shell first ℓ_1 and subsequently $-\ell_{12}$. Since $-\ell_{12,0}\big|_{\ell_{1,0}=q_{1,0}^{(p,+)}} = \ell_{2,0} + q_{1,0}^{(p,+)} - p_0$ the identification of the outer residue gives

$$\begin{aligned} &\mathrm{Res}\left(\mathrm{Res}\left(G_F(1,2,12),\left\{\ell_{1,0}\to q_{1,0}^{(p,+)}\right\}\right),\left\{\ell_{2,0}\to q_{12,0}^{(p,+)} - q_{1,0}^{(p,+)} + p_0\right\}\right) \\ &\quad = \mathrm{Res}\left(\mathrm{Res}\left(G_F(1,2,12),\left\{\ell_{1,0}\to q_{1,0}^{(p,+)}\right\}\right),\left\{-\ell_{12,0}\to q_{12,0}^{(p,+)}\right\}\right) \qquad (2.57) \end{aligned}$$

$=$ 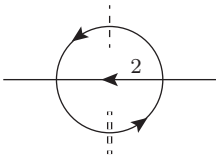

$= G_D(1,\overline{12};2)\,.$

The second contribution originates in setting on shell first $-\ell_{12}$ and then ℓ_1, noting that $-\ell_{1,0} = \ell_{12,0} + \ell_{2,0} - p_0$ and $\ell_{12,0} = -q_{12,0}^{(p,+)}$ due to the previous residue. The contribution is then given by

$$\begin{aligned}
&\mathrm{Res}\left(\mathrm{Res}\left(G_F(1,2,12),\left\{\ell_{1,0}\to q_{12,0}^{(p,+)}-\ell_{2,0}+p_0\right\}\right),\left\{\ell_{2,0}\to -q_{1,0}^{(p,+)}+q_{12,0}^{(p,+)}+p_0\right\}\right)\\
&\quad=\mathrm{Res}\left(\mathrm{Res}\left(G_F(1,2,12),\left\{-\ell_{12,0}\to q_{12,0}^{(p,+)}\right\}\right),\left\{-\ell_{1,0}\to -q_{1,0}^{(p,+)}\right\}\right) \qquad (2.58)\\
&\quad= \quad = -G_D(\overline{12},1;2)\,,
\end{aligned}$$

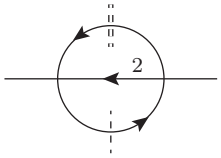

where the minus sign stems from rewriting the outer residue in terms of $\ell_{1,0}$. The cancellation between these two nested residues is guaranteed since both contributions are multiplied only by the same ambiguous Heavyside function $\Theta(-\mathrm{Im}(q_{12,0}^{(p,+)} - q_{1,0}^{(p,+)}))$.

Following the same procedure in evaluating all of the nested residues the sunrise diagram is thus given by the sum of only three contributions:

$$\begin{aligned}
\mathcal{A}_{\ominus}^{(2)}(p) = \int_{\vec{1},\vec{2}} \Bigg[&\mathrm{Res}\left(\mathrm{Res}\left(G_F(1,2,12),\left\{\ell_{1,0}\to q_{1,0}^{(p,+)}\right\}\right),\left\{\ell_{2,0}\to q_{2,0}^{(p,+)}\right\}\right)\\
&+\mathrm{Res}\left(\mathrm{Res}\left(G_F(1,2,12),\left\{\ell_{1,0}\to q_{12,0}^{(p,+)}-\ell_{2,0}+p_0\right\}\right),\left\{\ell_{2,0}\to q_{2,0}^{(p,+)}\right\}\right)\\
&+\mathrm{Res}\left(\mathrm{Res}\left(G_F(1,2,12),\left\{\ell_{1,0}\to q_{12,0}^{(p,+)}-\ell_{2,0}+p_0\right\}\right),\left\{\ell_{2,0}\to q_{1,0}^{(p,+)}+q_{12,0}^{(p,+)}+p_0\right\}\right)\Bigg]\\
=\int_{\vec{1},\vec{2}} &\left[G_D(1,2;12)+G_D(\overline{12},2;1)+G_D(\overline{12},\overline{1};2)\right]\,. \qquad (2.59)
\end{aligned}$$

This intermediate integrand-level expression is not unique, most notably it depends on which energy integral was solved first. The corresponding expression for starting with the integration in $\ell_{2,0}$ is obtained from Eq. (2.59) through the exchange $1 \leftrightarrow 2$. Taking advantage of the symmetry under the exchange of the on-shell indices one may then write the result in a compact form as

$$\mathcal{A}_{\ominus}^{(2)}(p) = \int_{\vec{1},\vec{2}} \sum_{i\in\{1,2,12\}} G_D(1,\ldots,i-1,\overline{i+1},\ldots,\overline{12};i)\,. \qquad (2.60)$$

Further simplifications of the sunrise amplitude prove useful. As a first step one may notice that the denominators of the three contributions are made up of only three factors which can all be written in the style of Eq. (2.26) as

$$\lambda^{\pm\pm\pm} = \pm q_{1,0}^{(p,+)} \pm q_{2,0}^{(p,+)} \pm q_{12,0}^{(p,+)} + p_0 \,. \tag{2.61}$$

Abbreviating the factors responsible for causal singularities as $\lambda^{+++} = \lambda^+$ and $\lambda^{---} = -\lambda^-$ the amplitude can then be expressed as

$$\begin{aligned} &\mathcal{A}_{\ominus}^{(2)}(p) \\ &\quad = \int_{\vec{1},\vec{2}} \left[\frac{1}{4q_{1,0}^{(+)} q_{2,0}^{(+)}} \frac{1}{-\lambda^- \lambda^{--+}} + \frac{1}{4q_{2,0}^{(+)} q_{12,0}^{(+)}} \frac{1}{\lambda^{--+} \lambda^{+-+}} + \frac{1}{4q_{1,0}^{(+)} q_{12,0}^{(+)}} \frac{1}{\lambda^{+-+} \lambda^{+}} \right] . \end{aligned} \tag{2.62}$$

Adding up both terms that contain either λ^{--+} or λ^{+-+} shows that this factor indeed appears in the added numerator and can thus be canceled. For the first two terms this gives

$$\begin{aligned} &\frac{q_{12,0}^{(+)}}{-\lambda^- \lambda^{--+}} + \frac{q_{1,0}^{(+)}}{\lambda^{--+} \lambda^{+-+}} \\ &\qquad = \frac{q_{12,0}^{(+)} (q_{1,0}^{(+)} - q_{2,0}^{(+)} + q_{12,0}^{(+)} + p_0) - q_{1,0}^{(+)} (q_{1,0}^{(+)} + q_{2,0}^{(+)} + q_{12,0}^{(+)} - p_0)}{-\lambda^- \lambda^{--+} \lambda^{+-+}} \\ &\qquad = -\frac{q_{1,0}^{(+)} + q_{12,0}^{(+)}}{\lambda^- \lambda^{+-+}} \,. \end{aligned} \tag{2.63}$$

In the same fashion the third term can be added on to give an expression that only depends on those denominators that lead to causal thresholds and gives the very compact expression

$$\mathcal{A}_{\ominus}^{(2)}(p) = -\int_{\vec{1},\vec{2}} \frac{1}{2q_{1,0}^{(+)}\, 2q_{2,0}^{(+)}\, 2q_{12,0}^{(+)}} \left(\frac{1}{\lambda^-} + \frac{1}{\lambda^+} \right) \,. \tag{2.64}$$

This form is now also locally symmetric under the exchange of $1 \leftrightarrow 2$. As shown in previous sections, the appearance of unphysical singularities, corresponding to the limits $\lambda^{\pm-+} \to 0$, does not pose a fundamental problem since these terms always cancel between the dual contributions. Nonetheless, the ability to write a loop amplitude in a form explicitly free of unphysical singularities represents a milestone, especially for numerical applications where the cancellation potentially requires high numerical precision and correspondingly large computation power.

Indeed, the cancellations leading to this so-called *causal representation* can be reached already before performing the second iteration of the residue theorem. After evaluating the integral in $\ell_{1,0}$ one has, with a computation analogous to the one above,

$$\begin{aligned}
&\mathcal{A}^{(2)}(p) \qquad (2.65)\\
&= \int_{\vec{1},2} G_F(2) \left[\frac{1}{2q_{1,0}^{(+)}} \frac{1}{(-q_{1,0}^{(p,+)} - \ell_{2,0} - q_{12,0}^{(p,+)} + p_0)(-q_{1,0}^{(p,+)} - \ell_{2,0} + q_{12,0}^{(p,+)} + p_0)} \right.\\
&\qquad \left. + \frac{1}{2q_{12,0}^{(+)}} \frac{1}{(-q_{1,0}^{(p,+)} - \ell_{2,0} + q_{12,0}^{(p,+)} + p_0)(q_{1,0}^{(p,+)} - \ell_{2,0} + q_{12,0}^{(p,+)} + p_0)} \right]\\
&= \int_{\vec{1},2} \frac{1}{2q_{1,0}^{(+)} q_{12,0}^{(+)}} \frac{G_F(2)}{\left(\ell_{2,0} - (-q_{1,0}^{(p,+)} - q_{12,0}^{(p,+)} + p_0)\right)\left(\ell_{2,0} - (q_{1,0}^{(p,+)} + q_{12,0}^{(p,+)} + p_0)\right)} .
\end{aligned}$$

This alternative integrand has only two singularities in the negative half-plane of $\ell_{2,0}$ at

$$\left\{ q_{2,0}^{(p,+)}, q_{1,0}^{(p,+)} + q_{12,0}^{(p,+)} + p_0 \right\} \subset S_2 \,. \qquad (2.66)$$

Not only is the amount of residues to be considered reduced but the superficially problematic terms with unclear imaginary part do not appear in this integrand. Thus the cancellation shown in Eq. (2.58) depending on the explicit usage of the Heavyside function is redundant. The reduction in the amount of contributions is relatively small for the sunrise diagram but can be considerable in more involved amplitudes. Even for the analytic calculation of the residues in order to obtain the dual amplitude it may be reasonable to simplify the integrand after each application of the residue theorem.

The results obtained for the sunrise diagram, while important in and of itself, can be extended to much more general diagrams. For this purpose we defined several classes of multiloop topologies and derived their LTD representations in Ref. [3].

To start with, there is the extension of the general sunrise diagram to the multiloop case shown in Fig. 2.10, which we named *maximal loop topology* (MLT). This type of L-loop diagram consists of $L+1$ sets of internal momenta, defined through the integration momenta $\{\ell_1, \ldots, \ell_L\}$ and the linear combination $\ell_{L+1} = -\sum_{i=1}^{L} \ell_i + p$, with p being a sum of external momenta. Each set may consist of more than one internal momentum depending on the configuration of external

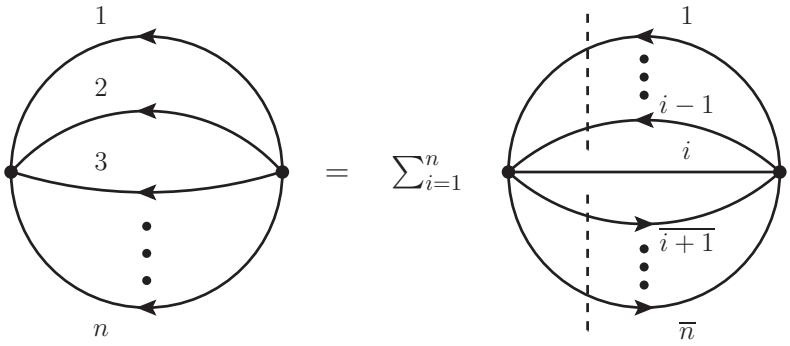

Figure 2.10: The maximal loop topology in the Feynman representation on the left and after solving the energy component of the loop integrals through the application of the residue theorem on the right. Dashed lines indicate internal propagators that have been set on shell and bars indicate that the momentum flow has been reversed. Figure taken from Ref. [3].

momenta connected to the amplitude. Its Feynman representation is given by

$$\mathcal{A}^{(L)}_{\rm MLT} = \int_{1,\dots,L} G_F(1,\dots,L+1)\,, \tag{2.67}$$

which for $L = 2$ amounts to the general two-loop sunrise diagram of Eq. (2.40). In the two-loop case the MLT is the only possible topology and is thus sufficient for the description of any scattering amplitude at the two-loop level. Starting from the evaluation of the nested residues for several representative multiloop integrals we have derived through induction that

$$\mathcal{A}^{(L)}_{\rm MLT} = \int_{\vec{1},\dots,\vec{L}} \sum_{i=1}^{n} G_D^{(L)}(1,\dots,i-1,\overline{i+1},\dots,\overline{n};i)\,, \tag{2.68}$$

giving thus a compact LTD representation for any diagram classified through the MLT topology. Non-trivial numerators can be added straight-forwardly through the replacement $G_D \to \mathcal{A}_D$ and including the numerator in the calculation of the nested residues. The singular structure of the MLT topology can be described in terms of two categories. On the one hand more than one propagator of a given set of internal momenta can go on shell at the same time. In this case the discussion reduces to the analysis of a one-loop diagram, essentially considering the

remaining loop momenta to be constant. On the other hand the occurrence of on-shell propagators in different sets leads to singularities specific to the multiloop case. While some of these singularities are of a physical nature others are of unphysical origin and cancel between paired dual contributions as shown previously in Eq. (2.58) for the sunrise diagram. Notably, the causal representation of the sunrise amplitude in Eq. (2.64) can be achieved for any scalar MLT amplitude with only one internal propagator per set, giving thus

$$\mathcal{A}^{(L)}_{\rm MLT} = -\int_{\vec{1},\ldots,\vec{L}} \frac{1}{x_{1,L}} \left(\frac{1}{\lambda^{-}_{1,L}} + \frac{1}{\lambda^{+}_{1,L}} \right) \tag{2.69}$$

with $x_{1,L} = \prod_{i=1}^{L+1} 2q^{(+)}_{i,0}$. The causal singularities are encoded in

$$\lambda^{\pm}_{1,L} = \sum_{i=1}^{L} q^{(p,+)}_{i,0} \pm p\,. \tag{2.70}$$

A comparable expression that is explicitly free of unphysical singularities can also be found for amplitudes with multiple powers of propagators, non-scalar integrals or more than one propagator per set.

The next type of structure, that first appears in three-loop amplitudes, contains one additional set of momenta classified through the sum of two integration momenta which may be chosen to be ℓ_1 and ℓ_2. The additional set is thus identified through $\ell_{12} = -\ell_1 - \ell_2 + p_{12}$, where p_{12} is the external momentum coupled to the vertex connecting the internal lines 1, 2 and 12. This topology, which we call *next-to-maximal loop topology* (NMLT), can be written in terms of convolutions of MLT and tree-level amplitudes through the compact expression

$$\begin{aligned}\mathcal{A}^{(L)}_{\rm NMLT}(1,\ldots,L+1,12) = {} & \mathcal{A}^{(2)}_{\rm MLT}(1,2,12) \otimes \mathcal{A}^{(L-2)}_{\rm MLT}(3,\ldots,L+1) \\ & + \mathcal{A}^{(1)}_{\rm MLT}(1,2) \otimes \mathcal{A}^{(0)}(12) \otimes \mathcal{A}^{(L-1)}_{\rm MLT}(\overline{3},\ldots,\overline{L+1})\,.\end{aligned} \tag{2.71}$$

The decomposition into the different contributing subtopologies shown here and graphically represented in Fig. 2.11 results in the sum of two contributions. The first term is the convolution of the generalized sunrise amplitude, involving the sets $1,2$ and 12, with the MLT amplitude of the remaining sets. In the second term the set 12 remains off shell, while the MLT amplitudes therein have to be interpreted heuristically, with either 1 or $\overline{2}$ and all of the inverted sets containing on-shell propagators. The interpretation of its lowest order appearance at three

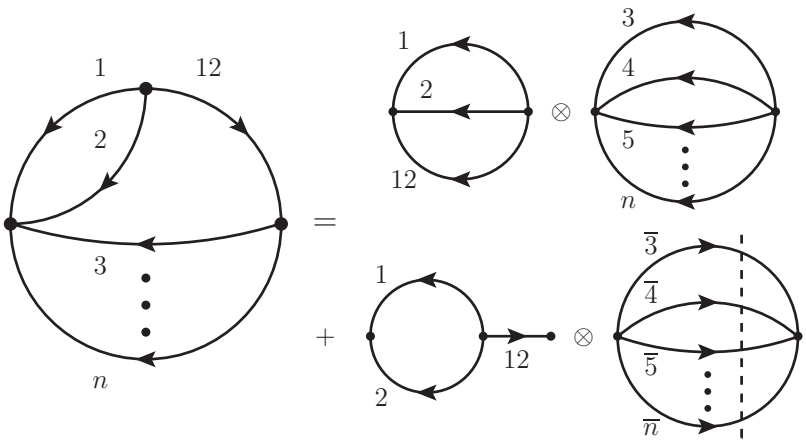

Figure 2.11: The next-to-maximal loop topology in the Feynman representation on the left and in the LTD representation on the right. Dashed lines indicate that an internal propagator within the corresponding set is on shell and bars that the momentum flow has been reversed. Where not already indicated differently the MLT subtopologies are treated according to Eq. (2.68). Figure taken from [3].

loops gives the dual expressions

$$\mathcal{A}^{(2)}_{\text{MLT}}(1,2,12)\otimes\mathcal{A}^{(1)}_{\text{MLT}}(3,4) \tag{2.72}$$
$$=\int_{1,2,3}\left(\mathcal{A}^{(3)}_D(\overline{2},\overline{12},\overline{4};1,3)+\mathcal{A}^{(3)}_D(1,\overline{12},\overline{4};2,3)\ +\mathcal{A}^{(3)}_D(1,2,\overline{4};12,3)+(\overline{4}\leftrightarrow 3)\right)$$

and for the second term

$$\mathcal{A}^{(1)}_{\text{MLT}}(1,2)\otimes\mathcal{A}^{(0)}(12)\otimes\mathcal{A}^{(2)}_{\text{MLT}}(\overline{3},\overline{4}) \tag{2.73}$$
$$=\int_{1,2,3}\left(\mathcal{A}^{(3)}_D(\overline{2},\overline{3},\overline{4};1,12)+\mathcal{A}^{(3)}_D(1,\overline{3},\overline{4};2,12)\right)\ .$$

The singular structure of the NMLT amplitudes is thus entirely determined by the previously considered MLT topology. This is particularly interesting considering the causal representation found for the MLT amplitudes, which thus may be extended to the study of the NMLT case.

With a generalization of the Mercedes-Benz topology, which we called *next-to-next-to-maximal loop topology*, we have studied another similar decomposition in Ref. [3] and more recently general results for up to four loops have been presented in Ref. [82].

2.5 Regularization of singularities

Having obtained the dual representation of a given amplitude some additional steps are necessary to allow its application in the context of a physical observable.

2.5.1 Local renormalization of UV singularities

The issue caused by singularities related to the high-energy regime of the loop integration is treated on the level of the whole theory through the process of renormalization. As mentioned in Chapter 1, this involves redefining the parameters appearing in the theory to absorb the UV divergences. It leaves the theory itself finite and results in all loop amplitudes well-behaved in the UV. In order to redefine the parameters in the appropriate manner the singularities must first be parametrized through DREG and the renormalized parameters themselves depend on the space-time dimension d. In the context of LTD the goal is to perform calculations in the physical four spacetime dimensions without resorting to DREG during the major part of the calculations. This implies that each amplitude must be regularized by subtracting an expression mirroring its UV behavior to produce a finite result

$$\mathcal{A}_{\mathrm{R}} = \mathcal{A} - \mathcal{A}^{\mathrm{cnt}}_{\mathrm{UV}} \,. \tag{2.74}$$

This subtraction is done locally at the level of the integrand such that the whole expression being integrated over is free from problematic UV behaviour and the integral converges immediately. This procedure is equivalent to the renormalization of the theory itself as long as the counterterm $\mathcal{A}^{\mathrm{cnt}}_{\mathrm{UV}}$ can be evaluated in DREG to reproduce the d-dependent expression in agreement with the chosen renormalization scheme. We use the expression *local renormalization* in this context.

The original method of obtaining the UV counterterm for a LTD calculation as presented in Ref. [83–85] is based on Ref. [86] and involves expanding the amplitude, while still in the Feynman representation, around the UV propagator

$$G_F(q_{\mathrm{UV}};\mu_{\mathrm{UV}}) = \frac{1}{q^2_{\mathrm{UV}} - \mu^2_{\mathrm{UV}} + \imath 0} \,. \tag{2.75}$$

The internal momentum therein is given by $q_{\mathrm{UV}} = \ell + k_{\mathrm{UV}}$ where k_{UV} can be chosen arbitrarily. For the one-loop example of the scalar two-point function Eq. (2.17) the leading order expansion around the UV propagator gives the counterterm

$$\mathcal{A}^{(1)}_{\mathrm{UV}} = \int_\ell \left(G_F(\ell;\mu_{\mathrm{UV}})\right)^2 \,, \tag{2.76}$$

when $k_{\rm UV} = 0$ is chosen. Using DREG the counterterm integrates to

$$\begin{aligned}\mathcal{A}^{(1)}_{\rm UV} &= \frac{\Gamma(1+\epsilon)}{(4\pi)^{2-\epsilon}} \frac{1}{\epsilon} \left(\frac{\mu^2_{\rm UV}}{\mu^2}\right)^{-\epsilon} \\ &= \frac{1}{16}\left(\frac{1}{\varepsilon} - \gamma_E + \log(4\pi) + \log\left(\frac{\mu^2}{\mu^2_{\rm UV}}\right) + \mathcal{O}(\varepsilon)\right) .\end{aligned} \tag{2.77}$$

Note that this indeed cancels the divergent part of the integrated result as presented in Eq. (1.30) and implements the standard $\overline{\rm MS}$ renormalization scheme when identifying the parameter $\mu_{\rm UV}$ with the DREG renormalization scale μ.

The application of the LTD to this integrand must take into account the pole of order two in the counterterm. Using Eq. (2.9) its dual integrand is obtained as

$$\mathcal{A}^{(1)}_{\rm UV} = \int_\ell \frac{\tilde{\delta}(\ell; \mu_{\rm UV})}{2\left(\ell^{(+)}_{0,\rm UV}\right)^2} , \tag{2.78}$$

where the UV on-shell energy is given by $\ell^{(+)}_{0,\rm UV} = \sqrt{\boldsymbol{\ell}^2 + \mu^2_{\rm UV}}$. The local UV behavior of this counterterm is exactly the same as the one present in the dual integrand of the scalar two-point function, independently of the considered values of the loop momentum, as long as a coordinate system is chosen where the dependence on the integration angle is trivial. Subtracting this expression from the unrenormalized amplitude at integrand-level thus provides an expression free of problematic UV behavior whose integral converges without the need to modify the spacetime dimensions.

In concrete applications of the LTD it has been seen that significant simplifications of the dual integrands are often possible. An example for this is the one-loop description of the decay of the Higgs boson into two photons [72–74] discussed in Chapter 3. In cases like this it would be cumbersome to find an expression in the Feynman representation that corresponds to the UV behavior seen in the simplified dual integrand. Expanding the integrand only after applying the LTD and possible simplifications allows to obtain a concise expression. Clearly, agreement of the integrated result in d dimensions with the DREG result is still required.

The procedure for renormalization of two-loop amplitudes within the LTD formalism has been described in Refs. [73, 74] and is based on extending the expansion of the integrand up to logarithmic order around the UV propagator,

given in the multiloop notation as

$$G_F(i_{\rm UV}) = G_F(q_{i,\rm UV}) = \frac{1}{q_{i,\rm UV}^2 - \mu_{\rm UV}^2 + \imath 0}, \tag{2.79}$$

where $q_{i,\rm UV} = \ell_i + k_{i,\rm UV}$ and $k_{i,\rm UV}$ is customarily set to 0. Concretely, for loop momenta ℓ_j, ℓ_k with $j,k \in \{1,2\}$ this amounts to applying the transformations

$$\begin{aligned}
\mathcal{S}_{j,\rm UV} \;&:\; \{\ell_j^2 \mid \ell_j \cdot k\} \to \{\lambda^2\, q_{j,\rm UV}^2 + (1-\lambda^2)\mu_{\rm UV}^2 \mid \lambda q_{j,\rm UV} \cdot k\}\;, \quad k \in \{\ell_k, p\} \\
\mathcal{S}_{\rm UV^2} \;&:\; \{\ell_j^2 \mid \ell_j \cdot \ell_k \mid \ell_j \cdot p\} \to \\
&\quad \{\lambda^2 q_{j,\rm UV}^2 + (1-\lambda^2)\mu_{\rm UV}^2 \mid \lambda^2 q_{j,\rm UV} \cdot q_{k,\rm UV} - (1-\lambda^2)/2\mu_{\rm UV}^2 \mid \lambda q_{j,\rm UV} \cdot p\}\;,
\end{aligned} \tag{2.80}$$

multiplying the amplitude with λ^4 for the single limits or λ^8 for the double-UV limit and the subsequent expansion for $\lambda \to \infty$, truncating the corresponding series in λ after the logarithmic order.

The effect of the transformations above on the Feynman propagators with momenta ℓ_i and internal masses m_i, including the subleading terms up to λ^{-4}, is given by

$$\begin{aligned}
\mathcal{S}_{i,\rm UV} G_F(i) &= \mathcal{S}_{\rm UV^2} G_F(i) \qquad (2.81)\\
&= \lambda^{-2} G_F(i_{\rm UV}) \left[1 - \lambda^{-2}\left(-m_i^2 + \mu_{\rm UV}^2\right) G_F(i_{\rm UV})\right] \\
\mathcal{S}_{i,\rm UV} G_F(ij) &= \lambda^{-2} G_F(i_{\rm UV}) \big[1 - \lambda^{-1} 2\ell_i \cdot \ell_j G_F(i_{\rm UV}) \qquad (2.82)\\
&\quad - \lambda^{-2} G_F(i_{\rm UV}) \left(\ell_j^2 + \mu_{\rm UV}^2 - m_{ij}^2 - (2\ell_i \cdot \ell_j)^2 G_F(i_{\rm UV})\right)\big] \\
\mathcal{S}_{\rm UV^2} G_F(ij) &= \lambda^{-2} G_F(ij_{\rm UV}) \left[1 - \lambda^{-2}\left(-m_{ij}^2 + \mu_{\rm UV}^2\right) G_F(ij_{\rm UV})\right]\;. \qquad (2.83)
\end{aligned}$$

Choosing different linear combinations of the loop momenta to be integrated over, the transformations have to be changed in order to reproduce the leading order behavior of the transformations above. The renormalized amplitude is obtained by subtracting the various counterterms

$$\mathcal{A}_R^{(2)} = \mathcal{A}^{(2)} - \mathcal{A}_{1,\rm UV}^{(2)} - \mathcal{A}_{2,\rm UV}^{(2)} - \mathcal{A}_{\rm UV^2}^{(2)}\;, \tag{2.84}$$

where $\mathcal{A}_{i,\rm UV}^{(2)} = \mathcal{S}_{i,\rm UV}\mathcal{A}^{(2)}$ and $\mathcal{A}_{\rm UV^2}^{(2)} = \mathcal{S}_{\rm UV^2}\left(\mathcal{A}^{(2)} - \mathcal{A}_{1,\rm UV}^{(2)} - \mathcal{A}_{2,\rm UV}^{(2)}\right)$.

Applying this formalism to the test amplitude

$$\begin{aligned}
\mathcal{I}(\ell_1,\ell_2) &= G_F(1,2^2,12) \qquad (2.85)\\
&= \frac{1}{\left(\ell_1^2 - M^2 + \imath 0\right)\left(\ell_2^2 - M^2 + \imath 0\right)^2 \left((\ell_1+\ell_2)^2 - M^2 + \imath 0\right)}
\end{aligned}$$

leads to the counterterms

$$\begin{aligned}\mathcal{I}_{1,\mathrm{UV}} &= G_F(1^2_{\mathrm{UV}}, 2^2) \ , \\ \mathcal{I}_{2,\mathrm{UV}} &= 0 \ , \\ \mathcal{I}_{\mathrm{UV}^2} &= G_F(1_{\mathrm{UV}}, 2^2_{\mathrm{UV}}) \left(G_F(12_{\mathrm{UV}}) - G_F(1_{\mathrm{UV}})\right) \ ,\end{aligned} \tag{2.86}$$

which successfully cancel the amplitude's UV singularities at the local level.

The same successful cancellation for the full $H \to gg$ amplitude was achieved in Refs. [73, 74] by including subleading terms in λ. The applicability of this formalism was expected and announced for a general two-loop amplitude.

A very special example with a high degree of ultravioletness is the massless sunrise amplitude Eq. (2.41), whose result as obtained through DREG before renormalization is given by

$$\mathcal{A}^{(2)}_{\ominus} = -\,\mu^{4\varepsilon}\,\frac{\Gamma(-1+2\epsilon)\,\Gamma(1-\epsilon)^3}{(4\pi)^{4-2\epsilon}\,\Gamma(3-3\epsilon)}\,(-p^2 - i0)^{1-2\epsilon} \ , \tag{2.87}$$

which corresponds to $(4\pi)^{-4}$ times the result obtained in [87] and has a simple pole in ε as seen through the expansion

$$\mathcal{A}^{(2)}_{\ominus} = -(S_\varepsilon^{\overline{\mathrm{MS}}})^2 p^2 \left(\frac{1}{4\varepsilon} - \frac{1}{2}\,\log\left(-\frac{p^2}{\mu^2} - i0\right) + \frac{13}{8}\right) + \mathcal{O}(\varepsilon) \ , \tag{2.88}$$

with

$$S_\varepsilon^{\overline{\mathrm{MS}}} = (4\pi)^{\varepsilon-2}\exp(-\varepsilon\,\gamma_E) \ . \tag{2.89}$$

Using the proposed transformations of Eq. (2.80) the single-UV counterterms are given by

$$\left(\mathcal{A}^{(2)}_{\ominus}\right)_{i,\mathrm{UV}} = \int_{1,2} \frac{1}{(\ell_i^2 - \mu^2_{\mathrm{UV}} + i0)^2(\ell_j^2 + i0)} = \int_{1,2} G_F(i^2_{\mathrm{UV}}, j) \ . \tag{2.90}$$

Similarly, the double-UV counterterm, when expanding up to logarithmic order in λ, takes the form

$$\begin{aligned}\left(\mathcal{A}^{(2)}_{\ominus}\right)_{\mathrm{UV}^2} = \int_{1,2} \Big[& G_F\left(1_{\mathrm{UV}}, 2_{\mathrm{UV}}, 12_{\mathrm{UV}}\right) - G_F\left(1^2_{\mathrm{UV}}, 2_{\mathrm{UV}}\right) - G_F\left(1_{\mathrm{UV}}, 2^2_{\mathrm{UV}}\right) \\ & - \frac{d-4}{d} p^2 G_F\left(1_{\mathrm{UV}}, 2_{\mathrm{UV}}, 12^2_{\mathrm{UV}}\right) \\ & + \frac{4}{d}\,\mu^2_{\mathrm{UV}} p^2 G_F\left(1_{\mathrm{UV}}, 2_{\mathrm{UV}}, 12^3_{\mathrm{UV}}\right) + 2\mu^2_{\mathrm{UV}} G_F\left(1^2_{\mathrm{UV}}, 2^2_{\mathrm{UV}}\right) \\ & - \mu^2_{\mathrm{UV}} G_F\left(1_{\mathrm{UV}}, 2_{\mathrm{UV}}, 12_{\mathrm{UV}}\right)\left(G_F\left(1_{\mathrm{UV}}\right) + G_F\left(2_{\mathrm{UV}}\right) + G_F\left(12_{\mathrm{UV}}\right)\right) \Big]\end{aligned} \tag{2.91}$$

after applying the integral identities $(\ell_i\cdot p)^2 \to \ell_i^2 p^2/d$ and $\ell_i\cdot p\, \ell_j\cdot p \to \ell_i\cdot\ell_j\, p^2/d$.

For these counterterms to produce the renormalized sunrise amplitude when subtracted from Eq. (2.41) they must reproduce the counterterms expected from DREG. While differences in the subtracted finite pieces can still be addressed by adding on subleading terms the cancellation of the UV singularity should be expected to be achieved immediately. Evaluating the obtained expressions using DREG one finds that in the case of the single-counterterms the two loop integrals factorize giving

$$\left(\mathcal{A}^{(2)}_{\ominus}\right)_{i,\mathrm{UV}} = \int_j \frac{1}{(\ell_j^2+\imath 0)} \int_i \frac{1}{(\ell_i^2-\mu^2_{\mathrm{UV}}+\imath 0)^2} = 0\,, \tag{2.92}$$

since the first integral is scaleless and thus vanishes in DREG.

The double-UV counterterm of the sunrise amplitude can be written in terms of master integrals using the tool for Feynman integral reduction *FIRE* [88] as implemented in MATHEMATICA through *FeynHelpers* [89], leading to the result

$$\begin{aligned}\left(\mathcal{A}^{(2)}_{\ominus}\right)_{\mathrm{UV}^2} = \left(\frac{\widetilde{S}_\varepsilon}{16\pi^2}\right)^2 \left(\frac{\mu^2_{\mathrm{UV}}}{\mu^2}\right)^{-2\varepsilon} \Bigg[\frac{2p^2}{3\varepsilon^2} + \frac{1}{\varepsilon}\left(\frac{7p^2}{12} - 5\mu^2_{\mathrm{UV}}\right) \\ + \left(-\frac{2}{9}p^2\left(\frac{21}{2} + 2\sqrt{3}\mathrm{Cl}_2(\frac{\pi}{3})\right) - 11\mu^2_{\mathrm{UV}} - \frac{43p^2}{24}\right)\Bigg]\,.\end{aligned} \tag{2.93}$$

where $\widetilde{S}_\varepsilon = (4\pi)^\varepsilon\Gamma(1+\varepsilon)$ and the Clausen function of order two is $\mathrm{Cl}_2(x) = \frac{i}{2}(\mathrm{Li}_2(-\imath x) - \mathrm{Li}_2(\imath x))$. The most immediate problem is the presence of the double-pole in the counter-term. Since the result of the amplitude itself only has a simple pole, subtracting the counterterms obtained here does *not* lead to a finite and much less a renormalized result. A deeper investigation of this special case is still required to extend local UV renormalization to the most general multiloop case.

2.5.2 Soft and collinear singularities

While the treatment of soft and collinear singularities is not a focus of this work it is worth sketching their regularization in the context of LTD since therein lies one of the central advantages of the method. As seen in Section 2.3 soft singularities appear in dual integrands as an endpoint singularity at $\boldsymbol{\ell}^2 = 0$ when integrating over the loop three-momentum along the positive-energy solution of the on-shell hyperboloid of a massless particle, which takes the form of a light-cone. Subtracting the low-energy limit of the dual integrand up to a minimum three-momentum

allows to construct a well-behaved and convergent integral. Since the collinear singularities are restricted to the limited range of the loop three-momentum that corresponds to the overlap between two light-cones a counterterm may be constructed to subtract the problematic part as well. It is important to emphasize that the cancellation of the singular structures takes place locally at integrand-level: no divergent terms proportional to negative powers of ε are produced. This is the case in the typical subtraction schemes, where the divergent result is regularized by subtracting a suitable counterterm. In contrast, the LTD allows to sum over the degenerate soft and collinear states stemming from virtual and real contributions by employing a suitable mapping between the loop three-momentum appearing in the virtual contribution and the three-momentum appearing in the phase-space integral of the real-emission contribution. In that sense, it is directly the IR-safe observable that is calculated and no subtractions are necessary.

This concept has been introduced under the name *four dimensional unsubtraction* (FDU) in Refs. [83–85, 90, 91]. Concretely, the construction of a NLO cross-section involves the simultaneous calculation of the one-loop virtual correction with m final-state particles and the exclusively real cross-section with an additional final-state particle

$$\sigma^{\mathrm{NLO}} = \int_m d\sigma_{\mathrm{V}}^{(1,\mathrm{R})} + \int_{m+1} d\sigma_{\mathrm{R}}^{(1)} \,, \tag{2.94}$$

where the $m+1$ particle phase-space integral of the real contribution effectively differs from the one of the virtual contribution by an additional integral over the three-momentum of the emitted massless particle. Through the application of the LTD the virtual contribution also includes an additional integral over the loop three-momentum. The overall integrations of both contributions are thus technically analogous. Naively pulling both integrands under the same integration is doomed to fail since the position of the soft singularities in the three-momentum space of either the loop momentum or the external momentum do not coincide. To achieve a local cancellation it is necessary to find the appropriate mapping between, on the one hand, the loop three-momentum in the virtual contribution and, on the other hand, the external three-momentum of the emitted particle and its emitter.

The method of FDU thus allows to cancel soft and collinear divergences locally without altering the space-time dimensions by introducing mappings of momenta between the virtual and real kinematics. Using this technique no overtly divergent expressions are generated and numerical instabilities in the calculation of observables can be avoided.

2.6 New developments and applications

As seen above, applying the LTD one obtains a function to be integrated over the Euclidean space of the loop three-momenta. In addition, the LTD representation exhibits a clear and localized singular structure that enables the local cancellation of IR singularities and thus the direct calculation of IR-safe observables in the physical four space-time dimensions using the FDU method. A novel local subtraction scheme for the computation of NLO contributions to scattering amplitudes has been presented recently in Ref. [92], including a discussion of singularities caused by the wave-function renormalization and initial state singularities.

Especially the causal representation found for the sunrise amplitude, as seen in Eq. (2.64), and for the MLT topology, Eq. (2.69), has led to great advances in the field. It has been seen for several topological families of multi-loop multi-leg Feynman integrals that it is possible to bring them into an integrand-level representation exhibiting a similar causal structure, a variety of examples are provided in Refs. [81,82] and technical proofs of the multiloop formalism are presented in Ref. [93]. As a consequence the occurrence of non-causal spurious singularities is avoided. While these are guaranteed to cancel, and are thus only a minor inconvenience during analytical calculations, they can lead to significant numerical instabilities and generally require resource-intensive high numerical precision. Alterations of the LTD formalism for multiloop numerical integrations, like averages over the positive and negative energy modes in Ref. [94], and formulations for the application of contour deformation have been presented in Refs. [78,79]. The causal representations have then recently been extended by using novel algebraic relations. These have led to all-order causal formulae that were proposed in Ref. [95]. Recently the automatized framework LOTTY [96] has been introduced to implement the causal application of LTD.

At the same time, the causal structure of multi-loop diagrams was investigated from a geometrical point of view in Ref. [97]. In this work concepts from graph theory were applied in order to determine the connections between the causal singularities and the entangled thresholds appearing in a given diagram. Numerical calculations performed using the geometric algorithm for obtaining the causal structure have proven to be extremely efficient.

In addition, it was observed that the two possible on-shell states of a Feynman propagator, describing a particle or antiparticle moving forward or backward in time, can be encoded efficiently within one qubit. Based on this connection applications of quantum algorithms to the calculation of Feynman diagrams have been investigated using the causal LTD representation in Ref. [98]. Especially

the geometrical interpretation proved useful in the development of the quantum algorithms where a modification of Grover's quantum algorithm has been used for efficiently identifying the causal configurations.

Lastly, the effective three-dimensional nature of the LTD integrand leads to an additional characteristic: in comparison to the original Feynman amplitude, a function of Minkowski four-momenta, the size of scalar products appearing in the dual integrand can be directly compared to external scales. This allows the development of a well-defined formalism of asymptotic expansions of the integrand. Specific asymptotic expansions in the context of LTD have been presented for the first time for the process $H \to \gamma\gamma$ at one loop [72]. In the next chapter we summarize these results and study the convergence behavior of the applied expansions.

Chapter 3

Asymptotic expansions in four spacetime dimensions in the $H \to \gamma\gamma$ amplitude

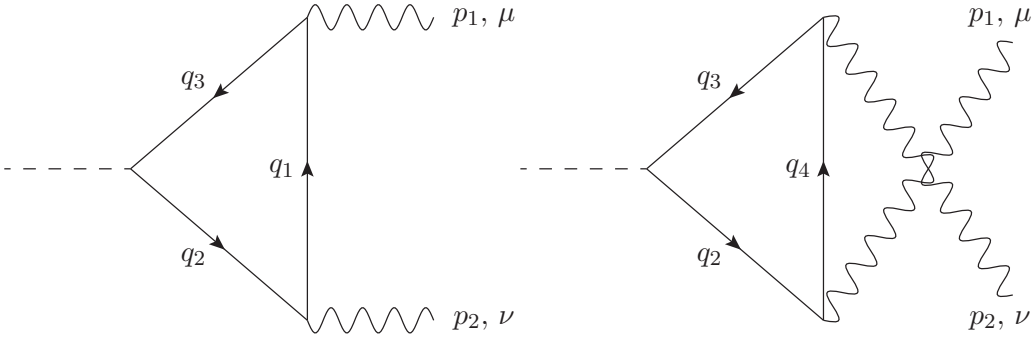

Figure 3.1: Two of the diagrams contributing to the process $H \to \gamma\gamma$ at leading order.

The most extensively studied physical processes within the framework of LTD is the Higgs boson production through gluon fusion and the Higgs boson decay into two photons. Even though these two processes involve different diagrammatic contributions they may be described by the same underlying amplitude [72–74]. During the examination of the one-loop amplitude asymptotic expansions were found, from which the idea for the development of a formalism for asymptotic expansions within the context of the LTD evolved. Being thus fundamental for the present work the dual amplitude and its expansions found in Ref. [72] will be reviewed in this chapter. We study in detail the integrand-level convergence behavior in different asymptotic limits.

3.1 The dual amplitude for $H \to \gamma\gamma$

One of the most important channels for Higgs boson production at the LHC is gluon-gluon fusion. Being massless gluons do not couple directly to the Higgs boson in the SM, instead their interaction, even at leading order, occurs through a loop of massive quarks, mostly top quarks. Similarly, the Higgs boson's decay into two photons goes through a loop of either quarks, charged scalars or W bosons. Interestingly, it was found in Ref. [72] that all of these amplitudes can be written in a universal manner, differing only in terms of a few real coefficients. While this universality is a noteworthy quality of these amplitudes it is of no consequence to the asymptotic expansions. Here I will thus only describe the top quark contribution to the $H \to \gamma\gamma$ amplitude aiming for compactness, for the general expressions one may refer to Refs. [72, 74].

According to the Feynman rules of the SM the top quark contribution for

Higgs boson decay into two photons at leading order is given by

$$\imath\mathcal{M}^{(1)}_{H\to\gamma\gamma} = -\frac{4e^2}{9}\left(\varepsilon^{\mu}(p_1)\right)^*\left(\varepsilon^{\nu}(p_2)\right)^*\mathcal{A}^{(1)}_{\mu\nu}\,, \tag{3.1}$$

with e being the electromagnetic coupling and ε the polarization vector of the external photons with momenta p_1 and p_2. The two contributing diagrams are given in Fig. 3.1 and the corresponding expression for $\mathcal{A}_{\mu\nu}$, as obtained from the interaction Lagrangians in Eq. (1.54) and Eq. (1.64), is

$$\begin{aligned}\mathcal{A}^{(1)}_{\mu\nu} = \frac{2M_t}{v}\int_\ell G_F(q_1,q_2,q_3)\,\mathrm{Tr}\left[(\not{q}_2+M_t)\,\gamma_\nu\,(\not{q}_1+M_t)\,\gamma_\mu\,(\not{q}_3+M_t)\right] \\ +\{q_1\leftrightarrow q_4,\mu\leftrightarrow\nu\}\,,\end{aligned} \tag{3.2}$$

where the internal momenta $q_1 = \ell + p_1$, $q_2 = \ell + p_1 + p_2$, $q_3 = \ell$ and $q_4 = \ell + p_2$ have been defined. Since the Yukawa coupling facilitating this interaction is proportional to the quark mass the contributions of the lighter quarks are severely suppressed compared to the top quark. This outweighs the lower probability for producing heavier particles in the loop and justifies the common omission of the light quarks in Higgs physics.

For easier manipulation of the amplitude it is convenient to decompose it into scalar form factors multiplied by the tensor structures which Lorentz invariance permits to appear in the result

$$\mathcal{A}^{(1)}_{\mu\nu} = \sum_{i=1}^{5}\mathcal{A}^{(1)}_i\,T^i_{\mu\nu}\,. \tag{3.3}$$

Defining $s_{12} = (p_1+p_2)^2$ the tensor basis is given by

$$T^{\mu\nu,i} = \left\{g^{\mu\nu} - \frac{2p_1^\nu\,p_2^\mu}{s_{12}}, g^{\mu\nu}, \frac{2p_1^\mu\,p_2^\nu}{s_{12}}, \frac{2p_1^\mu\,p_1^\nu}{s_{12}}, \frac{2p_2^\mu\,p_2^\nu}{s_{12}}\right\}\,. \tag{3.4}$$

The polarization vector of a photon is transversely polarized, meaning that its scalar product with the momentum of the photon vanishes. The contributions $\mathcal{A}^{(1)}_3$, $\mathcal{A}^{(1)}_4$ and $\mathcal{A}^{(1)}_5$ thus do not contribute to the decay amplitude into real photons. An additional physical restriction on the amplitude is imposed by gauge symmetry which demands that

$$p_1^\mu\mathcal{A}_{\mu\nu} = p_2^\nu\mathcal{A}_{\mu\nu} = 0\,. \tag{3.5}$$

This condition can only be fulfilled if $\mathcal{A}^{(1)}_2$ vanishes after integration, leaving $\mathcal{A}^{(1)}_1$ as the only physically relevant term.

The scalar form factors, and in particular $\mathcal{A}_1^{(1)}$, can be obtained through projection operators $P_i^{\mu\nu}$ fulfilling the conditions $P_i^{\mu\nu} T_{\mu\nu}^j = \delta_{ij}$. The only necessary operator is thus given by

$$P_1^{\mu\nu} = \frac{1}{d-2}\left(g^{\mu\nu} - \frac{2p_2^\mu\, p_1^\nu}{s_{12}} - (d-1)\frac{2p_1^\mu\, p_2^\nu}{s_{12}}\right) \tag{3.6}$$

and produces

$$\mathcal{A}_1^{(1)} = P_1^{\mu\nu}\mathcal{A}_{\mu\nu}^{(1)}\ . \tag{3.7}$$

Later on in the calculation it becomes apparent that subtracting the vanishing contribution of $\mathcal{A}_2^{(1)}$ simplifies intermediate expressions, making use of the second projector

$$\mathcal{A}_2^{(1)} = P_2^{\mu\nu}\mathcal{A}_{\mu\nu}^{(1)} = \frac{2p_1^\mu\, p_2^\nu}{s_{12}}\mathcal{A}_{\mu\nu}^{(1)}\ . \tag{3.8}$$

To facilitate analytic simplifications it is most convenient to apply the LTD on the scalar coefficients through the master formula of Eq. (2.16). Since the amplitude Eq. (3.2) contains four different internal momenta q_i one obtains the four dual contributions

$$\mathcal{A}_1^{(1)}\left(\tilde{\delta}\left(q_i\right)\right) = g_t \int_\ell \tilde{\delta}\left(q_i\right)\ \left(\frac{s_{12}M_t^2}{\left(2q_i\cdot p_1\right)\left(2q_i\cdot p_2\right)}c_1 + c_2\right)\ , \qquad i\in\{1,4\} \tag{3.9}$$

$$\mathcal{A}_1^{(1)}\left(\tilde{\delta}\left(q_2\right)\right) = g_t \int_\ell \tilde{\delta}\left(q_2\right)\ \frac{s_{12}}{s_{12}-2q_2\cdot p_{12}+\imath 0} \times\left(\left(\frac{s_{12}M_t^2}{(2q_2\cdot p_1)(2q_2\cdot p_2)}c_1 + c_2\right)\frac{2q_2\cdot p_{12}}{s_{12}} + c_3\right)\ ,$$

$$\mathcal{A}_1^{(1)}\left(\tilde{\delta}\left(q_3\right)\right) = g_t \int_\ell \tilde{\delta}\left(q_3\right)\ \frac{-s_{12}}{s_{12}+2q_3\cdot p_{12}} \times\left(\left(\frac{s_{12}M_t^2}{(2q_3\cdot p_1)(2q_3\cdot p_2)}c_1 + c_2\right)\frac{2q_3\cdot p_{12}}{s_{12}} + c_3\right)\ .$$

with $g_t = \frac{2M_t^2}{s_{12}v}$ and the coefficients c_i given by

$$c_1 = \frac{8}{d-2} - \frac{s_{12}}{M_t^2}, \quad c_2 = -\frac{4d}{d-2}, \quad c_3 = 8\ . \tag{3.10}$$

It is generally not advisable to employ random shifts in the loop integration momenta of the distinct dual contributions since the computational simplicity of the

formalism relies on the local cancellation of non-causal singularities. Nonetheless, the four contributions in Eq. (3.9) can be written in terms of a single loop momentum after some considerations.

These simplifications are possible by choosing to work in the center-of-mass frame with $\boldsymbol{p}_1 + \boldsymbol{p}_2 = 0$ and $p_{1,0} = p_{2,0} = s_{12}/2$, where the on-shell loop energies are given by

$$q_{1,0}^{(+)} = \sqrt{(\boldsymbol{\ell} + \boldsymbol{p}_1)^2 + M_t^2}\,, \quad q_{4,0}^{(+)} = \sqrt{(\boldsymbol{\ell} + \boldsymbol{p}_2)^2 + M_t^2}\,, \tag{3.11}$$

$$\ell_0^{(+)} = q_{2,0}^{(+)} = q_{3,0}^{(+)} = \sqrt{\boldsymbol{\ell}^2 + M_t^2}\,. \tag{3.12}$$

The relevant property needed for rewriting all dual contributions in terms of a single loop momentum is based on the observation that the integrands, after projection, are Lorentz scalars by design - except for the delta functional. Being invariant under Lorentz transformations a shift in the loop momentum is unproblematic since it is justified *locally* and is thus independent of the integration procedure. As for the delta functional $\tilde{\delta}\,(q)$ it is sufficient to look at its definition to see that the identity

$$\tilde{\delta}\,(q_i) = \tilde{\delta}\,(\ell)\,\frac{\ell_0^{(+)}}{q_{i,0}^{(+)}} \tag{3.13}$$

holds, being especially simple for q_2 and $q_3 = \ell$. Adding up the dual contributions in Eq. (3.9) and setting to zero those terms that are fully antisymmetric in the loop momentum one obtains the form

$$\begin{aligned}\mathcal{A}_1^{(1)} = g_t\, s_{12} \int_\ell \tilde{\delta}\,(\ell) \Bigg[& \frac{2 s_{12}}{s_{12}^2 - (2\ell\cdot p_{12} - i0)^2}\, c_3 \\ & + \left(\frac{\ell_0^{(+)}}{q_{1,0}^{(+)}} + \frac{\ell_0^{(+)}}{q_{4,0}^{(+)}} + \frac{2(2\ell\cdot p_{12})^2}{s_{12}^2 - (2\ell\cdot p_{12} - i0)^2} \right) \left(\frac{M_t^2}{(2\ell\cdot p_1)(2\ell\cdot p_2)}\, c_1 + c_2 \right) \Bigg]\,.\end{aligned} \tag{3.14}$$

In the same manner the dual contributions to $\mathcal{A}_2^{(1)}$ can be obtained and combined to give

$$\mathcal{A}_2^{(1)} = g_t \frac{c_3}{2}\, s_{12} \int_\ell \tilde{\delta}\,(\ell) \left(\frac{\ell_0^{(+)}}{q_{1,0}^{(+)}} + \frac{\ell_0^{(+)}}{q_{4,0}^{(+)}} - 2 \right)\,, \tag{3.15}$$

which, since it integrates to zero in DREG, may be combined with the physical scalar form factor as

$$\begin{aligned}\mathcal{A}^{(1)} &= \mathcal{A}_1^{(1)} - 2\frac{c_2}{c_3}\mathcal{A}_2^{(1)} \\ &= g_t\, s_{12} \int_\ell \widetilde{\delta}(\ell) \left[\left(\frac{\ell_0^{(+)}}{q_{1,0}^{(+)}} + \frac{\ell_0^{(+)}}{q_{4,0}^{(+)}} + \frac{2(2\ell\cdot p_{12})^2}{s_{12}^2 - (2\ell\cdot p_{12} - i0)^2} \right) \frac{M_t^2}{(2\ell\cdot p_1)(2\ell\cdot p_2)}\, c_1 \right. \\ &\quad \left. + \frac{2s_{12}}{s_{12}^2 - (2\ell\cdot p_{12} - i0)^2}\, c_{23} \right],\end{aligned} \tag{3.16}$$

defining the coefficient $c_{23} = c_2 + c_3 = 4(d-4)/(d-2)$ which vanishes in the limit $d \to 4$.

The term proportional to c_{23} showcases a peculiarity of this calculation. At first glance one would assume the $H \to \gamma\gamma$ amplitude to be finite - while it is a one-loop integral there is no pointlike $H\gamma\gamma$ interaction in the SM and therefore no parameter in the theory that could absorb an appearing UV divergence. Nonetheless, the traditional result cannot be reproduced by naively setting $d = 4$ at the beginning of the calculation. Here we can see why: Maintaining $c_{23} \sim (d-4) \neq 0$ allows us to identify a logarithmic divergence in the integral

$$2g_t \int_\ell \widetilde{\delta}(\ell) \frac{s_{12}^2}{s_{12}^2 - (2\ell\cdot p_{12} - i0)^2}\, c_{23} = -\lim_{\Lambda\to\infty} \frac{g_t s_{12}}{16\pi^2}\, c_{23} \cdot \log(\Lambda) + \text{finite terms}\,, \tag{3.17}$$

which corresponds to a pole in ε. Being multiplied by $c_{23} \sim \varepsilon$ one obtains a finite, non-vanishing contribution which must be properly accounted for through systematic local renormalization of the amplitude. While the final result is finite, it is therefore not permissible to set $d = 4$ at integrand-level before having introduced the appropriate counterterm ensuring a nonambiguous outcome. For a more complete discussion of the appearance of arbitrary, regularization dependent parameters introduced by divergent integrals in finite but superficially divergent amplitudes one may refer to Ref. [99].

The counterterm needed for this calculation must display the integrand's UV behavior and vanish upon integration in DREG, as in the traditional method no renormalization is needed. In Ref. [72] the appropriate counterterm was determined to be

$$\mathcal{A}_{\text{UV}}^{(1)} = -g_t\, s_{12}\, c_{23} \int_\ell \widetilde{\delta}(q_{\text{UV}}) \frac{1}{2(q_{\text{UV},0}^{(+)})^2} \left(1 + \frac{1}{(q_{\text{UV},0}^{(+)})^2} \frac{3\mu_{\text{UV}}^2}{d-4} \right), \tag{3.18}$$

with $q^{(+)}_{\mathrm{UV},0} = \sqrt{\ell^2 + \mu^2_{\mathrm{UV}}}$. Similarly, a counterterm would have to be derived to be able to integrate either $\mathcal{A}^{(1)}_1$ or $\mathcal{A}^{(1)}_2$ separately. While subtracting a multiple of $\mathcal{A}^{(1)}_2$ is in principle not necessary for this calculation, abstaining from it would require recalculating the appropriate counterterm. Using $\mathcal{A}^{(1)}_{\mathrm{UV}}$ the renormalized amplitude before integration is then given by

$$\begin{aligned}\mathcal{A}^{(1)}_{\mathrm{R}}\Big|_{d=4} &= \left(\mathcal{A}^{(1)} - \mathcal{A}^{(1)}_{\mathrm{UV}}\right)\Big|_{d=4} \\ &= g_t\, s_{12} \int_{\vec{\ell}} \left[\frac{1}{2\ell^{(+)}_0}\left(\frac{\ell^{(+)}_0}{q^{(+)}_{1,0}} + \frac{\ell^{(+)}_0}{q^{(+)}_{4,0}} + \frac{2(2\ell\cdot p_{12})^2}{s^2_{12} - (2\ell\cdot p_{12} - i0)^2}\right)\frac{M_t^2}{(2\ell\cdot p_1)(2\ell\cdot p_2)}\, c_1 \right. \\ &\qquad \left. + \frac{3\mu^2_{\mathrm{UV}}}{4(q^{(+)}_{\mathrm{UV},0})^5}\hat{c}_{23}\right], \qquad \hat{c}_{23} = \frac{c_{23}}{d-4}\,,\end{aligned} \tag{3.19}$$

where the terms proportional to $c_{23} \sim (d-4)$ and finite upon integration have been dropped. Solving the integral over the loop three-momentum leads to the known result

$$\mathcal{A}^{(1)}_{\mathrm{R}}\Big|_{d=4} = \frac{g_t\, s_{12}}{16\pi^2}\left(\frac{M_t^2}{s_{12}}\log^2\left(\frac{\beta-1}{\beta+1}\right)c_1 + 2\hat{c}_{23}\right), \quad \beta = \sqrt{1 - \frac{4M_t^2}{s_{12}+i0}}. \tag{3.20}$$

Note that the renormalization scale μ_{UV} disappears after integration as would be expected in a finite amplitude.

3.2 Large mass expansion

An example for an asymptotic expansion below threshold, that is for an integrand free of singularities, appears for the limit of one large mass. The expansion consists of replacing the expression in the round brackets of Eq. (3.19) by a version expanded in the quantity

$$\kappa(\boldsymbol{\ell}) = \frac{s_{12}}{(2\ell^{(+)}_0)^2} = \frac{s_{12}}{4(\boldsymbol{\ell}^2 + M_t^2)}\,, \tag{3.21}$$

which is a valid expansion parameter in all the range of the loop momentum whenever $M_t^2 \gg s_{12}$ as assumed in this scenario. A straight-forward expansion can be found for the last term in the bracket, which originates from the product of the two dual propagators $G_D(q_3; q_2)$ and $G_D(q_2; q_3)$. Note that in the considered

limit the imaginary prescription is superfluous. We thus have

$$\frac{1}{s_{12}^2 - (2\ell \cdot p_{12})^2} = -\frac{1}{s_{12}(2\ell_0^{(+)})^2 \ (1 - \kappa(\boldsymbol{\ell}))} = -\frac{1}{s_{12}(2\ell_0^{(+)})^2} \sum_{n=0}^{\infty} [\kappa(\boldsymbol{\ell})]^n \ . \quad (3.22)$$

The fractions of on-shell energies may also be written in terms of κ as

$$\frac{\ell_0^{(+)}}{q_{i,0}^{(+)}} = \left(1 + \frac{2\boldsymbol{\ell} \cdot \boldsymbol{p}_i + \boldsymbol{p}_i^2}{(\ell_0^{(+)})^2}\right)^{-\frac{1}{2}} = \frac{1}{\sqrt{1 \mp 2z\sqrt{\kappa(\boldsymbol{\ell})} + \kappa(\boldsymbol{\ell})}} \ , \quad i \in \{1, 4\} \ , \quad (3.23)$$

conveniently defining

$$z = \frac{2\boldsymbol{\ell} \cdot \boldsymbol{p}_1}{\ell_0^{(+)} \sqrt{s_{12}}} \ . \quad (3.24)$$

The expression thus obtained coincides with generating function in the definition of the Legendre Polynomials $P_n(z)$, giving an expansion for the energy ratio with

$$\frac{\ell_0^{(+)}}{q_{i,0}^{(+)}} = \sum_{n=0}^{\infty} P_n(\pm z) \left[\kappa(\boldsymbol{\ell})\right]^{\frac{n}{2}} \ . \quad (3.25)$$

Since $P_n(-z) = (-1)^n P_n(z)$ the two fractions can be combined to give

$$\frac{\ell_0^{(+)}}{q_{1,0}^{(+)}} + \frac{\ell_0^{(+)}}{q_{4,0}^{(+)}} = 2\sum_{n=0}^{\infty} P_{2n}(z) \left[\kappa(\boldsymbol{\ell})\right]^n \ . \quad (3.26)$$

The additional factor of scalar products may be expressed in terms of the introduced variables as

$$\frac{1}{(2\ell \cdot p_1)(2\ell \cdot p_2)} = \frac{1}{4(\ell_0^{(+)})^4} \ \frac{1}{(1 - z^2)\, \kappa(\boldsymbol{\ell})} \ , \quad (3.27)$$

allowing for the combination of the obtained results to give the large-mass expansion at integrand-level

$$\mathcal{A}_{\mathrm{R}}^{(1)}\Big|_{d=4} \overset{M_t^2 \gg s_{12}}{=} g_t \, s_{12} \int_{\vec{\ell}} \left[\frac{M_t^2}{4(\ell_0^{(+)})^5} \left(\sum_{n=1}^{\infty} \frac{P_{2n}(z) - 1}{1 - z^2} \left(\kappa(\boldsymbol{\ell})\right)^{n-1}\right) c_1 + \frac{3\mu_{\mathrm{UV}}^2}{4(q_{\mathrm{UV},0}^{(+)})^5} \, \hat{c}_{23}\right] . \quad (3.28)$$

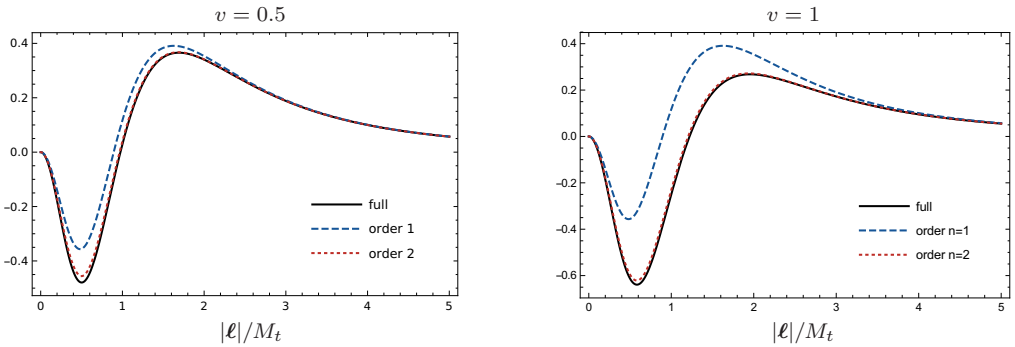

Figure 3.2: The convergence behavior at integrand-level of the large-mass expansion in Eq. (3.28) for the physical values of the masses, evaluated for the loop three-momentum $\boldsymbol{\ell}$ being orthogonal ($v = 0.5$) or parallel ($v = 1$) to $\boldsymbol{p}_1$.

Table 3.1: The values obtained through integration of the large-mass expansion Eq. (3.28) and their relative errors with respect to the full result 0.5545 GeV. Evaluation with physical values for the parameters.

	integrated result / GeV	rel. error
$n = 1$	0.8057	37 %
$n = 2$	0.5724	3 %
$n = 3$	0.5560	0.3 %

Since all of the expansions employed are well-justified in the whole range of integration the expanded amplitude converges at integrand-level. Taking into account that the expansion parameter $\kappa(\boldsymbol{\ell})$ goes to zero for large integration momenta the convergence in the high-energy region should improve. To test this expected behavior we set the numerical values to those consistent with the decay of an on-shell Higgs boson, $M_t = 172.76\,\text{GeV}$ and $\sqrt{s_{12}} = M_H = 125.10\,\text{GeV}$ [8]. In this scenario the expansion parameter is limited by $\kappa(\boldsymbol{\ell}) < 0.13$. As can be seen in Fig. 3.2, already at second order in the expansion a very good agreement with the full integrand is reached for all choices of the angle between the loop three-momentum and the external momenta. The integrated values for the same choice of parameters are given in Table 3.1.

The rational coefficients appearing in the result after analytic integration are expanded in an additional step leading to the expression given in Ref. [74]. The ensuing polynomial in the small quantity $r_t = s_{12}/M_t^2$ is given for the lowest

orders by

$$\mathcal{A}_{\mathrm{R}}^{(1)}\Big|_{d=4} \overset{M_t^2 \gg s_{12}}{=} \frac{s_{12}}{16\pi^2 v}\left(-\frac{4}{3} - \frac{7}{90} r_t - \frac{1}{126} r_t^2 - \frac{13}{12600} r_t^3 - \frac{8}{51975} r_t^4 + \mathcal{O}(r_t^5) \right) . \tag{3.29}$$

3.3 Small mass expansion

A relevant difference to the previous example appears when considering the kinematics above threshold with $s_{12} > 4M_t^2$. Thus another expansion has been developed for the small-mass limit $M_t^2 \ll s_{12}$.

In this limit the product of dual propagators in the renormalized integrand of Eq. (3.19) is considered again. Defining the small expansion parameter for this limit as $m_t^2 = -M_t^2/(s_{12} + \imath 0)$, the denominator of this expression may be separated into terms of different order in m_t^2 as

$$\begin{aligned} \frac{1}{s_{12}^2 - (2\ell \cdot p_{12} - i0)^2} &= \frac{-1/s_{12}}{4\boldsymbol{\ell}^2 - s_{12}(4 + m_t^2)} \\ &= \frac{-1/s_{12}}{4\boldsymbol{\ell}^2 - s_{12}(1 + m_t^2)^2 - s_{12} m_t^2 (2 - m_t^2)} . \end{aligned} \tag{3.30}$$

Since the last term in the denominator is proportional to the expansion parameter it is identified as a small quantity and the expression is thus expanded as

$$\frac{1}{s_{12}^2 - (2\ell \cdot p_{12} - i0)^2} = -\frac{1}{s_{12}} \sum_{n=1}^{\infty} \frac{\left(s_{12}\, m_t^2 (2 - m_t^2)\right)^{n-1}}{\left(4\boldsymbol{\ell}^2 - s_{12}(1 + m_t^2)^2\right)^n} . \tag{3.31}$$

This expansion is well justified both when $\boldsymbol{\ell}$ is negligibly small as well as when it dominates the denominator of the expansion. The condition justifying the expansion only breaks down in the part of the integration range where $4\boldsymbol{\ell}^2 \approx s_{12}(1+m_t^2)^2$. This corresponds to the physical threshold of the amplitude around which a locally convergent expansion cannot be expected.

Approximating the sum of energy ratios, $\ell_0^{(+)}/q_{1,0}^{(+)} + \ell_0^{(+)}/q_{4,0}^{(+)}$, by 2 and using z as defined previously the complete expansion of Eq. (3.19) in the small-mass

Table 3.2: The values obtained through numerical integration of the small-mass expansion Eq. (3.32) and their relative errors with respect to the full result $(8.92 + 1.86\imath)\,\mathrm{GeV}$. Evaluation with parameters $s_{12} = 5M_t^2$, $M_t = 172.76\,\mathrm{GeV}$, $\mu_{\mathrm{UV}} = 200\,\mathrm{GeV}$ and $\imath 0 = \imath 10^{-6}$.

	integrated result / GeV	rel. error Re	Im
$n = 1$	$8.38 + 3.12\imath$	5.9 %	50 %
$n = 2$	$8.84 + 2.22\imath$	0.7 %	18 %
$n = 3$	$8.88 + 2.00\imath$	0.1 %	7 %

limit is given by

$$\mathcal{A}_{\mathrm{R}}^{(1)}\Big|_{d=4} \overset{M_t^2 \ll s_{12}}{=} g_t\, s_{12} \int_{\vec{\ell}} \left[\frac{3\mu_{\mathrm{UV}}^2}{4(q_{\mathrm{UV},0}^{(+)})^5}\, \hat{c}_{23} - \frac{m_t^2}{(\ell_0^{(+)})^3(1-z^2)} \left(1 - \sum_{n=1}^{\infty} \frac{4(\ell_0^{(+)})^2 \big(s_{12}\, m_t^2 (2 - m_t^2)\big)^{n-1}}{\big(4\boldsymbol{\ell}^2 - s_{12}(1+m_t^2)^2\big)^n} \right) c_1 \right], \tag{3.32}$$

where the denominator can be simplified further by substituting the integration variable through $\ell \to M_t/2(x^{1/2} - x^{-1/2})$ as

$$4\boldsymbol{\ell}^2 - s_{12}(1+m_t^2)^2 = -\frac{s_{12} m_t^2}{x}(x + m_t^2)(x + m_t^{-2})\,. \tag{3.33}$$

A similar procedure is shown with more detail in Section 4.1.

For a numerical evaluation any value above threshold may be chosen, for $s_{12} = 5M_t^2$ the integrand-level convergence can be seen in Fig. 3.3. While the expansion's behavior around the pole does not mirror the full integrand the pole itself is reproduced with the pole position slightly moved

$$|\boldsymbol{\ell}|_{\mathrm{div}} = \frac{\sqrt{s_{12}}}{2}\left(1 - \frac{2M_t^2}{s_{12}}\right) \quad \to \quad \frac{\sqrt{s_{12}}}{2}\sqrt{1 - \frac{4M_t^2}{s_{12}}}\,. \tag{3.34}$$

The apparently slow convergence in the real part of the integrand when setting the integration momentum parallel to the external momentum is due to the simple replacement of the energy ratios by a constant.

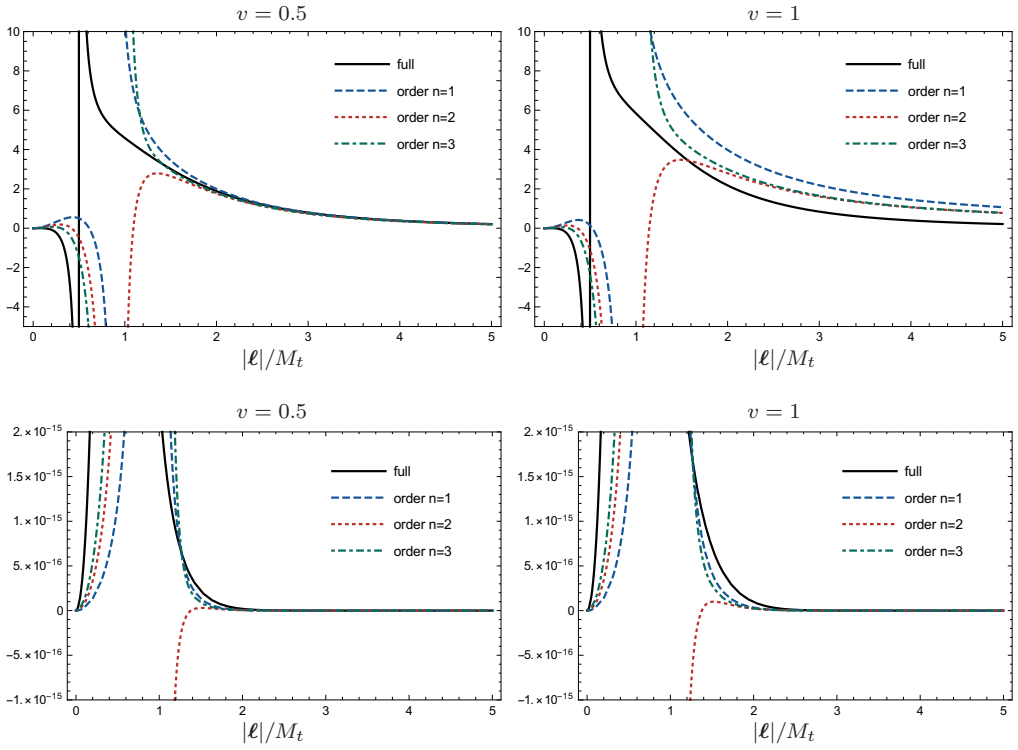

Figure 3.3: The convergence behavior at integrand-level of the small-mass expansion in Eq. (3.32) for $s_{12} = 5M_t^2$, evaluated for the loop three-momentum $\boldsymbol{\ell}$ being orthogonal ($v = 0.5$) or parallel ($v = 1$) to $\boldsymbol{p}_1$. The real part of the integrand is shown in the top row and the imaginary part in the bottom row.

Numerical integration of the amplitude by path deformation is straight-forward and results in the values found in Table 3.2. Convergence at integrand-level is thus achieved very effectively.

The result after analytic integration and a posterior expansion of the rational coefficients is given in Ref. [74] as a polynomial in m_t^2

$$\mathcal{A}_{\mathrm{R}}^{(1)}\Big|_{d=4} \overset{M_t^2 \ll s_{12}}{=} \frac{M_t^2}{8\pi^2 v}\Big(-4 + L_t^2 - 4(1-L_t)L_t\, m_t^2 + 2(2-5L_t)m_t^4 + 4(1+8L_t/3)m_t^6\Big) + \mathcal{O}(m_t^{10})\,,$$

with the logarithm $L_t = \log(m_t^2)$ appearing in the coefficients.

3.4 Results and opportunities

Using the $H \to \gamma\gamma$ amplitude the authors of Refs. [72–74] have derived expansions which cover two kinematical limits. The Euclidean nature of the dual integrands has allowed them to define these expansions in such a way that they do in fact converge already at integrand-level which we have analyzed here. Thus their use is well justified. Convergence of the integrated expansion is fast and the full result's Taylor expansion can be recovered by applying an additional expansion to the rational coefficients obtained in the analytic integration of the expanded integrand.

The formalism described here is far from generic: it does not only depend on the specific amplitude used but also on choices made during the calculation. It would be perfectly acceptable to combine the two contributing diagrams already when defining the amplitude. This can be achieved by redefining the loop momentum. In fact, algorithms like those implemented in the MATHEMATICA package FeynArts [100] do this automatically. Using this alternative, but equivalent, amplitude does of course lead to the same result after integration, but since the integrand differs the very specific expansions used here cannot be applied if one wants to demonstrate local convergence. The decision to maintain the separate treatment of the two diagrams is well justified, since it reduces the angular dependence of the integrand. Nonetheless, it would be desirable to obtain a more general approach easily applicable to a wider range of amplitudes or choices during manual simplification. Similarly, choosing to subtract the $\mathcal{A}_2$ contribution is not necessary, but abstaining from it leads to a different counterterm and overall a different integrand to which the very specific expansions used here cannot be applied.

The objective of this work is thus to develop expansions that may be used in a wider range of amplitudes in the context of the LTD.

Chapter 4

General asymptotic expansions at one loop and beyond

The asymptotic expansions found for the amplitude of $H \to \gamma\gamma$ [72] are a proof-of-concept showing that convergent integrand-level expansions can be succesfully formulated in the context of the LTD. The expansions found therein are very specific to the considered amplitude and its analytic implementation: a simple shift in the loop momentum in one of the contributing diagrams would already demand reformulating the expansions in a way that is not straight-forward. This is only one of many arbitrary choices during the calculation that have an impact on whether the found expansions may be applied. A way of formulating asymptotic expansions in a general way is thus needed.

Formulating a systematic approach to introduce asymptotic expansions in dual integrands has been the main goal of our work. The objective was to find expansions that converge well both at integrand- and at integral-level and ideally simplify both the analytic and the numerical integration. These expansions were to be non-specific such that they may be applied to any given one-loop amplitude, with the long-term goal being the extension of the formalism to multiloop scenarios. It is at this point that the method's application to physical calculations can provide additional tools to the phenomenology of the SM and beyond the SM.

The structure of this chapter is as follows. General guidelines for the expansion of dual propagators are layed out in Section 4.1. Those rules are then applied at one-loop level to the scalar two-point function in Section 4.2 as well as the scalar three-point function in Section 4.3, in both cases for a variety of limits. Since we aim towards obtaining an expansion that is well-defined also at integrand-level and simplifies integrands sufficiently to obtain loop analytic results at higher orders and multiple scales, we analyze in Section 4.4 the multiloop case of the Maximal Loop Topology (MLT) defined in Ref. [3], which is the most symmetric multiloop configuration and is used as the building block to construct more complex topologies.

4.1 Asymptotic expansions of dual propagators

The behavior of scattering amplitudes is ruled by their analytic properties. Aiming for asymptotic expansions at integrand-level, we must therefore consider in detail the analysis of propagators which are the objects that give rise to singularities. While the numerator plays a role in determining whether the amplitude has a UV divergence this is not relevant for the discussion that follows about asymptotic expansions: within LTD the singular UV behavior is neutralized through local renormalization before integration. An example of this will be shown in Section 4.2.

The dual propagators can manifest non-causal or unphysical singularities on top of the physical divergences related to causal threshold and IR singularities. These unphysical divergences appear only when the various terms in the sum of residues in a dual integrand are considered separately. Identifying the conditions under which both causal and unphysical singularities appear as well as their position in the integration space is necessary groundwork for asymptotically expanding an amplitude and was therefore discussed in detail in Section 2.3.

Having identified the propagators of an amplitude that lead to singularities, we can now reparameterize any of the dual propagators in the following form that is more suitable for asymptotic expansions

$$\tilde{\delta}\left(q_i\right)\, G_D\left(q_i;q_j\right) = \frac{\tilde{\delta}\left(q_i\right)}{2q_i\cdot k_{ji} + \Gamma_{ij} + \Delta_{ij} - \imath 0\eta\cdot k_{ji}}\ , \tag{4.1}$$

where $\Gamma_{ij} + \Delta_{ij} = k_{ji}^2 + m_i^2 - m_j^2$. If $\Gamma_{ij} + \Delta_{ij}$ vanishes the dual propagator is not expanded. Otherwise the starting point for the asymptotic expansion is to demand that the condition

$$|\Delta_{ij}| \ll |2q_i\cdot k_{ji} + \Gamma_{ij}| \tag{4.2}$$

be fulfilled for the whole range of the loop integration space except for small regions around physical divergences. The distinctive feature of LTD is that since dual propagators only appear in integrands where one loop momentum has been set on shell, the condition has to be fulfilled in the Euclidean space of the loop three-momentum. Whenever it is satisfied, the dual propagator can be expanded as

$$G_D\left(q_i;q_j\right) = \sum_{n=0}^{\infty} \frac{\left(-\Delta_{ij}\right)^n}{\left(2q_i\cdot k_{ji} + \Gamma_{ij} - i0\eta\cdot k_{ji}\right)^{n+1}}\ , \tag{4.3}$$

or in the case of amplitudes with propagators raised to multiple powers, as often occurs in multiloop amplitudes, by using the generalized binomial theorem

$$\left(G_D\left(q_i;q_j\right)\right)^m = \sum_{n=0}^{\infty} \binom{-m}{n} \frac{\left(\Delta_{ij}\right)^n}{\left(2q_i\cdot k_{ji} + \Gamma_{ij} - i0\eta\cdot k_{ji}\right)^{n+m}}\ . \tag{4.4}$$

A special case of the above is the situation when $k_{ji}^2 + m_i^2 - m_j^2$ is much smaller than the scalar product $2q_i\cdot k_{ji}$. Then we must identify $\Gamma_{ij} = 0$ and the expansion above simplifies as follows:

$$G_D\left(q_i;q_j\right) = \sum_{n=0}^{\infty} \frac{\left(-\Delta_{ij}\right)^n}{\left(2q_i\cdot k_{ji}\right)^{n+1}}\ . \tag{4.5}$$

The asymptotic expansion of the dual propagators given in Eq. (4.3) is the basis for the majority of the examples that will be presented in this work. In the following, we will discuss how to select the functions Γ_{ij} and Δ_{ij} for a given kinematical limit. Further simplifications arise whenever $\mathbf{k}_{ji} = 0$. In that case, with the change of variables $|\boldsymbol{q}_i| = m_i/2\,(x_i - x_i^{-1})$, the denominator of the expanded dual propagator takes an easily integrable form. For the case of $\Gamma_{ij} = 0$ the denominator of Eq. (4.5) is given by

$$2q_i \cdot k_{ji} = k_{ji,0}\, m_i \, \left(x_i + x_i^{-1}\right) \,, \tag{4.6}$$

leading to integrals of the form

$$\int_1^\infty \mathrm{d}x \, \frac{\left(x^2-1\right)^2}{x^3} \left(\frac{x}{x^2+1}\right)^n \overset{n\geq 2}{=} \frac{8}{n(n^2-4)} \, {}_2F_1\left(-1+\frac{n}{2}, n, 2+\frac{n}{2}, -1\right) \,, \tag{4.7}$$

when integrating over only one propagator, with the result being expressed in terms of the hypergeometric function ${}_2F_1$. This can be extended to the more general case of Eq. (4.3) where the denominator can be written as

$$2q_i \cdot k_{ji} + \Gamma_{ij} - \imath 0\, \eta \cdot k_{ji} = Q_i^2 \, (x_i + r_{ij}) \left(x_i^{-1} + r_{ij}\right) \,. \tag{4.8}$$

The relations between the parameters of the simplified denominators, Q_i^2 and r_{ij}, and those of G_D, Γ_{ij}, m_i and $k_{ji,0}$, are given by the equations

$$\begin{aligned} \Gamma_{ij} &= Q_i^2 \left(1 + |r_{ij}|^2\right) \,, \\ r_{ij} &= \frac{m_i k_{ji,0}}{Q_i^2(1+\imath 0)} \,, \end{aligned} \tag{4.9}$$

where it has to be ensured that $|r_{ij}| \leq 1$. Effectively, this imposes restrictions on how the parameters Γ_{ij} and r_{ij} can be chosen. The infinitesimal imaginary prescription of r_{ij} accounts properly for the complex prescription of the original dual propagator and therefore of its causal thresholds. As will be seen in the examples of the following sections this type of expansion facilitates the analytical integration based on integrals of the form

$$\int_1^\infty \frac{\mathrm{d}x_i}{x_i(x_i + r_{ij})(x_i^{-1} + r_{ij})} = \frac{\log(r_{ij})}{r_{ij}^2 - 1}, \qquad |r_{ij}| < 1 \,. \tag{4.10}$$

When considering propagators with singularities it is of great importance to keep track of the correct imaginary prescription. This has been seen in Chapter 2 to be

of particular importance for the cancellation between unphysical singularities to take place. On the other hand it becomes somewhat less important when having made the distinction between causal and unphysical singularities: the sign of the imaginary prescription in propagators with causal singularities is always positive. Since the integration variable x_i runs only over positive values the singularity only appears when $\mathrm{Re}(r_{ij}) < 0$. It is then clear that the correct sheet of the logarithms stemming from expressions like Eq. (4.10) when evaluated at negative values of r_{ij} is achieved with

$$r_{ij} = \frac{m_i k_{ji,0}}{Q_i^2} + \imath 0\,. \tag{4.11}$$

For the class of limits where one hard scale Q is available, we can identify $Q_i^2 = \pm Q^2$ with the sign determined by the sign of the hard scale in the expression $k_{ji}^2 + m_i^2 - m_j^2$. This immediately allows to write down the expanded dual propagator for the majority of limits like the one of a large mass or large external momentum. Asymptotic expansions around thresholds deserve a special treatment since all the scales are of the same order and, therefore, a hard scale cannot be clearly identified. Even when approaching the physical threshold from below and thus considering a dual propagator without pole on the real axis, its behavior is still strongly influenced by the threshold singularity. In cases like this it is necessary to consider the trajectory of the pole in the non-expanded propagator

$$G_D(q_i; q_j) = \frac{x_i}{k_{ji,0}\, m_i\, (x_i - x_+)(x_i - x_-)}\,, \tag{4.12}$$

more carefully. The pole positions are given by

$$x_\pm = -\frac{k_{ji,0}^2 + m_i^2 - m_j^2 \pm \lambda^{1/2}(k_{ji,0}^2, m_i^2, m_j^2)}{2 k_{ji,0} m_i}\,, \tag{4.13}$$

in terms of the modified Källén function

$$\begin{aligned} &\lambda(k_{ji,0}^2, m_i^2, m_j^2) \\ &\quad = (k_{ji,0}^2 - (m_i + m_j)^2)(k_{ji,0}^2 - (m_j - m_j)^2 - \imath 0 k_{ji,0}(k_{ji,0}^2 + m_i^2 - m_j^2)\,. \end{aligned} \tag{4.14}$$

It is thus possible to bring the non-expanded propagator into the shape desired for integration through the identification $r_{ij} = -x_+$ or $r_{ij} = -x_+^{-1} = -x_-$. The advantage of the expansion is that it showcases the amplitude's analytic structure in the specific limit both in the integrand and in the integrated result. The

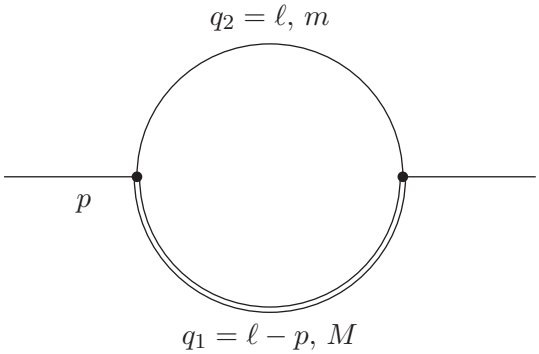

Figure 4.1: Scalar two-point function with internal masses $M > m$.

parameters found for those limits where a hard scale is available can be reproduced by expanding the poles $x_\pm$ and identifying r_{ij} accordingly. The appropriate choice between the potential divergences x_+ and x_- is the one whose absolute value is smaller than 1.

For the threshold expansion, identified through the definition $k^2_{ji,0} = (m_i + m_j)^2(1-\beta)$ one finds for the behavior of the pole positions in the limit $\beta \to 0^\pm$ that

$$x_\pm|_{\beta\to 0^\pm} = -\mathrm{sign}(k_{ji,0}) \left(1 \pm \sqrt{-\frac{m_j\,\beta}{m_i} - \imath 0 k_{ji,0}} + \mathcal{O}(\beta)\right) . \tag{4.15}$$

We can then deduce the correct r_{ij} and Q_i^2 parameters for the asymptotic threshold expansion and bring the dual propagator into the desired form of Eq. (4.8). With the rules layed out in this section it is thus straight-forward to write down the asymptotic expansion of the dual propagator for any kinematic limit.

In the following sections we will apply these general ideas to benchmark one-loop integrals, and will present their asymptotic expansions in several kinematical limits within the LTD formalism.

4.2 Asymptotic expansions of the scalar two-point function with two internal masses

A first benchmark application of the expansion of dual propagators is the asymptotic expansion of the scalar two-point function with two different internal masses. This is represented by the diagram in Fig. 4.1 and the corresponding amplitude

in the Feynman representation is

$$\mathcal{A}^{(1)} = \int_\ell G_F(q_1; M)\, G_F(q_2; m)\,, \tag{4.16}$$

with $q_1 = \ell - p$ and $q_2 = \ell$. The calculation of this amplitude in the context of DREG has already been discussed in Section 1.2 and in Section 2.3, where its analytic structure has been exposed. The momentum flow, assuming $p_0 > 0$, has been chosen specifically to avoid the appearance of non-causal or unphysical singularities. As seen, these types of integrand singularities, if they appear, always cancel in the sum of dual amplitudes.

We are interested in the asymptotic expansion of the renormalized amplitude, which is well defined in four spacetime dimensions at integrand-level

$$\mathcal{A}^{(1,R)} = \mathcal{A}^{(1)} - \mathcal{A}^{(1)}_{\rm UV}\Big|_{d=4}\,. \tag{4.17}$$

Here $\mathcal{A}^{(1)}_{\rm UV}$ is a local UV counterterm that suppresses the singular behavior of the unintegrated amplitude for large loop momenta, determined as described in Section 2.5.1. Its Feynman and dual representations are given by

$$\mathcal{A}^{(1)}_{\rm UV} = \int_\ell (G_F(\ell; \mu_{\rm UV}))^2 = \int_\ell \frac{\tilde{\delta}\,(\ell; \mu_{\rm UV})}{2\left(\ell^{(+)}_{0,\rm UV}\right)^2}\,, \quad \ell^{(+)}_{0,\rm UV} = \sqrt{\boldsymbol{\ell}^2 + \mu^2_{\rm UV}}\,, \tag{4.18}$$

where $\mu_{\rm UV}$ is an arbitrary scale. Its integrated form takes the shape

$$\mathcal{A}^{(1)}_{\rm UV} = \frac{\Gamma(1+\epsilon)}{(4\pi)^{2-\epsilon}}\,\frac{1}{\epsilon}\,\left(\frac{\mu^2_{\rm UV}}{\mu^2}\right)^{-\epsilon}\,, \tag{4.19}$$

and implements the standard $\overline{MS}$ renormalization scheme when identifying the parameter $\mu_{\rm UV}$ with the DREG renormalization scale μ. The full analytic expression of the renormalized scalar two-point function is well known through standard techniques

$$\begin{aligned}\mathcal{A}^{(1,R)} = \frac{1}{16\pi^2}\Bigg[2 &+ \frac{p^2 + M^2 - m^2}{2p^2}\log\left(\frac{\mu^2_{\rm UV}}{M^2}\right) + \frac{p^2 + m^2 - M^2}{2p^2}\log\left(\frac{\mu^2_{\rm UV}}{m^2}\right) \\ &+ \frac{\lambda^{1/2}\left(p^2, m^2, M^2\right)}{p^2}\log\left(\frac{m^2 + M^2 - p^2 + \lambda^{1/2}\left(p^2, m^2, M^2\right)}{2mM}\right)\Bigg]\,,\end{aligned} \tag{4.20}$$

which is symmetric under the exchange $m \leftrightarrow M$. This expression will be used to check the validity of the asymptotic expansions presented in the next sections.

4.2.1 Master asymptotic expansion

The dual representation of the renormalized scalar two-point function (Eq. (4.17)) is given by

$$\mathcal{A}^{(1,R)} = -\int_\ell \Bigg[\tilde{\delta}\,(q_1;M)\;G_D(q_1;\ell) + \tilde{\delta}\,(\ell;m)\;G_D(\ell;q_1) + \frac{1}{2}\,\tilde{\delta}\,(\ell;\mu_{\mathrm{UV}})\;\left(\ell_{0,\mathrm{UV}}^{(+)}\right)^{-2}\Bigg] = \int_0^\infty \mathrm{d}|\boldsymbol{\ell}|\;a(\boldsymbol{\ell})\,, \tag{4.21}$$

where the appearing dual propagators are

$$G_D(q_1;\ell) = \frac{1}{2q_1\cdot p + p^2 - m^2 + M^2 - \imath 0\, p_0}\,, \tag{4.22}$$

$$G_D(\ell;q_1) = \frac{1}{-2\ell\cdot p + p^2 + m^2 - M^2 + \imath 0\, p_0}\,. \tag{4.23}$$

Setting $p = (p_0, \mathbf{0})$ with $p_0 > 0$, the on-shell energies and scalar products are $q_{1,0}^{(+)} = \sqrt{\boldsymbol{\ell}^2 + M^2}$, $\ell_0^{(+)} = \sqrt{\boldsymbol{\ell}^2 + m^2}$, $q_1\cdot p = q_{1,0}^{(+)} p_0$ and $\ell\cdot p = \ell_0^{(+)} p_0$. With this choice of reference frame the dual representation and its asymptotic expansion are particularly convenient as the integrand no longer has any angular dependence. We have reproduced the renormalized result through direct integration of Eq. (4.21).

The general propagator expansion of Eq. (4.3) can be applied directly to the propagators of this amplitude and gives the general expanded integrand as

$$\mathcal{A}^{(1,R)} = -\frac{1}{16\pi^2}\left[\sum_{i,j=1,2}\frac{m_i^2}{Q_i^2}\sum_{n=0}^{\infty}\left(-\frac{\Delta_{ij}}{Q_i^2}\right)^n I^{(n)}(r_{ij},m_i) + I_{\mathrm{UV}}(\mu_{\mathrm{UV}})\right], \tag{4.24}$$

where $m_1 = M$ and $m_2 = m$. The remaining integrals are contained in

$$I^{(n)}(r_{ij},m_i) = \lim_{\Lambda\to\infty}\int_1^{\frac{\Lambda+\sqrt{\Lambda^2+m_i^2}}{m_i}} \mathrm{d}x\;\frac{(x^2-1)^2\,x^{-3}}{[(x+r_{ij})\,(x^{-1}+r_{ij})]^{n+1}}\,, \tag{4.25}$$

and

$$I_{\mathrm{UV}}(\mu_{\mathrm{UV}}) = \lim_{\Lambda\to\infty}\int_1^{\frac{\Lambda+\sqrt{\Lambda^2+\mu_{\mathrm{UV}}^2}}{\mu_{\mathrm{UV}}}} \mathrm{d}x\;\frac{2(x^2-1)^2\,x^{-1}}{(x^2+1)^2}\,. \tag{4.26}$$

We have introduced a cutoff Λ because the individual contributions are still singular in the UV. The sum of all of them is UV finite, however. Therefore, we

can safely work in four spacetime dimensions and then take the limit $\Lambda \to \infty$ after integration. Notice that the cutoff is a valid regulator because it acts on the Euclidean space of the loop three-momentum. The results of these integrals, up to order $n = 2$, are given by

$$\begin{aligned} I^{(n)}(r_{ij}, m_i) &\overset{n=0}{=} \lim_{\Lambda\to\infty} \left[\frac{2\Lambda}{m_i\, r_{ij}} - \left(1 + \frac{1}{r_{ij}^2}\right) \log\left(\frac{2\Lambda}{m_i}\right) + \left(1 - \frac{1}{r_{ij}^2}\right) \log\left(r_{ij}\right) \right] \\ &\overset{n=1}{=} \lim_{\Lambda\to\infty} \left[-\frac{1}{r_{ij}^2} \left(1 - \log\left(\frac{2\Lambda}{m_i}\right) - \frac{1 + r_{ij}^2}{1 - r_{ij}^2} \log\left(r_{ij}\right)\right)\right] \\ &\overset{n=2}{=} \frac{1}{\left(1 - r_{ij}^2\right)^2} \left(\frac{1 + r_{ij}^2}{2r_{ij}^2} + \frac{2}{1 - r_{ij}^2} \log\left(r_{ij}\right)\right) \end{aligned} \tag{4.27}$$

and

$$I_{\mathrm{UV}}(\mu_{\mathrm{UV}}) = \lim_{\Lambda\to\infty} \left[2 \log\left(\frac{2\Lambda}{\mu_{\mathrm{UV}}}\right) - 2 \right] . \tag{4.28}$$

A noteworthy feature of this expansion is that the UV divergence lessens with each order in the expansion. Indeed, all the contributions with $n \geq 2$ are UV finite, and can be calculated directly by extending the upper limit of the integral to infinity. The linearly UV divergent terms appearing at $n = 0$ cancel between the two dual amplitudes and the logarithmic dependence on the UV cutoff Λ of both terms at $n = 0$ and $n = 1$ is canceled by the UV counterterm. Since these cancellations happen locally in momentum space, numerical integration in the UV limit is straightforward.

Still without having to specify the kinematic limit to be considered, the integrated version of the asymptotic expansion of the renormalized amplitude then takes the general form

$$\mathcal{A}^{(1,R)} = \frac{1}{16\pi^2} \sum_{i,j} \left[2 + c_{0,i} \log\left(\frac{\mu_{\mathrm{UV}}}{m_i}\right) + \sum_{k=0}^{\infty} \left(c_{1,i}^{(k)} + c_{2,i}^{(k)} \log\left(r_{ij}\right)\right) \right] . \tag{4.29}$$

The coefficient $c_{0,i}$ is given by

$$c_{0,i} = \frac{m_i^2}{Q_i^2} \left(1 + \frac{1}{r_{ij}^2} \left(1 + \frac{\Delta_{ij}}{Q_i^2}\right)\right) = \frac{p^2 + m_i^2 - m_j^2}{p^2} , \tag{4.30}$$

and the coefficients $c_{1,i}^{(k)}$ and $c_{2,i}^{(k)}$ needed for the first few orders of the expansion

Table 4.1: The coefficients of the asymptotic expansions for the scalar two-point function in different kinematical limits. For the threshold limit the identification $p^2 = (m+M)^2(1-\beta)$ is made.

	$M^2 \gg \{m^2, p^2\}$	$p^2 \gg \{m^2, M^2\}$	$\beta \to 0^{\pm}$
$G_D(q_1;\ell)$			
Γ_{12}	M^2+p^2	p^2+M^2	$2Mp\,\cosh\left(\sqrt{-\frac{m\,\beta}{M}-\imath 0}\right)$
Δ_{12}	$-m^2$	$-m^2$	$p^2+M^2-m^2-\Gamma_{12}$
r_{12}	$\frac{\sqrt{p^2}}{M}$	$\frac{M}{\sqrt{p^2}}$	$\exp\left(\sqrt{-\frac{m\,\beta}{M}-\imath 0}\right)$
Q_1^2	M^2	p^2	$M\,p\,\exp\left(-\sqrt{-\frac{m\,\beta}{M}-\imath 0}\right)$
$G_D(\ell;q_1)$			
Γ_{21}	$-M^2-\frac{m^2\,p^2}{M^2}$	p^2+m^2	$2m\,p\,\cosh\left(\sqrt{-\frac{M\,\beta}{m}+\imath 0}\right)$
Δ_{21}	$p^2+m^2+\frac{m^2\,p^2}{M^2}$	$-M^2$	$p^2+m^2-M^2-\Gamma_{21}$
r_{21}	$\frac{m\sqrt{p^2}}{M^2}$	$-\frac{m}{\sqrt{p^2}}+\imath 0$	$-\exp\left(\sqrt{-\frac{M\,\beta}{m}+\imath 0}\right)$
Q_2^2	$-M^2$	p^2	$m\,p\,\exp\left(-\sqrt{-\frac{M\,\beta}{m}+\imath 0}\right)$

are given by

$$
\begin{aligned}
c_{1,i}^{(k)} &= -\frac{m_i^2}{Q_i^2}\left\{0, \frac{-\Delta_{ij}}{Q_i^2}\frac{-1}{r_{ij}^2}, \left(\frac{-\Delta_{ij}}{Q_i^2}\right)^2 \frac{1+r_{ij}^2}{2r_{ij}^2(1-r_{ij}^2)^2}, \left(\frac{-\Delta_{ij}}{Q_i^2}\right)^3 \frac{1+10r_{ij}^2+r_{ij}^4}{6r_{ij}^2(1-r_{ij}^2)^4}\right\},\\
c_{2,i}^{(k)} &= -\frac{m_i^2}{Q_i^2}\left\{1-\frac{1}{r_{ij}^2}, \frac{-\Delta_{ij}}{Q_i^2}\frac{1+r_{ij}^2}{r_{ij}^2(1-r_{ij}^2)}, \left(\frac{-\Delta_{ij}}{Q_i^2}\right)^2 \frac{2}{(1-r_{ij}^2)^3},\right.\\
&\qquad\qquad \left.\left(\frac{-\Delta_{ij}}{Q_i^2}\right)^3 \frac{2(1+r_{ij}^2)}{(1-r_{ij}^2)^5}\right\}.
\end{aligned}
\tag{4.31}
$$

Each term of the expansion is suppressed by extra powers of Δ_{ij}. The n-th

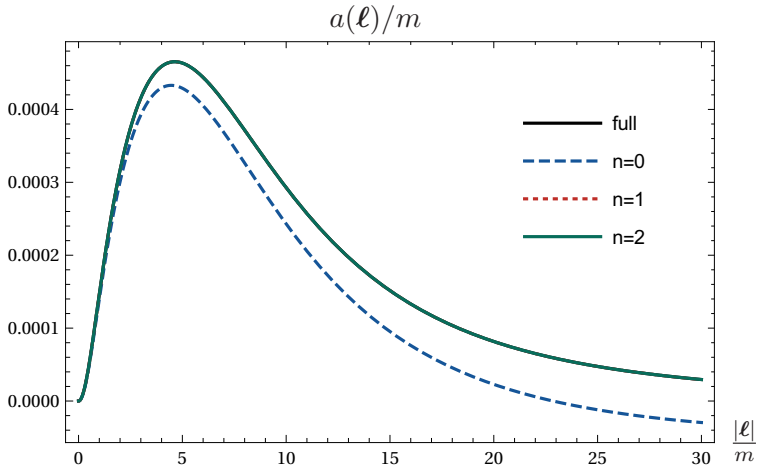

Figure 4.2: The convergence behavior of the integrand-level large-mass expansion of the scalar two-point function in Eq. (4.24) for $M/m = 10$, $p^2/m^2 = 3$ and $\mu_{\mathrm{UV}} = M$.

renormalized order of the integrated expansion, starting at $n = 1$, is given by

$$\mathcal{A}_{(n)}^{(1,R)} = \frac{1}{16\pi^2} \sum_{i,j} \left[2 + c_{0,i} \log\left(\frac{\mu_{\mathrm{UV}}}{m_i}\right) + \sum_{k=0}^{n} \left(c_{1,i}^{(k)} + c_{2,i}^{(k)} \log\left(r_{ij}\right) \right) \right]. \tag{4.32}$$

The order $n = 0$, while possible to consider at integrand-level in the low-energy regime, is not fully renormalized and thus is not considered in the integrated expansion.

4.2.2 Asymptotic expansions for different kinematical limits

We now consider explicitly different kinematical limits and the corresponding asymptotic expansions. In all the numerical evaluations of this chapter the smaller mass is set to $m = 1\,\mathrm{GeV}$ for simplicity. In the limit of one large mass, $M^2 \gg \{m^2, p^2\}$, the expansion parameters, as obtained by following Section 4.1, are $Q_1^2 = -Q_2^2 = M^2$, $r_{12} = \sqrt{p^2}/M$, and $r_{21} = m\sqrt{p^2}/M^2$. The functions Γ_{ij} and Δ_{ij} are summarized in Table 4.1. For the values $M/m = 10$ and $p^2/m^2 = 3$, and setting the renormalization scale $\mu_{\mathrm{UV}} = M$, the relative error at integrand-level of each dual contribution separately lies below 10^{-3} (10^{-4}) for $n = 1$ ($n = 2$) for the whole range of the loop momentum. The convergence of the integrand can be seen in Fig. 4.2. For the integrated result the relative error is 2.7% at first

Table 4.2: The values obtained through integration of the expansion Eq. (4.32) in the large mass limit and their relative errors with respect to the full result 0.006 127 7 with the parameters $M/m = 10$, $p^2/m^2 = 3$ and $\mu_{\mathrm{UV}} = M$.

	integrated result	rel. error
$n = 1$	0.005 963 8	2.7 %
$n = 2$	0.006 125 4	0.038 %
$n = 3$	0.006 127 7	0.000 76 %

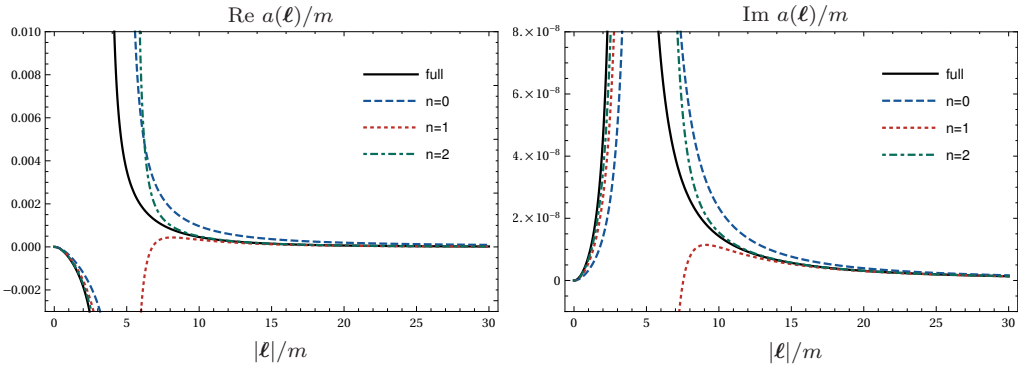

Figure 4.3: The convergence behavior of the integrand-level expansion in the limit of a large external momentum of the scalar two-point function in Eq. (4.24) for $\sqrt{p^2}/m = 10$, $\sqrt{p^2}/M = 2$, $\mu_{\mathrm{UV}} = M$ and $\imath 0 = \imath 10^{-3}$.

renormalized order in the expansion ($n = 1$) and decreases to 0.04% for $n = 2$. Results for the first three orders are given in Table 4.2.

With the limit of a large external momentum, $p^2 \gg \{m^2, M^2\}$, a scenario above threshold has been just as successful. The election of the expansion parameters for this case is also summarized in Table 4.1. Since this kinematical configuration is above threshold the asymptotic expansion should feature an imaginary part just as the original integral. The imaginary part is generated through $\log(r_{21})$, with $r_{21} = -m/\sqrt{p^2} + \imath 0$ where the positive imaginary part accounts for the correct Riemann sheet. As can be seen in Fig. 4.3, using the parameters $\sqrt{p^2}/m = 10$, $\sqrt{p^2}/M = 2$, $\mu_{\mathrm{UV}} = M$ and $\imath 0 = \imath 10^{-3}$, the integrand-level convergence is given for all values of the integration momentum that do not lie in the direct vicinity of the singularity whose general behavior and posi-

Table 4.3: The values obtained through integration of the expansion Eq. (4.32) in the limit of a large external momentum and their relative errors with respect to the full result $0.007\,92 + 0.014\,59\imath$ with the parameters $\sqrt{p^2}/m = 10$, $\sqrt{p^2}/M = 2$, $\mu_{\mathrm{UV}} = M$.

	integrated result		rel. error	
	Re	Im	Re	Im
$n = 1$	0.008 12	0.014 62	2.5 %	0.24 %
$n = 2$	0.007 94	0.014 60	0.20 %	0.061 %
$n = 3$	0.007 92	0.014 59	0.023 %	0.016 %

tion is reproduced. The convergence of the integrated expansions is provided in Table 4.3.

A more involved kinematic scenario is given by expansions around the unitarity threshold, which is identified by

$$\beta = 1 - p^2/(m+M)^2 \to 0^{\pm}\,. \tag{4.33}$$

This involves two separate limits, with the limit $\beta \to 0^+$ approaching the threshold from below and $\beta \to 0^-$ approaching the threshold from above. Since the integrand in the second case contains a physical threshold singularity it is evident that an accurate description of the singularity in the expansion is essential. However, the behavior of the amplitude is deeply affected by the threshold singularity even below the threshold. This can be understood by considering the position of the singularity in the diverging propagator

$$G_D(\ell; q_1) = -\frac{x}{m(m+M)\sqrt{1-\beta}\left((x - x_{\mathrm{div}}^{(+)})(x - x_{\mathrm{div}}^{(-)})\right)}\,, \tag{4.34}$$

where the loop momentum is parameterized as $|\boldsymbol{\ell}| = M/2(x - x^{-1})$ and the integrand diverges for

$$x \to x_{\mathrm{div}}^{(\pm)} = \frac{1}{\sqrt{1-\beta}}\frac{m+M}{2m}\left(\frac{2m}{m+M} - \beta \pm \sqrt{\beta\left(\beta - \frac{4mM}{(m+M)^2}\right)}\right)\,. \tag{4.35}$$

Note that $x_{\mathrm{div}}^{(+)} = (x_{\mathrm{div}}^{(-)})^{-1}$.

After the variable change the integration over x goes along $[0, \infty)$. When evaluating the amplitude below the unitarity threshold, $\beta > 0$, both $x_{\mathrm{div}}^{(+)}$ and

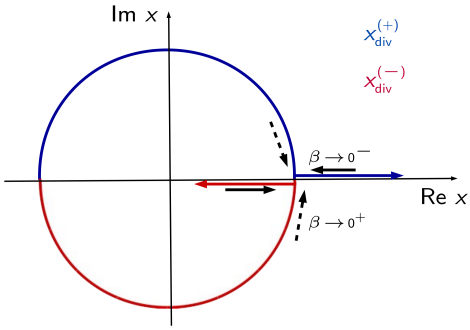

Figure 4.4: The position of the singularities of the unexpanded dual propagator in terms of the threshold parameter $\beta = 1 - p^2/(m+M)^2$ after the change of variable $|\boldsymbol{\ell}| = M/2\,(x - x^{-1})$. The integration path goes from the point where the singularities reach the real axis until infinity.

$x_{\text{div}}^{(-)}$ are complex numbers and thus do not lead to a divergence on the path of integration. Both pole positions become real above the threshold, $\beta < 0$, but while $x_{\text{div}}^{(-)} < 1$ the second pole position $x_{\text{div}}^{(+)}$ is larger than 1 and thus lies within the integration range. When approaching the unitarity threshold at $\beta = 0$ both pole positions move towards the starting point of the integration at $x = 1$, as illustrated in Fig. 4.4. Evaluating the integral when approaching the threshold from below thus means that both complex poles lie very close to the start point of the integration and have a significant influence on the integrand. Not taking into account the poles explicitly while defining an expansion in this limit can lead to a severely distorted expanded integrand and should be avoided. For both limits it is thus essential to define the expansion parameters through an expansion of the pole positions as given for a generic limit in Eq. (4.15).

Close to the unitary threshold the pole positions are well approximated by a Taylor expansion in β as

$$x_{\text{div}}^{(\pm)}\Big|_{\beta\to 0} = 1 \pm \sqrt{\frac{M}{m}}\sqrt{-\beta} - \frac{M}{2m}\beta + \mathcal{O}(\beta^{3/2})\,, \tag{4.36}$$

allowing to identify

$$r_{21} = -\,x_{\text{div}}^{(-)}\Big|_{\beta\to 0} = -1 + \sqrt{\frac{M}{m}}\sqrt{-\beta} + \imath 0\,, \tag{4.37}$$

such that $|r_{21}| < 1$ is guaranteed. Q_2^2 follows by applying Eq. (4.9). The first dual propagator $G_D(q_1;\ell)$ is free of threshold singularities and thus the simple choice

Table 4.4: The values obtained through integration of the expansion Eq. (4.32) in the threshold limit from below (above), the relative error of the real part with respect to the full result $0.011\,46$ $(0.015\,259\,9 + 0.005\,27i)$ and the ratio between real and imaginary part. The parameters used are $M/m = 3$, $\beta = \pm 0.1$ and $\mu_{\mathrm{UV}} = M$.

$\beta > 0$	integrated result		error	
	Re	Im	rel. error Re	Im/Re
$n = 1$	$0.011\,64$	$0.000\,141$	$1.5\,\%$	0.012
$n = 2$	$0.011\,42$	$0.000\,041$	$0.38\,\%$	0.0036
$n = 3$	$0.011\,45$	$-0.000\,017$	$0.11\,\%$	-0.0015
$\beta < 0$	integrated result		rel. error	
	Re	Im	Re	Im
$n = 1$	$0.015\,295\,0$	$0.005\,65$	$0.23\,\%$	$7.1\,\%$
$n = 2$	$0.015\,260\,9$	$0.005\,40$	$0.0067\,\%$	$2.5\,\%$
$n = 3$	$0.015\,259\,9$	$0.005\,32$	$0.000\,30\,\%$	$0.95\,\%$

$Q_1^2 = p^2$ is sufficient, leading to $r_{21} = m/\sqrt{p^2}$. The expressions obtained thus for the parameters can be used both when approaching the threshold from below and from above. In the latter the complex logarithm produces an imaginary part which is canceled by the also complex coefficients such that a real amplitude is obtained, except for a small imaginary part that goes to zero quickly when increasing the precision of the expansion. The convergence behavior of the integrands is shown in Fig. 4.5. Good convergence of the integrated expansion is achieved both for the limit below and the one above threshold. The relative error of the real part of the result for $\beta = -0.1$ ($\beta = 0.1$) is $0.23\,\%$ ($1.5\,\%$) for $n = 1$ and 7×10^{-5} ($0.38\,\%$) for $n = 2$. The imaginary part in the expansion below threshold converges towards zero with the ratio of imaginary over real part being 0.012 at $n = 1$ and 0.0036 at $n = 2$. The relative error of the imaginary part in the expansion above threshold is $7.1\,\%$ at $n = 1$ and $2.5\,\%$ at $n = 2$. All numeric values for the expansion orders $n \in [0, 4]$ are summarized in Table 4.4. The errors obtained through this expansion can be reduced by various orders of magnitude by including one more order in the expansion of the singularity: $r_{21} = -1 + \sqrt{M/m}\sqrt{-\beta} + M/(2m)\beta$. Numerical results for this variation are given in Appendix B, Fig. B.1 and Table B.1.

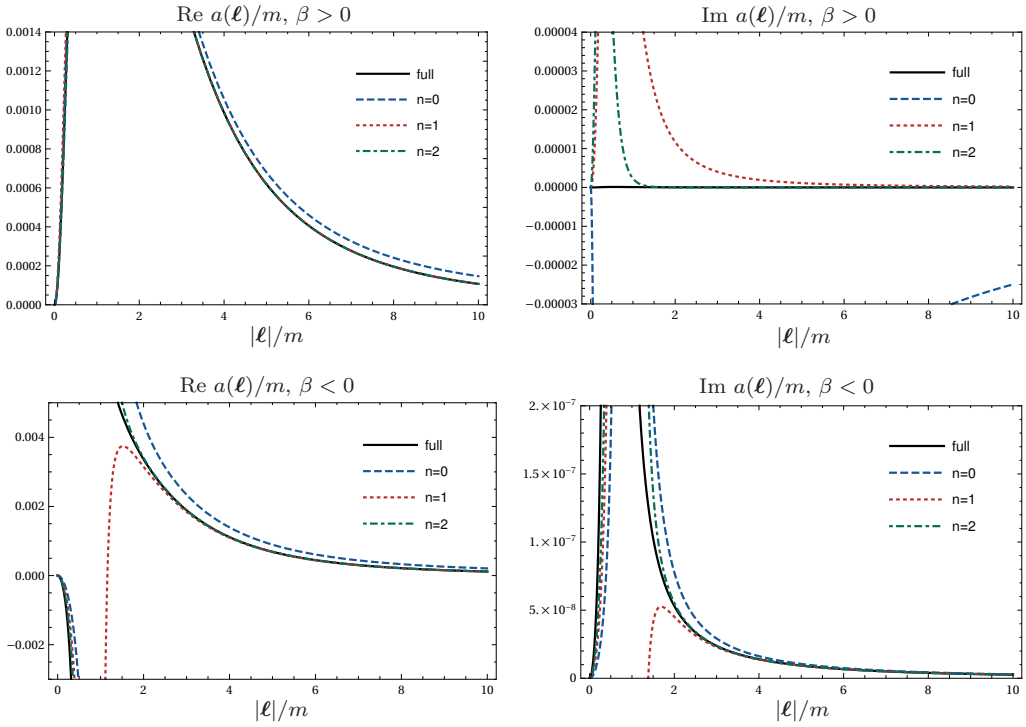

Figure 4.5: The convergence behavior of the integrand-level expansion in the threshold limit of the scalar two-point function in Eq. (4.24) for $M/m = 3$. In the upper row the integrand is shown for the expansion below the unitarity threshold, $\beta = 0.1$, and in the lower row above threshold, $\beta = -0.1$. Evaluation with $\mu_{\mathrm{UV}} = M$ and $\imath 0 = \imath 10^{-4}$.

It may be noted that the more precise formulation of r_{21} coincides with the first orders of a different expansion:

$$-\exp\left[-\sqrt{\frac{M}{m}}\sqrt{-\beta}\right] = -1 + \sqrt{\frac{M}{m}}\sqrt{-\beta} + \frac{M}{2m}\beta + \mathcal{O}(\beta^{3/2})\,. \tag{4.38}$$

We thus identify $\log(-r_{21}) = -\sqrt{M/m}\sqrt{-\beta+\imath 0}$, define symmetrically $\log(r_{12}) = \sqrt{m/M}\sqrt{-\beta-\imath 0}$ and derive the remaining expansion parameters therefrom. These are summarized in Table 4.1. This compact result is thus obtained by exponentiating the expanded expression determining the position of the threshold in the complex plane given by Eq. (4.15). Note that going beyond the formalism

Table 4.5: The values obtained through integration of the expansion Eq. (4.32) in the threshold limit from below (above) using exponentiated parameter, the relative error of the real part with respect to the full result 0.011 46 $(0.015\,259\,9 + 0.005\,272\,87\imath)$. The parameters used are $M/m = 3$, $\beta = \pm 0.1$ and $\mu_{\mathrm{UV}} = M$.

$\beta > 0$	integrated result		error
	Re	Im	rel. error Re
$n = 1$	0.011 458 8	-2.9×10^{-19}	0.033 %
$n = 2$	0.011 462 7	-5.7×10^{-18}	0.0011 %
$n = 3$	0.011 462 6	2.2×10^{-16}	4.9×10^{-7}

$\beta < 0$	integrated result		rel. error	
	Re	Im	Re	Im
$n = 1$	0.015 260 0	0.005 275 26	5.6×10^{-6}	0.045 %
$n = 2$	0.015 259 9	0.005 272 95	1.0×10^{-8}	0.0015 %
$n = 3$	0.015 259 9	0.005 272 87	2.5×10^{-11}	6.1×10^{-7}

described in Section 4.1 through exponentiation is not necessary for obtaining a convergent expression, as seen above, but it facilitates a simpler and more intuitive understanding of the expansion. The expressions for Δ_{ij} and Q_i^2 fulfill the necessary asymptotic behavior as

$$\frac{m_i^2}{Q_i^2} = \frac{m_i}{m+M} + \mathcal{O}(\beta^{1/2})\,, \qquad \frac{\Delta_{ij}}{Q_i^2} = \mathcal{O}(\beta^2)\,. \tag{4.39}$$

The first dual propagator $G_D(q_1;\ell)$ is free of threshold singularities and leads to a real expansion independently of the sign of β. The expressions obtained for both r_{12} and r_{21} are valid both when approaching the threshold from below and from above because the infinitesimal imaginary component accompanying β is fixed by the complex prescription of the dual propagators. As can be seen in Fig. 4.6 the integrand-level convergence is significantly improved through exponentiating the parameters r, especially in the real part. Also the integrated results are moved closer towards the full result as can be seen in Table 4.5. Note especially, that the imaginary parts of the expanded result below threshold are in the order of magnitude of numerical fluctuations and an effectively real result is generated.

In all the kinematical regions studied, we have achieved the asymptotic ex-

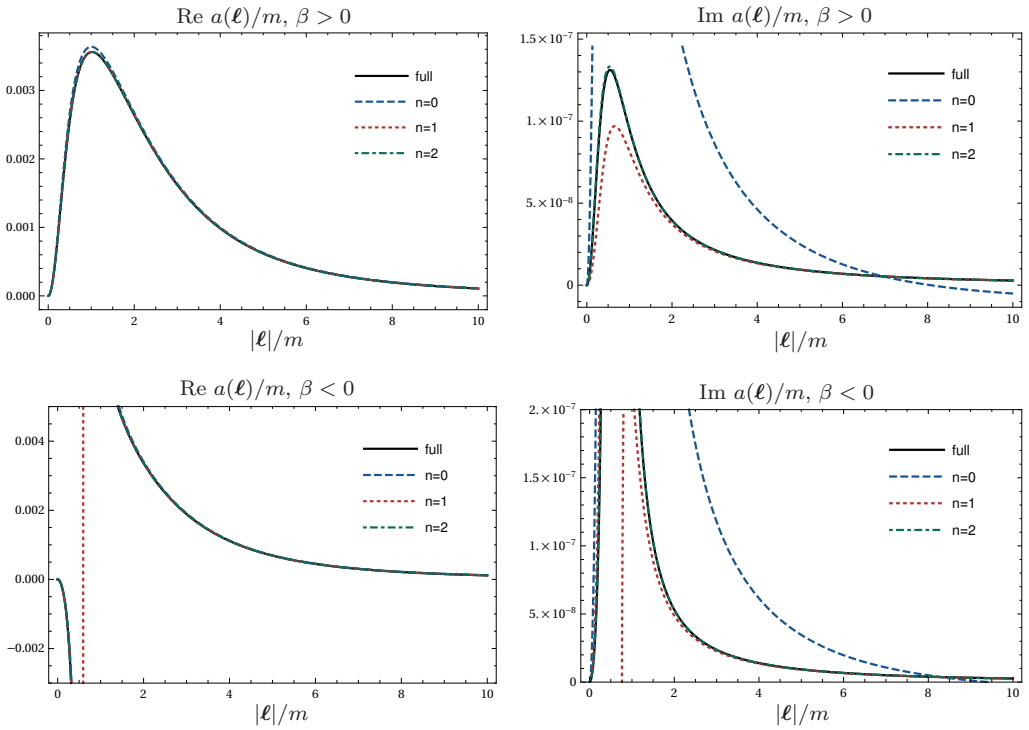

Figure 4.6: The convergence behavior of the integrand-level expansion in the threshold limit of the scalar two-point function in Eq. (4.24) for $M/m = 3$, using exponentiated parameters. In the upper row the integrand is shown for the expansion below the unitarity threshold, $\beta = 0.1$, and in the lower row above threshold, $\beta = -0.1$. Evaluation with $\mu_{\mathrm{UV}} = M$ and $\imath 0 = \imath 10^{-4}$.

pansions by conveniently selecting the expansion parameters that are used in the master expression, Eq. (4.29), which describes all these limits at once. In each limit fast convergence was achieved both at integrand- and at integral-level.

4.2.3 Comparison with *Expansion by Regions*

It is of interest to see how the expansions developed above hold up in comparison with the established method of Expansion by Regions (EbR) [58–65]. Within this successful method the integrand of the Feynman amplitude, written in terms of Minkowski momenta, is expanded by dividing the space of the loop momenta into distinct regions. In each region, the integrand is expanded into a Taylor

series with respect to the parameters considered small therein. Consecutively, the expanded integrands are integrated over the whole integration domain, not just within the region where the expansion was justified. The scaleless integrals that may appear are set to zero as commonly done within DREG. While Expansion by Regions has been successful for many types of amplitudes a general proof of validity is still pending. One may raise a few issues with the procedure above which will be mentioned in the context of its application to the scalar two-point function in Eq. (4.16). We center the discussion on the limit of one large mass, $M^2 \gg \{m^2, p^2\}$.

While in a general loop integral many types of regions can appear, in this particular example there are only two regions, the hard region with $\ell \sim M$ and the soft region with $\ell \sim \{m, \sqrt{p^2}\}$[1]. The scalar product between the loop momentum and the external momentum inherits the scaling of the momentum itself, that is for the hard region one performs the replacements

$$\{\ell^2, M^2\} \to \lambda^2 \, \{\ell^2, M^2\} \,, \qquad p \cdot \ell \to \lambda \, p \cdot \ell \,, \tag{4.40}$$

and expands for $\lambda \to \infty$. The assumed relationship between the large loop momentum and both its square and its scalar products does not account for cancellations between the energy component and the spatial components which will take place when integrating over the unrestricted components of the loop momentum. The Taylor series with the prescriptions above and comparable ones for the soft region leads to the expanded integrands

$$\begin{aligned} \mathcal{A}^{(1)}_{\text{hard}} = \int_\ell \left(\frac{1}{\ell^2} + \frac{m^2}{(\ell^2)^2} + \frac{m^4}{(\ell^2)^3} + \dots \right) \\ \cdot \left(\frac{1}{\ell^2 - M^2} + \frac{2p\cdot\ell - p^2}{(\ell^2 - M^2)^2} + \frac{4(p\cdot\ell)^2 + p^2}{(\ell^2 - M^2)^3} + \dots \right) , \end{aligned} \tag{4.41}$$

$$\begin{aligned} \mathcal{A}^{(1)}_{\text{soft}} = \int_\ell \frac{1}{\ell^2 - m^2} \\ \cdot \left(-\frac{1}{M^2} - \frac{(p-\ell)^2}{M^4} - \frac{(p-\ell)^4}{M^6} + \dots \right) . \end{aligned} \tag{4.42}$$

The first order of the expansion at integrated level is achieved by combining the UV counterterm with the first term appearing in the hard region

$$\int_\ell \frac{1}{\ell^2(\ell^2 - M^2)} - \mathcal{A}^{(1)}_{\text{UV}} = \frac{1 - \log\left(\frac{M^2}{\mu^2_{\text{UV}}}\right)}{16\pi^2} + \mathcal{O}(\epsilon) \,. \tag{4.43}$$

[1] To be precise, the scaling is assumed for the momentum in the *Euclidean sense*, i.e. $|\ell| = \sqrt{\ell_0^2 + \boldsymbol{\ell}^2}$.

The soft region does not contribute at this order. For the next order one must select all terms in the expansion at integrand-level which will lead to contributions of order M^{-2}. This includes the first term of the expansion in the soft region and three terms from the hard region. The result achieved in this way is indeed the Taylor series ($\mathcal{T}$) of the full result

$$\mathcal{T}\mathcal{A}^{(1,R)}(M,\infty) = \frac{1}{16\pi^2}\left(1 - \log\left(\frac{M^2}{\mu_{\rm UV}^2}\right) + \frac{p^2 - 2m^2\log\left(\frac{M^2}{m^2}\right)}{2M^2} + \dots\right). \quad (4.44)$$

In direct comparison, we give here the first renormalized order of the series achieved through the general expansion of the dual propagator Eq. (4.32) in the limit of one large mass:

$$\mathcal{A}_{n=1}^{(1,R)} = \frac{1}{16\pi^2}\left(1 - \log\left(\frac{M^2}{\mu_{\rm UV}^2}\right) - \frac{m^2}{M^2}\right. \quad (4.45)$$
$$\left. - \frac{m^2(M^2+m^2+p^2)}{M^4 - m^2p^2}\log\left(\frac{M^2}{m^2}\right) + \frac{m^2((p^2)^2 - m^2M^2)}{(M^2-p^2)(M^4-m^2p^2)}\log\left(\frac{M^2}{p^2}\right)\right).$$

By including the next term of the expansion ($n = 2$) and then expanding the rational coefficients for $M^2 \gg \{m^2, p^2\}$, we recover the expected Taylor series. Higher terms of the Taylor series can be obtained by including more terms in the dual expansion, $n \geq 3$. The asymptotic expansions in Eq. (4.44) and Eq. (4.45) display the same logarithmic dependence, although they differ in the rational coefficients accompanying the logarithms, which partially encode higher orders in the expansion. This is due to the fact that Δ_{12} includes subleading terms. The expression in Eq. (4.45) also contains a logarithmic dependence on $\log\left(M^2/p^2\right)$, which is formally one order higher than Eq. (4.44) and cancels when more orders in the dual expansion are included.

The relative error obtained by the two expansions with respect to the full result, Eq. (4.20), is numerically of the same order of magnitude. For the values of $M = 10m$, $p^2 = 3m^2$ and $\mu_{\rm UV} = M$ the relative error obtained including only the leading term in EbR is 3.3% compared to the 2.7% obtained by expanding the dual propagator as described above. Including one more order in the expansion the results are given by 0.14% and 0.038%, respectively. The comparison of the results obtained in EbR with those based on the expansion of the dual propagator is summarized in Table 4.6, demonstrating that the results of EbR can be exactly reproduced through the expansion of the coefficients in Eq. (4.29) whenever sufficient terms in the dual expansion have been included.

Table 4.6: The relative errors with respect to the full result of the dual expansion as given from Eq. (4.32) (both the direct result of this expansion and considering only the leading behavior of the coefficients at large M) compared with the result obtained through Expansion by Regions. Numerical evaluation with parameters $M = 10\,m$, $p^2 = 3\,m^2$, and $\mu_{\mathrm{UV}} = M$.

	G_D expansion	$\mathcal{O}(M^{-2})$	$\mathcal{O}(M^{-4})$		EbR
$n = 1$	2.67%	2.45%	2.68%	$\mathcal{O}(M^{-0})$	3.34%
$n = 2$	0.0375%	0.135%	0.0300%	$\mathcal{O}(M^{-2})$	0.135%
$n = 3$	$7.60 \cdot 10^{-6}$	0.135%	$6.18 \cdot 10^{-5}$	$\mathcal{O}(M^{-4})$	$6.18 \cdot 10^{-5}$

There is a distinction in the application of the two methods which we would like to emphasize. In EbR it is essential to consider the terms of the expansion at integrand-level to pick out only those which will contribute at a given order of the result. Failing to do so does not only lead to numerical differences but will generally lead to divergent results. This is due to the cancellation between UV and IR singularities appearing in the expansions of the soft and hard region. In contrast, UV renormalization within the method of expanding the dual propagators only involves the lowest orders of the integrand-level expansion. Including higher terms is optional for improving numerical precision and for this purpose it is possible to straight-forwardly include any amount of terms without needing to ensure cancellations between separate regions.

4.2.4 Asymptotic expansion by dual regions

The properties of dual amplitudes can also be exploited in a more direct way to facilitate asymptotic expansions. After applying LTD to the integrand of a Feynman integral the loop momentum is restricted to on-shell values. Thus, the direct expansion of the integrand into a Taylor series with respect to whichever scale is considered to be small or large is unambiguous. These asymptotic expansions can be done anywhere within the integration domain and depend on the size of the Euclidean loop three-momentum. For example, in the case of the two-point function in the limit of one large mass, $M^2 \gg \{m^2, p^2\}$, two regions in the loop three-momentum can be distinguished. One soft region with $\boldsymbol{\ell}^2 \ll M^2$, and one hard region with $\boldsymbol{\ell}^2 \gg \{m^2, p^2\}$ and $\boldsymbol{\ell}^2 \sim M^2$. We call these regions in the loop three-momentum *dual regions* because they become accessible only after obtaining a Euclidean integration domain through the application of LTD.

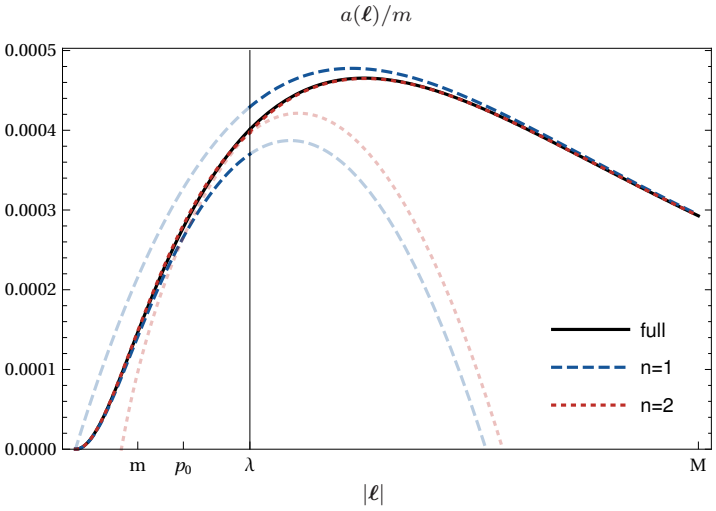

Figure 4.7: The convergence at integrand-level of the expansion given in Eq. (4.46) for the values $M = 10\,m$, $p^2 = 3\,m^2$, and $\mu_{\text{UV}} = M$.

The Euclidean integration domain can then be split up into two well-defined integrand-level expansions as

$$\begin{aligned}\mathcal{A}^{(1,R)} &= \int_0^\infty \mathrm{d}|\boldsymbol{\ell}|\; a(\boldsymbol{\ell}) \\ &= \int_0^\lambda \mathrm{d}|\boldsymbol{\ell}|\; \mathcal{T}a(M,\infty) + \int_\lambda^\infty \mathrm{d}|\boldsymbol{\ell}|\; \mathcal{T}a(\{\boldsymbol{\ell},M\},\infty)\,,\end{aligned} \tag{4.46}$$

where $a(\boldsymbol{\ell})$ is the unintegrated form of the renormalized amplitude defined in Eq. (4.21) and $m < \lambda < M$. The integrand-level convergence and the behavior around the matching scale λ is shown in Fig. 4.7.

Analytic integration of this type of expansion is straight-forward, as the integrand simplifies significantly. Including only the first order of the Taylor expansion in the soft region one obtains the result

$$\begin{aligned}\mathcal{A}^{(1,R)}_{\text{soft,n=0}} &= \int_0^\lambda \mathrm{d}|\boldsymbol{\ell}|\; \mathcal{T}_0\, a(M,\infty) \\ &= \frac{-2}{16\pi^2}\left(\frac{\lambda^3}{M^3} + \frac{m^2}{M^2}\mathrm{Sinh}\left(\frac{\lambda}{m}\right)^{-1} - \frac{\lambda m}{M^2}\sqrt{1+\frac{\lambda^2}{m^2}}\right)\,,\end{aligned} \tag{4.47}$$

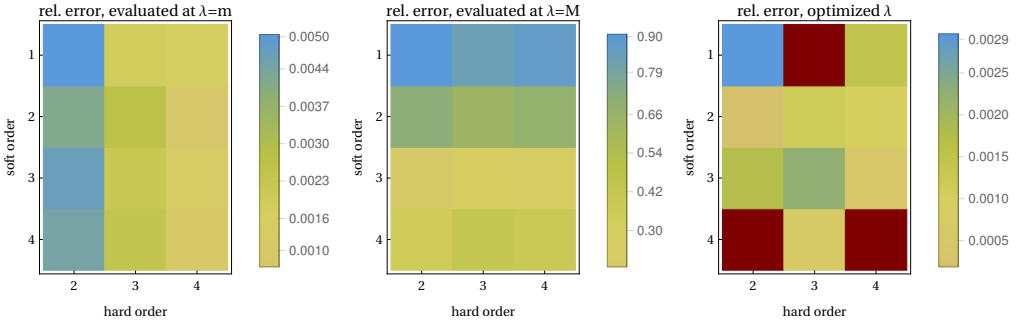

Figure 4.8: The relative error of the integrated expansion in Eq. (4.46), comparing the three scenarios of switching between soft and hard region at $\lambda = m$, $\lambda = M$ or by choosing the value of λ that corresponds to an extremum. The order of the expansion in the soft (hard) region is increased along the vertical (horizontal) axis. The values for the scales are $M = 10\,m$, $p^2 = 3\,m^2$, and $\mu_{\mathrm{UV}} = M$. In three combinations of integrand-level expansions the result did not have any extrema in λ and thus could not be optimized as per the method described, recognizable on the right by the dark red squares. Since the orders of the soft and the hard expansion can be chosen independently, one can easily avoid unfavorable combinations.

while in the hard region

$$\begin{aligned} \mathcal{A}^{(1,R)}_{\mathrm{hard,n=0}} &= \int_{\lambda}^{\infty} \mathrm{d}|\boldsymbol{\ell}|\; \mathcal{T}_0\, a(\{\boldsymbol{\ell}, M\}, \infty) \\ &= \frac{1}{16\pi^2}\left(1 - \frac{2\lambda^2}{M^2}\left(1 - \frac{1}{\sqrt{1+\frac{M^2}{\lambda^2}}}\right)\right) . \end{aligned} \tag{4.48}$$

Since adding additional orders to either expansion does not produce any artificial singularities, in contrast to the separate but interconnected expansions when applying EbR, any given order of the expansion in the soft region can be combined with any other order in the hard region. Very precise results can thus be achieved already at low orders in the expansion, as can be seen in Fig. 4.8 for the case of order 2 in both expansions. This property allows a more efficient use of numerical resources by using a precise expansion in the dual region with the most impact on the result while leaving the expansions in other dual regions with a very basic approximation.

The integrated results obtained by using Taylor expansions at integrand-level contribute to more than one order in M. Nonetheless, the Taylor series of the

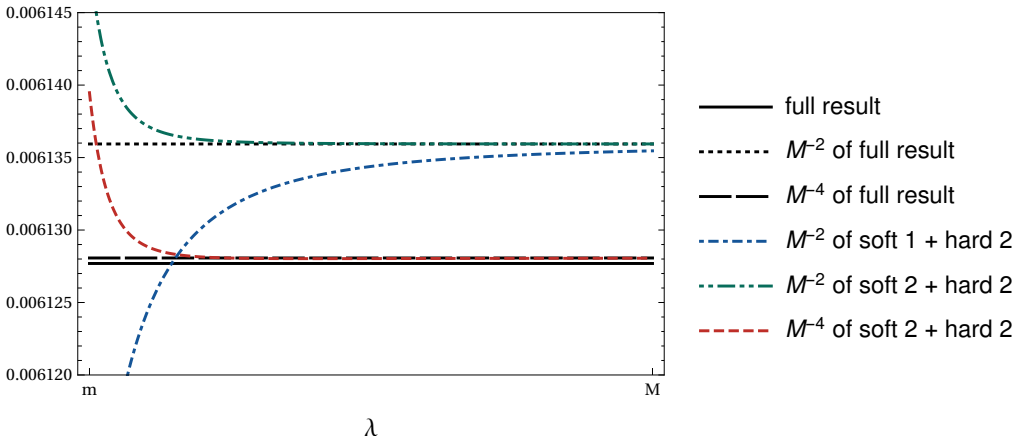

Figure 4.9: Recovery of the Taylor series of the full result for the scalar two-point function by applying an additional expansion to the *integrated* result of Eq. (4.46) at $M = 10\,m$, $p^2 = 3\,m^2$, and $\mu_{\mathrm{UV}} = M$.

full result, coinciding with the EbR result, can be recovered. To achieve this the integrated results, still depending on an undetermined λ, are to be expanded a second time for $M \to \infty$. As can be seen in Fig. 4.9 the Taylor series of the full result is then recovered by setting $\lambda = M$. The order M^x of the full result's Taylor series can be obtained as the order M^x of the integrated expansions whenever the soft and hard region's expansion have included sufficient terms to have introduced the order M^x in the result.

While the soft and hard regions depend on each other solely in terms of the matching scale, and the local renormalization is guaranteed in any case, a comparable accuracy in both regions requires to combine the $(n+1)$-th term of the hard region with the n-th term of the soft region. We consider this combination of expansion orders in the soft and hard region to be the n-th term of the overall expansion. In Fig. 4.10, we show the result of the asymptotic expansion in Eq. (4.46) as a function of the matching scale λ at different orders. We achieve good order-to-order convergence at the integrated level of the expansion for a wide range of values for λ.

As is to be expected, evaluation of the integrated result at the edges of the allowed range for λ does not lead to ideal agreement with the full result. The range of values of λ for which the amplitude is well approximated increases with rising order in the expansion. An example of this can be seen in Fig. 4.10. For a given order, an appropriate point of evaluation can be obtained by setting

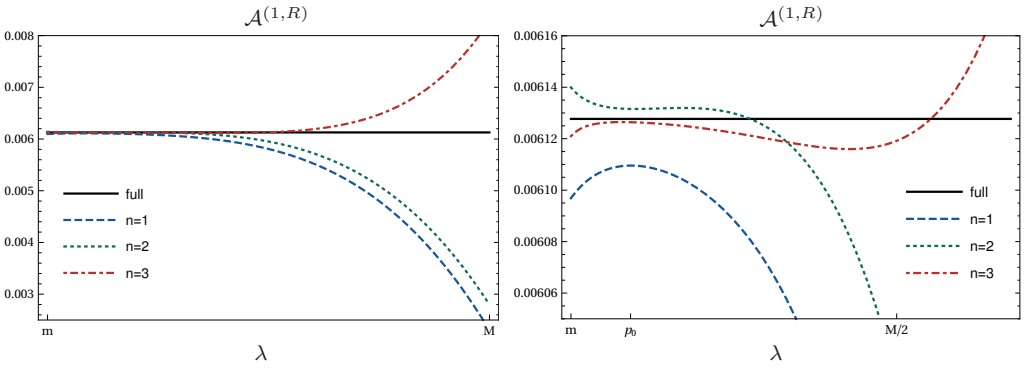

Figure 4.10: The convergence of the integrated results of the expansion in Eq. (4.46) at overall order n given for the values $M = 10\,m$, $p^2 = 3\,m^2$, and $\mu_{\mathrm{UV}} = M$, in the range of $m < \lambda < M$, with the image on the right showing a closeup of the region where the optimal value of λ can be identified.

Table 4.7: Integrated results of the expansion in Eq. (4.46) at overall order n evaluated at $\lambda = m$, $\lambda = 3M/4$ and $\lambda = p_0$, with parameters $M = 10\,m$, $p^2 = 3\,m^2$, and $\mu_{\mathrm{UV}} = M$, compared to the full result of $\mathcal{A}^{(1,R)} = 0.006128$.

n	$\mathcal{A}^{(1,R)}(m)$	rel. error	$\mathcal{A}^{(1,R)}(3M/4)$	rel. error	$\mathcal{A}^{(1,R)}(p_0)$	rel. error
1	0.006097	0.50%	0.004803	24%	0.006110	0.30%
2	0.006140	0.20%	0.005100	18%	0.006132	0.063%
3	0.006121	0.11%	0.006473	5.5%	0.006126	0.021%

the derivative with respect to λ and determining the position of the extrema. Coincidentally, the values obtained thus lie very close to $\lambda = p_0$. Numerical results for different choices of λ are presented in Table 4.7.

The behavior portrayed here has been seen as well in a modification of the scalar-two point function which has been rendered UV-finite by increasing the power of one of the propagators, with the only relevant difference being that the same order of both the soft and the hard integrand-level expansion had to be combined to achieve similar accuracy in both the soft and the hard region. The main advantage of this Taylor series inspired expansion method is its easy application and potential for automatization.

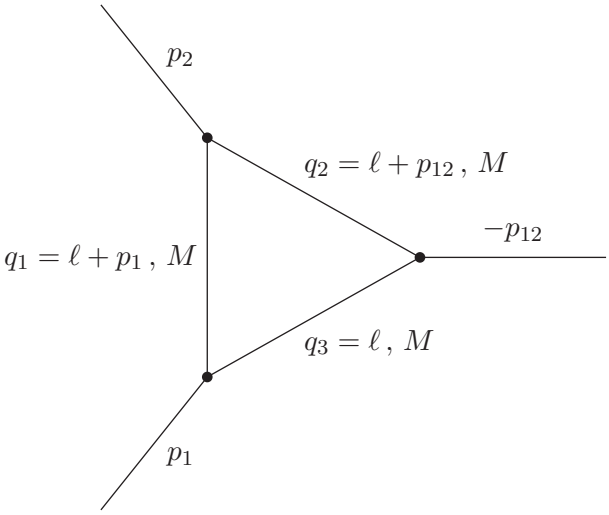

Figure 4.11: The three-point function with equal internal masses.

4.3 Asymptotic expansion of the scalar three-point function

As a benchmark application with more external legs, we consider the scalar three-point function at one-loop as shown in figure 4.11 with all the internal masses set to the same value

$$\mathcal{A}_3^{(1)} = \int_\ell G_F(q_1, q_2, q_3; M)\,, \tag{4.49}$$

where $G_F(q_1, q_2, q_3; M) = \prod_{i=1}^{3} G_F(q_i, M)$, with $q_1 = \ell + p_1$, $q_2 = \ell + p_1 + p_2$ and $q_3 = \ell$. Applying LTD to this integral leads to the dual representation

$$\mathcal{A}_3^{(1)} = -\int_\ell \left[\tilde{\delta}\,(q_1)\, G_D(q_1; q_2, q_3) + \tilde{\delta}\,(q_2)\, G_D(q_2; q_1, q_3) + \tilde{\delta}\,(q_3)\, G_D(q_3; q_1, q_2)\right], \tag{4.50}$$

with $G_D(q_i; q_j, q_k) = G_D(q_i; q_j)\, G_D(q_i; q_k)$ based on the dual propagators given as in Eq. (4.1). The three different linear combinations of external momenta that appear in the dual propagators are $k_{12} = -k_{21} = -p_2$, $k_{13} = -k_{31} = p_1$, and $k_{23} = -k_{32} = p_1 + p_2$. Only one of these can be chosen to have a vanishing three-momentum, for example by using the center-of-mass system of p_1 and p_2,

with $\mathbf{p}_{12} = 0$. The complete dual integrand thus only has angular dependence in the scalar products $q_i \cdot p_1$ and $q_i \cdot p_2$.

Assuming that all the internal particles running in the loop have the same mass M and the external particles are massless ($p_1^2 = p_2^2 = 0$ and $p_{12}^2 = s_{12}$, with $p_{12,0} > 0$) the LTD representation condenses to

$$\mathcal{A}_3^{(1)} = -\int_\ell \Bigg\{ -\frac{\tilde{\delta}\,(q_1; M)}{2q_1 \cdot p_{12}} \left(\frac{1}{2q_1 \cdot p_1} + \frac{1}{2q_1 \cdot p_2} \right) + \frac{\tilde{\delta}\,(\ell; M)}{(-2\ell \cdot p_2)(-2\ell \cdot p_{12} + s_{12} + \imath 0)} + \frac{\tilde{\delta}\,(\ell; M)}{(2\ell \cdot p_1)(2\ell \cdot p_{12} + s_{12})} \Bigg\}, \tag{4.51}$$

with the on-shell energies $q_{1,0}^{(+)} = \sqrt{(\boldsymbol{\ell} + \mathbf{p}_1)^2 + M^2}$ and $q_{2,0}^{(+)} = q_{3,0}^{(+)} = \ell_0^{(+)} = \sqrt{\boldsymbol{\ell}^2 + M^2}$. Thus, the on-shell energies in the second and third on-shell cuts are identical.

We may use the following integral identity

$$\int_\ell \frac{\tilde{\delta}\,(q_1; M)}{(2q_1 \cdot p_{12})(2q_1 \cdot p_i)} = \int_\ell \frac{\tilde{\delta}\,(\ell; M)}{(2\ell \cdot p_{12})(2\ell \cdot p_i)}\,, \tag{4.52}$$

to consequently rewrite Eq. (4.51) as

$$\mathcal{A}_3^{(1)} = \int_\ell \frac{\tilde{\delta}\,(\ell; M)\; s_{12}}{(2\ell \cdot p_{12})(2\ell \cdot p_1)} \left\{ \frac{1}{-2\ell \cdot p_{12} + s_{12} + \imath 0} + \frac{1}{2\ell \cdot p_{12} + s_{12}} \right\}. \tag{4.53}$$

Notice that now both terms in this expression are UV finite. Therefore, they can be integrated over the loop three-momentum separately without the necessity of introducing a cut-off.

The loop three-momentum can be parameterized as

$$\ell = |\ell| \left(2\sqrt{v(1-v)}\hat{e}_\perp, 1 - 2v \right), \tag{4.54}$$

where $\hat{e}_\perp$ is the unit vector perpendicular to $\mathbf{p}_1$. The angular dependence then takes the shape

$$2\ell \cdot p_i = \sqrt{s_{12}}\,(\ell_0^{(+)} \mp |\boldsymbol{\ell}|(1-2v))\,, \qquad i = 1, 2\,. \tag{4.55}$$

In this expression the two angular integrations are related by the change of variables $v \to 1 - v$ and thus

$$\int_0^1 \frac{dv}{2\ell \cdot p_i} = \frac{1}{2\sqrt{s_{12}}\,|\boldsymbol{\ell}|} \log\left(\frac{\ell_0^{(+)} + |\boldsymbol{\ell}|}{\ell_0^{(+)} - |\boldsymbol{\ell}|} \right), \quad i = 1, 2\,, \tag{4.56}$$

where the usual change of variables $|\boldsymbol{\ell}| = M/2\,(x - x^{-1})$ with $x > 1$ can be employed to obtain the full analytic result

$$\mathcal{A}_3^{(1)} = \frac{1}{32\pi^2 s_{12}} \log^2\left(\frac{\sqrt{s_{12}(s_{12}-4M^2)} + 2M^2 - s_{12}}{2M^2}\right). \tag{4.57}$$

The large mass expansion is straightforward and it is free of thresholds, i.e. the $\imath 0$ prescription can be dropped when $r = s_{12}/M^2 \ll 1$. We need to consider both $G_D(q_2; q_3)$ and $G_D(q_3; q_2)$ in the context of the general propagator expansion. Since in both propagators the condition $\Gamma + \Delta = s_{12} < M\sqrt{s_{12}}$ holds we must identify $\Gamma = 0$ and $\Delta = s_{12}$. Thus the asymptotic expansions of the propagators are given by

$$G_D(q_2; q_3) = \frac{1}{-2q_2 \cdot p_{12} + s_{12}} = \sum_{n=0}^{\infty} \frac{(-s_{12})^n}{(-2q_2 \cdot p_{12})^{n+1}} \tag{4.58}$$

and

$$G_D(q_3; q_2) = \frac{1}{2q_3 \cdot p_{12} + s_{12}} = \sum_{n=0}^{\infty} \frac{(-s_{12})^n}{(2q_3 \cdot p_{12})^{n+1}}\,. \tag{4.59}$$

Combining the two expanded propagators one obtains a single asymptotic expansion as

$$G_D(q_2; q_3) + G_D(q_3; q_2) = -\frac{2}{s_{12}} \sum_{n=1}^{\infty} \left(\frac{s_{12}}{2\ell \cdot p_{12}}\right)^{2n}, \tag{4.60}$$

leading to the expanded amplitude

$$\mathcal{A}_3^{(1)}(s_{12} \ll M^2) = -\int_\ell \frac{\tilde{\delta}\,(\ell; M)}{(2\ell \cdot p_{12})(\ell \cdot p_1)} \sum_{n=1} \left(\frac{s_{12}}{2\ell \cdot p_{12}}\right)^{2n}. \tag{4.61}$$

Integration leads to the following result for the large mass expansion:

$$\mathcal{A}_3^{(1)}(s_{12} \ll M^2) = -\frac{1}{16\pi^2}\frac{1}{2M^2}\left(1 + \frac{r}{12} + \frac{r^2}{90}\right) + \mathcal{O}(r^3)\,. \tag{4.62}$$

For $M/\sqrt{s_{12}} = 3$ the relative error of the result is $9 \cdot 10^{-3}$ with only the first term of the expansion and reduces to $1 \cdot 10^{-4}$ and $2 \cdot 10^{-6}$ when including up the second and third term of the expansion, respectively.

In the small mass limit, $2M/\sqrt{s_{12}} \ll 1$, the general expansion of the dual propagators can be applied as well. The expansion parameters are

$$\begin{aligned} \Gamma_{32} = \Gamma_{23} \equiv \Gamma &= s_{12}\left(1+\frac{M^2}{s_{12}}\right), \\ r_{32} = -r_{23} &= -\frac{M}{\sqrt{s_{12}}} + \imath 0\,, \\ Q_2^2 = Q_3^2 &= s_{12}\,. \end{aligned} \tag{4.63}$$

This leads to the expanded amplitude

$$\begin{aligned} \mathcal{A}_3^{(1)}(s_{12} \gg M^2) = \int_\ell \frac{\tilde{\delta}\,(\ell;M)\,s_{12}}{(2\ell\cdot p_{12})(2\ell\cdot p_1)} \\ \cdot \sum_{n=0}^{\infty}\left\{\frac{M^{2n}}{(-2\ell\cdot p_{12}+\Gamma)^{n+1}} + \frac{M^{2n}}{(2\ell\cdot p_{12}+\Gamma)^{n+1}}\right\}. \end{aligned} \tag{4.64}$$

Alternatively, both propagators in the sum may be combined as

$$\mathcal{A}_3^{(1)} = \int_\ell \frac{\tilde{\delta}\,(\ell;M)}{(2\ell\cdot p_{12})(2\ell\cdot p_1)}\,\frac{2s_{12}^2}{\left(-(2\ell\cdot p_{12})^2 + s_{12}^2 + \imath 0\right)}\,, \tag{4.65}$$

and expanded similarly to the general expansion so as to obtain the final expanded form at integrand level

$$\mathcal{A}_3^{(1)}(s_{12} \gg M^2) = \int_\ell \frac{\tilde{\delta}\,(\ell;M)\;s_{12}^2}{(2\ell\cdot p_{12})(\ell\cdot p_1)} \sum_{n=0}^{\infty} \frac{\left(s_{12}^2 r_{23}^2\,(2+r_{23}^2)\right)^n}{\left(-(2\ell\cdot p_{12})^2+\Gamma^2\right)^{n+1}}\,. \tag{4.66}$$

Also in this variation of the expansion it is possible to simplify the denominator in terms of the integration variable x by making use of

$$-(2\ell\cdot p_{12})^2 + s_{12}^2\,(1+r_{23}^2)^2 = s_{12}^2\,(x^2-r_{23}^2)(x^{-2}-r_{23}^2)\,. \tag{4.67}$$

Analytic integration up to $n=1$ gives the result

$$\begin{aligned} \mathcal{A}_3^{(1)}(s_{12} \gg M^2) = \frac{1}{16\pi^2}\,\frac{1}{2(1+r_{23}^2)^2 s_{12}}\Bigg(\log^2\left(-r_{23}^2\right) \\ + \frac{r_{23}^2(r_{23}^2+2)\log\left(-r_{23}^2\right)}{1+r_{23}^2}\left(\frac{2}{1-r_{23}^2} + \frac{\log\left(-r_{23}^2\right)}{1+r_{23}^2}\right) + \mathcal{O}\left(r_{23}^4\right)\Bigg). \end{aligned} \tag{4.68}$$

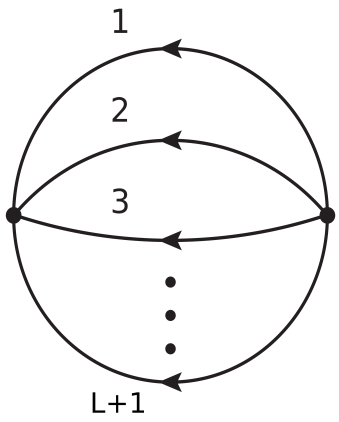

Figure 4.12: Maximal Loop Topology at L loops with arbitrary internal masses. External momenta are not shown.

Using the numerical values $\sqrt{s_{12}}/M = 3$ the relative error of this result is 33% (7.5%) in the real (imaginary) part including only the first term of the expansion and reduces to 7.5% (0.04%) and 1.5% (0.26%) when including up the second and third term of the expansion, respectively. The relative errors obtained by integrating Eq. (4.64) are slightly better but of the same order of magnitude with 26% (2.7%) with only the first term and 3.0% (1.3%) and 0.31% (0.27%) when including up the second and third term of the expansion, respectively. Even better results can be obtained by obtaining the parameters through expansion of the singularity position of the full propagator as discussed in Eq. (4.15). In this case already at first order the relative error lies at 3.9%.

4.4 Asymptotic expansion of multiloop integrals from the causal LTD representation

A new LTD representation of multiloop amplitudes has been presented recently [3] and was introduced in Section 2.4, which is manifestly causal and, therefore, free of the unphysical singularities. We will focus in this section on the class of multiloop integrals known as Maximal-Loop-Topology (MLT), which are represented by the diagram in Fig. 4.12 and are defined as

$$\mathcal{A}^{(L)}_{\rm MLT}(p) = \int_{\ell_1,\ldots,\ell_L} G_F(q_1,\ldots,q_{L+1})\,, \tag{4.69}$$

where $G_F(q_1,\ldots,q_{L+i}) = \prod_{s=1}^{L+1} G_F(q_s)$, and L is the number of loops. The momenta of the internal propagators are $q_s = \ell_s$, with $s \in [1,\ldots,L]$, and $q_{L+1} = -\sum_{s=1}^{L} \ell_s + p$. The internal masses, m_s, are arbitrary. The one-loop two-point function corresponds to the special case $q_1 = \ell_1$ and $q_2 = -\ell_1 + p$. The causal LTD representation of Eq. (4.69) is extremely compact and is given by

$$\mathcal{A}^{(L)}_{\rm MLT}(p) = -\int_{\vec{\ell}_1,\ldots,\vec{\ell}_L} \frac{1}{x_{L+1}} \left(\frac{1}{\lambda^-_{L+1}} + \frac{1}{\lambda^+_{L+1}} \right) , \tag{4.70}$$

where

$$x_{L+1} = \prod_{s=1}^{L+1} 2q^{(+)}_{s,0} , \qquad \lambda^\pm_{L+1} = \sum_{s=1}^{L+1} q^{(p,+)}_{s,0} \pm p_0 . \tag{4.71}$$

Here $q^{(p,+)}_{s,0} = \sqrt{\vec{q}_s^{\,2} + m_s^2 - i0}$ are the on-pole energies and p_0 is the energy component of the external momentum.

The causal representation in Eq. (4.70) is particularly suitable to achieve the asymptotic expansion in the limit $p^2 \ll m_s^2$. Assuming $p = (p_0, \mathbf{0})$, we obtain

$$\mathcal{A}^{(L)}_{\rm MLT}(p^2 \ll m_s^2) = -2 \sum_{n=0}^{\infty} (p^2)^n \int_{\vec{\ell}_1,\ldots,\vec{\ell}_L} \frac{\left(\lambda^0_{L+1}\right)^{-1-2n}}{x_{L+1}} , \tag{4.72}$$

where $\lambda^0_{L+1} = \sum_{s=1}^{L+1} q^{(+)}_{s,0}$. Notice that there is no dependence on p_0 neither in x_{L+1} nor in λ^0_{L+1}, and therefore the asymptotic integrals on the right-hand side of Eq. (4.72) are a function of the internal masses exclusively to all loop orders.

Chapter 5

Asymptotic expansions in highly boosted Higgs boson production

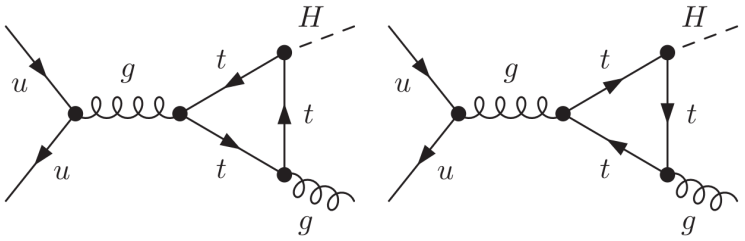

Figure 5.1: Contributing diagrams to the process $q\bar{q} \to Hg$ at LO through a top quark loop. The incoming particles can be any light quark-antiquark pair, with the main contributions coming from either a $u\bar{u}$ or a $d\bar{d}$ pair.

5.1 Motivation and contributions to highly boosted Higgs boson production

The dynamics involving the Higgs boson are of strong interest given that it is the only known scalar particle. As was mentioned in Chapter 1, one of the processes of high interest is the production of Higgs bosons with large transverse momentum $p_\perp$. For a Higgs boson to be sufficiently boosted to enter this scenario it must have been produced concurrently with another parton. The regime of small transverse momentum has been calculated at NLO with a point-like interaction encoding the top-quark loop [48,50], first attempts at the full calculation necessary for obtaining the large transverse momentum distribution have been published recently and rely on either numerical integration [56] or expansions in the Integration by Parts identities [46]. It is exactly this part of the $p_\perp$ distribution which is needed in order to rule out an additional point-like effective Higgs-gluon-gluon coupling. Amplitudes contributing to the production of a Higgs boson and either a gluon or a quark at the LHC are thus a good opportunity to apply the technique for asymptotic expansions to a benchmark physical process.

5.2 Amplitude and projections for $q\bar{q} \to Hg$

In its general form the amplitude for the process $q(-p_1)+\bar{q}(-p_2) \to H(h)+g(p_3)$ can be written as

$$i\mathcal{M} = c \cdot \varepsilon^*_\mu(p_3)\ \bar{v}(-p_2)\mathcal{A}^\mu u(-p_1)\,. \tag{5.1}$$

The reduced amplitude $\mathcal{A}^\mu$ is a function only of the external momenta, of which one may be eliminated using momentum conservation

$$h = -p_1 - p_2 - p_3 \,. \tag{5.2}$$

Since the masses of up and down quark are much smaller than the Higgs boson or top quark mass they can be treated as massless. Like the external gluon their momenta fulfill $p_1^2 = p_2^2 = p_3^2 = 0$ while the Higgs momentum is restricted by $h^2 = M_H^2$. In the context of LTD it is customary to define all momenta to be outgoing, meaning that the physically incoming particles have negative energy values, e.g. $E(q) = -p_{1,0} > 0$. The Mandelstam variables are given by

$$s = 2p_1 \cdot p_2, \quad t = 2p_1 \cdot p_3 = M_H^2 + 2p_2 \cdot h \quad \text{and} \quad u = 2p_2 \cdot p_3 = M_H^2 + 2p_1 \cdot h \,, \tag{5.3}$$

and are related through $s + t + u = M_H^2$.

The Feynman diagrams of the leading order contribution are shown in Fig. 5.1 and give

$$\imath\mathcal{M}^{(1)} = \frac{\imath\, e g_s^3 M_t^2 T^c_{\beta\alpha}}{s\; M_W \sin\theta_W}\; \varepsilon^*_\mu(p_3)\; \bar{v}(-p_2)\gamma_\nu u(-p_1)\mathcal{A}^{(1),\mu\nu} \,, \tag{5.4}$$

where the index (1) signaling the one-loop nature of the amplitude will be dropped in the following since no higher-order contributions are considered yet. The reduced amplitude can be written in a particularly short form when the direction of the integration momentum is shifted in the second diagram, leading to both contributions being exactly equal. Defining the momenta running through the loop as $q_0 \equiv \ell$, $q_3 \equiv \ell + p_3$ and $q_{12} \equiv \ell - p_1 - p_2$ allows to choose a coordinate system where all angular dependence in the propagator giving rise to the unitary threshold can be eliminated. The reduced amplitude is then given by

$$\mathcal{A}^{\mu\nu} = \int_\ell \frac{1}{2M_t} \mathrm{Tr}\left\{(\not{q}_{12} + M_t)\gamma^\nu(\not{q}_3 + M_t)\gamma^\mu(\not{q}_0 + M_t)\right\} G_F(q_0, q_{12}, q_3) \,. \tag{5.5}$$

Solving the trace and dropping the terms that do not contribute due to the transversality of the external gluon, $\varepsilon^*(p_3) \cdot p_3 = 0$, as well as the Dirac equation, $\bar{v}(-p_2)\not{p}_2 = \not{p}_1 u(-p_1) = 0$, this amounts to

$$\mathcal{A}^{\mu\nu} = \int_\ell G_F(q_0, q_3, q_{12}) \left[-g^{\mu\nu}\left(2\ell^2 - 2M_t^2 + M_H^2 - s\right) + 2p_{12}^\mu p_3^\nu + 8\ell^\mu \ell^\nu\right] \,. \tag{5.6}$$

For the leading order amplitude one may note that a separate dependence on the quark momenta p_1 and p_2 is introduced to the amplitude only through the spinors while $A^{\mu\nu}$ only depends on the sum $p_{12} = p_1 + p_2$ due to the topology of the contributions. When defining a basis for decomposing the amplitude into scalar form factors it is therefore convenient to choose basis vectors for $\mathcal{A}^{\mu\nu}$ that do not depend on the external momenta independently,[1] such as

$$\mathcal{B}^{\mu\nu} = \{g^{\mu\nu} - \frac{p_{12}^\mu p_3^\nu}{p_{12}\cdot p_3},\ g^{\mu\nu},\ p_3^\mu p_{12}^\nu,\ p_{12}^\mu p_{12}^\nu, p_3^\mu p_3^\nu\}\,. \tag{5.7}$$

The basis vectors have been chosen in this specific form instead of a different linear combination to exploit the Ward identity which for this amplitude amounts to

$$0 = (p_3)_\mu\ \mathcal{A}^{\mu\nu}\,. \tag{5.8}$$

The last three basis vectors are of the form $p_i^\mu p_{12}^\nu$ and thus vanish when applying the Dirac equation given by $\not{p}_1 u(-p_1) = \bar{v}(-p_2)\not{p}_2 = 0$ for massless particles. Furthermore, the square of the gluon momentum is zero, $p_3^2 = 0$, and since

$$(p_3)_\mu\ \left(g^{\mu\nu} - \frac{p_{12}^\mu p_3^\nu}{p_{12}\cdot p_3}\right) = 0\,, \tag{5.9}$$

the Ward identity applied to the remaining amplitude forces the condition

$$(p_3)_\mu\ \mathcal{A}^{\mu\nu} = \text{const.}\cdot (p_3)^\nu \overset{!}{=} 0\,. \tag{5.10}$$

Thus after performing all required integrations the coefficient of the second element of the basis must vanish. Physically relevant is only the first element of the basis.

Taking this into account the integrated result is significantly simplified and necessarily takes the form

$$\mathcal{A}^{\mu\nu} = F_{12}\ \left(g^{\mu\nu} - \frac{p_{12}^\mu p_3^\nu}{p_3 p_{12}}\right)\,, \tag{5.11}$$

leaving to be calculated only the scalar form factor F_{12} which can be obtained using the projector

$$P_{12}^{\mu\nu} = \frac{1}{d-2}\left(g^{\mu\nu} - \frac{p_{12}^\mu p_3^\nu}{p_{12}\cdot p_3}\right) - \frac{2}{t+u}\frac{d-1}{d-2}\ p_3^\mu p_{12}^\nu + \frac{4s}{(t+u)^2}\frac{d-1}{d-2}\ p_3^\mu p_3^\nu. \tag{5.12}$$

[1] For higher order calculations the needed additional terms can be obtained through the replacement $p_{12} \to p_1 - p_2$ although different choices for the basis are more convenient.

This leads to the integral

$$
\begin{aligned}
F_{12} &= P_{12}^{\mu\nu}\mathcal{A}_{\mu\nu} \\
&= \int_\ell G_F(q_0,q_3,q_{12}) \left[8\frac{(d-1)}{(d-2)}\frac{s\ (2\ell\cdot p_3)^2}{(M_H^2-s)^2} \right. \\
&\qquad \left. - \frac{16\ d}{(d-2)}\frac{(\ell\cdot p_3)(\ell\cdot p_{12})}{M_H^2-s} + \frac{8}{(d-2)}\ell^2 - M_H^2 + s \right].
\end{aligned}
\tag{5.13}
$$

Through Passarino-Veltman tensor reduction [36] within the standard approach one finds the decomposition into the master integrals B_0 and C_0 as

$$
\begin{aligned}
F_{12} = &- i\pi^2 \left[+ 2\mathrm{B}_0\left(M_H^2, M_t^2, M_t^2\right)\frac{d-4}{d-2}((M_H^2-s)) \right. \\
&+ \frac{1}{d-2}\frac{4\ s}{(M_H^2-s)}\left(\mathrm{B}_0\left(s, M_t^2, M_t^2\right) - \mathrm{B}_0\left(M_H^2, M_t^2, M_t^2\right)\right) \\
&\left. + \left(M_H^2 - s - \frac{8M_t^2}{d-2}\right)\mathrm{C}_0\left(0, s, M_H^2, M_t^2, M_t^2, M_t^2\right) \right].
\end{aligned}
\tag{5.14}
$$

Using the known results for the scalar integrals B_0 and C_0 as quoted in Appendix A the analytical result for F_{12} is given by

$$
\begin{aligned}
F_{12} = \frac{1}{32\pi^2}\Bigg[&\left(1 - \frac{4M_t^2}{M_H^2-s}\right)\left(\log^2\left(\frac{\sqrt{s\left(s-4M_t^2\right)}+2M_t^2-s}{2M_t^2}\right)\right. \\
&\left. - \log^2\left(\frac{\sqrt{M_H^2\left(M_H^2-4M_t^2\right)}+2M_t^2-M_H^2}{2M_t^2}\right)\right) \\
&+ \frac{4s}{M_H^2-s}\left(\sqrt{1-4\frac{M_t^2}{M_H^2}}\log\left(\frac{\sqrt{M_H^4-4M_H^2M_t^2}+2M_t^2-M_H^2}{2M_t^2}\right)\right. \\
&\left. \left. - \sqrt{1-4\frac{M_t^2}{s}}\log\left(\frac{\sqrt{s^2-4sM_t^2}+2M_t^2-s}{2M_t^2}\right)\right) + 4\Bigg].
\end{aligned}
\tag{5.15}
$$

5.3 LTD application, dual representation and integration

The calculation within the LTD formalism starts with the evaluation of the scalar form factor in Eq. (5.13). Applying the LTD theorem gives

$$
\begin{aligned}
F_{12} = -\int_\ell N(\ell) \Bigg[& \widetilde{\delta}(q_0)\; G_D(q_0;q_3) G_D(q_0;q_{12}) \\
& + \widetilde{\delta}(q_3)\; G_D(q_3;q_0) G_D(q_3;q_{12}) \\
& + \widetilde{\delta}(q_{12})\; G_D(q_{12};q_0) G_D(q_{12};q_3) \Bigg] ,
\end{aligned}
\tag{5.16}
$$

with the three dual contributions, including the numerator $N(\ell)$ explicitly, given by

$$
\begin{aligned}
F_{12}\left(\tilde{\delta}\left(q_0\right)\right) = & \int_\ell \frac{-\tilde{\delta}\left(q_0\right)}{-2p_{12}\cdot q_0 + s} \frac{2p_3\cdot q_0}{M_H^2 - s} \\
& \times \left[c_3 + \left(\frac{M_t^2\left(M_H^2 - s\right)}{\left(2p_{12}\cdot q_0\right)\left(2p_3\cdot q_0\right)} c_1 + c_2 \right) \frac{p_{12}\cdot q_0}{p_3\cdot q_0} \right] , \\
F_{12}\left(\tilde{\delta}\left(q_3\right)\right) = & \int_\ell \frac{\tilde{\delta}\left(q_3\right)}{M_H^2 - s} \Bigg[- c_2 \\
& + \frac{1}{2h\cdot q_3 + M_H^2} \left(\left(\frac{M_t^2 (M_H^2 - s)}{\left(2p_3\cdot q_3\right)^2} c_1 - c_2 + c_3 \right) \left(2p_3\cdot q_3\right) - \frac{8}{d-2} M_H^2 - 4s \right) \Bigg] , \\
F_{12}\left(\tilde{\delta}\left(q_{12}\right)\right) = & -\int_\ell \frac{\tilde{\delta}\left(q_{12}\right) s}{2p_{12}\cdot q_{12} + s + \imath 0} \Bigg[\frac{c_2 - 2c_3}{(M_H^2 - s)s} \left(2p_{12}\cdot q_{12} + s\right) \\
& + c_3 \frac{M_H^2 - 2h\cdot q_{12}}{(M_H^2 - s)s} + \left(\frac{s M_t^2}{M_H^2 - 2h\cdot q_{12}} \frac{M_H^2 - s}{s^2} c_1 + c_2 \right) \frac{1}{(M_H^2 - s)} \\
& + \frac{1}{(M_H^2 - s)^2} \frac{1}{M_H^2 - 2h\cdot q_{12}} \Bigg(\frac{8p_{12}\cdot q_{12}}{d-2} \left(\frac{2(M_H^2 - s)^2}{s} + \left((d-4)s + 3dM_H^2\right) \right) \\
& + 8M_H^2 (s + \frac{M_H^2}{d-2}) + (2p_{12}\cdot q_{12})^2 (-c_2 \frac{M_H^2}{s} + 4) \Bigg) \Bigg] .
\end{aligned}
\tag{5.17}
$$

The coefficients found in these expressions are similar to the ones in the calculation for $H \to \gamma\gamma$ [72,74] and are given by

$$\begin{aligned} c_1 &= \frac{8}{d-2} - \frac{M_H^2 - s}{M_t^2}\,, \\ c_2 &= -\frac{4d}{d-2}\,, \\ c_3 &= 8\frac{d-1}{d-2}\frac{s}{M_H^2 - s}. \end{aligned} \tag{5.18}$$

For the integration of the amplitude it is necessary to choose a coordinate system. It is convenient to define the external momenta as

$$\begin{aligned} h^\mu &= \frac{1}{2\sqrt{s}}\left(s + M_H^2,\ \mathbf{0},\ s - M_H^2\right) \\ p_3^\mu &= \frac{s - M_H^2}{2\sqrt{s}}\left(1,\ \mathbf{0},\ -1\right) \\ p_{12}^\mu &= \sqrt{s}\left(-1,\ \mathbf{0},\ 0\right)\,. \end{aligned} \tag{5.19}$$

The loop momentum ℓ may be parameterized as

$$\ell^\mu = \left(\ell_0,\ |\boldsymbol{\ell}|\ 2\sqrt{v(1-v)}\ \mathbf{e}_\perp,\ |\boldsymbol{\ell}|\ (1-2v)\right)\,, \tag{5.20}$$

which can be simplified in the on-shell case by defining $\ell_0 = \sqrt{\boldsymbol{\ell}^2 + M_t^2} \equiv M_t\sqrt{\xi^2+1}$ and then gives

$$\ell^\mu = M_t\left(\sqrt{\xi^2+1},\ \xi\ 2\sqrt{v(1-v)}\ \mathbf{e}_\perp,\ \xi\ (1-2v)\right)\,. \tag{5.21}$$

The scalar products between the loop momentum and the external momenta evaluate to

$$\begin{aligned} p_{12}\cdot\ell &= -\sqrt{s}\ell_0 \\ p_3\cdot\ell &= \frac{\sqrt{s}}{2}\left(1 - \frac{M_H^2}{s}\right)\left((1-2v)M_t\xi + \ell_0\right) \\ h\cdot\ell &= \frac{\sqrt{s}}{2}\left(\left(\frac{M_H^2}{s} - 1\right)(1-2v)\,M_t\xi + \left(\frac{M_H^2}{s} + 1\right)\ell_0\right)\,. \end{aligned} \tag{5.22}$$

Taking into account that the considered amplitude is very similar to the one discussed in Chapter 3 one would expect that also here a local counterterm is

necessary to regulate the amplitude's UV behavior. Indeed, when looking at the UV limit of the integrand after setting $d = 4$

$$F_{12}^{(d=4)} = \int_0^1 \frac{\mathrm{d}v}{2\pi^2} \int_0^\infty \mathrm{d}|\boldsymbol{\ell}|\, f_{12}(\boldsymbol{\ell}, v) \tag{5.23}$$

one finds that the integrand appears to produce a logarithmic divergence

$$f_{12}(\ell, v) = \left(-9v^2 + 9v - \frac{3}{2}\right) \frac{1}{|\boldsymbol{\ell}|} + \mathcal{O}(|\boldsymbol{\ell}|^{-2})\,. \tag{5.24}$$

However, this term and further terms even in $\boldsymbol{\ell}$ disappear when evaluating the integral over v revealing the leading contribution in the UV to be of $\mathcal{O}(|\boldsymbol{\ell}|^{-3})$, giving

$$\int_0^1 \mathrm{d}v\, f_{12}(\ell, v) = \frac{-M_H^4 + 4M_H^2 s - 3s^2}{24s} \frac{1}{|\boldsymbol{\ell}|^3} + \mathcal{O}(|\boldsymbol{\ell}|^{-5})\,. \tag{5.25}$$

The UV is thus well-defined and a local renormalization is unnecessary. The integration can be performed in four spacetime dimensions without further considerations. For numerical stability it may still be convenient to subtract the vanishing contribution in Eq. (5.24) to obtain a locally well-behaved integrand.

The numerical integration below the production threshold of the top-antitop pair in the loop is thus straight-forward and confirms the analytical result. Above this threshold the amplitude has a physically relevant pole stemming from the contribution with q_2 set on-shell, giving rise to

$$G_F(\ell)\tilde{\delta}\left(\ell - p_{12}\right) = \frac{\tilde{\delta}\left(q_{12}\right)}{-2\sqrt{s}\, q_{12,0}^{(+)} + s}\,. \tag{5.26}$$

With the coordinates chosen, this term is independent of the integration angle and diverges for $|\boldsymbol{\ell}| \to \frac{1}{2}\sqrt{s - 4M_t^2}$. The numerical solution obtained by contour deformation agrees perfectly with the analytical result.

As in the case of the scalar two-point function the most convenient choice for defining the internal momenta is not for them to be composed of pure sums without negative signs. Indeed, when choosing to define the amplitude in terms of the entirely positive internal momenta ℓ, $\ell + p_3$ and $\ell + p_{12} + p_3$ the propagator giving rise to the physical singularity has the shape

$$G_F(\ell + p_{12} + p_3)\tilde{\delta}\left(\ell\right) = \frac{\tilde{\delta}\left(\ell\right)}{2p_{12,0}\sqrt{\left(\boldsymbol{\ell} + \boldsymbol{p}_3\right)^2 + m^2} - 2\boldsymbol{p}_{12}\cdot\boldsymbol{\ell} - 2\boldsymbol{p}_{12}\cdot\boldsymbol{p}_3}\,, \tag{5.27}$$

where the angular dependence persists independently of the coordinate choice. This leads to a significant inconvenience since the singularity appears in the integrand along a line in the $\{|\boldsymbol{\ell}|, v\}$-space - depending on the kinematics of the process even at $\boldsymbol{\ell} = 0$. A succesful numerical integration has still been achieved by stabilizing the integration around the singularities through subtraction of the numerators at this point and integration of the isolated singularity analytically as

$$\frac{f(|\boldsymbol{\ell}|,\theta)}{s-\sqrt{s}\sqrt{4(|\boldsymbol{\ell}|-\ell_1)(|\boldsymbol{\ell}|-\ell_2)+s}} = \frac{f(|\boldsymbol{\ell}|,\theta)-f(\ell_i,\theta)}{s-\sqrt{s}\sqrt{4(|\boldsymbol{\ell}|-\ell_1)(|\boldsymbol{\ell}|-\ell_2)+s}} + \frac{f(\ell_i,\theta)}{s-\sqrt{s}\sqrt{4(|\boldsymbol{\ell}|-\ell_1)(|\boldsymbol{\ell}|-\ell_2)+s}}. \tag{5.28}$$

For the implementation the integration area is divided into various regions with

$$\cos\theta_{\min} = \sqrt{M_H^4 - 2M_H^2 s + 4M_t^2 s}/|s - M_H^2| \tag{5.29}$$

being the minimal angle below which the physical singularity appears as shown in Fig. 5.2. The various regions for integration are then given by

1. divergent dual contribution over $(\theta, 0, \theta_{\min}), (|\boldsymbol{\ell}|, 0, \ell_{\mathrm{mid}})$, where $\ell_{\mathrm{mid}} = \ell_1(\theta = \theta_{\min}) = \frac{1}{2}\sqrt{\frac{M_H^4}{s} - 2M_H^2 + 4M_t^2}$.

2. divergent dual contribution over $(\theta, 0, \theta_{\min}), (|\boldsymbol{\ell}|, \ell_{\mathrm{mid}}, \ell_{\mathrm{cut}})$, where $\ell_{\mathrm{cut}} = \ell_2 + (\ell_2 - \ell_{\mathrm{mid}})$.

3. non-divergent dual contributions over $(\theta, 0, \theta_{\min}), (|\boldsymbol{\ell}|, 0, \ell_{\mathrm{cut}})$

4. high-energy region: full integrand over $(\theta, 0, \pi), (|\boldsymbol{\ell}|, \ell_{\mathrm{cut}}, \Lambda)$.

5. low-energy, high-angle region: full integrand over $(\theta, \theta_{\min}+\varepsilon, \pi), (|\boldsymbol{\ell}|, 0, \ell_{\mathrm{cut}})$. While $\varepsilon \geq 0.0000005$ is necessary for the integral to converge, lowering ε towards this value shows good convergence.

Clearly, the result is independent of how the internal momenta are defined. Nonetheless, defining them as pure sums complicates the integration significantly and due to noncausal singularities requires changes in the developed technique for asymptotic expansions when applying it to the diverging propagator.

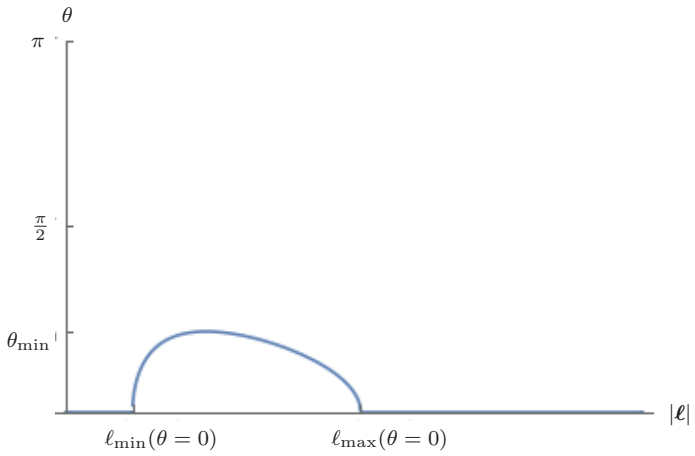

Figure 5.2: The area over which the integration needs to be performed. Singularities stemming from Eq. (5.27) appear along the line shown when the amplitude is defined with the internal momenta ℓ, $\ell + p_3$ and $\ell + p_{12} + p_3$.

5.4 Asymptotic expansions of the integrand

The dual integrand derived above can be expanded using the technique described in Section 4.1 as will be demonstrated in the following. Among the propagators appearing in the amplitude the one with the most significant physical importance is the one giving rise to the unitarity threshold

$$G_F(\ell)\tilde{\delta}\left(q_{12}\right) = \frac{\tilde{\delta}\left(q_{12}\right)}{2p_{12}\cdot q_{12} + s + \imath 0}\,. \tag{5.30}$$

It may be expanded as per Eq. (4.3) as

$$G_D(q_{12};q_0)\tilde{\delta}\left(q_{12}\right) = \sum_{n=0}^{\infty} \frac{(-\Delta_{20})^n}{(2q_{12}\cdot k_{02} + \Gamma_{20} - i0\eta\cdot k_{02})^{n+1}}\,, \tag{5.31}$$

where in the naming of the indices the replacement $12 \to 2$ has been made to simplify the notation: $\Gamma_{\{12\}0}$ is written as Γ_{20}.

5.4.1 Large mass expansion

The kinematics below the unitarity threshold is defined through

$$p_{12}^2 = s \leq 4M_t^2\,, \tag{5.32}$$

barring thus the quarks in the loop from forming an on-shell intermediate state. This condition is automatically fulfilled when considering the scenario of a very large mass in the loop

$$M_t^2 \gg \{s, M_H^2\} \tag{5.33}$$

and leads to the situation that

$$|2p_{12}\cdot q_{12}| = 2\sqrt{s}\,\sqrt{\ell^2 + M_t^2} \gg s\,. \tag{5.34}$$

The parameter Γ_{20} is correspondingly set to zero and $\Delta_{20} = s$ is identified. The appropriate expansion for the propagator is thus given by

$$G_D(q_{12}; q_0) \overset{M_t^2 \gg s}{=} \sum_{n=0}^{\infty} \frac{(-s)^n}{(2p_{12}\cdot q_{12})^{n+1}}\,. \tag{5.35}$$

The expanded form factor is obtained by the modification

$$F_{12}^{M_t^2\gg s} = F_{12}\left(\tilde{\delta}\,(q_0)\right) + F_{12}\left(\tilde{\delta}\,(q_3)\right) + F_{12}^{M_t^2\gg s}\left(\tilde{\delta}\,(q_{12})\right)\,, \tag{5.36}$$

where

$$\begin{aligned}
&F_{12}^{M_t^2\gg s}\left(\tilde{\delta}\,(q_{12})\right) = \\
&-\int_\ell \tilde{\delta}\,(q_{12})\, s \sum_{n=0}^{\infty} \frac{(-s)^n}{(2p_{12}\cdot q_{12})^{n+1}} \Bigg[\left(\frac{sM_t^2}{M_H^2 - 2h\cdot q_{12}} \frac{M_H^2 - s}{s^2} c_1 + c_2 \right) \frac{1}{(M_H^2 - s)} \\
&+ \frac{c_2 - 2c_3}{(M_H^2 - s)s}\,(2p_{12}\cdot q_{12} + s) + c_3 \frac{M_H^2 - 2h\cdot q_{12}}{(M_H^2 - s)s} \\
&+ \frac{1}{(M_H^2 - s)^2} \frac{1}{M_H^2 - 2h\cdot q_{12}} \left(\frac{8p_{12}\cdot q_{12}}{d-2} \left(\frac{2(M_H^2 - s)^2}{s} + \left((d-4)s + 3dM_H^2\right) \right) \right. \\
&\left. + 8M_H^2 (s + \frac{M_H^2}{d-2}) + (2p_{12}\cdot q_{12})^2 (-c_2 \frac{M_H^2}{s} + 4) \right) \Bigg]\,.
\end{aligned} \tag{5.37}$$

Choosing physical masses $M_t = 172.76\,\text{GeV}$, $M_H = 125.1\,\text{GeV}$ [8] and the center-of-mass energy $s = 0.1M_t^2$ the integrand-level convergence is satisfactory as can be seen in Fig. 5.3 and the integrated results have an acceptable relative error compared to the full result starting only at order $n = 3$ as can be seen in Table 5.2.

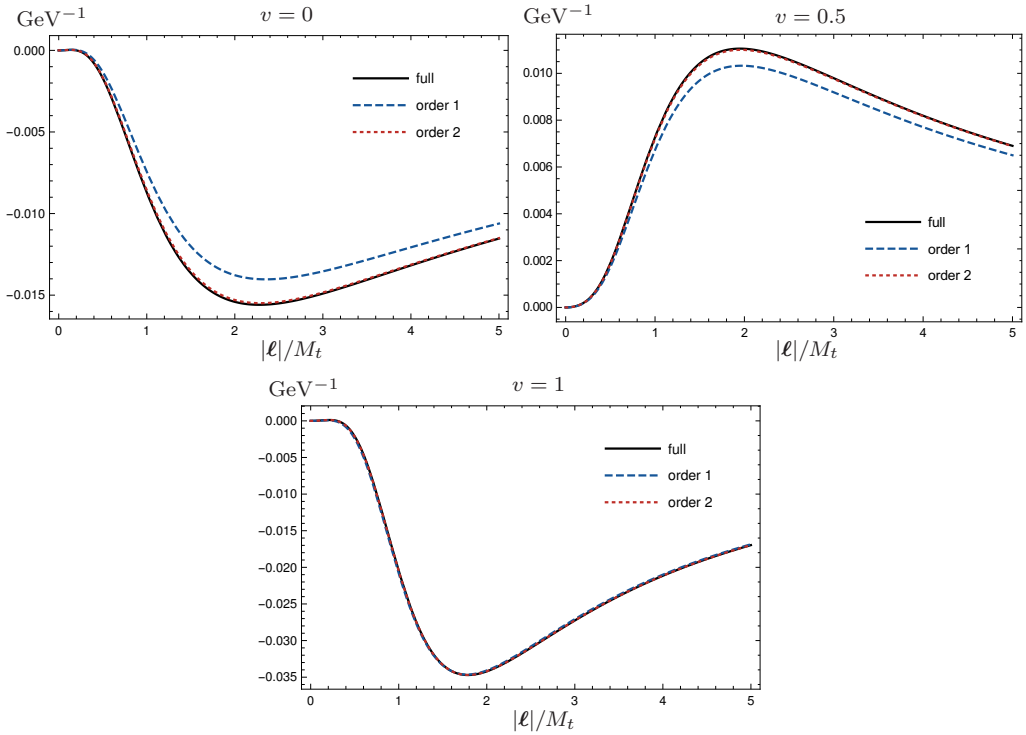

Figure 5.3: The convergence behavior of the integrand-level large-mass expansion of the form factor F_{12} in Eq. (5.36) for the physical values of the masses, evaluated for the loop three-momentum $\boldsymbol{\ell}$ being orthogonal ($v = 0.5$), parallel ($v = 0$) or antiparallel ($v = 1$) to the momentum $\boldsymbol{p}_3$ of the final-state gluon.

Table 5.1: The values obtained through integration of the large-mass expansion Eq. (5.36) and their relative errors with respect to the full result 0.000 934. Evaluation with physical values for the masses and $s = 0.1M_t^2$.

	integrated result	rel. error
$n = 1$	$-0.004\,979$	$-290\,\%$
$n = 2$	$0.000\,828$	$12\,\%$
$n = 3$	$0.000\,927$	$0.7\,\%$

5.4.2 Large center-of-mass energy expansion

With the particle running through the loop being much lighter than the energy entering the loop

$$s \gg \{M_t^2, M_H^2\}\,, \tag{5.38}$$

the process takes place above threshold. Thus the propagator has a singularity on the integration path which must be correctly imitated by the expansion. According to the guidelines laid out in Section 4.1 the parameters shall be chosen as

$$Q_{20}^2 = s\,, \quad \Gamma_{20} = s + M_t^2\,, \quad r_{20} = -\frac{M_t}{\sqrt{s}} + \imath 0\,. \tag{5.39}$$

This leads to the expanded propagator

$$G_D(q_{12}; q_0)\tilde{\delta}\left(q_{12}\right) \overset{M_t^2 \ll s}{=} \sum_{n=0}^{\infty} \frac{\left(M_t^2\right)^n}{\left(2p_{12}\cdot q_{12} + s + M_t^2 + \imath 0\right)^{n+1}}\,. \tag{5.40}$$

The expanded integrand in the limit of a large center-of-mass energy is obtained by replacing the diverging propagator in the third dual contribution, as was done for the large mass expansion, giving

$$F_{12}^{s\gg M_t^2} = F_{12}\left(\tilde{\delta}\left(q_0\right)\right) + F_{12}\left(\tilde{\delta}\left(q_3\right)\right) + F_{12}^{s\gg M_t^2}\left(\tilde{\delta}\left(q_{12}\right)\right)\,, \tag{5.41}$$

Table 5.2: The values obtained through integration of the large center-of-mass energy expansion in Eq. (5.41) and their relative errors with respect to the full result $F_{12} = -0.005\,998 - 0.025\,854\imath$. Evaluation with physical values for the masses and $s = 10M_t^2$.

	integrated result		rel. error	
	Re	Im	Re	Im
$n = 1$	$-0.003\,656$	$-0.024\,999$	49 %	3.4 %
$n = 2$	$-0.005\,897$	$-0.025\,931$	1.7 %	-0.30 %
$n = 3$	$-0.005\,993$	$-0.025\,867$	0.081 %	-0.050 %

where

$$
\begin{aligned}
&F_{12}^{s\gg M_t^2}\left(\tilde{\delta}\left(q_{12}\right)\right) = \\
&-\int_\ell \tilde{\delta}\left(q_{12}\right) s \sum_{n=0}^{\infty} \frac{\left(M_t^2\right)^n}{\left(2p_{12}\cdot q_{12} + s + M_t^2 + \imath 0\right)^{n+1}} \\
&\times \left[\left(\frac{sM_t^2}{M_H^2 - 2h\cdot q_{12}} \frac{M_H^2 - s}{s^2} c_1 + c_2\right) \frac{1}{(M_H^2 - s)}\right. \\
&+ \frac{c_2 - 2c_3}{(M_H^2 - s)s}\left(2p_{12}\cdot q_{12} + s\right) + c_3 \frac{M_H^2 - 2h\cdot q_{12}}{(M_H^2 - s)s} \\
&+ \frac{1}{(M_H^2 - s)^2} \frac{1}{M_H^2 - 2h\cdot q_{12}} \left(\frac{8p_{12}\cdot q_{12}}{d-2}\left(\frac{2(M_H^2 - s)^2}{s} + \left((d-4)s + 3dM_H^2\right)\right)\right. \\
&\left.\left. + 8M_H^2\left(s + \frac{M_H^2}{d-2}\right) + \left(2p_{12}\cdot q_{12}\right)^2\left(-c_2\frac{M_H^2}{s} + 4\right)\right)\right].
\end{aligned}
\tag{5.42}
$$

As expected integrand-level convergence breaks down only around the singularity and is good in the remainder of the integration range as can be seen in Fig. 5.4. The integrated results converge to the full result much faster than what was observed for the large mass expansion as shown in Table 5.2.

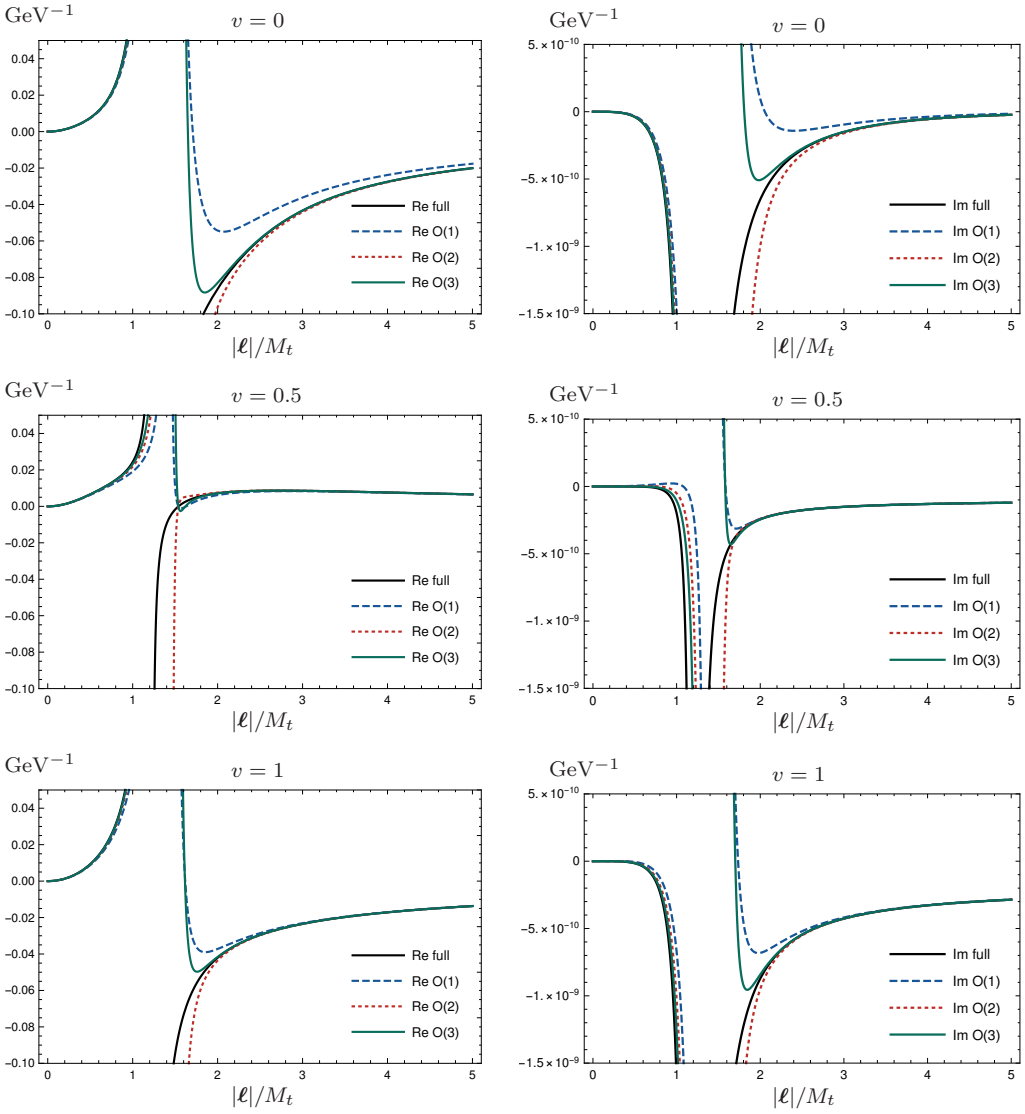

Figure 5.4: The convergence behavior of the integrand-level large center-of-mass energy expansion of the form factor F_{12} in Eq. (5.41) for the physical values of the masses, $s = 10M_t^2$ and $i0 = \imath 10^{-3}$, evaluated for the loop three-momentum $\boldsymbol{\ell}$ being orthogonal ($v = 1.5$), parallel ($v = 0$) or antiparallel ($v = 0$) to the momentum $\boldsymbol{p}_3$ of the final-state gluon.

Chapter 6

Summary and outlook

The experimental advances of the past decades have permitted exhaustive tests of the SM of particle physics revealing almost no discrepancies between observations and theory predictions. Various arguments, however, lead to the expectation that the SM does not provide a complete description of fundamental particle physics. In order to determine the structure of BSM physics one of the available options is the construction of ever larger particle accelerators allowing to explore particle interactions at even higher energies. An appealing alternative lies in the pursuit of precision observables: with the vast available data of current and future LHC runs it is essential to develop methods beyond the state-of-the-art for increasing the precision of theory predictions. Current limitations in perturbative calculations of scattering amplitudes are connected to the escalating difficulty when increasing either the number of loops, external legs or contributing energy scales.

While the traditional procedure for the calculation of scattering amplitudes relies on regularizing the appearing integrals through changing the number of space-time dimensions, an alternative regularization scheme has been introduced during the last decades based on solving the integral over the energy-component of the loop four-momentum by applying Cauchy's residue theorem. Known under the name of loop-tree duality, this novel method allows to work with integrands depending only on Euclidean three-momenta, which facilitates cancellations of both ultraviolet and infrared singularities already at integrand-level and thus renders the change of dimensions unnecessary.

After a short overview of QFT and the SM this thesis has presented a derivation of the one-loop formula of the LTD from the application of the residue theorem. We have put special emphasis on the emergence of singularities in the dual integrand and the distinction between those of physical origin from spurious

ones. This allowed us to show clearly the cancellations between non-physical divergences appearing in different parts of the dual integrand and analyze the kinematic limits in which divergences related to normal and anomalous thresholds appear. The extension of the formalism to the two-loop case has been exemplified through the detailed calculation of the sunrise amplitude, show-casing how the cancellation of non-physical divergences perseveres at higher orders. We have provided an entirely causal representation of the sunrise amplitude and extended this to its generalization to the multiloop case described by the MLT. Further multiloop topologies have been defined and important relations between their singular structures developed.

The main part of this thesis has been focused on the description of asymptotic expansions in the context of the LTD which had first been described for the one-loop amplitude describing the decay of the Higgs boson into two photons. This amplitude and its calculation using the LTD has been reviewed here and the asymptotic expansions have been rederived. A detailed analysis of their integrand- and integral-level convergence behavior has been carried out.

With the goal of generalizing these asymptotic expansions and making them applicable to a wider range of scattering amplitudes we have started by developing a procedure for the expansion of the dual propagator as it encodes the singular structure of a dual integrand. Applying this we have developed several benchmark asymptotic expansions of Feynman integrals in the LTD formalism. These asymptotic expansions take place at integrand-level in the Euclidean space of the loop three-momentum, where the hierarchies among internal and external scales are more evident than in the Minkowski space of the four-momentum. The method is well-defined since convergence to the full integral is achieved both in the final result and, remarkably, at integrand-level, giving ample justification for applying these expansions. Additionally, we have shown that the UV behavior of the individual contributions to the asymptotic expansion does not increase when including higher orders in the expansion. Renormalization is completed locally in four space-time dimensions including only the first terms of the expansion. Both of these aspects are an improvement compared to the commonly used method of Expansion by Regions and a numerical comparison between the methods showed comparably fast convergence.

We have presented explicit results for the scalar two- and three-point functions at one loop in different kinematical limits. Specifically, we have achieved with a single expression a universal description of several asymptotic limits of the two-point function by conveniently selecting certain parameters of this expression. Examples of the integrand-level convergence have been provided for a variety of

kinematic situations, including scenarios above threshold and the threshold limit itself. The recent developments in the realization of the LTD representation at all orders appear especially suitable to facilitating asymptotic expansions. We have provided an additional example to all loop orders by exploiting the simplicity of the causal representation.

As a first application to a physically relevant amplitude highly boosted Higgs boson production has been examined, being a good candidate due to the various appearing energy scales. We have utilized the general expansion of the dual propagator to obtain asymptotic expansions for the amplitude describing the production of a Higgs boson and a gluon from a quark-antiquark pair. Both a kinematic limit below and above threshold have been considered and the integrand-level convergence analyzed.

Further work is still needed to make the developed asymptotic expansions applicable to arbitrary multiloop amplitudes. Describing relevant physical scattering amplitudes with high precision exactly in those parts of the kinematic space where their impact on observables relevant for BSM physics is greatest will allow the more efficient use of numerical resources and hopefully contribute to the ongoing endeavour of improving our understanding of the most fundamental processes found in nature.

Chapter 7

Resum

La descripció conjunta de les interaccions electrofeble i forta en termes d'una teoria quàntica de camps (TQC) s'anomena el model estàndard de física de partícules (ME). Ha tingut un gran èxit en descriure i explicar una àmplia gamma d'observacions tant en física de partícules com en astrofísica a una alta precisió i, per tant, s'ha acordat, almenys com una teoria efectiva en un rang d'energia limitat, entre tots els físics. De fet, habitualment s'afirma que el ME funciona *massa bé*, ja que és força difícil trobar discrepàncies entre les prediccions del ME i les observacions. No obstant, hi ha inconsistències fonamentals que el ME no pot resoldre com l'asimetria matèria-antimatèria observada a l'univers actual o les masses dels neutrins. En els intents de determinar quin sector del ME necessita ser modificat, experiments en física de partícules com els del Gran Col·lisionador d'Hadrons del CERN (GCH) continuen augmentant la precisió i el seu rang d'energia. D'altra banda, les tècniques actuals de càlcul teòric tenen dificultats per assolir un grau de precisió comparable amb els experiments. Facilitar la inclusió de contribucions quàntiques d'ordre superior addicionals a les prediccions TQC està, per tant, a l'avantguarda de la investigació actual. Un breu resum de la TQC i alguns detalls sobre el ME es recullen al capítol 1 d'aquesta tesi i es resumeixen a la secció 7.2.1.

Entre d'altres, s'ha proposat el marc de la dualitat arbre-bucle (DAB) per proporcionar una alternativa al mètode tradicional en la TQC pertorbativa. Aquest mètode té l'avantatge de permetre realitzar càlculs sense canviar el nombre de dimensions de l'espaitemps. Tant els seus fonaments com els nous desenvolupaments per determinar una representació completament causal a primer ordre i més enllà es troben al capítol 2 i es resumeixen a la secció 7.2.2.

Les teories per a la física més enllà del ME (MEME) es desvien de la predicció del ME en un rang d'energia o límit cinemàtic específic d'alguns processos. Per tant, només és necessari calcular una predicció precisa en aquests límits rellevants. La DAB proporciona un punt de partida ideal per al desenvolupament d'expansions asimptòtiques a nivell d'integrand, ja que l'integrand DAB és una funció dels 3-moments euclidis. D'aquesta manera s'eviten les cancel·lacions entre diferents components del 4-moment de Minkowski, que dificulten la determinació clara de les escales relatives dins de les expressions de l'integrand. Les primeres ampliacions asimptòtiques en el context de la DAB es van trobar en l'amplitud de desintegració del bosó de Higgs en dos fotons, estudiada a l'ordre principal. El càlcul d'aquest procés es proporciona al capítol 3, on també s'estudia la naturalesa i el comportament de convergència de les expansions involucrades.

La part principal d'aquesta tesi, en el capítol 4, és el desenvolupament d'un enfocament sistemàtic per determinar les expansions asimptòtiques pel propa-

gador dual i, per tant, les amplituds DAB. Les ampliacions trobades es posen a prova a nivell d'un bucle, proporcionant també les expansions asimptòtiques per a una configuració important amb més d'un bucle (*multiloop* d'ara endavant). Al capítol 5 s'explora una aplicació al procés físicament rellevant de la producció de partícules Higgs amb un gran moment transversal.

7.1 Objectius

Les expansions asimptòtiques trobades per a l'amplitud de $H \to \gamma\gamma$ [72] són una prova de concepte que mostra que les expansions convergents a nivell d'integrand es poden formular de manera exitosa en el context de la DAB. No obstant, les expansions trobades són molt específiques de l'amplitud considerada i la seva forma analítica: un simple canvi en el moment del bucle en un dels diagrames ja exigiria reformular fonamentalment les expansions, sent aquesta una de les moltes opcions arbitràries durant el càlcul que tenen un impacte en si les expansions trobades es poden aplicar. Per tant, es necessita una manera més general de formular expansions asimptòtiques.

La formulació d'un enfocament sistemàtic per introduir expansions asimptòtiques en els integrands duals ha estat l'objectiu principal d'aquest treball. L'objectiu era trobar expansions que convergiren bé tant a nivell d'integrand com a nivell d'integral i simplificar idealment tant la integració analítica com la numèrica. Aquestes ampliacions no han de ser específiques, de manera que es puguen aplicar a qualsevol amplitud d'un sol bucle, amb l'objectiu a llarg termini d'extendre el formalisme a escenaris *multiloop*. És en aquest punt que l'aplicació del mètode DAB als càlculs físics pot proporcionar eines addicionals a la fenomenologia del ME i més enllà del ME.

7.2 Metodologia

7.2.1 La teoria quàntica de camps i el Modèl Estàndard

El tipus de marc teòric necessari per descriure les interaccions de les partícules subatòmiques ha de ser capaç de complir un conjunt de requisits. A causa de les petites escales de distància implicades, inversament relacionades amb l'energia dels processos a través de la relació d'incertesa, es necessita una teoria quàntica. Aquesta teoria ha de ser capaç de relacionar infinitament molts graus de llibertat per tal de descriure conceptes com el camp electromagnètic, o vist des d'un angle diferent, la producció de parells d'antípartícula-partícula des del buit en qualsevol

punt de l'espaitemps. Amb velocitats properes a la velocitat de la llum també és necessari incorporar la relativitat especial al formalisme. Una de les construccions teòriques que compleixen aquestes condicions és una *teoria quàntica de camps* (TQC), i de fet, s'espera que en qualsevol marc que sigui necessari per unir la física de partícules amb gravetat a l'escala de Planck, la teoria efectiva corresponent que descriu la naturalesa a escales d'energia accessibles en els experiments actuals de física de partícules sigui una TQC.

L'objectiu general en física de partícules és predir la probabilitat de dispersió i desintegració d'esdeveniments. Aquests es produeixen de forma natural o es provoquen accelerant partícules a energies extremadament altes i facilitant la seva col·lisió en experiments a gran escala com el GCH. La probabilitat que un estat asimptòtic inicial de les partícules evolucioni en un estat asimptòtic final s'escriu generalment en termes d'una amplitud invariant de Lorentz $\imath\mathcal{M}$. L'amplitud es pot calcular a partir de la lagrangià $\mathcal{L}$ d'una TQC. Aquest està format mínimament per termes cinètics que contenen els quadrats d'un tipus de camp. Els termes addicionals amb tres o més camps del mateix o diferent tipus, s'anomenen termes d'interacció.

Qualsevol procés de dispersió conté una quantitat infinita de termes amb diverses potències de la interacció definida al lagrangià. En aquelles TQC on l'acoblament que apareix en el terme d'interacció és petit, aquests termes es poden ordenar en potències de l'acoblament. Llavors l'expansió en l'acoblament es pot utilitzar per calcular un procés fins a un ordre especificat i, per tant, per limitar, però definir, la precisió. Aquest procediment es coneix com a *teoria de la pertorbacions* i permet escriure l'amplitud en una expansió pertorbativa. Per a una teoria amb l'acoblament λ això equival a

$$\mathcal{M} = \lambda\mathcal{M}^{(1)} + \lambda^2\mathcal{M}^{(2)} + \lambda^3\mathcal{M}^{(3)} + \mathcal{O}\left(\lambda^4\right) , \tag{7.1}$$

amb la contribució de l'ordre inicial (LO, per les sigles en anglès) denotada per $\mathcal{M}^{(1)}$, la contribució de l'ordre següent a l'inicial (NLO) per $\mathcal{M}^{(2)}$ i la contribució del següent ordre (NNLO) per $\mathcal{M}^{(3)}$. Hi ha diverses tècniques per obtenir els termes que contribueixen a l'expansió pertorbativa en qualsevol ordre donat. En un nivell pràctic, l'enfocament esquemàtic és més convenient, on les partícules es representen per línies i les interaccions per vèrtexs.

Per una TQC amb un camp escalar ϕ, amb un terme d'interacció ϕ^4, l'expansió pertorbativa es pot visualitzar com

$\mathcal{M} =$ 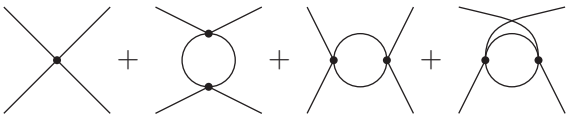 $+ \mathcal{O}\left(\lambda^3\right) .$ (7.2)

En aquests anomenats *diagrames de Feynman* les línies i vèrtexs tenen definicions matemàtiques clares derivades del lagrangià anomenades *regles de Feynman*. En concret, els vèrtexs sempre inclouen un factor de l'acoblament rellevant. Els diagrames de Feynman com el primer de Eq. (7.2), on cada línia pertany a una partícula asimptòtica, s'anomenen diagrames a nivell d'arbre. El seu valor es pot llegir directament utilitzant les regles de Feynman. Els diagrames amb circuits tancats s'anomenen diagrames de bucle - el seu càlcul implica resoldre una integral sobre el moment de quatre dimensions que passa a través del bucle, que en molts casos condueix a singularitats i altres dificultats tècniques. Les línies internes corresponen als propagadors de Feynman que són funcions potencialment divergents

$$G_F(q) = \frac{1}{q^2 - m^2 + \imath 0}\,, \tag{7.3}$$

on q és el 4-moment que corre al llarg d'aquesta línia i m la massa de la partícula que representa. Aquest propagador està ben definit només amb el regulador imaginari infinitesimal $\imath 0$ que circumventa la singularitat explícita quan la partícula es troba a la capa de masa (*on shell*, d'ara endavant).

L'ocurrència d'una divergència en integrals de bucle no és l'excepció, sinó la norma. De fet, els càlculs d'ordre superior en TQC pertorbativa a sovint impliquen haver de tractar amb expressions que no poden ser avaluades per si soles i en quatre dimensions espai-temporals. No obstant, els observables físics han de ser necessàriament finits i, de fet, TQC només es va convertir en una eina acceptada i àmpliament utilitzada en física de partícules quan s'havien trobat mètodes per reescriure expressions divergents d'una manera ben definida i consistent. Aquest procés d'eliminació de singularitats, sovint fent-les explícites en termes d'un paràmetre infinitesimal, s'anomena *regularització*.

Mentre que els llindars unitaris i anòmals són una part integral d'una amplitud de dispersió i les singularitats espúries cancel·len durant el càlcul, les divergències relacionades amb la regió d'alta energia de la integral (UV) i les divergències originades a la regió de baixa energia de la integral (IR) s'han de regularitzar i tractar amb cura per tal d'obtenir resultats inequívocs per als observables físics.

En la tècnica de regularització més comuna, els càlculs es realitzen en dimensions d'espai-temps $d = 4 - 2\varepsilon$. Això deixa les expressions problemàtiques matemàticament ben definides sempre que ε no sigui zero. Per tant, es pot trobar un resultat explícit i la seva dependència del paràmetre ε codifica la singularitat d'una manera inexorable. Aquesta idea va ser introduïda per 't Hooft i Veltman [16], i independentment per Giambiagi i Bollini [17], en els anys setanta i és coneguda sota el nom de *regularització dimensional* (REGDI).

En restar un contraterme que conté la mateixa estructura divergent l'amplitud és llavors finita i les dimensions es poden establir al valor físic

$$\mathcal{A}_R^{(1)} = \mathcal{A}^{(1)} - \mathcal{A}_{\mathrm{UV}}^{(1)}\Big|_{d=4}. \tag{7.4}$$

La qualitat més sorprenent d'aquest enfocament és que conserva totes les simetries fonamentals de la teoria usada. Això fa que sigui possible no només regularitzar una amplitud específica, sinó també fer que tota la teoria estigui ben definida en límit ultraviolat d'energia (UV). Aquest procés es basa en el reconeixement de que els paràmetres que apareixen en el lagrangià, com ara masses i acoblaments, no són necessàriament les propietats físicament mesurables de les partícules descrites per la teoria. Durant l'anomenada *renormalització* els paràmetres nus del lagrangià es redefineixen per absorbir les divergències UV combinant l'amplitud no normalitzada amb el contraterme. A la teoria renormalitzada i el seu lagrangià, escrit en termes de les masses observades i els acoblaments, totes les amplituds estan immediatament lliures de les singularitats del UV.

Els paràmetres de la teoria renormalitzada depenen explícitament de la dimensió no física, de manera que aquest tipus de sostracció sistemàtica només és possible dins la REGDI. No obstant això, després d'haver identificat els contratermes necessaris en la REGDI és possible utilitzar aquestes mateixes expressions també en altres marcs, fins i tot en quatre dimensions. La resta directa del contraterme i el càlcul de l'amplitud renormalitzada en quatre dimensions és suficient per al càlcul d'un observable específic.

Com S. Weinberg va afirmar famosament, per construir una TQC només cal conèixer els graus de llibertat rellevants, és a dir, les partícules que interaccionen a l'escala d'energia considerada, i les simetries del sistema considerat [42]. El lagrangià consisteix llavors de tots els termes possibles que contenen els camps permesos i respecten les simetries, incloses les transformacions contínues de Lorentz. Mitjançant l'ús d'aquest lagrangià per calcular un observable s'obté l'element de matriu S més general possible que està d'acord amb les simetries assumides, l'analítica, la unicitat pertorbativa i el principi de descomposició de cúmuls. Per a les partícules fonamentals conegudes, es pot construir un lagrangià utilitzant les simetries observades experimentalment. La unió de tots els operadors renormalitzables que apareixen en aquest lagrangià defineix el model estàndard de física de partícules.

Les partícules considerades dins de l'àmbit de la física de partícules s'agrupen en fermions, amb espí semienter, i bosons, amb espí enter. Les partícules que medien les interaccions fonamentals són els bosons. Per a l'electromagnetisme, aquests són els fotons, i els seus homòlegs per a la interacció forta s'anomenen

gluons. Les interaccions febles es medien a través dels bosons massius $W.\pm$ i Z i, finalment, hi ha el bosó Higgs, relacionat amb el mecanisme per a la generació de masses. Entre els fermions, que constitueixen el contingut de matèria del ME, hi ha el quark *up* i *down*, que són els components principals de protons i neutrons. A més a més, existeixen dues còpies més pesades d'aquest conjunt: en general, hi ha sis quarks afectats per la interacció forta, organitzats en parells de masses creixents

$$\begin{bmatrix} u \\ d \end{bmatrix}, \quad \begin{bmatrix} c \\ s \end{bmatrix}, \quad \begin{bmatrix} t \\ b \end{bmatrix}. \tag{7.5}$$

Els fermions fonamentals restants no afectats per la interacció forta s'anomenen leptons. Aquest grup es compon de versions més pesades de l'electró i els corresponents neutrins:

$$\begin{bmatrix} \nu_e \\ e^- \end{bmatrix}, \quad \begin{bmatrix} \nu_\mu \\ \mu^- \end{bmatrix}, \quad \begin{bmatrix} \nu_\tau \\ \tau^- \end{bmatrix}. \tag{7.6}$$

Les diferències entre els conjunts semblen estar només en la massa i, per tant, es consideren tres famílies. Els fermions, les seves corresponents antipartícules, el bosó de gauge i el bosó de Higgs són el que entenem actualment com a partícules fonamentals i, com a tals, són els camps les interaccions dels quals són descrites pel ME.

A més del requisit bàsic de que les lleis de la física, també de la física de partícules, no depenguin de la posició o la velocitat de l'observador, és a dir, que han de ser invariants sota transformacions ortocrones de Lorentz, el ME es construeix sobre la base de simetries de *gauge*. Aquestes simetries estan relacionades amb el fet de que els camps utilitzats per descriure les interaccions de partícules no són ells mateixos objectes físics que es poden mesurar directament. Les diferents configuracions sense rellevància física escollides per als camps han de conduir a exactament el mateix resultat mesurable. Les operacions que converteixen una d'aquestes configuracions permeses en una altra s'anomenen *transformacions de gauge*. Les simetries de gauge relacionades amb la interacció electrofeble i forta formen el grup de simetria del ME

$$SU(3)_C \otimes SU(2)_L \otimes U(1)_Y . \tag{7.7}$$

El primer subgrup d'aquests està relacionat amb la interacció forta. Les partícules observables que es veuen afectades per aquesta interacció forta són els hadrons. Aquests es produeixen com barions fermiònics i mesons bosònics i tots dos encara tenen una estructura interna. Essencialment, els mesons s'identifiquen

amb l'estat lligat d'un quark i un antiquark, mentre que els (anti-)barions corresponen a un estat de tres (anti-)quarks. S'ha establert experimentalment a través de la mesura dels factors de la forma de protó en experiments de dispersió inelàstica profunda que els quarks es comporten com a partícules gairebé lliures a distàncies molt curtes, el que porta a un requisit experimental anomenat *llibertat asimptòtica*.

Com tots els estats asimptòtics són singlets de color, la simetria que defineix la interacció forta és la invariància sota les rotacions en l'espai de color tridimensional. La transformació de simetria corresponent es pot utilitzar per construir la teoria de gauge de la cromodinàmica quàntica (CDQ).

Per construir tot l'espectre hadrònic cal introduir un nou nombre quàntic associat als quarks, la càrrega de color: sense ell les estadístiques de Fermi-Dirac es violarien en el sector bariònic. El color en si mateix no es pot observar directament, ja que tots els estats asimptòtics són singlets de color que condueixen al segon requisit experimental d'una teoria que descriu la interacció forta: a causa de la seva càrrega de color, els quarks no poden aparèixer fora dels estats lligats, amb el color neutre. Aquest concepte s'anomena *confinament*. Amb la mesura de la relació entre les desintegracions hadròniques i leptòniques del leptó τ^-, el nombre de colors es va determinar a ser tres.

La interacció electrofeble descrita pel ME conté, d'una banda, la interacció electromagnètica mediada per fotons entre partícules amb càrrega elèctrica, que es descrita per l'anomenada electrodinàmica quàntica (EDQ). Per altra banda, es descriuen també les interaccions febles que acoblen a tots els fermions fonamentals a través dels bosons de gauge massius Z i $W^{\pm}$. Aquestes interaccions tenen en comú que els seus acoblaments són suficientment petits per a un tractament pertorbatiu: les amplituds de transició es poden expandir en termes d'acoblaments electromagnètics i febles i calcular fins al nivell necessari de precisió.

En estudiar les distribucions d'energia i angulars de la desintegració β s'ha revelat que la direcció dels productes de desintegració depenen l'espí de les partícules implicades. De fet, només els fermions esquerrans i els antifermions dretans semblaven participar en aquest tipus d'interaccions que implicaven el canvi de sabor d'un leptó massiu. L'observació addicional als experiments de dispersió amb neutrins de que el nombre de leptons de qualsevol sabor es conserva per separat, distingint així els neutrins dels antineutrins, així com els arguments teòrics que exigeixen un comportament correcte de la teoria a altes energies ha estat suficient per al desenvolupament de la teoria electrofeble. En aquest procés, els bosons vectorials i les seves masses van ser predites, confirmant-se la seva existència en experiments posteriors.

Els processos com les desintegracions β estan mediats pels bosons vectorials carregats $W^{\pm}$. Tenint en compte que només els fermions esquerrans (dretans) es veuen afectats per aquestes anomenades corrents *carregades*, és clar que dues simetries discretes importants es trenquen al màxim: la paritat, que gira el signe de la coordenada espacial i, per tant, intercanvia les partícules esquerranes amb les seves contraparts dretanes, i la conjugació de càrrega, que substitueix les partícules per les seves antipartícules i viceversa.

Altres processos com la dispersió d'electrons-positrons són mediats per bosons vectorials neutres: el fotó sense massa i el bosó massiu de Z. Com que cap d'aquests dos té càrrega electromagnètica, aquestes interaccions es coneixen com *corrents neutres*. Tots dos bosons vectorials s'uneixen sempre a un fermió i l'antifermió corresponent, conservant el sabor.

Perquè incloure les masses en la teoria, s'ha de trencar la simetria de gauge electrofeble. Això es pot aconseguir mantenint el lagrangià completament simètric, i per tant renormalitzable, però trencant la simetria espontàniament. En el cas del ME, la *ruptura espontània de la simetria* (RES) es realitza en forma del mecanisme de Higgs.

Unint les descripcions de la interacció forta a través de CDQ i la interacció electrofeble, el lagrangià complet del ME després de la RES és donat per

$$\mathcal{L}_{\mathrm{ME}} = \mathcal{L}_{\mathrm{CDQ}} + \mathcal{L}_{\mathrm{electrofèble}} + \mathcal{L}_{\mathrm{escalar}} + \mathcal{L}_{\mathrm{Yukawa}} \,. \tag{7.8}$$

Aquesta teoria ha estat extremadament exitosa en descriure no només una gran varietat d'experiments en col·lisionadors de partícules, sinó també en intents cosmològics per desxifrar l'origen i l'evolució de l'univers. Aquesta teoria ha segut testejada amb gran precisió, calculantse correccions en certs observables amb fins a cinc bucles en EDQ.

7.2.2 La dualitat arbre-bucle

S'han desenvolupat diverses tècniques en els últims anys per fer front al problema de quantificar integrals no integrables, moltes d'elles resumides en la referènca [9], entre elles la dualitat arbre-bucle (DAB) [3, 4, 66–82]. La base de la DAB és l'ús del teorema de residus de Cauchy per integrar una component del moment del bucle. Les amplituds de bucle es poden expressar com una suma de residus que es reformulen com les anomenades amplituds duals. Aquestes consisteixen en sumes d'objectes semblants a les amplituds a nivell d'arbre que han de ser integrades en el que essencialment és una integral d'espai de fase.

L'amplitud general de dispersió amb un sol bucle amb N potes externes en la

representació de Feynman és donada per

$$\mathcal{A}_N^{(1)} = \int_\ell a_N^{(1)} = \int_\ell \mathcal{N}\left(\ell, \{p_k\}_N\right) \left(\prod_{i=1}^{N} G_F(q_i)\right) \ , \tag{7.9}$$

amb la mesura integral de bucle $\int_\ell$, en dimensions de l'espaitemps $d = 4 - 2\varepsilon$, ve donada per l'Eq. (A.13). En aquesta expressió, $\mathcal{N}\left(\ell, \{p_k\}_N\right)$ és una funció del moment del bucle ℓ i dels moments externs $\{p_k\}_N$. Els propagadors de Feynman $G_F(q_i)$ porten moments $q_i = \ell + k_i$, on k_i són combinacions lineals dels moments externs.

La formulació original del teorema de la dualitat arbre-bucle tal com es presenta a Ref. [66] permet aplicar el teorema de residus de Cauchy i reescriure el resultat en la forma compacta

$$\mathcal{A}_N^{(1)} = -\int_\ell \mathcal{N}\left(\ell, \{p_k\}_N\right) \sum_{i=1}^{N} \tilde{\delta}\left(q_i\right) \left(\prod_{j\neq i} G_D\left(q_i; q_j\right)\right) \ , \tag{7.10}$$

on $\tilde{\delta}\left(q_i\right) = 2\pi i \ \theta(q_{i,0})\delta(q_i^2 - m_i^2)$ es una versió modificada del funcional delta i el propagador dual es dona per

$$G_D(q_i; q_j) = \left. \frac{1}{2q_i \cdot k_{ji} + m_i^2 + k_{ji}^2 - m_j^2 - \imath 0 \eta \cdot k_{ji}} \right|_{q_{i,0}=q_{i,0}^{(+)}} . \tag{7.11}$$

amb la energia *on shell* $q_{j,0}^{(+)} = \sqrt{\boldsymbol{q}^2 + m^2}$ i $k_{ji} = q_j - q_i$. En aquesta expressió, η és un vector temporal arbitrari future-like. Un moment intern diferent es posa *on shell* en cadascun dels sumands de l'Eq. (7.10), que s'anomenen convencionalment contribucions duals (també anomenades de vegades amplituds o talls duals). En cadascuna d'aquestes contribucions, el component d'energia del moment del bucle es fixa a través del funcional delta deixant per resoldre només la integral sobre el 3-moment euclidi. D'aquesta manera, s'aconsegueix representar la integral d'un bucle com una suma d'objectes semblants a amplituds de nivell d'arbre, en el sentit de que, amb un propagador intern *on shell*, les integrals de cada una de les contribucions duals s'assemblen a la integral d'espai de fase sobre una amplitud de nivell d'arbre, tal i com s'il·lustra a Fig. 7.1.

7.3 Resultats i conclusions: expansions asimptòtiques generals en un bucle i més enllà

El comportament de les amplituds de dispersió es regeix per les seves propietats analítiques. Com que aspirem a trobar expansions asimptòtiques a nivell

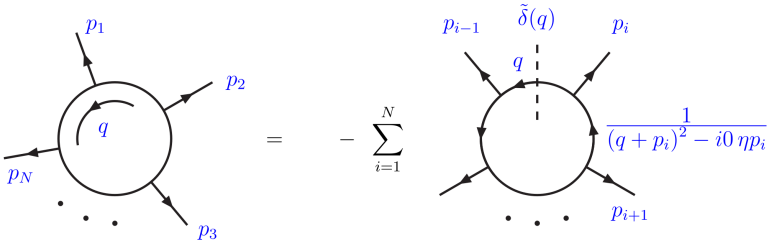

Figure 7.1: Una amplitud d'un sol bucle amb N partícules externes expressada a l'esquerra en la representació de Feynman i a la dreta després de l'aplicació de la DAB com es dona a 7.10. Figura extreta de [66].

d'integrand, hem de considerar detalladament l'anàlisi dels propagadors, que són els objectes que donen lloc a singularitats. Els propagadors duals poden manifestar singularitats no causals, a més de les divergències físiques relacionades amb la frontera causal i les singularitats IR. Aquestes divergències no físiques només apareixen quan els diversos termes de la suma de residus en un integrand dual es consideren per separat. Cal identificar les condicions en les quals apareixen tant les singularitats causals com les no físiques, així com la seva posició en l'espai d'integració abans d'expandir asimptòticament una amplitud.

Podem parametritzar qualsevol dels propagadors duals en la següent forma més adequada per a expansions asimptòtiques

$$\tilde{\delta}\left(q_i\right) G_D\left(q_i; q_j\right) = \frac{\tilde{\delta}\left(q_i\right)}{2q_i \cdot k_{ji} + \Gamma_{ij} + \Delta_{ij} - \imath 0 \eta \cdot k_{ji}} \tag{7.12}$$

amb $\Gamma_{ij} + \Delta_{ij} = k_{ji}^2 + m_i^2 - m_j^2$. Si $\Gamma_{ij} + \Delta_{ij}$ desapareix el propagador dual no s'expandeix. En cas contrari, el punt de partida per a l'expansió asimptòtica és exigir que la condició

$$|\Delta_{ij}| \ll |2q_i \cdot k_{ji} + \Gamma_{ij}| \tag{7.13}$$

es compleixi per a tot el rang de l'espai d'integració del bucle. L'única excepció a aquesta regla són les petites regions que envolten les divergències físiques. La característica distintiva del DAB és que com que els propagadors duals només apareixen en integrands on s'ha posat un moment de bucle *on shell*, la condició s'ha de complir en l'espai euclidià del 3-moment del bucle. Aleshores, el propa-

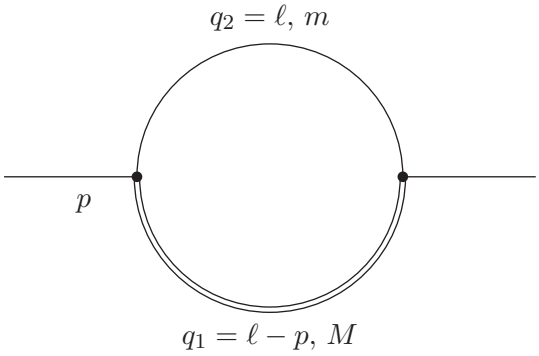

Figure 7.2: Funció escalar de dos punts amb dues masses internes diferents.

gador dual s'expandeix com

$$G_D\left(q_i; q_j\right) = \sum_{n=0}^{\infty} \frac{\left(-\Delta_{ij}\right)^n}{\left(2q_i \cdot k_{ji} + \Gamma_{ij} - i0\eta \cdot k_{ji}\right)^{n+1}} \,. \tag{7.14}$$

Una primera aplicació de l'expansió dels propagadors duals és l'expansió asimptòtica de la funció escalar de dos punts amb dues masses internes diferents. Això es representa pel diagrama de Fig. 7.2 i l'amplitud renormalitzada corresponent en la representació de Feynman és

$$\mathcal{A}^{(1,R)} = \left(\int_\ell G_F(q_1; M)\, G_F(q_2; m) - \left(G_F(\ell; \mu_{\rm UV})\right)^2 \right) \Big|_{d=4} \,, \tag{7.15}$$

amb $q_1 = \ell - p$ i $q_2 = \ell$. $\mu_{\rm UV}$ és una escala arbitrària. L'expressió analítica completa de la funció escalar de dos punts renormalitzada és ben coneguda a través de tècniques estàndard

$$\begin{aligned} \mathcal{A}^{(1,R)} = \frac{1}{16\pi^2} \Bigg[2 + \frac{p^2 + M^2 - m^2}{2p^2} \log\left(\frac{\mu_{\rm UV}^2}{M^2}\right) + \frac{p^2 + m^2 - M^2}{2p^2} \log\left(\frac{\mu_{\rm UV}^2}{m^2}\right) \\ + \frac{\lambda^{1/2}\left(p^2, m^2, M^2\right)}{p^2} \log\left(\frac{m^2 + M^2 - p^2 + \lambda^{1/2}\left(p^2, m^2, M^2\right)}{2mM} \right) \Bigg] \,. \end{aligned} \tag{7.16}$$

La representació dual de la funció escalar renormalitzada de dos punts és

$$\begin{aligned} \mathcal{A}^{(1,R)} = -\int_\ell \Bigg[\tilde{\delta}\left(q_1; M\right)\, G_D(q_1; \ell) + \tilde{\delta}\left(\ell; m\right)\, G_D(\ell; q_1) \\ + \frac{1}{2}\, \tilde{\delta}\left(\ell; \mu_{\rm UV}\right)\, \left(\ell_{0,\rm UV}^{(+)}\right)^{-2} \Bigg] = \int_0^\infty {\rm d}|\boldsymbol{\ell}|\, a(\boldsymbol{\ell}) \,. \end{aligned} \tag{7.17}$$

Aplicant l'expansió del propagador dual s'obté l'expansió asimptòtica de la funció de dos punts escalars. L'ordre renormalitzat n-èsima de l'expansió ve donat per

$$\mathcal{A}_{(n)}^{(1,R)} = \frac{1}{16\pi^2}\sum_{i,j}\left[2 + c_{0,i}\log\left(\frac{\mu_{\text{UV}}}{m_i}\right) + \sum_{k=0}^{n}\left(c_{1,i}^{(k)} + c_{2,i}^{(k)}\log\left(r_{ij}\right)\right)\right]. \tag{7.18}$$

Tingueu en compte que no s'ha d'especificar un límit cinemàtic específic. El coeficient $c_{0,i}$ ve donat per

$$c_{0,i} = \frac{m_i^2}{Q_i^2}\left(1 + \frac{1}{r_{ij}^2}\left(1 + \frac{\Delta_{ij}}{Q_i^2}\right)\right) = \frac{p^2 + m_i^2 - m_j^2}{p^2}, \tag{7.19}$$

i els coeficients $c_{1,i}^{(k)}$ i $c_{2,i}^{(k)}$ per als primers ordres són

$$\begin{aligned}
c_{1,i}^{(k)} &= -\frac{m_i^2}{Q_i^2}\left\{0, \frac{-\Delta_{ij}}{Q_i^2}\frac{-1}{r_{ij}^2}, \left(\frac{-\Delta_{ij}}{Q_i^2}\right)^2 \frac{1+r_{ij}^2}{2r_{ij}^2(1-r_{ij}^2)^2}, \left(\frac{-\Delta_{ij}}{Q_i^2}\right)^3 \frac{1+10r_{ij}^2+r_{ij}^4}{6r_{ij}^2(1-r_{ij}^2)^4}\right\},\\
c_{2,i}^{(k)} &= -\frac{m_i^2}{Q_i^2}\left\{1 - \frac{1}{r_{ij}^2}, \frac{-\Delta_{ij}}{Q_i^2}\frac{1+r_{ij}^2}{r_{ij}^2(1-r_{ij}^2)}, \left(\frac{-\Delta_{ij}}{Q_i^2}\right)^2 \frac{2}{(1-r_{ij}^2)^3},\right.\\
&\qquad\left.\left(\frac{-\Delta_{ij}}{Q_i^2}\right)^3 \frac{2(1+r_{ij}^2)}{(1-r_{ij}^2)^5}\right\}.
\end{aligned} \tag{7.20}$$

Cada terme de l'expansió és suprimit per potències extra de Δ_{ij}.

Hem estudiat diverses regions cinemàtiques i hem aconseguit les expansions asimptòtiques seleccionant convenientment els paràmetres d'expansió que s'utilitzen en l'expressió general, Eq. (7.18), que descriu tots aquests límits alhora. En cada límit es va aconseguir una convergència ràpida tant a nivell d'integrand com a nivell d'integral. A la figura 7.3 es pot veure clarament com la expansió convergeix perfectament sempre que no siga en el punt exacte de la divergència física. Els resultats específics dels límits estudiats es poden veure en les figures 4.2, 4.3, 4.5, 4.6, B.1, i en les taules 4.2, 4.3, 4.4, 4.5, B.1.

Les propietats de les amplituds duals també es poden explotar d'una manera més directa per facilitar les expansions asimptòtiques. Després d'aplicar DAB a l'integrand d'una integral de Feynman, el moment del bucle està restringit als valors on-shell. Així, l'expansió directa de l'integrand en una sèrie de Taylor respecte a qualsevol escala que es consideri petita o gran és inequívoca. Aquestes expansions asimptòtiques es poden fer en qualsevol lloc dins del domini d'integració i depenen de la mida del 3-moment euclidià del bucle. Per exemple, en el cas de

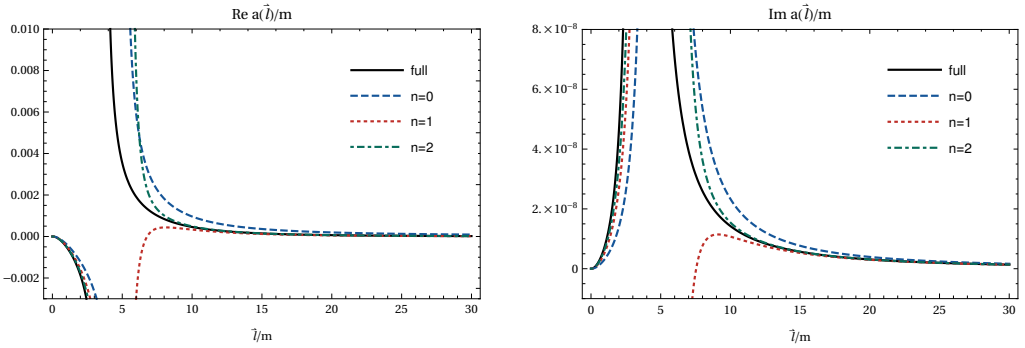

Figure 7.3: La convergència de l'expansió a nivell de integrand en el límit de un gran moment extern en la funció escalar de dos punts, Eq. (7.18), per als valors $\sqrt{p^2}/m = 10$, $\sqrt{p^2}/M = 2$, $\mu_{\rm UV} = M$ i $\imath 0 = \imath 10^{-3}$.

la funció de dos punts en el límit d'una gran massa, $M^2 \gg \{m^2, p^2\}$, es poden distingir dues regions en el 3-moment del bucle. Una regió tova amb $\boldsymbol{\ell}^2 \ll M^2$ i una regió dura amb $\boldsymbol{\ell}^2 \gg \{m^2, p^2\}$ i $\boldsymbol{\ell}^2 \sim M^2$. Anomenem a aquestes regions en el moment del bucle *regions duals* perquè només són accessibles després d'obtenir un domini d'integració euclidià a través de l'aplicació de DAB. El domini d'integració euclidià es pot dividir en dues expansions ben definides al nivell d'integrand com

$$\begin{aligned} \mathcal{A}^{(1,R)} &= \int_0^\infty \mathrm{d}|\boldsymbol{\ell}|\ a(\boldsymbol{\ell}) \\ &= \int_0^\lambda \mathrm{d}|\boldsymbol{\ell}|\ \mathcal{T}a(M,\infty) + \int_\lambda^\infty \mathrm{d}|\boldsymbol{\ell}|\ \mathcal{T}a(\{\boldsymbol{\ell}, M\},\infty) \end{aligned} \tag{7.21}$$

amb $m < \lambda < M$. La convergència al nivell d'integrand i el comportament propet de la escala λ es poden veure a la figura 7.4

També hem aplicat l'expansió del propagador dual a la funció escalar de tres punts. Com a primera aplicació a una amplitud físicament rellevant, la producció del bosó de Higgs ha estat examinada, sent un bon candidat a causa de les diverses escales d'energia que apareixen. Hem utilitzat l'expansió general del propagador dual per obtenir expansions asimptòtiques per a l'amplitud que descriu la producció d'un bosó Higgs i un gluó a partir d'un parell de quarks-antiquarks. S'ha considerat un límit cinemàtic per sota i per sobre de la frontera causal i s'ha analitzat la convergència a nivell d'integrand.

L'extensió del formalisme de DAB al cas de dos bucles s'ha exemplificat a través del càlcul detallat de l'amplitud del diagrama *posta de sol* (*sunset* en anglés) en la Fig. 2.8, mostrant com la cancel·lació de divergències no físiques

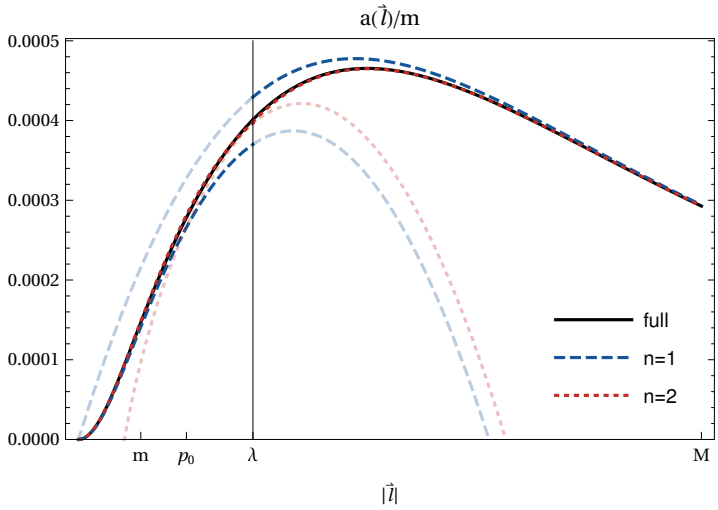

Figure 7.4: La convergència a nivell d'integrand de l'expansió en Eq. (7.21) per als valors $M = 10\,m$, $p^2 = 3\,m^2$, i $\mu_{\rm UV} = M$.

es manté en ordres superiors. Hem proporcionat una representació totalment causal de l'amplitud *posta de sol* i ho hem ampliat a la seva generalització al cas multiloop, la *topologia maximal de bucle* (MLT). Aquest tipus de diagrama L-bucle consisteix en conjunts $L+1$ de moments interns, definit a través dels moments d'integració $\{\ell_1, \ldots, \ell_L\}$ i la combinació lineal $\ell_{L+1} = -\sum_{i=1}^{L} \ell_i + p$, amb p com una suma de moments externs. La seva representació de Feynman la dona

$$\mathcal{A}^{(L)}_{\rm MLT} = \int_{1,\ldots,L} G_F(1,\ldots,L+1)\,, \tag{7.22}$$

que per $L = 2$ equival al diagrama general de dos bucles *posta de sol* de l'equació 2.40. En el cas de dos bucles, el MLT és l'única topologia possible i per tant és suficient per a la descripció de qualsevol amplitud de dispersió al nivell de dos bucles. A partir de l'avaluació dels residus per a diverses integrals *multiloop* representatives, hem derivat per inducció que

$$\mathcal{A}^{(L)}_{\rm MLT} = \int_{\vec{1},\ldots,\vec{L}} \sum_{i=1}^{n} G^{(L)}_D(1,\ldots,i-1,\overline{i+1},\ldots,\overline{n};i)\,, \tag{7.23}$$

donant així una representació DAB compacta per a qualsevol diagrama classificat a través de la topologia MLT. En particular, hem aconseguit una *representació*

causal per a l'amplitud escalar del MLT amb només un propagador intern per conjunt, donant així

$$\mathcal{A}^{(L)}_{\rm MLT} = -\int_{\vec{1},\ldots,\vec{L}} \frac{1}{x_{1,L}} \left(\frac{1}{\lambda^{-}_{1,L}} + \frac{1}{\lambda^{+}_{1,L}} \right) \tag{7.24}$$

amb $x_{1,L} = \prod_{i=1}^{L+1} 2q^{(+)}_{i,0}$. Les singularitats causals estan codificades en

$$\lambda^{\pm}_{1,L} = \sum_{i=1}^{L} q^{(p,+)}_{i,0} \pm p\,. \tag{7.25}$$

Una expressió comparable que està explícitament lliure de singularitats no físiques també es pot trobar per amplituds amb múltiples potències de propagadors, integrals no escalars, o més d'un propagador per conjunt. A més, s'han definit altres topologies *multiloop* i s'han desenvolupat importants relacions entre les seves estructures singulars.

La representació causal és particularment adequada per aconseguir l'expansió asimptòtica en el límit $p^2 \ll m_s^2$. Suposant $p = (p_0, \mathbf{0})$, obtenim

$$\mathcal{A}^{(L)}_{\rm MLT}(p^2 \ll m_s^2) = -2\sum_{n=0}^{\infty} (p^2)^n \int_{\vec{\ell}_1,\ldots,\vec{\ell}_L} \frac{\left(\lambda^0_{L+1}\right)^{-1-2n}}{x_{L+1}}\,, \tag{7.26}$$

amb $\lambda^0_{L+1} = \sum_{s=1}^{L+1} q^{(+)}_{s,0}$.

Encara es necessita més treball per fer que les expansions asimptòtiques desenvolupades siguin aplicables a amplituds *multiloop* arbitràries. La descripció d'amplituds de dispersió físicament rellevants amb alta precisió en aquelles parts de l'espai cinemàtic on l'impacte de la física MEME és major permetrà un ús més eficient dels recursos numèrics. Amb aquest fi, la DAB pot contribuir a l'esforç continu de millorar la nostra comprensió dels processos més fonamentals trobats a la natura.

Appendix A

Definitions, conventions and master integrals

For the metric tensor the convention used is the one common in particle physics

$$g_{\mu\nu} = g^{\mu\nu} = \begin{pmatrix} 1 & 0 & 0 & 0 \\ 0 & -1 & 0 & 0 \\ 0 & 0 & -1 & 0 \\ 0 & 0 & 0 & -1 \end{pmatrix} . \tag{A.1}$$

Four-momenta are denoted in terms of the Euclidean three-momentum $\boldsymbol{p} = \vec{p}$ by

$$p_\mu = (p^0, -\boldsymbol{p}) , \quad p^\mu = g^{\mu\nu} p_\nu = (p^0, \boldsymbol{p}) , \quad E_p = p^0 , \tag{A.2}$$

and the four-dimensional partial derivative is defined through

$$\partial_\mu = \frac{\partial}{\partial x^\mu} = \left(\frac{\partial}{\partial x^0}, \nabla \right) . \tag{A.3}$$

Whenever repeated indices appear a sum over them is implied. The scalar product is then given by

$$p \cdot q = p^\mu q_\mu = p^0 q^0 - \boldsymbol{p} \cdot \boldsymbol{q} . \tag{A.4}$$

The description of fermions in the context of Lorentz invariance demands the introduction of the Dirac algebra

$$\{\gamma^\mu, \gamma^\nu\} = 2 g^{\mu\nu} \times \mathbf{1}_n . \tag{A.5}$$

In four-dimensional Minkowski space the Dirac matrices are of at least $n = 4$ dimensions and a convenient choice is the chiral representation with

$$\gamma^0 = \begin{pmatrix} 0 & \mathbf{1}_2 \\ \mathbf{1}_2 & 0 \end{pmatrix}, \quad \gamma^i = \begin{pmatrix} 0 & \sigma^i \\ -\sigma^i & 0 \end{pmatrix} \tag{A.6}$$

in terms of the 2×2 identity matrix $\mathbf{1}_2$ and the Pauli matrices

$$\sigma^1 = \begin{pmatrix} 0 & 1 \\ 1 & 0 \end{pmatrix}, \quad \sigma^2 = \begin{pmatrix} 0 & -\imath \\ \imath & 0 \end{pmatrix}, \quad \sigma^3 = \begin{pmatrix} 1 & 0 \\ 0 & -1 \end{pmatrix}. \tag{A.7}$$

A short-hand notation for scalar products involving a Dirac matrix is

$$\not{p} = \gamma^\mu p_\mu \,. \tag{A.8}$$

The only fermions appearing in calculations in this thesis are quarks described by the relativistic spin-1/2 fields q (or q_f if the flavor f of the quark is relevant). The complementary definition of the conjugate field

$$\bar{q} = q^\dagger \gamma^0 \tag{A.9}$$

in terms of the Hermitian conjugate $q^\dagger$ is needed to define Lorentz-invariant terms for Lagrangians. The positive-frequency plane-wave solution of the free Dirac equation of a quark field is given by

$$q^{(+)} = u(p) e^{-ipx} \,, \tag{A.10}$$

introducing the Dirac spinor $u(p)$. The quark field is written as a linear combination of the positive- and negative-frequency solutions. In Feynman amplitudes, such as the one in Chapter 5, it is thus the positive-frequency spinors $u(p)$ and their negative-frequency equivalent $v(p)$, as well as their conjugates $\bar{u}$ and $\bar{v}$, that appear. Analogously, a vector field is written in terms of polarization vectors $\varepsilon_\mu(p)$. These appear in the calculations of Chapter 3 for photons and in Chapter 5 for the gluon.

The QCD Lagrangian is written using the $SU(2)_C$ generators

$$T^a = \frac{\lambda_c^a}{2} \tag{A.11}$$

which are given in terms of the Gell-Mann matrices

$$\lambda_c^1 = \begin{pmatrix} 0 & 1 & 0 \\ 1 & 0 & 0 \\ 0 & 0 & 0 \end{pmatrix}, \qquad \lambda_c^2 = \begin{pmatrix} 0 & -\imath & 0 \\ \imath & 0 & 0 \\ 0 & 0 & 0 \end{pmatrix}, \qquad \lambda_c^3 = \begin{pmatrix} 1 & 0 & 0 \\ 0 & -1 & 0 \\ 0 & 0 & 0 \end{pmatrix},$$
$$\lambda_c^4 = \begin{pmatrix} 0 & 0 & 1 \\ 0 & 0 & 0 \\ 1 & 0 & 0 \end{pmatrix}, \qquad \lambda_c^5 = \begin{pmatrix} 0 & 0 & -\imath \\ 0 & 0 & 0 \\ \imath & 0 & 0 \end{pmatrix}, \tag{A.12}$$
$$\lambda_c^6 = \begin{pmatrix} 0 & 0 & 0 \\ 0 & 0 & 1 \\ 0 & 1 & 0 \end{pmatrix}, \qquad \lambda_c^7 = \begin{pmatrix} 0 & 0 & 0 \\ 0 & 0 & -\imath \\ 0 & \imath & 0 \end{pmatrix}, \qquad \lambda_c^8 = \frac{1}{\sqrt{3}} \begin{pmatrix} 1 & 0 & 0 \\ 0 & 1 & 0 \\ 0 & 0 & -2 \end{pmatrix}.$$

The integration measures appearing in loop integrals are abbreviated as

$$\int_{\ell_i} = -\imath\, \mu^{4-d} \int \mathrm{d}^d \ell_i / (2\pi)^d \,, \tag{A.13}$$
$$\int_{\vec{\ell}_i} = -\,\mu^{4-d} \int \mathrm{d}^{d-1} \ell_i / (2\pi)^{d-1} \,, \tag{A.14}$$

with d being set to 4 whenever the proper regularization procedures have been performed.

The LTD theorem for a one-loop amplitude with N external legs $\mathcal{A}_N^{(1)}$ is given by

$$\mathcal{A}_N^{(1)} = -\int_\ell \mathcal{N}\left(\ell, \{p_k\}_N\right) \sum_{i=1}^{N} \tilde{\delta}\left(q_i\right) \left(\prod_{j \neq i} G_D\left(q_i; q_j\right) \right), \tag{A.15}$$

where

$$\tilde{\delta}\left(q_i\right) = 2\pi i\ \theta(q_{i,0}) \delta(q_i^2 - m_i^2) \tag{A.16}$$

and the dual propagator is given by

$$G_D(q_i; q_j) \equiv G_F(q_j)\Big|_{q_{i,0}=q_{i,0}^{(p,+)}} = \frac{1}{q_j^2 - m_j^2 - \imath 0\, \eta \cdot k_{ji}}\Bigg|_{q_{i,0}=q_{i,0}^{(+)}} \tag{A.17}$$
$$= \frac{1}{2q_i \cdot k_{ji} + m_i^2 + k_{ji}^2 - m_j^2 - \imath 0 \eta \cdot k_{ji}}\Bigg|_{q_{i,0}=q_{i,0}^{(+)}}.$$

The on-pole momenta

$$q_{q,0}^{(p,+)} = \sqrt{\boldsymbol{q}^2 + m^2 - \imath 0} \tag{A.18}$$

are on-shell momenta

$$q_{q,0}^{(+)} = \sqrt{\boldsymbol{q}^2 + m^2} \tag{A.19}$$

with the explicit imaginary part of the pole position.

For analytical integration after the application of LTD and local renormalization the following substitutions in the integral are useful:

$$\begin{aligned}
\int_\ell \tilde{\delta}\left(\ell\right)\ f_R(\ell_0, |\boldsymbol{\ell}|, \vartheta) &= -\frac{\imath}{(2\pi)^4} \int \mathrm{d}^3\ell_i \int \mathrm{d}\ell_0\ 2\pi\imath \frac{\delta(\ell_0 - \ell_0^{(+)})}{2\ell_0^{(+)}}\ f_R(\ell_0, |\boldsymbol{\ell}|, \cos\vartheta) \\
&= \frac{1}{(2\pi)^3} \int_0^\infty \mathrm{d}\boldsymbol{\ell}\ \boldsymbol{\ell}^2 \int_{-1}^1 \mathrm{d}\cos\vartheta \int_0^{2\pi} \mathrm{d}\varphi\ \frac{1}{2\ell_0^{(+)}}\ f_R(\ell_0^{(+)}, |\boldsymbol{\ell}|, \cos\vartheta) \\
&= \frac{1}{(2\pi)^2} \int_0^\infty m\mathrm{d}\xi\ m^2\xi^2 \int_0^1 2\mathrm{d}v\ \frac{1}{2\ell_0^{(+)}}\ f_R(\ell_0^{(+)}, m\xi, 1-2v) \\
&= \frac{m^3}{(2\pi)^2} \int_0^\infty \mathrm{d}\xi \int_0^1 \mathrm{d}v\ \frac{\xi^2}{\ell_0^{(+)}}\ f_R(\ell_0^{(+)}, m\xi, 1-2v)\,.
\end{aligned} \tag{A.20}$$

The Passarino-Veltman integrals [36] appearing in this thesis may be evaluated using Package-X [101] which is connected to FeynCalc [38, 39] through FeynHelpers [89]. The integrals B_0 and C_0 are defined such that their result is obtained in MATHEMATICA with

```
PaxEvaluate[B0[s,mt^2,mt^2],PaxImplicitPreFactor->-i/(2Pi)^D]
```

$$= \mathrm{B}_0\left(s, M_t^2, M_t^2\right)\,. \tag{A.21}$$

This corresponds to the following definitions and results:

$$\begin{aligned}
\mathrm{B}_0\left(s, M_t^2, M_t^2\right) &= \int_\ell \frac{\left(\imath\pi^2\right)^{-1}}{\left(\ell^2 + M_t^2\right)\left((\ell + p_{12})^2 + M_t^2\right)} \\
&= -\frac{\imath}{16\pi^4\hat{\varepsilon}} - \frac{\imath}{16\pi^4 s}\left[s\left(\log\left(\frac{\mu^2}{M_t^2}\right) + 2\right)\right. \\
&\quad \left. + \sqrt{s\left(s - 4M_t^2\right)}\log\left(\frac{\sqrt{s\left(s-4M_t^2\right)} + 2M_t^2 - s}{2M_t^2}\right)\right],
\end{aligned} \tag{A.22}$$

where $d = 4 - 2\varepsilon$, $1/\hat{\varepsilon} = 1/\varepsilon - \gamma_E + \log(4\pi)$ and $s = p_{12}^2$, and

$$\begin{aligned}\mathrm{C}_0\big(0, s, M_H^2, M_t^2, M_t^2, M_t^2\big) &= \int_\ell \frac{\big(\imath\pi^2\big)^{-1}}{\big(\ell^2 - M_t^2\big)\big((\ell - h)^2 - M_t^2\big)\big((\ell + p_{12})^2 - M_t^2\big)} \\ &= \frac{i}{32\pi^4\big(M_H^2 - s\big)}\left[\log^2\left(\frac{\sqrt{s\big(s - 4M_t^2\big)} + 2M_t^2 - s}{2M_t^2}\right)\right. \\ &\quad \left. - \log^2\left(\frac{\sqrt{M_H^2\big(M_H^2 - 4M_t^2\big)} + 2M_t^2 - M_H^2}{2M_t^2}\right)\right], \quad \text{(A.23)}\end{aligned}$$

where $M_H^2 = h^2$. Note that the square root appearing inside the second logarithm is inherently complex, leading the logarithm to be entirely imaginary. A real value is produced by the square.

Appendix B

Complementary numerical results

In comparison to the numerical results shown in Section 4.2.2 here are provided the numerical convergence both at integrand-level and of integrated results of the threshold expansion of the scalar two-point function when using an additional term in the expansion of the pole position

$$r_{21} = -1 + \sqrt{M/m}\sqrt{-\beta} + M/(2m)\beta\,, \tag{B.1}$$

while maintaining the value of r_{12} are shown in Fig. B.1 and Fig. B.1.

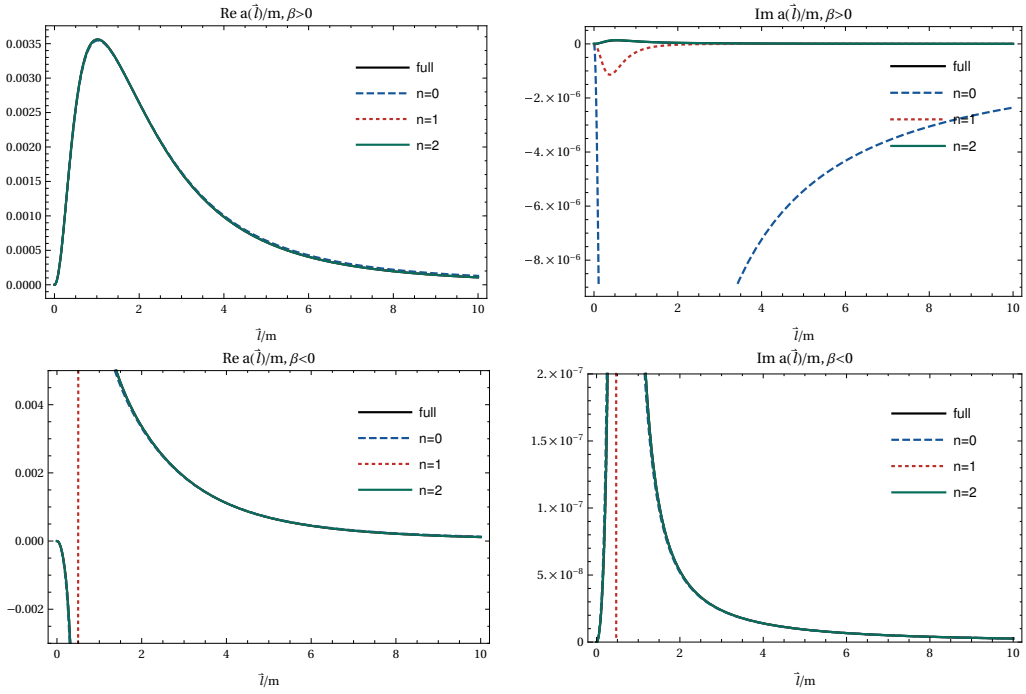

Figure B.1: The convergence behaviour of the integrand-level expansion in the threshold limit of the scalar two-point function in Eq. (4.24) for $M/m = 3$ including the third term in the pole expansion. In the upper row the integrand is shown for the expansion below the unitarity threshold, $\beta = 0.1$, and in the lower row above threshold, $\beta = -0.1$. Evaluation with $\mu_{\mathrm{UV}} = M$ and $\imath 0 = \imath 10^{-4}$.

Table B.1: The values obtained through integration of the expansion Eq. (4.32) in the threshold limit from below (above) including the third term in the pole expansion, the relative error of the real part with respect to the full result 0.011 46 ($0.015\,259\,9 + 0.005\,272\,87\imath$) and the ratio between real and imaginary part. The parameters used are $M/m = 3$, $\beta = \pm 0.1$ and $\mu_{\mathrm{UV}} = M$.

$\beta > 0$	integrated result		error	
	Re	Im	rel. error Re	Im/Re
$n = 1$	0.011 639 9	0.000 141	1.5 %	0.012
$n = 2$	0.011 419 0	0.000 041	0.38 %	0.0036
$n = 3$	0.011 450 2	−0.000 017	0.11	−0.0015
$\beta < 0$	integrated result		rel. error	
	Re	Im	Re	Im
$n = 1$	0.015 264 7	0.005 277 89	0.031 %	0.095 %
$n = 2$	0.015 259 9	0.005 272 61	2.3×10^{-6}	0.0049 %
$n = 3$	0.015 259 9	0.005 272 88	2.6×10^{-8}	3.0×10^{-6}

Bibliography

[1] J. J. Aguilera-Verdugo *et al.*, "A Stroll through the Loop-Tree Duality," *Symmetry* **13** no. 6, (2021) 1029, arXiv:2104.14621 [hep-ph].

[2] J. Plenter and G. Rodrigo, "Asymptotic expansions through the loop-tree duality," *Eur. Phys. J. C* **81** no. 4, (2021) 320, arXiv:2005.02119 [hep-ph].

[3] J. J. Aguilera-Verdugo, F. Driencourt-Mangin, R. J. Hernández-Pinto, J. Plenter, S. Ramirez-Uribe, A. E. Renteria Olivo, G. Rodrigo, G. F. R. Sborlini, W. J. Torres Bobadilla, and S. Tracz, "Open Loop Amplitudes and Causality to All Orders and Powers from the Loop-Tree Duality," *Phys. Rev. Lett.* **124** no. 21, (2020) 211602, arXiv:2001.03564 [hep-ph].

[4] J. J. Aguilera-Verdugo, F. Driencourt-Mangin, J. Plenter, S. Ramírez-Uribe, G. Rodrigo, G. F. R. Sborlini, W. J. Torres Bobadilla, and S. Tracz, "Causality, unitarity thresholds, anomalous thresholds and IR singularities from the loop-tree duality at higher orders," *JHEP* **12** (2019) 163, arXiv:1904.08389 [hep-ph].

[5] S. Holz, J. Plenter, C. W. Xiao, T. Dato, C. Hanhart, B. Kubis, U. G. Meißner, and A. Wirzba, "Towards an improved understanding of $\eta \to \gamma^*\gamma^*$," *Eur. Phys. J. C* **81** no. 11, (2021) 1002, arXiv:1509.02194 [hep-ph].

[6] J. J. Aguilera-Verdugo, F. Driencourt-Mangin, J. Plenter, S. Ramírez-Uribe, G. Rodrigo, G. F. R. Sborlini, W. J. Torres Bobadilla, and S. Tracz, "Unsubtractions at NNLO," *CERN Yellow Reports: Monographs* **3** (2020) 169–176.

[7] J. Plenter, "Asymptotic Expansions Through the Loop-Tree Duality," *Acta Phys. Polon. B* **50** (2019) 1983–1992.

[8] **Particle Data Group** Collaboration, P. A. Zyla *et al.*, "Review of Particle Physics," *PTEP* **2020** no. 8, (2020) 083C01.

[9] C. Gnendiger *et al.*, "To d, or not to d: recent developments and comparisons of regularization schemes," *Eur. Phys. J.* **C77** no. 7, (2017) 471, arXiv:1705.01827 [hep-ph].

[10] R. A. Fazio, P. Mastrolia, E. Mirabella, and W. J. Torres Bobadilla, "On the Four-Dimensional Formulation of Dimensionally Regulated Amplitudes," *Eur. Phys. J. C* **74** no. 12, (2014) 3197, arXiv:1404.4783 [hep-ph].

[11] G. Cullen *et al.*, "G*OSAM*-2.0: a tool for automated one-loop calculations within the Standard Model and beyond," *Eur. Phys. J. C* **74** no. 8, (2014) 3001, arXiv:1404.7096 [hep-ph].

[12] O. A. Battistel, A. L. Mota, and M. C. Nemes, "Consistency conditions for 4-D regularizations," *Mod. Phys. Lett. A* **13** (1998) 1597–1610.

[13] A. P. Baeta Scarpelli, M. Sampaio, B. Hiller, and M. C. Nemes, "Chiral anomaly and CPT invariance in an implicit momentum space regularization framework," *Phys. Rev. D* **64** (2001) 046013, arXiv:hep-th/0102108.

[14] A. P. Baeta Scarpelli, M. Sampaio, and M. C. Nemes, "Consistency relations for an implicit n-dimensional regularization scheme," *Phys. Rev. D* **63** (2001) 046004, arXiv:hep-th/0010285.

[15] R. Pittau, "A four-dimensional approach to quantum field theories," *JHEP* **11** (2012) 151, arXiv:1208.5457 [hep-ph].

[16] G. 't Hooft and M. J. G. Veltman, "Regularization and Renormalization of Gauge Fields," *Nucl. Phys. B* **44** (1972) 189–213.

[17] C. G. Bollini and J. J. Giambiagi, "Dimensional Renormalization: The Number of Dimensions as a Regularizing Parameter," *Nuovo Cim. B* **12** (1972) 20–26.

[18] T. Kinoshita, "Mass singularities of Feynman amplitudes," *J. Math. Phys.* **3** (1962) 650–677.

[19] T. D. Lee and M. Nauenberg, "Degenerate Systems and Mass Singularities," *Phys. Rev.* **133** (1964) B1549–B1562.

[20] Z. Kunszt and D. E. Soper, "Calculation of jet cross-sections in hadron collisions at order α_s^3," *Phys. Rev. D* **46** (1992) 192–221.

[21] S. Frixione, Z. Kunszt, and A. Signer, "Three jet cross-sections to next-to-leading order," *Nucl. Phys. B* **467** (1996) 399–442, arXiv:hep-ph/9512328.

[22] S. Catani and M. H. Seymour, "The Dipole formalism for the calculation of QCD jet cross-sections at next-to-leading order," *Phys. Lett. B* **378** (1996) 287–301, arXiv:hep-ph/9602277.

[23] S. Catani and M. H. Seymour, "A General algorithm for calculating jet cross-sections in NLO QCD," *Nucl. Phys. B* **485** (1997) 291–419, arXiv:hep-ph/9605323. [Erratum: Nucl.Phys.B 510, 503–504 (1998)].

[24] A. Gehrmann-De Ridder, T. Gehrmann, and E. W. N. Glover, "Antenna subtraction at NNLO," *JHEP* **09** (2005) 056, arXiv:hep-ph/0505111.

[25] S. Seth and S. Weinzierl, "Numerical integration of subtraction terms," *Phys. Rev. D* **93** no. 11, (2016) 114031, arXiv:1605.06646 [hep-ph].

[26] S. Catani and M. Grazzini, "An NNLO subtraction formalism in hadron collisions and its application to Higgs boson production at the LHC," *Phys. Rev. Lett.* **98** (2007) 222002, arXiv:hep-ph/0703012.

[27] S. Catani, L. Cieri, G. Ferrera, D. de Florian, and M. Grazzini, "Vector boson production at hadron colliders: a fully exclusive QCD calculation at NNLO," *Phys. Rev. Lett.* **103** (2009) 082001, arXiv:0903.2120 [hep-ph].

[28] M. Czakon, "A novel subtraction scheme for double-real radiation at NNLO," *Phys. Lett. B* **693** (2010) 259–268, arXiv:1005.0274 [hep-ph].

[29] P. Bolzoni, G. Somogyi, and Z. Trócsányi, "A subtraction scheme for computing QCD jet cross sections at NNLO: integrating the iterated singly-unresolved subtraction terms," *JHEP* **01** (2011) 059, arXiv:1011.1909 [hep-ph].

[30] V. Del Duca, C. Duhr, G. Somogyi, F. Tramontano, and Z. Trócsányi, "Higgs boson decay into b-quarks at NNLO accuracy," *JHEP* **04** (2015) 036, arXiv:1501.07226 [hep-ph].

[31] R. Boughezal, C. Focke, X. Liu, and F. Petriello, "W-boson production in association with a jet at next-to-next-to-leading order in perturbative QCD," *Phys. Rev. Lett.* **115** no. 6, (2015) 062002, arXiv:1504.02131 [hep-ph].

[32] J. Gaunt, M. Stahlhofen, F. J. Tackmann, and J. R. Walsh, "N-jettiness Subtractions for NNLO QCD Calculations," *JHEP* **09** (2015) 058, arXiv:1505.04794 [hep-ph].

[33] V. Del Duca, C. Duhr, A. Kardos, G. Somogyi, Z. Szőr, Z. Trócsányi, and Z. Tulipánt, "Jet production in the CoLoRFulNNLO method: event shapes in electron-positron collisions," *Phys. Rev. D* **94** no. 7, (2016) 074019, arXiv:1606.03453 [hep-ph].

[34] V. Del Duca, C. Duhr, A. Kardos, G. Somogyi, and Z. Trócsányi, "Three-Jet Production in Electron-Positron Collisions at Next-to-Next-to-Leading Order Accuracy," *Phys. Rev. Lett.* **117** no. 15, (2016) 152004, arXiv:1603.08927 [hep-ph].

[35] W. J. Torres Bobadilla *et al.*, "May the four be with you: Novel IR-subtraction methods to tackle NNLO calculations," *Eur. Phys. J. C* **81** no. 3, (2021) 250, arXiv:2012.02567 [hep-ph].

[36] G. Passarino and M. J. G. Veltman, "One Loop Corrections for e^+e^- Annihilation Into $\mu^+\mu^-$ in the Weinberg Model," *Nucl. Phys. B* **160** (1979) 151–207.

[37] W. R. Inc., "Mathematica, Version 13.0.0." https://www.wolfram.com/mathematica. Champaign, IL, 2021.

[38] R. Mertig, M. Bohm, and A. Denner, "FEYN CALC: Computer algebraic calculation of Feynman amplitudes," *Comput. Phys. Commun.* **64** (1991) 345–359.

[39] V. Shtabovenko, R. Mertig, and F. Orellana, "New Developments in FeynCalc 9.0" *Comput. Phys. Commun.* **207** (2016) 432–444, arXiv:1601.01167 [hep-ph].

[40] F. V. Tkachov, "A Theorem on Analytical Calculability of Four Loop Renormalization Group Functions," *Phys. Lett. B* **100** (1981) 65–68.

[41] K. G. Chetyrkin and F. V. Tkachov, "Integration by Parts: The Algorithm to Calculate beta Functions in 4 Loops," *Nucl. Phys. B* **192** (1981) 159–204.

[42] S. Weinberg, "Phenomenological Lagrangians," *Physica A* **96** no. 1-2, (1979) 327–340.

[43] T. Aoyama *et al.*, "The anomalous magnetic moment of the muon in the Standard Model," *Phys. Rept.* **887** (2020) 1–166, arXiv:2006.04822 [hep-ph].

[44] A. Pich, "Flavour Anomalies," *PoS* **LHCP2019** (2019) 078, arXiv:1911.06211 [hep-ph].

[45] G. Heinrich, "Collider Physics at the Precision Frontier," arXiv:2009.00516 [hep-ph].

[46] J. M. Lindert, K. Kudashkin, K. Melnikov, and C. Wever, "Higgs bosons with large transverse momentum at the LHC," *Phys. Lett. B* **782** (2018) 210–214, arXiv:1801.08226 [hep-ph].

[47] C. Anastasiou, C. Duhr, F. Dulat, E. Furlan, T. Gehrmann, F. Herzog, A. Lazopoulos, and B. Mistlberger, "High precision determination of the gluon fusion Higgs boson cross-section at the LHC," *JHEP* **05** (2016) 058, arXiv:1602.00695 [hep-ph].

[48] X. Chen, T. Gehrmann, E. W. N. Glover, and M. Jaquier, "Precise QCD predictions for the production of Higgs + jet final states," *Phys. Lett.* **B740** (2015) 147–150, arXiv:1408.5325 [hep-ph].

[49] R. Boughezal, C. Focke, W. Giele, X. Liu, and F. Petriello, "Higgs boson production in association with a jet at NNLO using jettiness subtraction," *Phys. Lett.* **B748** (2015) 5–8, arXiv:1505.03893 [hep-ph].

[50] R. Boughezal, F. Caola, K. Melnikov, F. Petriello, and M. Schulze, "Higgs boson production in association with a jet at next-to-next-to-leading order," *Phys. Rev. Lett.* **115** no. 8, (2015) 082003, arXiv:1504.07922 [hep-ph].

[51] X. Chen, J. Cruz-Martinez, T. Gehrmann, E. W. N. Glover, and M. Jaquier, "NNLO QCD corrections to Higgs boson production at large transverse momentum," *JHEP* **10** (2016) 066, arXiv:1607.08817 [hep-ph].

[52] J. M. Campbell, R. K. Ellis, and S. Seth, "H + 1 jet production revisited," *JHEP* **10** (2019) 136, arXiv:1906.01020 [hep-ph].

[53] R. K. Ellis, I. Hinchliffe, M. Soldate, and J. J. van der Bij, "Higgs Decay to $\tau^+\tau^-$: A Possible Signature of Intermediate Mass Higgs Bosons at the SSC," *Nucl. Phys.* **B297** (1988) 221–243.

[54] R. P. Kauffman, "Higgs boson p_T in gluon fusion," *Phys. Rev. D* **44** (1991) 1415–1425.

[55] R. Bonciani, V. Del Duca, H. Frellesvig, J. M. Henn, F. Moriello, and V. A. Smirnov, "Two-loop planar master integrals for Higgs→ 3 partons with full heavy-quark mass dependence," *JHEP* **12** (2016) 096, arXiv:1609.06685 [hep-ph].

[56] S. P. Jones, M. Kerner, and G. Luisoni, "Next-to-Leading-Order QCD Corrections to Higgs Boson Plus Jet Production with Full Top-Quark Mass Dependence," *Phys. Rev. Lett.* **120** no. 16, (2018) 162001, arXiv:1802.00349 [hep-ph].

[57] K. Becker *et al.*, "Precise predictions for boosted Higgs production," arXiv:2005.07762 [hep-ph].

[58] M. Beneke and V. A. Smirnov, "Asymptotic expansion of Feynman integrals near threshold," *Nucl. Phys. B* **522** (1998) 321–344, arXiv:hep-ph/9711391.

[59] V. A. Smirnov, "Applied asymptotic expansions in momenta and masses," *Springer Tracts Mod. Phys.* **177** (2002) 1–262.

[60] A. Pak and A. Smirnov, "Geometric approach to asymptotic expansion of Feynman integrals," *Eur. Phys. J. C* **71** (2011) 1626, arXiv:1011.4863 [hep-ph].

[61] B. Jantzen, "Foundation and generalization of the expansion by regions," *JHEP* **12** (2011) 076, arXiv:1111.2589 [hep-ph].

[62] B. Jantzen, A. V. Smirnov, and V. A. Smirnov, "Expansion by regions: revealing potential and Glauber regions automatically," *Eur. Phys. J. C* **72** (2012) 2139, arXiv:1206.0546 [hep-ph].

[63] G. Mishima, "High-Energy Expansion of Two-Loop Massive Four-Point Diagrams," *JHEP* **02** (2019) 080, arXiv:1812.04373 [hep-ph].

[64] B. Ananthanarayan, A. Pal, S. Ramanan, and R. Sarkar, "Unveiling Regions in multi-scale Feynman Integrals using Singularities and Power Geometry," *Eur. Phys. J. C* **79** no. 1, (2019) 57, arXiv:1810.06270 [hep-ph].

[65] T. Y. Semenova, A. V. Smirnov, and V. A. Smirnov, "On the status of expansion by regions," *Eur. Phys. J. C* **79** no. 2, (2019) 136, arXiv:1809.04325 [hep-th].

[66] S. Catani, T. Gleisberg, F. Krauss, G. Rodrigo, and J.-C. Winter, "From loops to trees by-passing Feynman's theorem," *JHEP* **09** (2008) 065, arXiv:0804.3170 [hep-ph].

[67] I. Bierenbaum, S. Catani, P. Draggiotis, and G. Rodrigo, "A Tree-Loop Duality Relation at Two Loops and Beyond," *JHEP* **10** (2010) 073, arXiv:1007.0194 [hep-ph].

[68] I. Bierenbaum, S. Buchta, P. Draggiotis, I. Malamos, and G. Rodrigo, "Tree-Loop Duality Relation beyond simple poles," *JHEP* **03** (2013) 025, arXiv:1211.5048 [hep-ph].

[69] S. Buchta, G. Chachamis, P. Draggiotis, I. Malamos, and G. Rodrigo, "On the singular behaviour of scattering amplitudes in quantum field theory," *JHEP* **11** (2014) 014, arXiv:1405.7850 [hep-ph].

[70] S. Buchta, *Theoretical foundations and applications of the Loop-Tree Duality in Quantum Field Theories*. PhD thesis, Valencia U., 2015. arXiv:1509.07167 [hep-ph].

[71] S. Buchta, G. Chachamis, P. Draggiotis, and G. Rodrigo, "Numerical implementation of the loop–tree duality method," *Eur. Phys. J. C* **77** no. 5, (2017) 274, arXiv:1510.00187 [hep-ph].

[72] F. Driencourt-Mangin, G. Rodrigo, and G. F. R. Sborlini, "Universal dual amplitudes and asymptotic expansions for $gg \to H$ and $H \to \gamma\gamma$ in four dimensions," *Eur. Phys. J.* **C78** no. 3, (2018) 231, arXiv:1702.07581 [hep-ph].

[73] F. Driencourt-Mangin, G. Rodrigo, G. F. R. Sborlini, and W. J. Torres Bobadilla, "Universal four-dimensional representation of $H \to \gamma\gamma$ at two loops through the Loop-Tree Duality," *JHEP* **02** (2019) 143, arXiv:1901.09853 [hep-ph].

[74] F. Driencourt-Mangin, *Four-dimensional representation of scattering amplitudes and physical observables through the application of the Loop-Tree Duality theorem*. PhD thesis, U. Valencia, 2019. arXiv:1907.12450 [hep-ph].

[75] E. T. Tomboulis, "Causality and Unitarity via the Tree-Loop Duality Relation," *JHEP* **05** (2017) 148, arXiv:1701.07052 [hep-th].

[76] R. Runkel, Z. Szőr, J. P. Vesga, and S. Weinzierl, "Causality and loop-tree duality at higher loops," *Phys. Rev. Lett.* **122** no. 11, (2019) 111603, arXiv:1902.02135 [hep-ph]. [Erratum: Phys.Rev.Lett. 123, 059902 (2019)].

[77] R. Baumeister, D. Mediger, J. Pečovnik, and S. Weinzierl, "Vanishing of certain cuts or residues of loop integrals with higher powers of the propagators," *Phys. Rev. D* **99** no. 9, (2019) 096023, arXiv:1903.02286 [hep-ph].

[78] Z. Capatti, V. Hirschi, D. Kermanschah, and B. Ruijl, "Loop-Tree Duality for Multiloop Numerical Integration," *Phys. Rev. Lett.* **123** no. 15, (2019) 151602, arXiv:1906.06138 [hep-ph].

[79] Z. Capatti, V. Hirschi, D. Kermanschah, A. Pelloni, and B. Ruijl, "Numerical Loop-Tree Duality: contour deformation and subtraction," *JHEP* **04** (2020) 096, arXiv:1912.09291 [hep-ph].

[80] F. Driencourt-Mangin, G. Rodrigo, G. F. R. Sborlini, and W. J. Torres Bobadilla, "Interplay between the loop-tree duality and helicity amplitudes," *Phys. Rev. D* **105** no. 1, (2022) 016012, arXiv:1911.11125 [hep-ph].

[81] J. J. Aguilera-Verdugo, R. J. Hernández-Pinto, G. Rodrigo, G. F. R. Sborlini, and W. J. Torres Bobadilla, "Causal representation of multi-loop Feynman integrands within the loop-tree duality," *JHEP* **01** (2021) 069, arXiv:2006.11217 [hep-ph].

[82] S. Ramírez-Uribe, R. J. Hernández-Pinto, G. Rodrigo, G. F. R. Sborlini, and W. J. Torres Bobadilla, "Universal opening of four-loop scattering amplitudes to trees," *JHEP* **04** (2021) 129, arXiv:2006.13818 [hep-ph].

[83] R. J. Hernández-Pinto, G. F. R. Sborlini, and G. Rodrigo, "Towards gauge theories in four dimensions," *JHEP* **02** (2016) 044, arXiv:1506.04617 [hep-ph].

[84] G. F. R. Sborlini, F. Driencourt-Mangin, R. Hernández-Pinto, and G. Rodrigo, "Four-dimensional unsubtraction from the loop-tree duality," *JHEP* **08** (2016) 160, arXiv:1604.06699 [hep-ph].

[85] G. F. R. Sborlini, F. Driencourt-Mangin, and G. Rodrigo, "Four-dimensional unsubtraction with massive particles," *JHEP* **10** (2016) 162, arXiv:1608.01584 [hep-ph].

[86] S. Becker, C. Reuschle, and S. Weinzierl, "Numerical NLO QCD calculations," *JHEP* **12** (2010) 013, arXiv:1010.4187 [hep-ph].

[87] R. Scharf and J. B. Tausk, "Scalar two loop integrals for gauge boson selfenergy diagrams with a massless fermion loop," *Nucl. Phys. B* **412** (1994) 523–552.

[88] A. V. Smirnov and V. A. Smirnov, "FIRE4, LiteRed and accompanying tools to solve integration by parts relations," *Comput. Phys. Commun.* **184** (2013) 2820–2827, arXiv:1302.5885 [hep-ph].

[89] V. Shtabovenko, "FeynHelpers: Connecting FeynCalc to FIRE and Package-X," *Comput. Phys. Commun.* **218** (2017) 48–65, arXiv:1611.06793 [physics.comp-ph].

[90] G. F. R. Sborlini, "Loop-tree duality and quantum field theory in four dimensions," *PoS* **RADCOR2015** (2016) 082, arXiv:1601.04634 [hep-ph].

[91] G. F. R. Sborlini, R. Hernández-Pinto, and G. Rodrigo, "From dimensional regularization to NLO computations in four dimensions," *PoS* **EPS-HEP2015** (2015) 479, arXiv:1510.01079 [hep-ph].

[92] R. M. Prisco and F. Tramontano, "Dual subtractions," *JHEP* **06** (2021) 089, arXiv:2012.05012 [hep-ph].

[93] J. Jesús Aguilera-Verdugo, R. J. Hernández-Pinto, G. Rodrigo, G. F. R. Sborlini, and W. J. Torres Bobadilla, "Mathematical properties of nested residues and their application to multi-loop scattering amplitudes," *JHEP* **02** (2021) 112, arXiv:2010.12971 [hep-ph].

[94] Z. Capatti, V. Hirschi, D. Kermanschah, A. Pelloni, and B. Ruijl, "Manifestly Causal Loop-Tree Duality," arXiv:2009.05509 [hep-ph].

[95] W. J. Torres Bobadilla, "Loop-tree duality from vertices and edges," *JHEP* **04** (2021) 183, arXiv:2102.05048 [hep-ph].

[96] W. J. T. Bobadilla, "Lotty – The loop-tree duality automation," *Eur. Phys. J. C* **81** no. 6, (2021) 514, arXiv:2103.09237 [hep-ph].

[97] G. F. R. Sborlini, "Geometrical approach to causality in multiloop amplitudes," *Phys. Rev. D* **104** no. 3, (2021) 036014, arXiv:2102.05062 [hep-ph].

[98] S. Ramírez-Uribe, A. E. Rentería-Olivo, G. Rodrigo, G. F. R. Sborlini, and L. Vale Silva, "Quantum algorithm for Feynman loop integrals," arXiv:2105.08703 [hep-ph].

[99] A. L. Cherchiglia, L. A. Cabral, M. C. Nemes, and M. Sampaio, "(Un)determined finite regularization dependent quantum corrections: the Higgs boson decay into two photons and the two photon scattering examples," *Phys. Rev. D* **87** no. 6, (2013) 065011, arXiv:1210.6164 [hep-th].

[100] T. Hahn, "Generating Feynman diagrams and amplitudes with FeynArts 3," *Comput. Phys. Commun.* **140** (2001) 418–431, arXiv:hep-ph/0012260.

[101] H. H. Patel, "Package-X: A Mathematica package for the analytic calculation of one-loop integrals," *Comput. Phys. Commun.* **197** (2015) 276–290, arXiv:1503.01469 [hep-ph].